

NDI-Phanes
with
Tailor-Made Optical Properties

Inauguraldissertation

zur
Erlangung der Würde eines Doktors der Philosophie
vorgelegt der
Philosophisch-Naturwissenschaftlichen Fakultät
der Universität Basel

von
Pascal Christian Hess
aus
Dürrenroth (BE), Schweiz
Basel, 2015

Originaldokument gespeichert auf dem Dokumentenserver der Universität Basel

edoc.unibas.ch



Dieses Werk ist unter dem Vertrag „Creative Commons Namensnennung-Keine kommerzielle Nutzung-Keine Bearbeitung 3.0 Schweiz“ (CC BY-NC-ND 3.0 CH) lizenziert. Die vollständige

Lizenz kann unter

creativecommons.org/licenses/by-nc-nd/3.0/ch/

eingesehen werden.

Genehmigt von der Philosophisch-Naturwissenschaftlichen Fakultät der Universität Basel
auf Antrag von

Prof. Dr. Marcel Mayor

Prof. Dr. Catherine Housecroft

Basel, den 16. September 2014

Prof. Dr. Jörg Schibler

Dekan



Namensnennung - Nicht-kommerziell - Keine Bearbeitung 3.0 Schweiz

(CC BY-NC-ND 3.0 CH)

Sie dürfen: Teilen — den Inhalt kopieren, verbreiten und zugänglich machen

Unter folgenden Bedingungen:



Namensnennung — Sie müssen den Namen des Autors/Rechteinhabers in der von ihm festgelegten Weise nennen.



Keine kommerzielle Nutzung — Sie dürfen das Material nicht für kommerzielle Zwecke nutzen.



Keine Bearbeitungen erlaubt — Sie dürfen diesen Inhalt nicht bearbeiten, abwandeln oder in anderer Weise verändern.

Wobei gilt:

- **Verzichtserklärung** — Jede der vorgenannten Bedingungen kann **aufgehoben** werden, sofern Sie die ausdrückliche Einwilligung des Rechteinhabers dazu erhalten.
- **Public Domain (gemeinfreie oder nicht-schützbarer Inhalte)** — Soweit das Werk, der Inhalt oder irgendein Teil davon zur Public Domain der jeweiligen Rechtsordnung gehört, wird dieser Status von der Lizenz in keiner Weise berührt.
- **Sonstige Rechte** — Die Lizenz hat keinerlei Einfluss auf die folgenden Rechte:
 - Die Rechte, die jedermann wegen der Schranken des Urheberrechts oder aufgrund gesetzlicher Erlaubnisse zustehen (in einigen Ländern als grundsätzliche Doktrin des **fair use** bekannt);
 - Die **Persönlichkeitsrechte** des Urhebers;
 - Rechte anderer Personen, entweder am Lizenzgegenstand selber oder bezüglich seiner Verwendung, zum Beispiel für **Werbung** oder Privatsphärenschutz.
- **Hinweis** — Bei jeder Nutzung oder Verbreitung müssen Sie anderen alle Lizenzbedingungen mitteilen, die für diesen Inhalt gelten. Am einfachsten ist es, an entsprechender Stelle einen Link auf diese Seite einzubinden.

Dedicated to my family

Abstract

The concept of *nanoscience* was introduced at the talk entitled “*Plenty of Room at the Bottom*” by Richard Feynman, the father of nanotechnology, in 1959. Nanoscience is an interdisciplinary field and involves biology, chemistry, material science, and physics. The electrical, optical, magnetic, and mechanical properties of materials change as we move from macro- to the nanoscale and, thus, allow us to design new functional *nanomaterials* with tailor-made properties. One of the approaches to nanoscale materials, varying in size between 1 and 100 nm, is the so-called “*bottom-up*” approach. Because of the great potential of nanodevices, they are of interest for industrial applications and, so far, billions of dollars have been invested into this field of research. The focus of this doctoral thesis was the synthetic aspect of new functional materials with tailor-made optical properties. All of the synthesized model compounds have one characteristic in common: they contain a naphthalene diimide (NDI) unit within their structure. The three objectives of this doctoral thesis are described in Chapter 2, while the introductory Chapter 1 explains (a) the chemical and (b) the optical properties of the NDI-derived compounds, and (c) the techniques to measure these properties at the nanoscale level. Each objective is described in more detail in Chapters 3–5 and the obtained results are discussed. Finally, the results are summarized in Chapter 6. In detail:

Chapter 1 provides an introduction to five topics (1) Cyclophanes, (2) Energy Transfers, (3) Naphthalene Diimides, (4) Molecular Electronics, and (5) Photoswitchable Phanes as Molecular Switches.

Chapter 2 describes the three objectives of this doctoral thesis, which are to investigate (a) the influence of the reduced motional freedom of the core substituents in a NDI-*phane* with two fixed bridges on the photoinduced charge transfer, (b) the photoinduced charge transfer in a linear cNDI integrated into a squeezable break junction, and (c) photoswitchable NDI-*phanes* as potential molecular switches.

Chapter 3 describes the design, synthesis, and characterization of a series of molecular figure-of-eight derivatives as well as their transient-absorption spectra, which are compared with that of the reference compound.

Chapter 4 describes the design, synthesis, and characterization of linear core-substituted NDIs and their subsequent integration into squeezable break junction setups to investigate photoinduced charge transfers.

Chapter 5 describes the design, synthesis, and characterization of photoswitchable NDI-*phanes*, as well the deposition of such NDI-*phanes* on a Ag (111) surface and the UV/Vis studies of the photoinduced isomerization processes.

Chapter 6 gives a summary of the obtained results of this thesis and provides an outlook

Chapter 7 provides the experimental details, including the characterization of all compounds described throughout the thesis.

Acknowledgements

First of all, I would like to express my deepest gratitude to Prof. Dr. Marcel Mayor for giving me the opportunity to work in his research group and his continuous support throughout my PhD studies. Marcel, you allowed me to work almost independently on the projects and explore the fascinating field of naphthalene diimide science, which I sincerely appreciate.

I would like to express my gratitude to Prof. Dr. Catherine Housecroft for co-refereeing my doctoral thesis and her time to read this doctoral thesis. Prof. Dr. Dennis Gillingham is acknowledged for chairing the examination committee.

Furthermore, my thanks go to three collaborators, with whom I cooperated closely in the last four years. I thank Prof. Dr. Eberhard Riedle and his former group member Dr. Igor Pugliesi in Munich for performing the transient-absorption measurements. I thank Dr. Yoram Selzer and his group member Michal Vadai in Tel Aviv for performing squeezable break junction measurements and explaining to me the physical details. I thank Prof. Dr. Richard Berndt and his group member Katharina Scheil in Kiel for performing the STM measurements and for many fruitful discussions.

My special thanks go to Gero Harzmann, Dr. Michal Juríček, and Dr. Gabriel Schäfer for proofreading this thesis, and to Michel Rickhaus for the beautiful artworks he created in the thesis.

I would like to thank Uli for introducing me to rock climbing, teaching me Austrian words, and pleasant times as my lab mate. I am grateful to Gero Harzmann for joining me so many times for a Döner and fun times at the conferences. I thank all the past and present members of the Mayor group for a nice working atmosphere, fruitful scientific discussions, and great times we had together outside the lab.

I dedicate a special thanks to all former and present group members in Lab 8, namely, Dr. Almudena Gallego, Dr. Ulrike Fluch, Dr. Jens Hermes, Dr. Fabian Sander, Lukas Felix, Mario Lehmann, Kenan Li (柯楠 李), and Kevin Weiland for the nice spirit in our lab during all these years.

Moreover, I would like to thank Dr. Daniel Häussinger, Heiko Gsellinger, and Kaspar Zimmermann for performing NMR experiments, Dr. Heinz Nadig for mass spectrometric analyses, Werner Kirsch and Sylvie Mittelheisser for elemental analyses, Dr. Markus Neuburger for X-ray diffraction analysis, Dr. Jonas Schönle for measuring the fluorescence quantum yields of the synthesized dyes, Mathias Fischer for the synthesis of 2,6-dichloronaphthalene-1,4,5,8-tetracarboxylic acid dianhydride, and Ruben Cal for helping me to use their NP-HPLC device.

I also want to thank Markus Ast, Francis Cabrera, Manuel Hermida, and Andreas Koller from the “Werkstatt”, Markus Hauri and Roy Lips from the “Materialausgabe”, and Brigitte Howald, Marina Mambelli, and Beatrice Erismann for their help.

I am wholeheartedly thankful also to my family. Without their constant support and love, none of the described work would have been possible.

Last but not least, I want to say thank you to my close friends Gabriel, Gian, Niels, and Toni.

Abstract	i
Acknowledgements	ii
Table of Contents	iii
Abbreviations	vi
1 Introduction	1
1.1 Cyclophanes.....	1
1.1.1 History, Synthesis, and Properties of Cyclophanes	1
1.1.2 Nomenclatures of Phanes	4
1.1.3 Naming of Synthesized Naphthalene Diimide-Phanes	6
1.2 Energy Transfers	9
1.2.1 Perrin–Jablonski Diagram.....	9
1.2.2 Absorption and Fluorescence Spectra.....	11
1.2.3 Transient-Absorption Spectroscopy.....	12
1.2.4 Fluorescence Quantum Yield	12
1.2.5 Quenching of Excited States	13
1.3 Naphthalene Diimides.....	14
1.3.1 Synthesis and Properties of Naphthalene Diimides	14
1.3.2 Naphthalene Diimide Motifs in Highly Strained Phanes	18
1.3.3 Naphthalene Diimides for Photoinduced Charge-Transfer Studies.....	21
1.4 Molecular Electronics.....	26
1.4.1 Scanning Probe Microscopy	26
1.4.2 Break Junctions	29
1.4.3 Immobilization of Organic Structures on Surfaces	32
1.5 Photoswitchable Phanes as Molecular Switches.....	33
1.5.1 History, Properties, and Isomerization Process Mechanisms of Stilbene	34
1.5.2 Stilbene Motifs in Highly-Strained Phanes.....	37
1.5.3 History, Properties, and Isomerization Process Mechanisms of Azobenzene	40
1.5.4 Azobenzene Motifs in Highly Strained Phanes	44
1.5.5 Dithienylethene—A Third Class of Photochromic Molecular Switches.....	47
2 Aim of the Work	49
3 Synthesis and Properties of Molecular 8 Derivatives	51
3.1 General Synthetic Strategy.....	52

3.1.1	Molecular Design of Molecular 8 Derivatives	52
3.1.2	Molecular Design of Reference Compounds.....	53
3.1.3	Retrosynthetic Analysis of Molecular 8 Derivatives.....	53
3.1.4	Retrosynthetic Analysis of Reference Compounds	55
3.2	Results and Discussion	56
3.2.1	Choice of the Protective Group.....	56
3.2.2	Synthesis of <i>S,S'</i> -Molecular 8	56
3.2.3	Synthesis of <i>N,N'</i> -Molecular 8	61
3.2.4	Synthesis of <i>O,O'</i> -Molecular 8.....	65
3.2.5	Synthesis of Reference Compounds	70
3.2.6	Overlay of Two Crystal Structures	72
3.2.7	Optical Properties of Molecular 8	72
3.2.8	Transient-Absorption Spectra	78
4	Synthesis and Properties of Linear cNDIs	79
4.1	General Synthetic Strategy.....	79
4.1.1	Molecular Design.....	79
4.1.2	Retrosynthetic Analysis	80
4.2	Results and Discussion	80
4.2.1	Synthesis of Linear cNDIs.....	80
4.2.2	Investigation of the Cleavage of the Protective Groups.....	82
4.2.3	Origin of the High Efficiency of the TMSE Protective Group Cleavage	83
4.2.4	Optical Properties.....	84
4.2.5	Physical Properties	85
5	Synthesis and Properties of Photoswitchable NDI-Phanes.....	86
5.1	General Synthetic Strategy.....	86
5.1.1	Molecular Design.....	86
5.1.2	First Generation Retrosynthetic Analysis of a NDI-Stilbenophane.....	87
5.1.3	Second Generation Retrosynthetic Analysis of a NDI-Stilbenophane.....	87
5.1.4	Retrosynthetic Analysis of NDI-Azobenzenophane	88
5.2	Results and Discussion	89
5.2.1	First Generation Synthesis of a NDI-Stilbenophane.....	89
5.2.2	Second Generation Synthesis of a NDI-Stilbenophane	89
5.2.3	Synthesis of a NDI-Azobenzenophane	95
5.2.4	Optical Properties.....	96
5.2.5	UV/Vis Study of Isomerization.....	97

5.2.6	¹ H-NMR Study of Isomerization.....	98
5.2.7	Immobilization of NDI-Azobenzophane on a Metallic Surface.....	106
6	Summary and Outlook.....	107
7	Experimental Section.....	110
7.1	General Information.....	110
7.2	Instrumentation.....	110
7.3	Synthesis of Molecular 8 Derivatives and Reference Compounds.....	115
7.4	Synthesis of Linear cNDIs.....	140
7.6	Syntheses of Linear cNDIs with Different Protecting Groups.....	183
7.8	Solid State Structures.....	205
7.8.1	Structure Determination by X-ray Diffraction Analysis.....	205
8	Appendix.....	206
8.1	Contributions.....	206
9	Literature.....	207

Abbreviations

A	Acceptor, Aliphatic, Acid	EI	Electron ionization
Å	Angstrom	equiv	Equivalent
AcCl	Acetyl chloride	ESI	Electrospray ionization
AcOH	Acetic acid	ET	Energy transfer
AFM	Atomic force microscopy	Et	Ethyl
AIBN	Azobisisobutyronitrile	et al.	And others
Alox	Aluminum oxide	Et ₂ O	Diethyl ether
BJ	Break junction	EtOAc	Ethyl acetate
Bn	Benzyl	EtOH	Ethanol
Boc	<i>tert</i> -Butyloxycarbonyl	EWG	Electron-withdrawing group
Boc ₂ O	Di- <i>tert</i> -butyl dicarbonate	Fmoc	9-Fluorenylmethyloxycarbonyl
Bp	Boiling point	FQY	Fluorescence quantum yield
BP	Bicycle-pedal	FRET	Fluorescence resonance energy transfer
calcd	Calculated	FT	Fourier-transform
cat.	Catalytic	GC	Gas chromatography
Cbz	Carbobenzyloxy	GPC	Gel permeation chromatography
CC	Column chromatography	h	Hextet
CM	Cross metathesis	HT	Hula-twist
cNDI	Core-substituted naphthalene diimide	hept	Heptet
CNOC	Commission on the Nomenclature of Organic Chemistry	HF	Hartree-Fock
concd	Concentrated	HMBC	Heteronuclear multiple-bond correlation
COSY	Correlation spectroscopy	HMQC	Heteronuclear multiple-quantum correlation
cPDI	Core-substituted perylene diimide	HOMO	Highest occupied molecular orbital
CT	Charge transfer	HPLC	High-performance liquid chromatography
d	Doublet	HRMS	High-resolution mass spectrometry
D	Donor	HWE	Horner-Wadsworth-Emmons
DART	Direct analysis at real time	i.e.	That is
DCC	<i>N,N'</i> -Dicyclohexylcarbodiimide	IC	Internal conversion
DCTB	(<i>E</i>)-2-[3-(4- <i>tert</i> -Butylphenyl)-2-methyl-2-propenylidene]malononitrile	IR	Infrared
DHP	4a,4b-Dihydrophenanthrene	ISC	Intersystem crossing
DIPEA	Diisopropylethylamine	IUPAC	International Union of Pure and Applied Chemistry
DMA	<i>N,N</i> -Dimethylacetamide	KIT	Karlsruhe Institute of Technology
DMAP	4-Dimethylaminopyridine	LMU	Ludwig Maximilian University
DME	1,2-Dimethoxyethane	LUMO	Lowest occupied molecular orbital
DMF	<i>N,N'</i> -Dimethylformamide	M	Molarity
DMI	1,3-Dimethyl-2-imidazolidinone	m	Multiplet (NMR), Medium (IR)
DMSO	Dimethylsulfoxid	MALDI	Matrix assisted laser desorption ionization
DTBP	Di- <i>tert</i> -butyl peroxide	MCBJ	Mechanically controllable break junction
<i>E</i>	Entgegen (configuration), Energy, Efficiency	Me	Methyl
e.g.	For example	MeCN	Acetonitrile
EA	Elemental analysis	MEM	β -Methoxyethoxymethyl ether
EDC	1,2-Dichloroethane	MeOH	Methanol
EDCI	1-Ethyl-3-(3-dimethylaminopropyl)carbodiimide	MOM	Methoxymethyl ether

EDG	Electron-donating group	MP	Melting point
MS	Mass spectroscopy	RCM	Ring-closing metathesis
MW	Microwave	RET	Resonance energy transfer
NBS	<i>N</i> -Bromosuccinimide	R _f	Retention factor
<i>n</i> -BuLi	<i>n</i> -Butyllithium	rt	Room temperature
NDA	Naphthalene dianhydride	S	Singlet (spin)
NDI	Naphthalene diimide	s	Singlet (NMR), Strong (IR)
NMR	Nuclear magnetic resonance	SAM	Self-assembled monolayer
NOE	Nuclear Overhauser effect	SBJ	Squeezable break junction
NOESY	Nuclear Overhauser effect spectroscopy	SM	Starting material
NP	Normal-phase	S _N 2	Bimolecular nucleophilic substitution
OBF	One-bond-flip	S _N Ar	Nucleophilic aromatic substitution
OPE	Oligo(<i>p</i> -phenylene ethynylene)	STM	Scanning tunneling microscopy
OPV	Oligo(<i>p</i> -phenylene vinylene)	t	Triplet (NMR),
ORTREP	Oak ridge thermal ellipsoid plot	T	Triplet (spin)
OSu	Succinimide	TAU	Tel Aviv University
p	Pentet	TBAF	Tetra- <i>n</i> -butylammonium fluoride
PG	Protective group	TBAH	Tetrabutylammonium hydroxide
Ph	Phenyl	^t Bu	<i>tert</i> -Butyl
pK _A	Acid dissociation constant at the logarithmic scale	TFA	Trifluoroacetic acid
PhMe	Methylbenzene	THF	Tetrahydrofuran
PhOH	Phenol	TLC	Thin-layer chromatography
PMB	<i>p</i> -Methoxybenzyl ether	TMS	Tetramethylsilane
ppm	Parts per million	TMSE	2-(Trimethylsilyl)ethyl
PSS	Photostationary state	TOF	Time of flight
PTLC	Preparative thin-layer chromatography	UHV	Ultrahigh vacuum
Py	Pyridine	UV	Ultraviolet
q	Quartet	UV/Vis	Ultraviolet/visible
quant.	Quantitatively	w	Weak (IR)
<i>R</i>	Distance	<i>Z</i>	Zusammen (configuration)
r	Rate	ZnChl	Zn chlorin

1 Introduction

The following introduction is divided into five sections (1) Cyclophanes, (2) Energy Transfers, (3) Naphthalene Diimides, (4) Molecular Electronics, and (5) Photoswitchable Phanes as Molecular Switches. These five topics are closely related to the main objectives of this thesis to investigate (a) the general assembly of various linear core-substituted naphthalene diimides (cNDIs) and NDI-phanes, (b) the influence of the reduced motional freedom of the core substituents in a NDI-phanes with two fixed bridges on the photoinduced charge-transfer process (c) the photoinduced charge transfer in a linear cNDI integrated into a squeezable break junction, and (d) photoswitchable NDI-phanes as potential molecular switches.

1.1 Cyclophanes

The aim of this chapter is to provide an insight into the history of cyclophanes and give examples of important cyclophanes. In a further step, the basic principle of π -interactions is explained and followed by the introduction of general methods for the successful assembly of (cyclo)phanes. In addition, different nomenclatures for naming (cyclo)phanes are described and the chapter is finally closed after a detailed tutorial on how the tailor-made target compounds of this doctoral thesis are named.

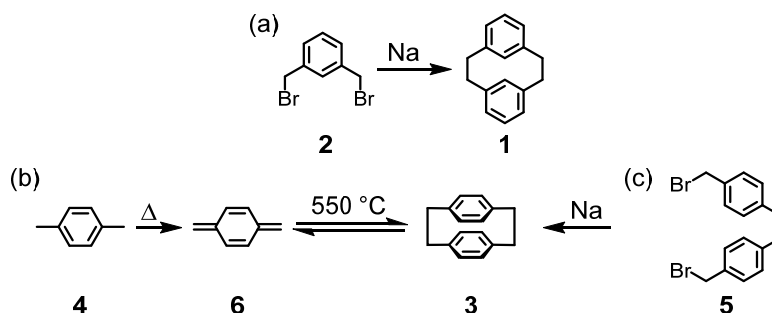
1.1.1 History, Synthesis, and Properties of Cyclophanes

Cram and Steinberg^[1] established the class name *cyclophane* for compounds consisting of an arene motif in which two positions are bridged by an aliphatic chain, forming a cycle ($n \geq 1$) seen in Figure 1.



Figure 1 General concept of cyclophane.

The history of cyclophanes started in 1899 with the successful synthesis^[2] of [2.2]metacyclophane **1** (Scheme 1a) by Pellegrin.



Scheme 1 Synthesis of: (a) [2.2]metacyclophane **1** by an intramolecular Wurtz reaction, (b) [2.2]paracyclophane **3** by pyrolysis, and (c) [2.2]paracyclophane **3** by Wurtz reaction.

He was able to assemble [2.2]metacyclophane **1** via an intermolecular Wurtz reaction of 1,3-bis(bromomethyl)benzene (**2**) with molten sodium. Next milestone and the beginning of the modern era of cyclophane history was the synthesis of [2.2]paracyclophane **3** (Scheme 1b) by Brown and Farthing^[3] in 1949. They were able, albeit non-selectively, to synthesize **3** by pyrolysis of 1,4-dimethylbenzene (**4**) at 550 °C. In 1951, Cram and Steinberg^[4] reported the first rational synthesis of **3**, as illustrated in Scheme 1c, by an intramolecular Wurtz reaction of 1,2-bis(4-(bromomethyl)phenyl)ethane (**5**) with molten sodium. Cram and Cram^[5] studied the influence of strain and the intermolecular interaction between the two π systems, also referred to as π - π interactions, in this three-dimensional aromatic molecule. Cyclophane **1** and **3** are perfectly suited to study π - π interactions for two reasons. Firstly, the arene motifs have well-defined relative orientations and, secondly, the arene motifs are held in close proximity to each other on the basis of the short aliphatic bridge. In detail, the arenes in cyclophane **1** and the arenes in cyclophane **3** have sandwich arrangements, also referred to as face-to-face conformations. Two benzene rings,^[6,7,8,9] as displayed in Figure 2, can interact in four possible arrangements, such as (a) face-to-face, (b) edge-to-face, (c) parallel displaced, and (d) T-shaped. The lowest-energy conformation is continually being discussed^[10,11] in the literature. Nevertheless, Tsuzuki et al.^[11] calculated the most important intramolecular interaction energies (E_{total}) in hexafluorobenzene–benzene and benzene–benzene arrangements. A hexafluorobenzene–benzene arrangement is predicted to have a parallel displaced ($E_{\text{total}} = -5.38$ kcal/mol) or a sandwich ($E_{\text{total}} = -5.07$ kcal/mol) orientation compared to a parallel displaced ($E_{\text{total}} = -2.48$ kcal/mol) or a T-shaped ($E_{\text{total}} = -2.46$ kcal/mol) orientation in a benzene dimer. The increased stability of the hexafluorobenzene–benzene arrangement is attributed to electrostatic and dispersion interactions. In case of the benzene–benzene dimer, only electrostatic interactions are stabilizing the T-shaped geometry and, vice versa, dispersion interactions enhance the stability of the parallel displaced arrangement.

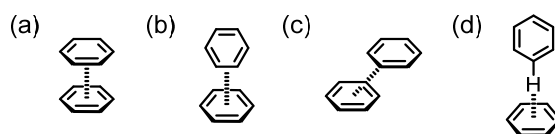


Figure 2 The four possible arrangements of two benzene rings: (a) face-to-face, (b) edge-to-face, (c) parallel displaced, and (d) T-shaped.

The latest review in this field by Iverson et al.^[12] is very interesting and is entitled “*Rethinking the term pi-stacking*”. According to the authors the terms “ π - π interactions” and “ π - π stacking” are used misnomers in literature and do not describe precisely the forces of a particular interaction. The reader can as well misleadingly connect these terms to a “*face-to-face arrangement*”. Consequently, these terms should not be used anymore and be replaced by more precise terms.

Moreover, an aromatic unit can have non-covalent interactions with an anion or a cation based on their π -acidity and π -basicity, respectively. Most aromatic moieties are π -basic with the electron

clouds above and below an electron-deficient aromatic plane, as seen in Figure 3a, implying a negative permanent quadrupole moment (Q_{zz}). Benzene has $Q_{zz} = -8.5 \text{ B}^{[13]}$ (B corresponds to Buckingham) and pyrene has $Q_{zz} = -13.8 \text{ B}^{[14]}$. An inverted permanent quadrupole moment, caused by the differences in electronegativity for hydrogen and fluorine relative to carbon and indicated by the plus sign, is observed in hexafluorobenzene^[15] with $Q_{zz} = +9.5 \text{ B}$ as displayed in Figure 3b.

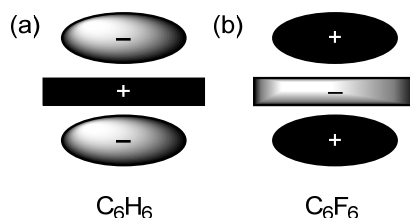


Figure 3 A schematic representation of (a) the permanent quadrupole moment in benzene, and (b) the inverted permanent quadrupole moment in hexafluorobenzene.

An *anion- π interaction* is a non-covalent contact between an electron-deficient aromatic system (a π -acidic compound, such as hexafluorobenzene) and an adjacent anion (e.g., a chloride anion). Likewise, a *cation- π interaction* is a non-covalent contact between an electron-rich aromatic system (a π -basic compound, such as benzene) and an adjacent cation (e.g., a sodium cation). Both interactions are a subclass of π -interactions to which (a) polar- π interactions, (b) metal- π interactions, (c) π - π interactions, and (d) π -donor- π -acceptor interactions are counted. Studies^[13,16,17] revealed that cation- π interactions are usually dominated by electrostatic (nature of the cation), solvatic (nature of the solvent), electronic (nature of the substituent on the aromatic moiety), and geometric (distance and geometry of both protagonists) contributions. In case of anion- π interactions, the contributions are reversed compared to cation- π interactions. The cation- π interaction can be used, for instance, in cyclophane host-guest chemistry as demonstrated^[18] by the group of Dougherty. By employing such interactions, they were able to perform the alkylation of quinolones in the presence of a cyclophane 8000 times faster than without a cyclophane, which facilitated the reaction rate as catalyst.

A next milestone in the history of cyclophanes was the successful synthesis (Figure 4) of the fully bridged [2₆]cyclophane **7**, also known as superphane, by Schirch and Boekelheide^[19] in 1979, followed by the preparation of [1.1]paracyclophane **8** by the group of Tsuji^[20] in 1993.

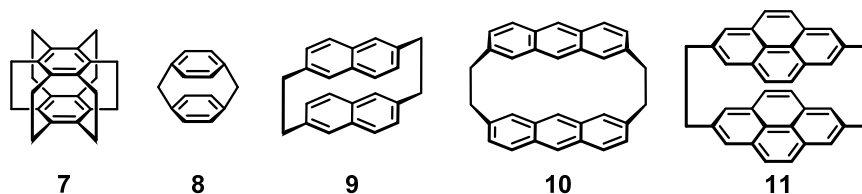


Figure 4 A series of important synthesized cyclophanes.

Not only the distance of the aliphatic bridge can be altered from narrow to wide as described above, but also the arene motifs (Figure 4) can be tailored leading to [2.2](2,6)naphthalenophane

9,^[21] [2.2](2,7)anthracenophane **10**,^[22] and [2.2](2,7)pyrenophane **11**.^[23,24,25] The concept of bridged aromatic compounds was adapted onto the synthesis of various cavitands, crown ethers, cryptands, and molecular machines. Most of these structures belong to the family ofphanes. From the synthetic point of view, there are a few criteria that should be considered to successfully assemble macrocycles (1) the synthesis of a molecular building block should involve just a few bond-formation steps to increase the overall yield; and (2) during the cyclization step, minimize or even prevent polymerization as a side reaction. Point (2) can be addressed by using (a) high-dilution principle or (b) template effect:

- (a) The high-dilution principle, also known as Ruggli–Ziegler dilution principle,^[26] favors cyclization over polymerization. This implies that the concentration of the reaction mixture must be in the range of 1 to 50 mM. A high-dilution synthesis can be achieved either by dissolving the starting material in a large amount of solvent or by slow addition of the reactant over hours or days with a syringe pump to the reaction flask. The latter is called pseudo-high-dilution principle and has one major drawback, namely, it is difficult to keep the reaction mixture strictly under an inert atmosphere. Oxygen or moisture may enter to the reaction flask and influences its outcome in a disadvantageous way.
- (b) Template effect is a very powerful tool to generate macrocycles of a specific size, as beautifully demonstrated by Anderson's^[27,28,29,30] porphyrin nanorings, Leigh's^[31,32,33,34] knots, and Stoddart's^[35,36,37,38] supramolecular structures. The specific interactions of the intermediate components with the reactant during the assembly reaction form the basic principle behind the template effect. The use of template thus allows for a size control of the macrocycle in most cases.

1.1.2 Nomenclatures of Phanes

The concept of Cram and Steinberg was further developed by Smith and Schubert, and in 1972, a subcommittee of the International Union of Pure and Applied Chemistry (IUPAC) Commission on the Nomenclature of Organic Chemistry (CNOC), consisting of Hirayama, Kaufmann, and Vögtle,^[1] started their pioneering work to establish a nomenclature of cyclophanes. This objective arised because many authors had used different nomenclature principles to name their cyclophanes. Meanwhile, Vögtle and Neumann envisioned to extend and systematize the work of Cram, Schubert, and Smith and developed their own nomenclature system, also referred to as phane nomenclature. They used the term *phane* for every compound having at least one homo- or heteroaromatic moiety and at least one n -membered bridge ($n \geq 0$). Therefore, the class ofphanes (Figure 5; X corresponds to NH, S, O, to name a few) can be divided into three subclasses (a) cyclophanes (benzophanes, in the case when the aromatic moiety is benzene); (b) heterophanes, in

the case when the aromatic moiety bears a heteroatom, for instance, pyridine; and (c) heteraphanes, in case when the heteroatom is in the aliphatic chain.

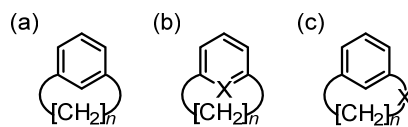


Figure 5 Three subclasses ofphanes: (a) benzophanes, (b) heterophanes, and (c) heteraphanes.

Two sets of numbers are put in front of the name that carries the suffix *-phane* (a) the numbers in the brackets indicate the length of the bridge, and (b) the numbers in the parentheses define the substitution pattern of the aromatic unit. If the term *ortho*, *meta*, or *para* is used to describe the substitution pattern of the aromatic motif, then the parentheses can be omitted. In case of cyclophanes bridged multiple times, the number of equally bridged units can be denoted by the number in subscript to the number in the parentheses. For example, superphane has six equal ethyl bridges and is therefore named $[2_6]$ cyclophane. According to the phane nomenclature, $[2.2]$ paracyclophane is named $[2.2]$ paracyclophane or $[2.2](1,4)$ cyclophane **3** (Figure 7a).

In 1979, N. Lozac'h et al.^[39,40] reported a tutorial for the nodal nomenclature. The term *nodal* is derived from the Latin word *nodus*, which means *knot*. The general concept of the nodal system is the *node principle*. According to which, each arene moiety is collapsed to a superatom that is represented as a node. These nodes are then connected, numbered, and named as an acyclic chain. In the case of $[2.2]$ metacyclophane **1**, the node simplification will result in a cyclohexane skeleton (Figure 6). The collapsed nodes are referred to as prefixes derived from the names of the corresponding arenes by changing their terminal letter *-e* to *-a*. (e.g, benzena) and added to the parentheses, where the substitution pattern of the arene is defined. The substitution pattern of the arene is put in front of the parentheses, followed by the acyclic chain name, whose terminal letters *-ne* are omitted. Finally, the suffix *-nodane* is added and the structure has its nodane name, for example, 1,4-di(1,3-benzena)cyclohexanodane **1**.

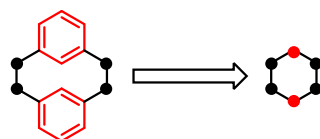


Figure 6 The node principle for naming 1,4-di(1,3-benzena)cyclohexanodane **1**.

The major advantage of the nodal and phane nomenclatures over the IUPAC nomenclature is the simplified naming of complex macrocycles as illustrated in Figure 7. The structure, as drawn in Figure 7a, is called according to the (a) phane nomenclature $[2.2]$ paracyclophane, $[2_2]$ paracyclophane, or $[2.2](1,4)$ cyclophane; (b) nodal nomenclature 1,4-di(1,4-benzena)cyclohexanodane; and (c) IUPAC nomenclature 1,4(1,4)-dibenzenacyclohexaphane (**3**). The more complex structure, as seen in Figure 7b, is known according to the (1) phane nomenclature as $[2.2](1,4)$ -naphthalenophane; (2) nodal nomenclature as 1,4-di(1,4-naphthalena)cyclohexanodane; (3) old IUPAC nomen-

clature as 6,7,14,15-tetrahydro-5,16:8,13-diethenodibenzo[a,g]cyclododecene; and (4) new IUPAC nomenclature as 1,4(1,4)-dinaphthalenacyclohexaphane (**12**).

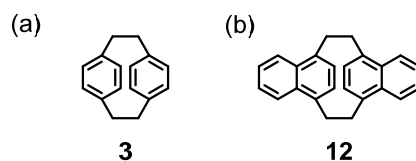


Figure 7 Two examples of naming phanes according to different nomenclatures, such as phane nomenclature, nodal nomenclature, and IUPAC nomenclature.

Nevertheless, the CNOC decided not to use the phane or nodal nomenclature (IUPAC recommendation) because they had developed their own nomenclature over the years.

1.1.3 Naming of Synthesized Naphthalene Diimide-Phanes

Within this doctoral thesis a modified nodal nomenclature is used for naming the synthesized naphthalene diimide-phanes (NDI-phanes). In general, all the molecular backbones are named after the IUPAC nomenclature and implemented into the nodal nomenclature for naming polycyclic systems.

According to this the molecular backbone of the molecular 8 derivatives (Figure 8a, X corresponds to S, NH, or O; see Chapter 3) is named according to the IUPAC nomenclature (Figure 8b), and results in case of (a) the 4,9-diphenylsulfanyl core-substituted NDI in 2,7-diphenyl-4,9-bis(phenylthio)benzo[*lmn*][3,8]phenanthroline-1,3,6,8(2*H*,7*H*)-tetraone; (b) the 4,9-diphenylamino core-substituted NDI in 2,7-diphenyl-4,9-bis(phenylamino)benzo[*lmn*][3,8]phenanthroline-1,3,6,8(2*H*,7*H*)-tetraone; and (c) the 4,9-diphenoxy core-substituted NDI in 2,7-diphenyl-4,9-bis(phenoxy)benzo[*lmn*][3,8]phenanthroline-1,3,6,8(2*H*,7*H*)-tetraone.

The rules **N-3.1** to **N-3.7** must be applied to name bicyclic phanes and out of these rules the rules **N-3.4** to **N-3.6** are the most important ones. In detail, the rule **N-3.1** defines a polycyclic system, and the rule **N-3.2** specifies that the main ring contains the greatest number of nodes. The rule **N-3.3** defines how to choose the main bridge, namely, it consists of the longest unbranched chain of nodes. This rule can be omitted in our case because only bicyclic phanes were synthesized. As already above-mentioned, the most important rules are **N-3.4** to **N-3.7** and are here cited^[39] as written in the original publication:

“Rule N-3.4 The numbering of a polycyclic graph begins at one of the nodes of the main ring to which the main bridge is attached (bridgehead) and proceeds in the direction that gives the lower locant to the other bridgehead. The main bridge is numbered sequentially after the main ring, beginning with the node of the main bridge connected to the node in the main ring having the locant 1. The secondary bridges are numbered successively in the same manner, beginning always with the longest bridge (or one of the longest bridges) connected to nodes of the graph previously numbered.”

When there is a choice between two or more bridges of the same length, the first to be numbered is the one attached to the node having the lowest locant in the part of the graph previously numbered. Each bridge is numbered beginning with the node of the bridge connected to the node of the part of the graph previously numbered having the lower locant.

Rule N-3.5 The descriptor of a polycyclic graph consists of square brackets enclosing: (a) a zero indicating the presence of a ring followed by an Arabic numeral indicating the number of nodes in the main ring; (b) a period followed by Arabic numerals denoting the number of nodes in each bridge, cited in the order of their numbering (see rule N-3.4); and (c) a pair of superscript locants for each bridge numeral, separated by a comma and cited in increasing numerical order, denoting the nodes in the part of the polycyclic graph already numbered to which each bridge is attached.

Rule N-3.6 When two or more alternative descriptors for a polycyclic graph can be derived because there is a choice for the main ring, main bridge, starting point and/or direction of numbering, Arabic numerals, in each descriptor, denoting the lengths of the bridges and the positions of the bridges in the graph are compared term by term in the order they appear (see rule N-3.5). The correct descriptor is the one with the preferred Arabic numeral at the first difference: if the first difference corresponds to a bridge length, the preferred numeral is higher; if the first difference appears in a superscript numeral (locant), the preferred numeral is lower.

Rule N-3.7 The name of a polycyclic graph consists of: (a) a descriptive prefix, such as “bicyclo-”, “tricyclo-”, etc., indicating the number of rings in the ring system; (b) the descriptor derived according to rules N-3.5 and N-3.6; (c) a multiplying prefix dictating the total number of nodes; and (d) the ending “-nodane”.

In our case, the NDI backbone with the core substituents in the positions 4 and 9 and the imide substituents in positions 2 and 7, as illustrated in Figure 8a, are collapsed to one node. After applying all the above-mentioned rules, the name bicyclo[09.8^{1,1}]heptadecanodane results. Last but not least, the arene substitution patterns of the four substituents on the NDI moiety must be defined. Each phenyl motif, as seen in Figure 8a, has a *meta*-substitution pattern and, as a result, the diction 3, 3', 3'', and 3''' (Figure 8b) can be used.

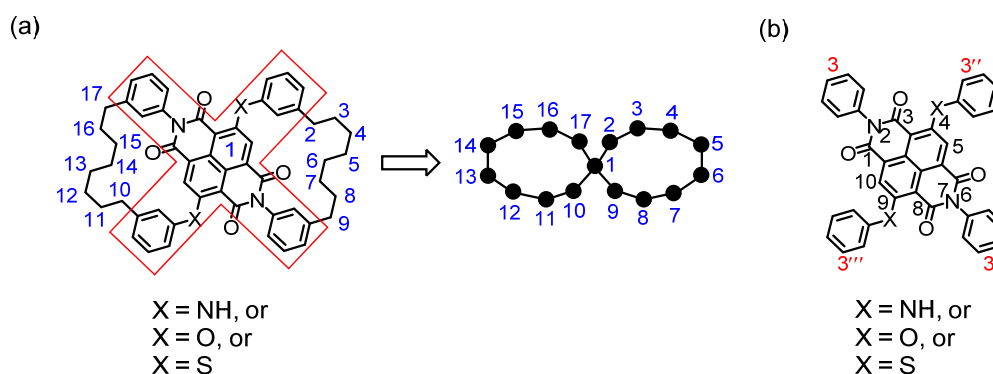


Figure 8 Applying the nodal nomenclature for naming properly the molecular 8 derivatives.

The name of a molecular 8 with a (a) 4,9-diphenylsulfanyl core substitution pattern is 1((3,3',3'',3''')-2,7-diphenyl-4,9-bis(phenylthio)benzo[*lmn*][3,8]phenanthroline-1,3,6,8(2*H*,7*H*)-tetraona)bicyclo[09.8^{1,1}]heptadecanodane, also referred to as *S,S'*-molecular 8; (b) 4,9-diphenylamino core substitution pattern is 1((3,3',3'',3''')-2,7-diphenyl-4,9-bis(phenylamino)benzo[*lmn*][3,8]phenanthroline-1,3,6,8(2*H*,7*H*)-tetraona)bicyclo[09.8^{1,1}]heptadecanodane, also referred to as *N,N'*-molecular 8; and (c) 4,9-diphenoxy core substitution pattern is 1((3,3',3'',3''')-2,7-diphenyl-4,9-bis(phenoxy)-benzo[*lmn*][3,8]phenanthroline-1,3,6,8(2*H*,7*H*)-tetraona)bicyclo[09.8^{1,1}]heptadecanodane, also referred to as *O,O'*-molecular 8.

In another objective, NDI-phanes with either a stilbene or an azobenzene switching unit were synthesized. Similar to the previous example, the NDI moiety is collapsed to a node as well as the stilbene and the azobenzene moiety, respectively, as illustrated in Figure 9a. The IUPAC name of the NDI moiety, as seen in Figure 9b, is benzo[*lmn*][3,8]phenanthroline-1,3,6,8(2*H*,7*H*)-tetraone, and the IUPAC names of the azobenzene and stilbene moiety (Figure 9b) are (*E*)-1,2-diphenyldiazene and (*E*)-1,2-diphenylethene, respectively. By applying the same rules (**N-3.4** to **N-3.7**), as for bicyclic systems, the following two names resulted. In case of the NDI-*phane* with an azobenzene moiety, the target structure is called (*E*)-1((2,7)-benzo[*lmn*][3,8]phenanthroline-1,3,6,8(2*H*,7*H*)-tetraona)-6((4,4')-1,2-diphenyldiazena)-4,8-dithiadecanodane, also referred to as NDI-azobenzenophane, and in case of a NDI-*phane* with a stilbene moiety, the structure is called (*E*)-1((2,7)-benzo[*lmn*][3,8]phenanthroline-1,3,6,8(2*H*,7*H*)-tetraona)-6((4,4')-1,2-diphenylethena)-4,8-dithiadecanodane, also referred to as NDI-stilbenophane.

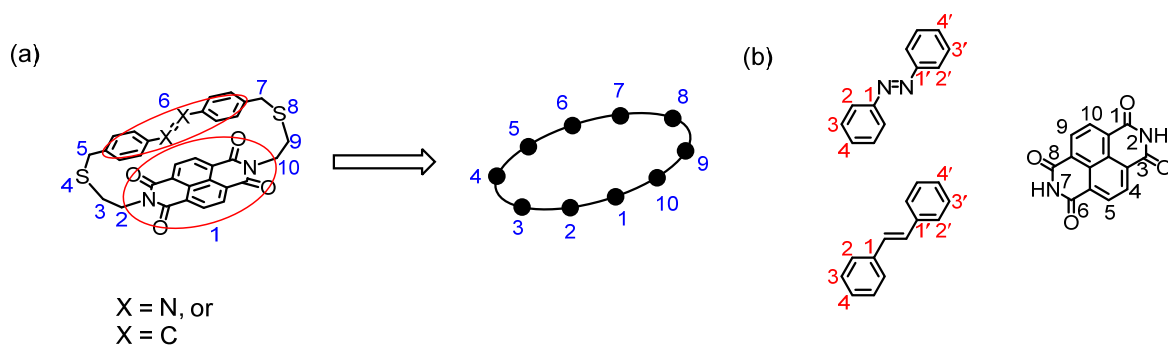


Figure 9 Applying the nodal nomenclature for naming the NDI-azobenzenophane and NDI-stilbenophane.

1.2 Energy Transfers

The aim of this chapter is to deliver an insight into energy and charge transfers and, therefore, the two terms are first defined. Secondly, the Perrin–Jablonski diagram will be described in detail to make the basic principles of the electronic states of a molecule and the transitions (energy transfers) between them comprehensible for the reader. Later on, the shape of the absorption and fluorescence spectra, and three examples of quenching processes of excited states are provided.

Energy transfer (ET) is defined^[41] by the IPUAC “*as the process by which a molecular entity absorbs light and a phenomenon originates from the excited state of another molecular entity. In mechanistic photochemistry the term has been reserved for the photophysical process in which an excited state of one molecular entity (the donor) is deactivated to a lower-lying state by transferring energy to a second molecular entity (the acceptor) which is thereby raised to a higher energy state. The excitation may be electronic, vibrational, rotational or translational. The donor and acceptor may be two parts of the same molecular entity, in which case the process is called intramolecular energy transfer*”.

Whereas, the expression charge transfer (CT) is defined^[42] by the IUPAC “*as an electronic transition in which a large fraction of an electronic charge is transferred from one region of a molecular entity, called the electron donor, to another, called the electron acceptor (intramolecular CT) or from one molecular entity to another (intermolecular CT). Typical for donor-acceptor complexes or multichromophoric molecular entities. In some cases the charge-transfer absorption band may be obscured by the absorption of the partners*”.

1.2.1 Perrin–Jablonski Diagram

An electron of a molecule in its ground states (S_0) can be excited very fast (10^{-15} s) by the absorption of a photon to an excited state (S_1 , S_2 , and S_3). The different excited states are denoted by the number in subscript and the different vibrational excited levels are indicated by the number in superscript, for example, S_m^n , with $m = 0-3$ and $n = 0-3$. If a molecule contains π -electrons from aromatic motifs (i.e., benzene, anthracene, pyrene, etc.) or n-electrons from functional groups (i.e., ketones, esters, double bonds, halogens, etc.), it can be excited as well. In principle, an electron is transferred from its highest occupied molecular orbital (HOMO) to its lowest unoccupied molecular orbital (LUMO). The transition, for example, of a non-bonding electron from the HOMO to its LUMO is denoted by $n \rightarrow \pi^*$. The energy of such a transition increases in the following order: $n \rightarrow \pi^* < \pi \rightarrow \pi^* < n \rightarrow \sigma^* < \sigma \rightarrow \pi^* < \sigma \rightarrow \sigma^*$.

There are two general rules (a) the longer is the π -electron system, the lower is the energy of the $\pi \rightarrow \pi^*$ transition and, consequently, the larger is the wavelength of the absorption band; and (b) the most likely transitions are the $n \rightarrow \pi^*$ and $\pi \rightarrow \pi^*$ transitions.

The release of the absorbed energy and the simultaneous relaxation of the electron to the ground state, also known as emission, can either occur by a non-radiative or a radiative transition via *photoluminescence* (including *fluorescence* or *phosphorescence*). Photoluminescence is a subclass of *luminescence*, also referred to as cold light. Because the phenomenon is not a result of heat (the opposite phenomenon is called incandescence), it is also known as cold light. The word *luminescence* is derived from the Latin word *lumen*, which means *light*.

As seen in Figure 10, the Perrin–Jablonski diagram^[43] illustrates (a) the absorption and emission process of a photon, (b) the different electronic states of a molecule, (c) the different vibrational levels of an electronic state, and (d) the transitions between them. To the class of non-radiative transitions^[44] belongs (1) vibrational relaxation, (2) internal conversion (IC), and (3) intersystem crossing (ISC). The vibrational relaxation with a lifetime of 10^{-12} to 10^{-10} s takes place if an electron relaxes to its lowest vibrational level in the same excited state, such as $S_1^2 \rightarrow S_1^0$. The resulting vibrational energy is transferred in solution either intra- or intermolecularly, leading to vibrational modes in the excited structure or to the surrounding solvent molecules through collision. Internal conversion with a lifetime of 10^{-11} to 10^{-9} s is a non-radiative transition from a higher to a lower excited state, for example, $S_2^2 \rightarrow S_1^2$. The relaxation after absorption of a photon to the lowest vibrational level of the first excited state, for example, $S_2^2 \rightarrow S_1^0$, takes place in the timescale of 10^{-13} to 10^{-11} s, and both internal conversion and vibrational relaxation are responsible for this process. This process is normally completed before the fluorescence process starts. The internal conversion of $S_1^0 \rightarrow S_0^0$ is very unlikely due to the large energy gap, but possible.^[44]

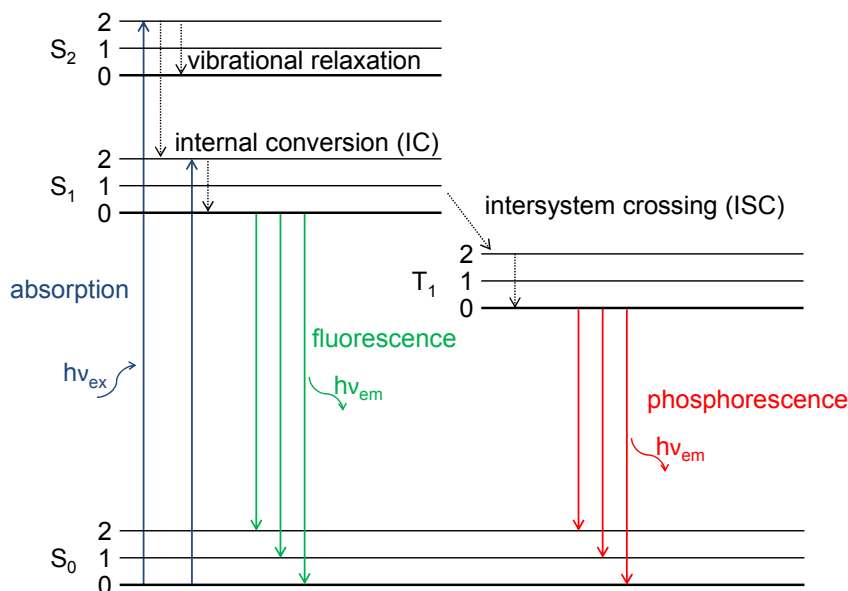


Figure 10 The Perrin–Jablonski diagram.

The radiative decay from an electronically excited singlet state to a singlet ground state $S_1^0 \rightarrow S_0^0$ is called fluorescence and has a much shorter lifetime (10^{-10} to 10^{-7} s) than phosphorescence (10^{-6} to 10^3 s). Intersystem crossing with a lifetime of 10^{-10} to 10^{-8} s is a spin forbidden and a

non-radiative transition from an excited singlet state (paired electrons) to a triplet state (unpaired electrons), namely, $S_1^0 \rightarrow T_1^0$. The spin forbidden radiative decay from an excited triplet state to a singlet ground state is called phosphorescence and is unfavored. As a result of the very slow decay, phosphorescence has a very long lifetime. Crossing between spin multiplicities is forbidden, but spin-orbital coupling may be large enough and, therefore, possible. The ISC transition is only significant in the presence of heavy atoms, such as Br, I, Pb, to name a few.

1.2.2 Absorption and Fluorescence Spectra

The Born-Oppenheimer approximation states that the motion of electrons is much faster than those of their nuclei. Thus, the transition from the ground to an excited state will most likely not affect the position of a nucleus. The resulting excited state is referred to as Franck-Condon state and the transition to the excited state is called vertical transition. As a consequence, the fluorescence spectrum appears often symmetrical to the absorption spectrum and is therefore like its mirror image as shown in Figure 11. The term *Stokes shift* is named after its discoverer and represents the difference in wavelengths of the band maxima (λ_{\max}) of the absorption and emission spectra of the same electronic transition. The phenomenon occurs when the emitted photon has less energy than the absorbed photon. In such a case, this energy difference is called Stokes shift (Figure 11) and, vice versa, *anti-Stokes shift*. Small Stokes shifts are generally observed in aprotic solvents and large Stokes shifts in protic solvents.

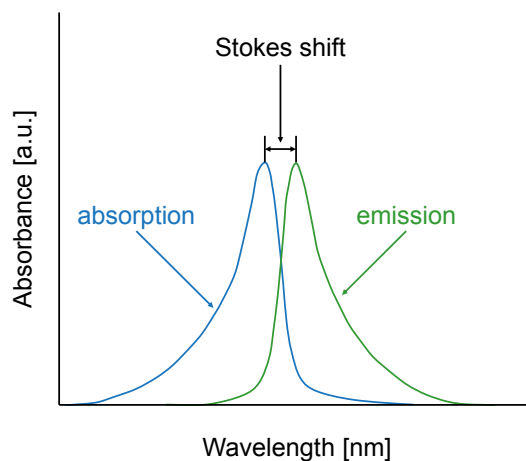


Figure 11 The Stokes shift and the illustrated mirror image of the absorption and emission spectra. Adapted from the webpage indicated in the literature.^[45]

There are some further terms, which must be introduced and defined. A shift to a longer wavelength (lower frequency) is called *bathochromic shift*, or *red-shift*, and a shift to a shorter wavelength is referred to as *hypsochromic shift*, or *blue-shift*. Such a shift can be caused, for instance, by the use of different solvents (solvatochromism), or molecules with substituents which can influence the absorption band maximum, to name a few. An increase in the molar absorption coefficient (ϵ) is called *hyperchromic effect* and the decrease of ϵ is called *hypochromic effect*.

1.2.3 Transient-Absorption Spectroscopy

Transient-absorption spectroscopy,^[46,47,48] also referred to as flash spectroscopy, is a powerful technique for probing and characterizing the electronic and structural properties of short-lived excited states of photochemically active molecules (pico- and femtosecond times domain). In 1999, Ahmed Zewail^[49] was awarded with the Nobel Prize in Chemistry “for his studies of the transition states of chemical reactions using femtosecond spectroscopy”.

In principle, the absorbance is detected at a particular wavelength or a range of wavelengths of a sample as a function of time after excitation by a flash of light. In a typical experimental setup the light for excitation (pump pulses) and the light for measuring the absorbance (probe) are generated by a pulsed laser. Transient-absorption spectroscopy is used to study, among others, photoinduced chemical reactions, electron transfer dynamics inside a molecular structure, and isomerization process from the (*Z*)- to the (*E*)-isomer, here referred to as *E* → *Z* isomerization process (*E* corresponds to *entgegen* and *Z* corresponds to *zusammen*). The study of electron transfer dynamics gives a kinetic profile of the formation and the decay through various stages of a photophysical pathway. A further development of femtosecond transient-absorption spectroscopy is attosecond^[50] transient-absorption spectroscopy.

1.2.4 Fluorescence Quantum Yield

The fluorescence quantum yield (FQY) is defined (Equation 1) as the ratio of the number of emitted photons to the number of absorbed photons and indicates the efficiency of the emission process in a molecule with photoluminescence properties.

$$\Phi_{\text{fl}} = \frac{\text{number of photons emitted}}{\text{number of photons absorbed}}$$

Equation 1 The fluorescence quantum yield.

The maximum FQY is 100% ($\Phi_{\text{fl}} = 1.0$) and it means that each absorbed photon is emitted over the whole duration of the radiative decay. The FQY is influenced by different parameters:

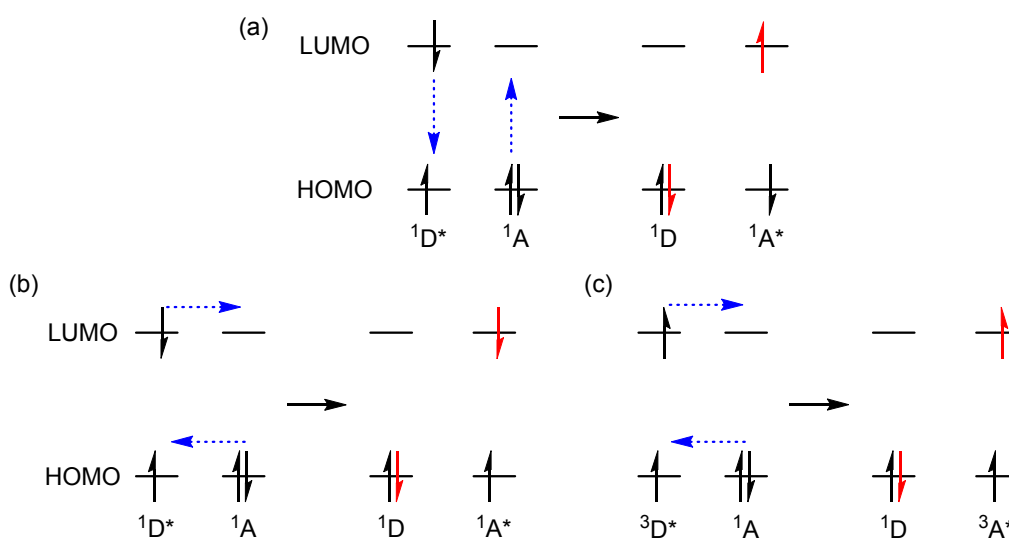
- (a) An increase of temperature results in a decreased FQY.
- (b) An increase of the size of π -electron system results in an increased FQY.
- (c) The FQY is dependent on the polarity of the solvent (proximity effect).
- (d) Azarenes (e.g., pyridine or quinoline) have a decreased FQY, but azarenes with a pyrrole motif (i.e., indole or carbazole) have increased FQY.
- (e) Internal rotations in a molecule often provide additional channels for non-radiative de-excitation ($\text{FQY}_{\text{rhodamine B}} < \text{FQY}_{\text{rhodamine 101}}$) and results in an increased FQY.
- (f) FQY is pH dependent.
- (g) Molecular oxygen or halide ions (e.g., chloride and iodide anions) will decrease the FQY as described in Chapter 1.2.5.

1.2.5 Quenching of Excited States

The lifetime of a molecule in its excited state can be decreased, or quenched, by various bimolecular processes, such as complex-formation, collision, electron transfer, or energy transfer. There are three main mechanisms responsible for this phenomena (a) resonance energy transfer (RET), (b) Dexter electron transfer (Dexter ET), and (c) static quenching.

In 1948, Förstner^[51] reported the first mechanism on non-radiative long-range (10–100 Å) transfer of excitation energy between a donor–acceptor (D–A) pair by RET, also known as fluorescence resonance energy transfer (FRET).^[52] The expression fluorescence resonance energy transfer is delusive because it is the electronic energy being transferred and not the fluorescence. The D–A pair can be within a large macromolecular structure and, as a result, the method can be used to measure the distance between two positions of interest. Specifically, the donor group is excited by a photon and relaxes to the lowest excited singlet state, S_1 . If the acceptor group is in close proximity (Scheme 2a) to the donor group, the donor group may transfer its energy to an electron of an acceptor group in its ground state (S_0) and, simultaneously, the donor group returns to its ground state (S_0). This process is referred to as resonance. Finally, the energy of the acceptor group is released as fluorescence (if the acceptor group is a fluorophore) or as heat and, simultaneously, the electron of the acceptor group returns to its ground state (S_0). The RET mechanism efficiency (E) depends strongly on the following three parameters with a decreasing order (1) the distance (R) between the D–A pair ($E = \propto 1/R^6$), (2) the spectral overlap of the emission spectrum of the donor with the absorption spectrum of the acceptor, and (3) the relative orientation of their transition dipole moments.

The second quenching mechanism (Scheme 2b–c) is known as Dexter ET mechanism and is named after its discoverer Dexter,^[53] who reported his results in 1953.



Scheme 2 HOMO and LUMO are shown for donor (D) and acceptor (A) before (left) and after ET (right): (a) RET mechanism, (b) singlet–singlet Dexter ET mechanism, and (c) triplet–triplet Dexter ET mechanism.

For an effective Dexter ET, a spatial overlap of the donor and the acceptor molecular orbitals as well as a short distance (5–10 Å) between them are required. In the course of the mechanism, an excited electron of a donor molecule, as illustrated in Scheme 2b–c, is transferred to the ground state of an acceptor molecule and, simultaneously, an electron from the ground state of the acceptor molecule is back-transferred to the ground state of the donor molecule. This exchange mechanism is allowed because of the Wigner’s spin conservation rule:



The Dexter ET mechanism efficiency (E) has an exponential dependence ($E = \alpha e^{-R}$) and decreases with increasing distance (R) between the D–A pair.

The efficiency of the third quenching mechanism—the static quenching—requires either the existence of a sphere of effective quenching or the formation of a ground-state non-fluorescent complex. The former case occurs if a quencher molecule (such as molecular oxygen or halide ions) is in close proximity to a fluorophore and forming a sphere (i.e., a fluorophore is in the radius of the quenching sphere). As a result, the fluorescence process efficiency will be significantly decreased. The latter case deals with the formation of a fluorophore/quencher (1:1) complex and, as a consequence, the photoluminescence process is quenched. Compared to RET and Dexter ET, the static quenching is strongly dependent on concentration, solvent, and temperature.

1.3 Naphthalene Diimides

The aim of this chapter is to describe in a first step the history, synthesis, and the most important chemical, physical, and optical properties of naphthalene diimides. After the general introduction, the few existing examples of the successful integration of naphthalene diimides into cyclic structures and their properties are provided. In the last part of the chapter, previous work on core-substituted naphthalene diimides for studying photoinduced charge-transfer processes is discussed.

1.3.1 Synthesis and Properties of Naphthalene Diimides

Core-substituted naphthalene diimides (cNDIs) are 1,4,5,8-naphthalenetetracarboxylic acid diimides (NDIs) with normally substituents in the positions 2 and 6 in case of the trivial name nomenclature, as seen in Figure 12a, and in the positions 4 and 9 in case of the IUPAC nomenclature as displayed in Figure 12b. The trivial name of, for example, cNDI **13** is *N,N'*-diphenyl-2,6-diphenylamino-1,4,5,8-naphthalenetetracarboxylic acid diimide (Figure 12a) and the official IUPAC name is 2,7-diphenyl-4,9-bis(phenylamino)benzo[*lmn*][3,8]phenanthroline-1,3,6,8(2*H*,7*H*)-tetraone (Figure 12b). Within this doctoral thesis the trivial name nomenclature is generally used to name unsubstituted NDIs and cNDIs. Only if necessary, the IUPAC nomenclature will be used.

In 1937, Vollmann et al.^[54] reported the successful synthesis (Figure 12a–b) of, among others, cNDI **13** and 2,6-dichloronaphthalene-1,4,5,8-tetracarboxylic acid dianhydride (Figure 12c; NDA **14**). Unfortunately, these compounds had a lack of interesting optical properties, a reason why this class of fluorophores was not in the focus of research for a long time.

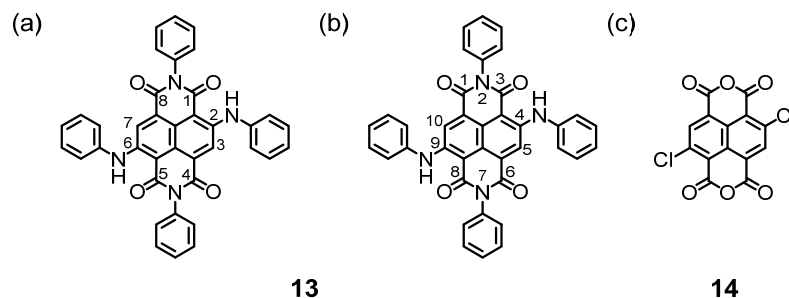
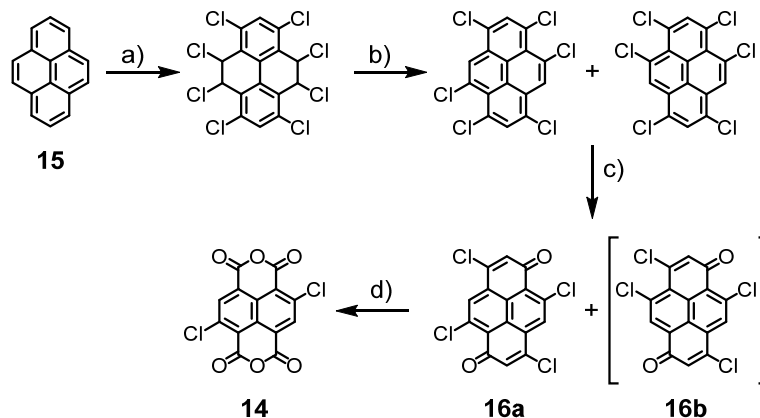


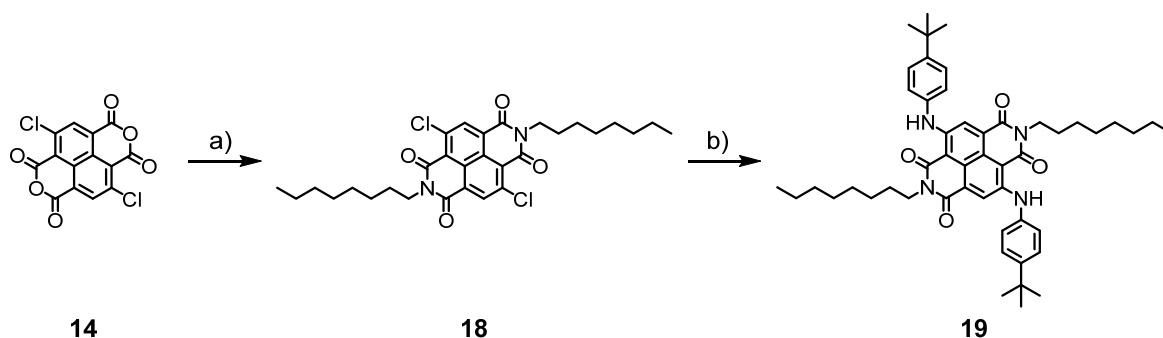
Figure 12 The chemical structures of NDA **13** and cNDI **14**.

The synthetic protocol for the synthesis of NDA **14** (Scheme 3) was later on adapted by Würthner et al.^[55] The modified synthesis started with the chlorination of pyrene (**15**) and a subsequent boiling of the reaction mixture in ethanolic KOH initiated HCl elimination. After oxidation in fuming nitric acid, the two regioisomers **16a** and **16b** were separated by precipitation out of the reaction mixture, purified by sublimation, and isomerically pure 2,5,7,10-tetrachloropyrene-3,8-quinone (**16a**) was isolated. A final oxidation with fuming nitric acid and concentrated sulfuric acid afforded the target structure **14** as a yellow solid.



Scheme 3 Synthesis of NDA **14** applying: (a) Cl₂ (g), 1,2,4-trichlorobenzene, 25–110 °C, 6 h, 36–38%; (b) KOH, EtOH, 80 °C, 5 h, 96–97%; (c) fuming HNO₃, 0–5 °C, 15 min, yield 32–45% of **16a** (regioisomer **16b** was not purified); (d) fuming HNO₃, concd. H₂SO₄, 100 °C, 5 min, 45–49%.

An illustrative example is given in Scheme 4 for the further functionalization of **14** by a twofold condensation reaction under acidic conditions in boiling acetic acid (AcOH) with *n*-octylamine (**17**) and is yielding cNDI **18**. Compound **18** can be converted by a subsequent twofold nucleophilic aromatic substitution reaction with a nucleophile like 4-*tert*-butylaniline in a polar aprotic solvent like *N,N'*-dimethylformamide (DMF) to the corresponding cNDI **19**, namely, *N,N'*-di-*n*-octyl-2,6-dimethylamino-1,4,5,8-naphthalenetetracarboxylic acid diimide.^[55]



Scheme 4 Synthesis of **19** applying: (a) **17**, AcOH, 120 °C, 10 min, 70%; (b) 4-*t*-Bu-C₆H₄-NH₂, DMF, 110 °C, 57%.

The powerful renaissance of cNDIs was initiated by Würthner et al.^[56] in 2002, who described new and highly interesting cNDIs that were used inter alia for RET mechanism studies as discussed in Chapter 1.3.3. In contrast to Vollman's aniline-based core substituents, Würthner et al. used aliphatic amino core substituents, which led to cNDIs with higher FQYs. Additionally, they synthesized cNDIs with different colors based on the nature of the core substituents. Moreover, the precise control of the reaction temperature and the choice of the solvent led to the formation of symmetrical and unsymmetrical cNDIs.

The first important property of cNDIs is colorability. The optical properties of cNDIs depend strongly on the core substituents in the positions 2 and 6 (IUPAC nomenclature: positions 4 and 9) of a particular cNDI, which can display various colors over the whole visible range.^[56] By tuning the HOMO–LUMO gap, the color of a cNDI^[57] is adjustable as illustrated in Figure 13. For example, the gap decreases from ethers core substituents (yellow color) to sulfides (red color), and to amines (blue color). The decreasing HOMO–LUMO gap with increasing HOMO and LUMO energies is a rare phenomenon and makes such cNDIs very attractive for various applications.

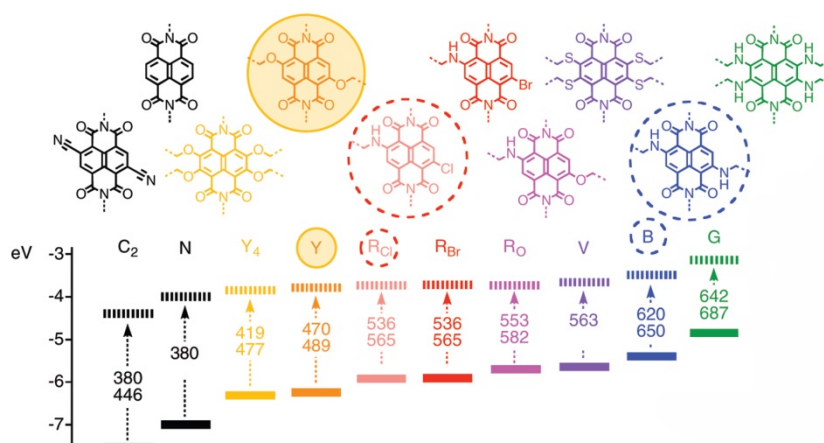


Figure 13 Effect of the core substituents on the color of cNDI. Reprinted with permission from Matile et al.^[57]

Changing the core substituents of a particular cNDI does not only affect the core-substituent transition band (bathochromic or hypsochromic shift) but also the FQY changes, ranging from low ($\Phi_{\text{fl}} = 0.01$), as reported by Vauthey et al.,^[58] to high ($\Phi_{\text{fl}} = 0.76$), as reported^[56] by Würthner et

al., values. In general, high FQYs are obtained in case of symmetrical secondary alkylamino-core-substituted NDIs due to multiple intramolecular hydrogen bondings between the hydrogen atom of the amine functionality with the oxygen atom of the carbonyl functionality compared to the low FQYs in case of symmetrical tertiary alkylamino- and arylamino-core-substituted NDIs.

The second important feature of NDIs is the ability to control the solubility and the aggregation by choosing appropriate imide substituents (Figure 12b; IUPAC nomenclature: positions 2 and 7). A NDI with a long and bulky substituent at each imide function features a high solubility, whereas a NDI with an aryl side-group at each imide function has a lower solubility.^[59]

These two abilities make cNDIs very attractive to various applications, for example, in the field of molecular sensors (Figure 14a; e.g., pH sensor^[59]) or as building blocks to form supramolecular structures by self-assembly aggregation (Figure 14b; acceptor-donor-donor-acceptor (AD-DA) array^[60]). The first application (Figure 14a), namely, pH sensor, works on the principle of different absorption band maxima caused by the removal of a proton in structure **20** to obtain structure **21**. Compared to the neutral structure **20** with an absorption band maximum at 454 nm, the anionic species **21** has its absorption band maximum at 550 nm. The observed red-shift can be ascribed to the conjugated resonance form in structure **21**. As a result of the aromatization in structure **21**, the more stable structure **22** is isolated.

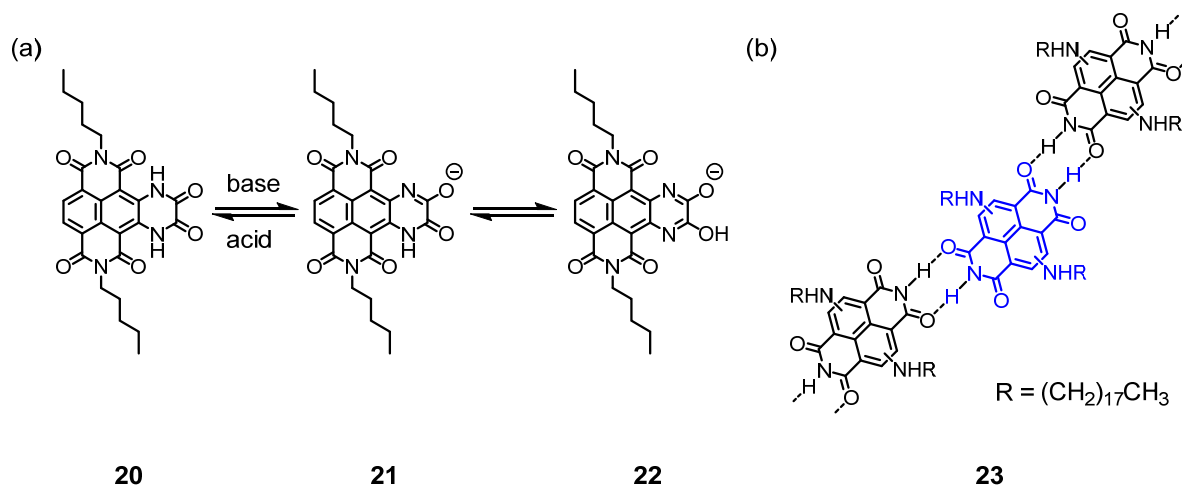


Figure 14 Two possible applications of cNDIs: (a) molecular pH sensor **20** is based on different absorption band maxima caused by the removal of a proton in **20**. This leads to structures **21** and **22**; and (b) AD-DA array (trimer-level) of this (*Z*)-type arrangement **23**. The chemical structure was proved by scanning tunneling microscopy (STM) analysis.

The second example (Figure 14b), namely, the AD-DA array, is a very good example of a supramolecular architecture with the possibility to form a (*Z*)- or (*E*)-type arrangement proved by STM analysis. The formation of this AD-DA pairing is caused by multiple intermolecular hydrogen bondings between the oxygen atom of the carbonyl functionality with the hydrogen atom at the *N*-terminus of the imide functionality to form the supramolecular tape **23**. This approach was further successfully applied to create bigger arrays, also referred to as supramolecular rosettes.^[61]

The abilities of cNDIs to create face-to-face arrangements,^[62] have anion- π interactions with π -acidic aromatic compounds,^[57,63] and transport charges are other important features of cNDIs and unsubstituted NDIs. The planar geometry of NDIs, compared to the slightly twisted core-substituted perylene diimides (cPDI)s, is essential for these abilities. In contrast to hexafluorobenzene with a high inverted permanent quadrupole ($Q_{zz} = +9.5$ B), an unsubstituted NDI has a calculated permanent quadrupole moment of $Q_{zz} = +18.6$ B,^[57] which is almost two times higher than in case of hexafluorobenzene. A 4,9-dichloro core-substituted NDI, as seen in Figure 15a, has a calculated permanent quadrupole moment of $Q_{zz} = +18.0$ B.^[57] The introduction of electron-withdrawing groups (EWGs) like cyano groups in the positions 4 and 9 of the naphthyl core will drastically increase the π -acidity ($Q_{zz} = +39.2$ B).^[14] Whereas the introduction of electron-donating groups (EDGs) like oxy substituents in the same positions will moderately lower the π -acidity (Figure 15b; $Q_{zz} = +8.0$ B)^[57] and heavily in case of secondary amino substituents (Figure 15c; $Q_{zz} = +2.3$ B).^[57]

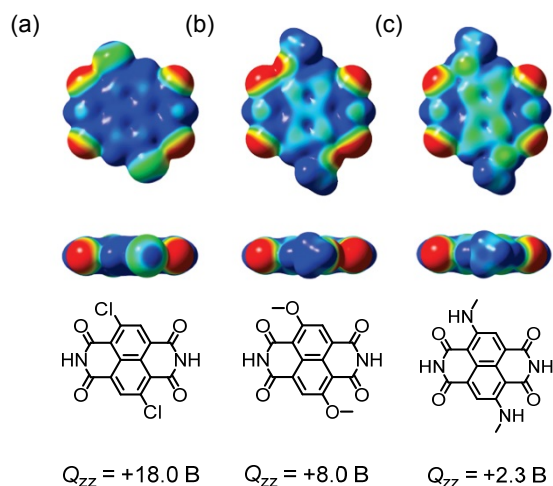


Figure 15 Permanent quadrupole moments of different core-substituted cNDIs. Reprinted with permission from Matile et al.^[57]

The ability of NDIs to transport charges was first reported by Miller et al.,^[64] who was able to detect the existence of delocalized radical anions in NDI π -stacks. A few years later, Katz et al.^[65] reported the successful synthesis of an air-stable *n*-semiconductor which contained an unsubstituted NDI. Outstanding work of Würthner et al.^[66,67] by the combination of the ability of photoinduced charge transfer and colorability, as discussed in Chapter 1.3.3, led to the formation of triads. Indeed, the pinnacle was the creation of the artificial photosystem developed by Matile et al.^[68]

1.3.2 Naphthalene Diimide Motifs in Highly Strained Phanes

NDIs are known for a long time, however, there are hardly any examples of NDIs integrated into supramolecular structures, such as phanes, catenanes, and rotaxanes. In the following section the most important examples are introduced and discussed.

In 1987, Lehn et al.^[62] succeeded in the preparation of [8.8]periophane **24** (Figure 16a), a phane bearing naphthalene diimide moieties instead of benzene moieties. They used this molecular receptor to study supramolecular host–guest interactions. In particular, they showed that an electron-deficient aromatic compound like nitrobenzene (Figure 16a) is able to bind inside the cavity between the two NDI units. Two decades later, Buncel and coworkers^[69] reported the syntheses of an unsymmetrical [3.4]periophane and a symmetrical [3.3]periophane **26** (Figure 16b). In contrast to Lehn’s long aliphatic octyl-bridge, their supramolecular assembly **26** has a very short aliphatic propyl-bridge and, consequently, the structure is extremely rigid. However, the authors only reported both syntheses, but did not investigate the possible host–guest interactions or the influence of the ring strain on the optical properties.

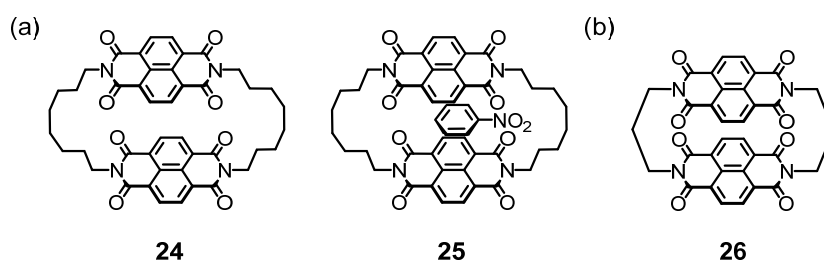


Figure 16 Illustration of (a) the chemical structure of Lehn’s [8.8]periophane **24** and the supramolecular host–guest structure **25** in which **24** binds a nitrobenzene molecule in its cavity; and (b) the chemical structure of Bunzel’s [3.3]periophane **26**.

Structures like rotaxanes and catenanes are highly interesting in the field of nanoscience and material science due to their ability to undergo translational isomerism upon external stimulus (see Chapter 1.5). Sander et al. reported the successful syntheses of two [2]catenanes via template-directed approaches applying in the first example a final ring-closing metathesis (RCM) reaction using first generation Grubbs catalyst^[70] (Figure 17) and in the second example either a final Glaser–Hay coupling^[71] using a copper(I) source or a final Mitsunobu alkylation reaction.^[71]

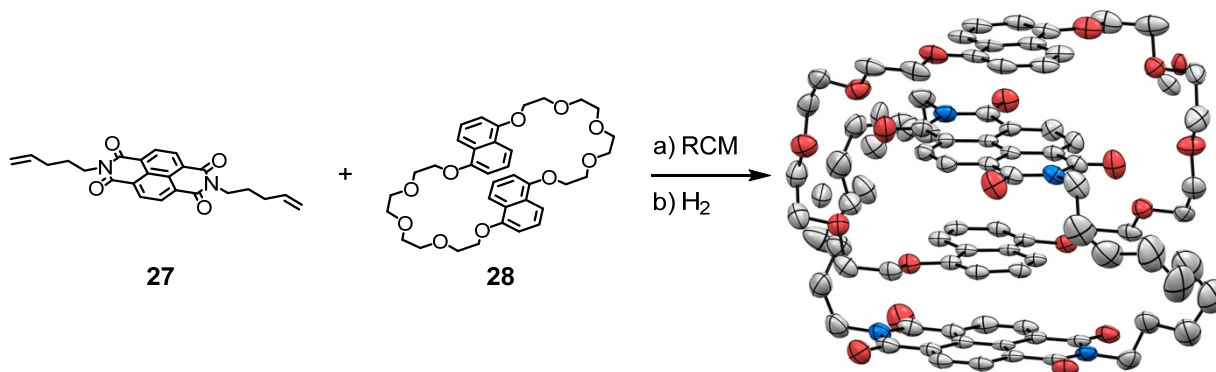


Figure 17 Illustration of the template-directed synthesis of Sander’s [2]catenane^[70] via a RCM reaction using two equivalents of the unsubstituted NDI **27** (π-electron deficient) and one equivalent of the crown ether derivative **28** (π-electron rich).

Some years later, Langford et al.^[72] demonstrated the successful assembly of another [2]catenane (Figure 18) via a template-directed synthesis. The target structure was obtained after a final oxidative Glaser–Hay coupling of the unsubstituted NDI **29** with the crown ether derivative **30**. The stability of the two presented [2]catenanes is attributed to the strong π -donor– π -acceptor interactions and the efficiency of the catenane formation process is caused by the permanent template effect for the resulting cyclophane. However, both [2]catenanes had a lack of potential applications, and the authors reported therefore only the successful integration of the NDI moieties into their supramolecular structures.

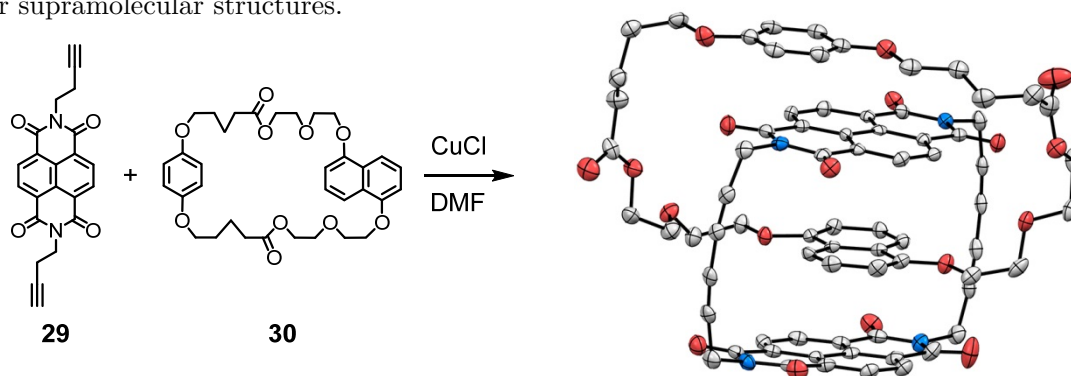


Figure 18 The key step of the template-directed synthesis of Langford's [2]catenane^[72] via an oxidative Glaser–Hay coupling using two equivalents of the unsubstituted NDI **29** and one equivalent of the crown ether derivative **30**.

Only very recently, Stoddart et al.^[73,74] not only achieved the successful integration of a modified version of Sander's [2]catenane^[71] into an electrochemically and thermally switchable donor–acceptor [c2]daisy chain rotaxane (Figure 19a) via a final azide–alkyne cycloaddition reaction but also the successful synthesis of mechanically interlocked molecules featuring through-space electron sharing (Figure 19b). In the former case, they demonstrated the precise control by the dual-mode switching behavior upon external stimuli.

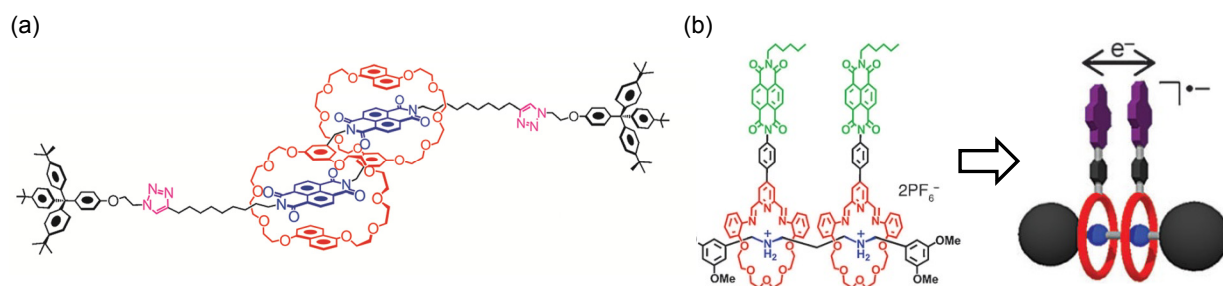


Figure 19 Structural formula of: (a) Stoddart's [c2]daisy chain rotaxane, and (b) the molecular machine suitable for through-space electron sharing. The figure on the left is reprinted with permission from Stoddart et al.^[73] and figure on the right is reprinted with permission from Stoddart et al.^[74]

Therefore, this kind of molecular structure could form the basis for the creation of molecular machines that can transform thermal or electrochemical energy into mechanical energy. In the latter case, the authors were able to synthesize mechanically interlocked molecules containing NDI

moieties with the ability to form π -stacks and, consequently, enabled an efficient through-space electron sharing. The efficiency of the through-space electron transport process decreased moderately as they increased the distance of the electron transport by an additional NDI stack (Figure 19b; e.g., by changing the number of NDI stacks between the two black balls from two to three units).

1.3.3 Naphthalene Diimides for Photoinduced Charge-Transfer Studies

To gain further insight into the mechanism of the charge-transfer process, simple model structures with cNDIs, such as structure **31** developed by Würthner et al.,^[56] were used. This particular system was mandatory for the creation of the more complex system, triad ZnChl-NDI_{NN}-NDI_{NO} **32**, reported by Würthner and coworkers.^[67] In detail, the first system (Figure 20) was synthesized to study the intramolecular RET mechanism. The authors found an efficient RET process from the NDI_{NCl} chromophore to the NDI_{NN} chromophore upon excitation at 500 nm (indicated with the red arrow). The energy-transfer efficiency was around 96% and a FQY of 30% was determined, compared to a FQY of 33% for direct excitation of NDI_{NN} at 622 nm.

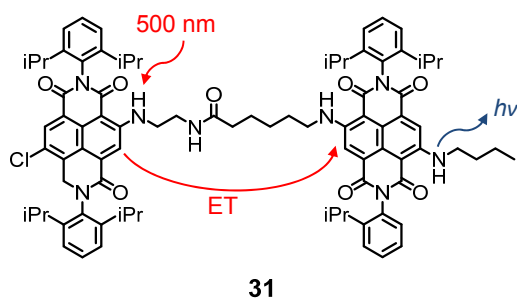


Figure 20 Bichromophoric compound **31** suitable for RET studies.

The photoinduced electron transport in the triad ZnChl-NDI_{NN}-NDI_{NO} **32** (Figure 21) led to intramolecular RET processes from the NDI_{NO} (excitation: red arrow; emission: purple arrow) and from the NDI_{NN} (excitation: blue arrow; emission: green arrow) after excitation at 540 and 612 nm, respectively, to the zinc chlorin (ZnChl) **33** rod antenna with an overall energy-transfer efficiency of 99%, and a light-harvesting efficiency of 63% compared to the parent ZnChl. Indeed, the authors were able to selectively excite the NDI_{NN} (blue arrow) or the NDI_{NO} (red arrow) chromophore based on the fact that both chromophores have different absorption band maximum of the charge-transfer transition of the core substituents to the NDI core. More precisely, they found that upon excitation of NDI_{NO} the excitation energy is directly transferred, to a certain extent, to the ZnChl rod antenna and not via NDI_{NN} to the ZnChl rod antenna. The bigger spectral overlap of the area of the emission spectrum of NDI_{NN} with the absorption spectrum of the ZnChl rod resulted in a more efficient RET process compared to NDI_{NO} with a smaller spectral overlap.

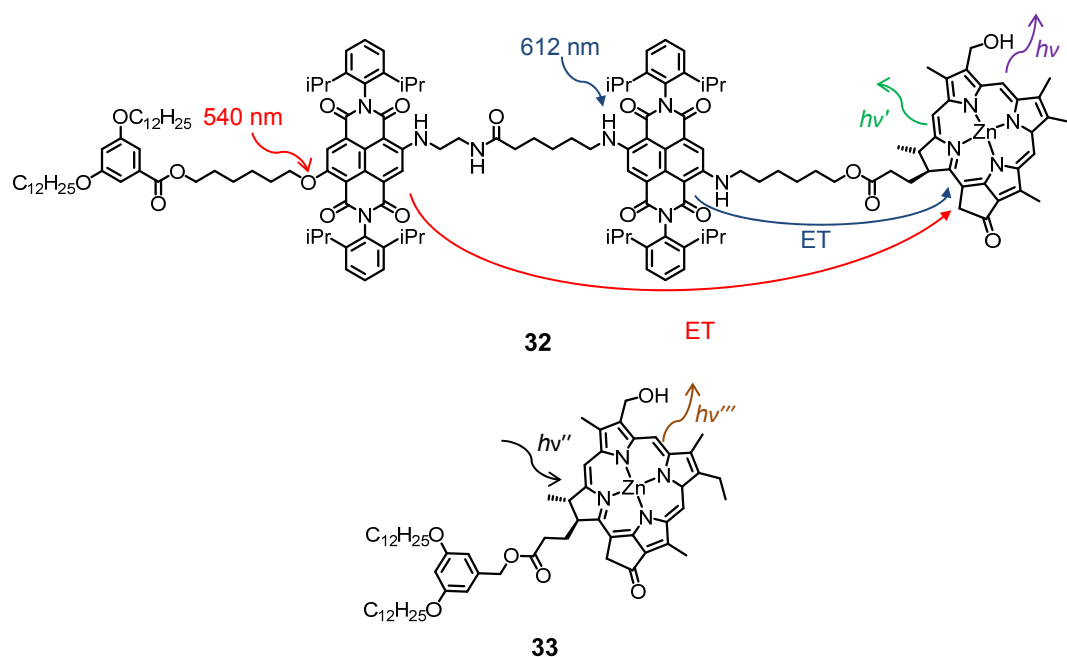


Figure 21 Structural formula of triad ZnChl-NDI_{NN}-NDI_{NO} **32** for studying selective intramolecular RET processes, and the parent ZnChl **33** as a comparison for calculating the light-harvesting efficiency.

Previous work in our research group (Figure 22) resulted in novel and unsymmetrical NDI-phanes **34–36** suitable for energy-transfer studies. In particular, Mayor et al.^[75] investigated the influence of the core substituents in the positions 2 and 6 (IUPAC nomenclature: positions 4 and 9) on the RET process efficiency.

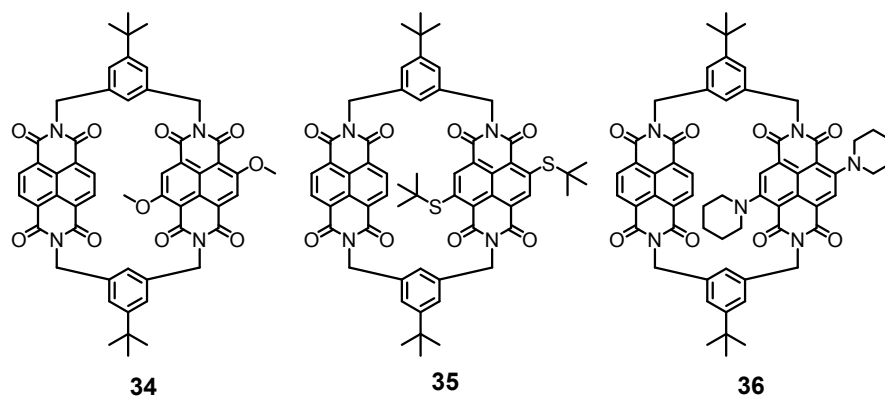


Figure 22 Three investigated NDI-Phanes **33–36**.

Their intramolecular RET studies (Figure 23a–c) revealed that an efficient RET process occurred in the case of a 2,6-dimethoxy-core-substituted NDI **34** (Figure 23a), a less efficient RET process was observed in case of a 2,6-di-*tert*-sulfanyl-core-substituted NDI **35** (Figure 23b), and no RET process was detected in case of a 2,6-dipiperidinyl-core-substituted NDI **36** (Figure 23c). The decreased RET process efficiency was explained by the smaller spectral overlap of the emission and absorption spectra of the donor–acceptor pair in case of **35**, and the missing spectral overlap of the emission and absorption spectra of the donor–acceptor pair in case of **36**. The distance between the

two NDI decks and the positions of the core substituents were the same, therefore, the observed effect was directly attributed to the core substituents.

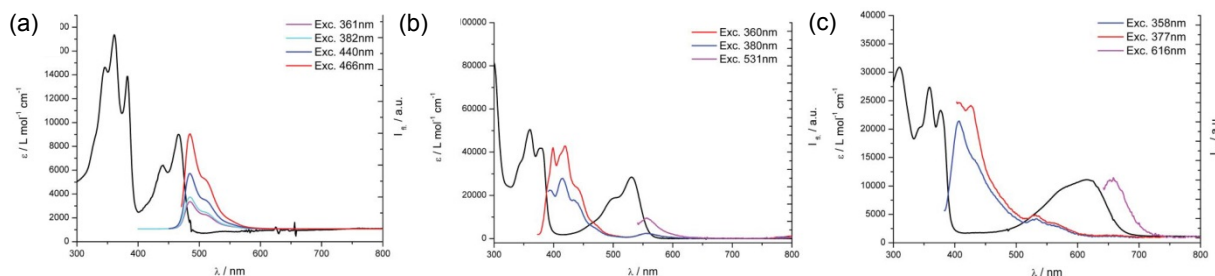


Figure 23 The absorption and emission spectra (black line: absorption spectra; colored lines: emission spectra at specific wavelengths) of: (a) the 2,6-dimethoxy-core-substituted NDI **34**, (b) the 2,6-di-*tert*-butylsulfanyl-core-substituted NDI **35**, and (c) the 2,6-dipiperidinyl-core-substituted NDI **36**. The RET process efficiency decreased in the following order: O > S > N. All pictures are reprinted from Gabutti.^[76]

In 2010, Pugliesi and coworkers^[77] reported the first time-resolved study of the rate of charge-transfer from different sulfanyl core substituents to the NDI moiety. To be more specific, the authors measured the fluorescence-quenching behavior of three different sulfanyl-core-substituted NDIs **37–39** (Figure 24a; Ph–NDI–Ph, Ph corresponds to phenyl, **37**; Bn–NDI–Bn, Bn corresponds to benzyl, **38**; and A–NDI–A, A corresponds to alkyl, **39**) by transient spectroscopy and found an ultrafast and efficient fluorescence quenching if a *tert*-butylphenylsulfanyl unit, such as Ph–NDI–Ph **37**, was used. In case of a benzylsulfanyl unit (Bn–NDI–Bn) **38**, on the contrary, they were not able to detect an ultrafast fluorescence quenching.

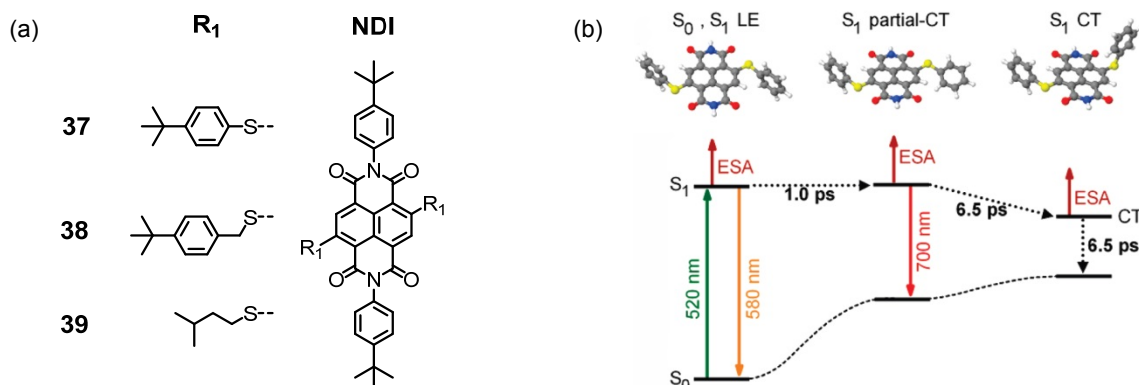


Figure 24 (a) Chemical structures of the investigated compounds: Ph–NDI–Ph **37**, Bn–NDI–Bn **38**, and A–NDI–A **39**; and (b) ab initio calculations of the minimum energy geometries in different states of **37** without terminal substituents, and the occurring charge transfer: (1) planarization of the sulfanyl core substituent after absorption of a photon, (2) partial charge transfer in the optically excited state, and (3) finally a full charge transfer combined with twisting out of the NDI plane. The figure on the right is reprinted with permission from Pugliesi et al.^[77]

A detailed ab initio study (Figure 24b; the *tert*-butyl group of each core substituent and the *tert*-butylphenyl substituent at each *N*-terminus were replaced by hydrogen atoms to reduce computational time) supported their experimental data. The combination of both findings revealed that after a photoinduced excitation an electron was transferred from the phenylsulfanyl substituent

ent (HOMO) to the naphthyl motif (LUMO) in two steps (1) a planarization of the phenylsulfanyl substituent occurred within 1.0 ps and was associated with a partial charge transfer, and (2) a complete charge transfer associated with a twisting of the phenylsulfanyl substituent out of the flat NDI plane took place within 6.5 ps. Finally, the excited molecule relaxed by a back charge-transfer within 6.5 ps through a nonradiatively decay back to the ground state. The lifetime of the excited state was extended in case of Bn–NDI–Bn **38** and, thereby, the slower charge transfer rate led to a detectable fluorescence process.

The authors observed, as displayed in Figure 25, in the evolution of the transient spectra (excitation at 522 nm) of Ph–NDI–Ph **37** and Bn–NDI–Bn **38** the decay of the excited state between 5–20 and 20–100 ps, respectively. Both spectra had the same shape before 0.3 ps and, consequently, indicated that the originally populated electronic states were similar.

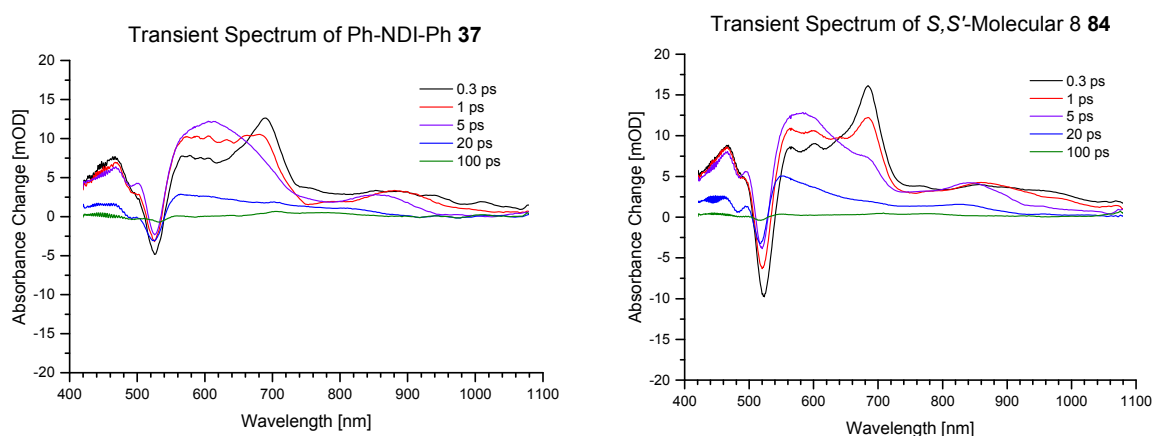


Figure 25 A comparison of the transient-absorption spectra of **37** (left) and **38** (right) displays the decay of the excited CT state between 5–20 ps in case of **37**, and the extended lifetime of the excited CT state in case of **38**. Both transient-absorption spectra were recorded in CHCl_3 at room temperature.

The relaxation dynamics in **37** and **38** were subsequently quantified by the analysis of the temporal evolution of the absorbance changes using a rate model, and revealed a single-exponential decay in case of **38** with a time constant of 36 ps. Neither a two-exponential decay nor a third time constant made the fit stable in case of **37**. The instability of the fit could be ascribed to two identical rates. Finally, the authors were able to postulate a stable fit for the measured signal $s(t)$ with the model function, as illustrated in Equation 2, and found a time constant (τ_{kk}) of 6.5 ps for **37**.

$$s(t) = A_e \cdot \exp\left(-\frac{t}{\tau_e}\right) + A_k \cdot \exp\left(-\frac{t}{\tau_{kk}}\right) + A_{k,t} \cdot t \cdot \exp\left(-\frac{t}{\tau_{kk}}\right)$$

Equation 2 A stable fitting model function for the decay of the excited state in **37**: A_e and τ_e are the amplitude and the time constant of the first exponential decay, respectively. A_k and $A_{k,t}$ are the first and second amplitude of the double decay, respectively, with the time constant τ_{kk} .

Furthermore, Pugliesi et al.^[78] were able to demonstrate that in the case of an amino-core-substituted NDI with a hydrogen atom at the amine functionality (N-H), as seen in Figure 26, the first step, namely, the planarization of the core substituent combined with a partial charge transfer, was not necessary. They explained this observation by the already quasi-planar geometry of the core substituent in the ground state on the basis of hydrogen bonding between the hydrogen atom of the amine functionality with the oxygen atom of the carbonyl functionality (highlighted with the yellow circle). As a consequence, the optically excited state, as seen in Figure 26a, possessed from the very beginning a quasi-planar geometry and a partial charge transfer occurred without changing the conformation. In the second step, as illustrated in Figure 24b, of this process, the amino core substituent twisted out of the NDI plane, and a full charge transfer occurred. The authors measured a similar timescale of this process like in case of **37**.

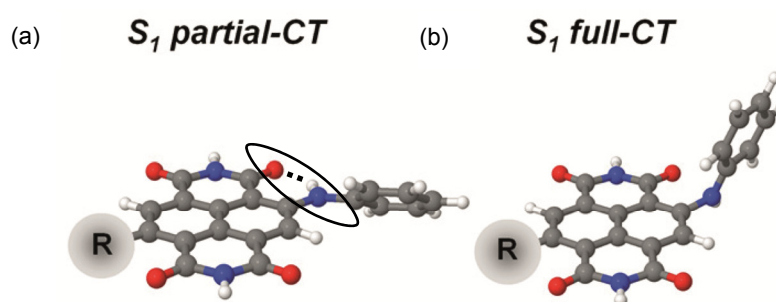


Figure 26 Different calculated minimum energy geometries in different states: (a) in the optical excited state the arylamine core substituent has already a quasi-planar conformation caused by hydrogen bonding (highlighted with the yellow circle), and a partial charge transfer occurs, and (b) in the full charge transfer state a full charge transfer occurred. Reprinted with permission from Pugliesi et al.^[78]

All these presented studies are examples of the charge-transfer process in cNDIs from the core substituents to the naphthyl moiety. There are also examples of the charge-transfer process from the imide substituents to the naphthyl moiety in NDIs^[79] and cNDIs.^[80,81,82] Such examples are not in the scope of this doctoral thesis because the objectives of this doctoral thesis are focused on the photoinduced charge transfer from the core substituents to the naphthalene chromophore.

1.4 Molecular Electronics

The aim of this chapter is to explain the current problem with electronic circuits and, consequently, give possible solutions to solve the problem. In a next step, two techniques in the field of scanning probe microscopy are introduced and subsequently explained. Followed by the introduction of two break junction setups and closed with the requirements to successfully integrate molecules into such setups.

The ultimate goal in nanotechnology research is the construction of nanoscale electronic circuits and components. The current top-down approach, which makes use of silicon chips, will soon reach its limits of the resolution of the silicon wafers. Beyond this point, silicon chips will become useless due to quantum tunneling effects (the so-called 14 nm resolution limit^[83]). The fact that computing power doubles roughly every two years was first described by Moore^[84] and, therefore, this law is called the Moore's law. A possible way to face this problem and to satisfy the tremendous demand to fabricate smaller, faster, and more powerful computers, is to use other fine materials like SiGe or Ge,^[85] or to replace the current top-down approach by the bottom-up approach. In this approach, the nanoscale electronic circuit can consist of a single molecule or a well-defined assembly of single molecules. Suitable molecules are on demand because they represent the smallest possible and stable unit of such circuits on an atomic level. Over the last decades, researchers have proven that molecular switches can be employed in such a molecular device.

1.4.1 Scanning Probe Microscopy

Scanning tunneling microscopy (STM) technique was patented by Binnig and Rohrer^[86] in 1981 and allowed researchers to image the molecular surface at the atomic level for the first time. To date, STM is a very powerful and important technique. For its discovery, Binnig and Rohrer were awarded with the Nobel Prize in Physics^[87] in 1986. When searching for “*scanning tunneling microscopy*”, around 40000 hits are found on SciFinder[®] as of 9th July 2014.

The probe (organic or inorganic molecule) must be first immobilized on a metallic surface (e.g., copper, silicon, silver, or gold), on a graphene layer, or on a transition metal dichalcogenide layer like MoS₂. In the first case, ultrahigh vacuum (UHV) must be applied due to the rapid oxidability of the metallic surface. However, if graphene or a transition-metal dichalcogenide layer is used instead, the subsequent measurements can be carried out at normal pressure. After the successful deposition of the sample on the surface, a metallic conducting tip (like Pt or W) with a close-to-single atom end is held in near proximity to the immobilized molecule (Figure 27a) and bias is applied. STM is working on the basis of two main major principles,^[88,89] quantum tunneling and piezoelectric effect. The latter one is responsible for a precise (Angstrom-level) position of the tip at a specific height. Through the vacuum gap between the tip and the surface, also referred to as barrier, electrons can pass because of a tunneling (Figure 27a). Tunneling is a quantum mechanical

effect, which is not possible in classical mechanics (particle-like nature), but in quantum mechanics (wave-particle duality) possible. In particular, the wave-like nature of an electron in quantum mechanics makes this process possible. Because an electron with a wave-like property will not end abruptly at a barrier, but taper off quickly. If the barrier is thin enough, the probability function extends to the region on the other side of the barrier. The number of electrons which are able to tunnel through the barrier is decreasing exponentially with the barrier thickness and, therefore, a very narrow gap is mandatory. If a positive bias is applied, the electrons are tunneling from the tip to the surface (empty states) and, vice versa, if a negative bias is applied the electrons are tunneling from the surface (occupied states) to the tip.

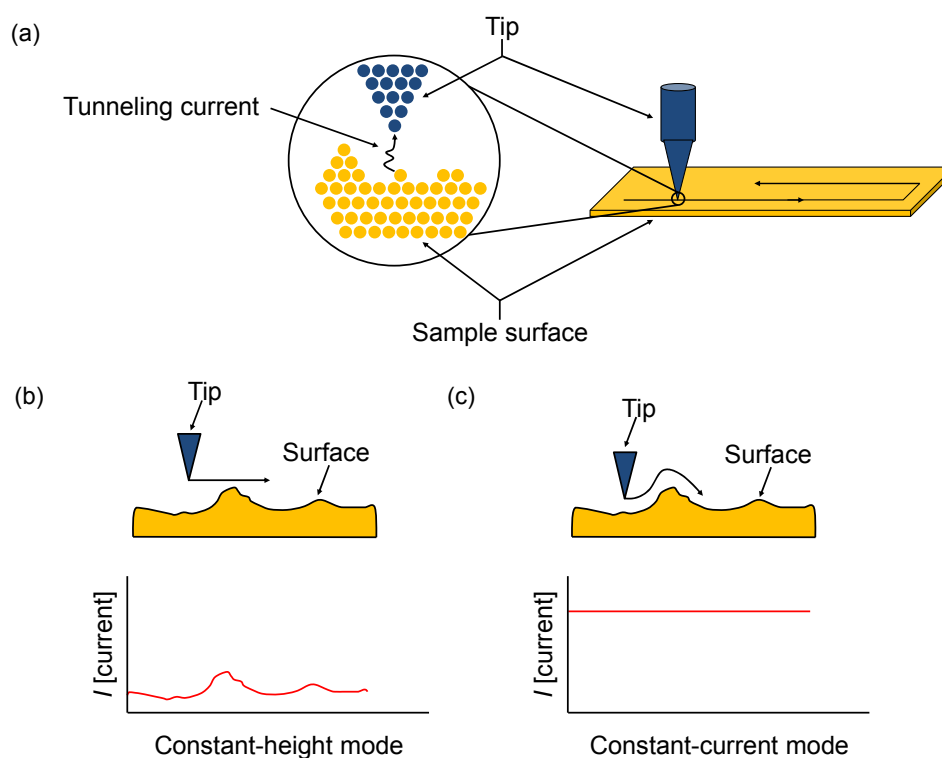


Figure 27 A schematic illustration of a STM setup: (a) magnification of the atomically sharp tip and the occurring tunneling effect, (b) STM operating in constant-height mode, and (c) STM operating in constant-current mode.

STM experiments have either a constant distance between the tip and the surface or a constant current passing from the surface to the tip (Figure 27b–c). In the former mode, the distance of the tip is kept constant throughout the entire experiment. During scanning, current varies in response to the topographic and electronic characteristics of the surface. The constant-distance mode requires a molecule to be flat. This mode is extremely useful to monitor dynamic processes in real-time analysis. In the latter mode, the current is kept constant, which requires a feedback loop to adjust the distance during the measurement. The current is proportional to the electronic states of a flat molecular surface and, therefore, a precise topographic image of the surface is observed. Compared with the constant-distance mode, this method is slower because the tip has to move slowly up and down to adjust the distance.

Another high-resolution imaging technique for measuring the topography of a surface is atomic force microscopy (AFM), which is a result of further development of the STM technique, introduced by Binnig.^[90] An AFM setup,^[91,92] as seen in Figure 28a, consists of a cantilever which is brought into close contact to the surface of investigation. The cantilever, as illustrated in Figure 28b, is made of Si or N_4Si_3 and its tip has a width of just a few nanometers. The narrower the gap between the tip of the cantilever and the surface is, the stronger are the interatomic forces (chemical bonding, London dispersion forces, and electrostatic forces). Stronger forces lead to deflection (Figure 28a; Hooke's law) of the cantilever and are measured by using a laser beam, reflected from the surface of the cantilever into a position-sensitive photodiode (consisting of two side-by-side photodiodes). The difference between the two photodiode signals is detected by a feedback loop and, thereby, indicates the position of the laser and the angular deflection of the cantilever.

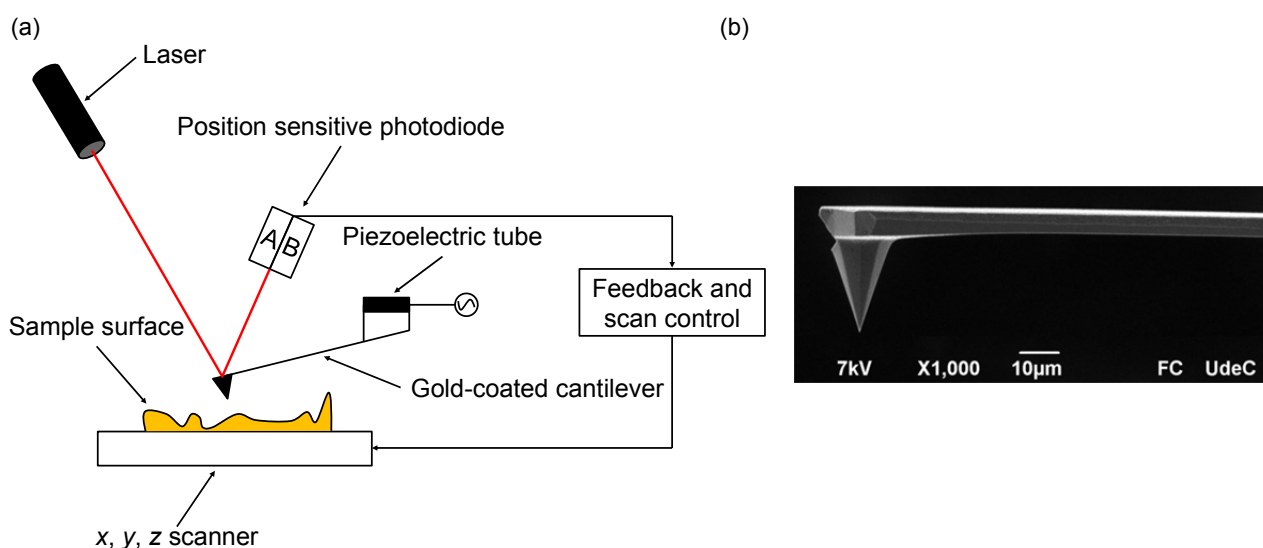


Figure 28 (a) A schematic illustration of an AFM setup, and (b) magnification of the cantilever. The picture on right is taken from the webpage indicated in the literature.^[93]

There are three imaging modes, which an AFM instrument^[92] can be operated with (a) static-contact mode, (b) non-contact mode, and (c) tapping mode. In the static-contact mode, the tip is in direct contact with the sample surface and the observed force is of repulsive nature. This method has a major disadvantage because it damages the sample on the surface. The non-contact mode is a dynamic mode and operates in a close distance (5–10 nm) between the tip and the surface, and in this case attractive forces are important. However, the resolution in this mode is lower than that for the contact mode due to the weaker forces. The tapping mode is also a dynamic mode, and it combines the advantages of the contact and non-contact modes. The resolution is similar to the contact mode but this mode is faster and causes less damage to the surface.

1.4.2 Break Junctions

The discovery of the break junction (BJ) setup is attributed to Ekin and Moreland.^[94] In their original work, they described the study of the electron tunneling phenomenon using a Nb–Sn break junction. Ruitenbeek and Muller^[95] improved and developed this technique further, and introduced also the term mechanically controllable break junction (MCBJ). The mechanically controllable break junction technique is used to study the electronic properties of a single molecule and the occurring charge-transfer process through a molecule. The working principle of the MCBJ technique is the following one. While elongating a metallic wire (e.g., a gold wire) both ends of which are fixed on a flexible substrate, a notch is created, and two fresh facing nanoelectrodes are produced (Figure 29a–c). The gap between these two electrodes can be altered by bending or relaxing of the substrate with a push-rod (z -direction), and reversibly closed and re-opened, if required. This feature is essential because the lifetime of a molecular junction at room temperature is only several minutes.

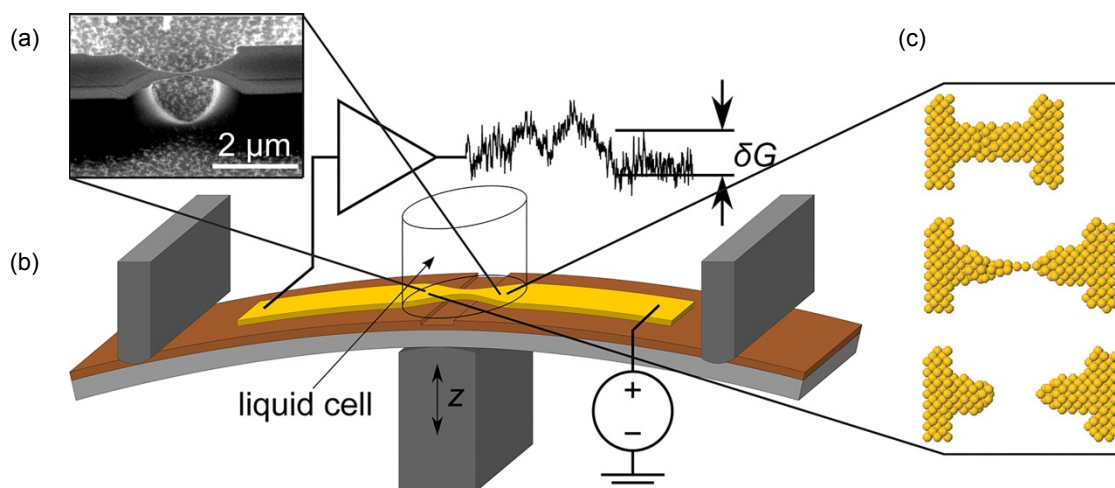


Figure 29 A schematic illustration of a typical MCBJ setup: (a) microscopic view of the wire at the breaking point, (b) the whole MCBJ setup at a macroscopic scale, and (c) illustration of the elongation of a gold wire at the atomic scale. Pictures on the left are reprinted from Brunner^[96] and the picture on the right is reprinted from Turanský et al.^[97]

Compared to the macroscopic scale where Ohm's law, as seen in Equation 3, is valid, the electrical conductance of a quantum conductor, as displayed in Equation 4, must be expressed with the Landauer formula.

$$G = \frac{I}{V}$$

Equation 3 Ohm's law: G is the conductance, V is the applied potential, and I is the current.

$$G_0 = \frac{2e^2}{h} = 77.5 \mu\text{S}$$

Equation 4 Landauer formula: G_0 is the conductance quantum, e is the electron charge, and h corresponds to Planck's constant.

At the very beginning of the bending process (Figure 30a, **1**), the measured conductance G is higher than G_0 ($G > G_0$) and at the breaking point (Figure 30a, **2**), the measured conductance G equals G_0 ($G = G_0$). This breaking point, also referred to as quantum point contact (QPC), was first reported independently by Van Weels^[98] and Wharam^[99] in 1988. Finally, the two electrodes are pulled apart (Figure 30a, **3** and **4**) and the measured conductance G is lower than G_0 ($G < G_0$). The conductance value of a single gold atom is set to $G_0 = 1$ and, as result, all conductance values of small molecules are less than G_0 .

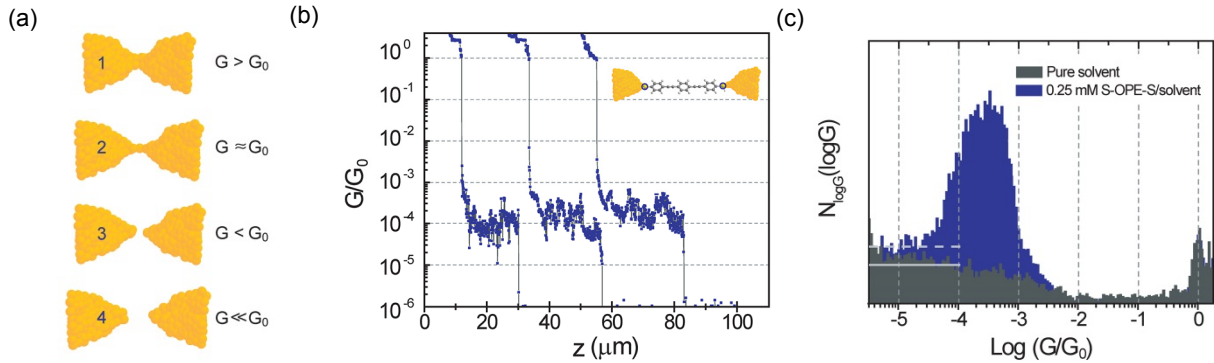


Figure 30 (a) A schematic illustration of the notch formation in a MCBJ setup, (b) three $\log G(z)$ curves with plateaus around $G = 10^{-4} G_0$, and (c) a logarithmic histogram $N_{\log G}(\log G)$ showing no distinct peak in case of pure solvent (black color) and a distinct peak in case of a molecule (purple color; S-OPE-S) bridged between two electrodes. All picture are adapted from Wu.^[100]

The ultimate goal of the MCBJ technique is to integrate a molecule inside the gap such that its two terminal anchoring groups, as discussed in Chapter 1.4.3, are each connected to one of the two electrodes and, thus, forming a bridge. Because such an integration is extremely difficult, hundreds of measurements must be recorded to obtain a statistical data set. After the analysis of the statistical data, the obtained conductance traces are plotted either as a $\log G(z)$ curve (Figure 30b) or as a logarithmic histogram $N_{\log G}(\log G)$ (Figure 30c). The plateau in the $\log G(z)$ curve, as illustrated in Figure 30b, and the distinct peak in the logarithmic histogram $N_{\log G}(\log G)$, as seen in Figure 30c, correspond to the measured conductance G of the bridging molecule.

The two main advantages of the MCBJ technique are (a) the high mechanical stability of the system towards mechanical vibrations because the electrodes are rigidly fixed to the substrate at a very short distance, and (b) the fresh preparation of the electrodes throughout the entire experiment reduces the probability of contamination.

The two main disadvantages of the MCBJ technique, however, are (1) the ability to measure only in one direction, and (2) the exact shape of the two electrodes is always unknown because of the uncontrollable details of the breaking process.

In contrast to the previous section where the charge transport in MCBJ under an applied bias voltage is discussed, in this section the photoinduced charge transport in molecular junctions is described.

A further development of the MCBJ is the squeezable break junction (SBJ), which can be used under ambient conditions at room temperature, first described by Hansma and coworkers^[101] in 1983 and further developed by Selzer et al.^[102] in 2013. The SBJ setup (Figure 31) consists of two glass slides and on each of these slides a gold electrode is deposited by evaporation. By applying mechanically controlled squeezing force against the top slide, the initial gap decreases and the electrodes are getting closer and closer to each other. The squeezing force is applied until the upper slide is in contact with the lower slide. If a molecule is in the junction, the conductance of the molecule is measured while the applied squeezing force is slowly released.

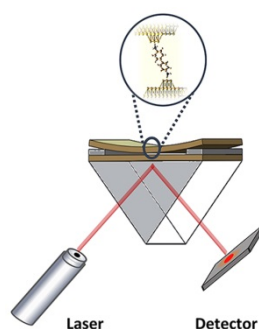


Figure 31 A schematic overview of the squeezable break junction setup. Reprinted with permission from Selzer and coworkers.^[102]

In the MCBJ and STM setup the configuration and geometry of the electrode changes, therefore it is impossible to obtain a plasmonic resonance curve. The SBJ technique, however, allows one to focus light with a laser beam and excite plasmons with a better precision and, therefore, more precisely tune the plasmonic resonance. This is accomplished by using a prism in a diminished total reflection configuration, also referred to as Kretschmann Configuration (for further reading, see literature^[103,104,105]).

In conclusion, the SBJ technique offers new possibilities to measure the photoinduced conductance of molecules.

1.4.3 Immobilization of Organic Structures on Surfaces

The immobilization of an organic structure on a surface is accomplished by the introduction of two anchoring groups in the organic structure and is essential for performing the previously mentioned techniques, such as MCBJ and SBJ. Ideal anchoring groups (e.g., $-\text{CN}$, $-\text{CO}_2\text{H}$, $-\text{NC}$, $-\text{NH}_2$, and $-\text{SH}$) must have a strong binding affinity to the surface (noble metal) and no or low charge-injection barrier. The charge-injection barrier^[106,107,108] (hole transport) is the energy difference between the Fermi-level of the gold electrode and the transport level (HOMO or LUMO) of the immobilized anchoring group. Whether, the hole transport goes through the HOMO or the LUMO state of the anchoring group is determined by the smaller energy gap of one of these two states with the Fermi-Level of the gold electrode. The sulfur ($-\text{SH}$) anchoring group was the first to be investigated^[109,110] and is still the most widely^[109,111] used anchoring group for break junctions and other techniques. For surface immobilization this anchoring has two main drawbacks (a) large variability in S–Au binding geometries, which causes multiple or/and broadened conductance traces;^[112] and (b) the oxidative disulfide formation, which causes polymerization in case of a bifunctional molecule or dimerization in case of a monofunctional molecule.

Taniguchi et al.^[107] found that selenium (0.9 eV) has a lower density of state than sulfur (1.2 eV) and, consequently, they measured a lower injection barrier for selenium than for sulfur. Selenium, however, is not the anchoring group of choice due to its toxicity. Moreover, they demonstrated that tellur forms an oxide and is therefore not suitable as an anchoring group.

Non-covalent binding of sulfur to a gold surface will result in a density of state of approximately 0.5 eV^[113] and a covalent binding of 1.2 eV,^[107] as above-mentioned. The latter binding mode is the major type of binding in sulfur–gold immobilization.

Tao and coworkers^[111] showed that the conductance of anchoring groups decreases in the following order: $-\text{SH} > -\text{NH}_2 > -\text{CO}_2\text{H}$. They attributed this outcome to the different electronic coupling efficiencies between the molecule and the electrode. Wandlowski and coworkers^[114] were studying the binding efficiency of 4,4'-disubstituted OPE ($p\text{-(X)-C}_6\text{H}_4\text{-HCCH-C}_6\text{H}_4\text{-}p\text{-(X)}$) derivatives bearing different anchoring groups ($-\text{SH}$, $-\text{NH}_2$, $-\text{CN}$, and $-\text{Py}$) by performing conductance experiments using MCBJs and STM-BJs techniques. The authors found the following tendency of decreasing stability: $-\text{Py} > -\text{SH} > -\text{NH}_2 > -\text{CN}$. The charge transport through the $-\text{CN}$ and $-\text{Py}$ anchoring groups occurs primarily through the LUMO^[115,116] and for $-\text{SH}$ and $-\text{NH}_2$ groups through the HOMO.^[117,118,119] Additionally, the length of the molecule^[120,121] (dithiol–alkane, oligothiophene, etc.), the conjugation (OPV)^[121] vs. oligo(p -phenylene ethynylene) (OPE)^[122], the topological connection^[123] (*ortho*, *meta*, and *para*) of the molecule, and the torsion angle^[124,125] (e.g., in biphenyl systems) have an influence on the conductance.

To conclude, the sulfur anchoring group is the most suitable one for the covalent binding of an anchoring group to gold and, thus, the most widely used one for conductance experiments.

1.5 Photoswitchable Phanes as Molecular Switches

The aim of this chapter is to provide an insight into the research topic of molecular switches and, therefore, the term is first explained. In a second step, two examples of photochromic molecular switches, namely, stilbene and azobenzene are described in detail. Therefore, the history, the synthesis, the properties, the isomerization mechanism, and their successful integration into various highly-strained phanes are described. The chapter is closed by the brief introduction of a third class of photochromic molecular switches, namely, dithienylethene.

In general, a molecular switch is a molecule that can exist in two or more different states and can be reversibly switched between these states as a response to external stimulus, such as biological impulse, pH, electrical current, light, or temperature. The class of molecular switches can be further divided into subclasses based on the nature of their switching mechanism. The main subclasses are host-guest molecular switches (e.g., crown ether switches^[126,127,128,129,130]), mechanically interlocked switches^[131] (e.g., Vögtle's^[132] photoswitchable catenane or Kaifer and Stoddart's^[133] molecular shuttle), nanoparticle switches (e.g., Zheludev's^[134] bistable Ga nanoparticles or Barth's^[135] porphyrin switch, which is the smallest possible atomistic switching unit to date), and photochromic molecular switches. The latter class (Figure 32) can bear the following motifs (a) diarylethene (stilbene), (b) diphenyldiazene (azobenzene), (c) dithienylethene, and (d) spiropyran, to name a few.

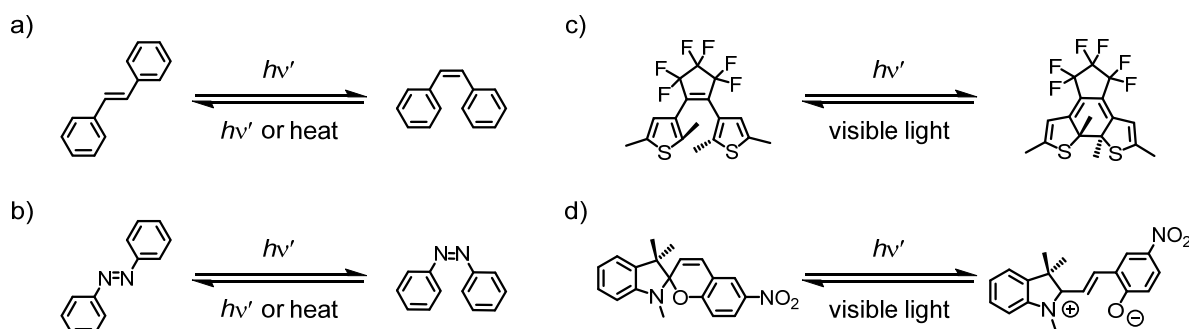


Figure 32 Four examples of photochromic molecular switches.

The first two examples in Figure 32 can exist as (*E*)- or as (*Z*)-isomer. In these systems, the *E* → *Z* isomerization process can be achieved upon irradiation with UV light and the reverse process (*Z* → *E*) either by irradiation with visible light or thermally in the dark. For a potential photochromic molecular switch to be useful, certain criteria must be fulfilled:

- the two states must have different properties
- the conversion between the two states must be efficient and selective upon irradiation with monochromatic light
- a high conversion must be obtained during a very short irradiation time
- the molecule must have a fast response time

- (e) the molecule should not show thermal isomerization between the two states and, therefore, allowing long-term storage of information
- (f) the switching process between the two states must be reversible over many cycles
- (g) upon irradiation of the switching unit with UV light the molecular backbone must be chemical inert

1.5.1 History, Properties, and Isomerization Process Mechanisms of Stilbene

The name *stilbene* is derived from the Greek word *stilbos*, which means *shining*. Stilbene belongs to the class of *diarylethene*, which has two aromatic moieties connected to each other by a C=C bond, and exists (Figure 33) in the form of two isomers, (*E*)-1,2-diphenylethylene (*E*)-**40**, also referred to as (*E*)-stilbene, and (*Z*)-1,2-diphenylethylene (*Z*)-**40**, also referred to as (*Z*)-stilbene. It is remarkable how the change of geometry influences the physical properties of the two isomers. The (*E*)-isomer is planar, sterically not hindered, and can, as a consequence, interact with itself or other molecules via π - π interactions. The (*Z*)-isomer, on the contrary, has an angular geometry and, as a result, is less stable. The decreased stability is reflected in the much lower melting point of (*Z*)-stilbene (5–6 °C)^[136] compared to the high melting point of (*E*)-stilbene (123–125 °C).^[137] The name 1,2-diphenylethylene as well as stilbene are valid and are fully accepted in the scientific community. The stilbene motif^[138] can be found in various molecules for applications, such as industrial dyes, optical brighteners, dye lasers, or even in plants as stilbenoids. In 1865, Märcker^[139] succeeded in the synthesis of (*E*)-**40** and in 1095, Straus^[140] reported the successful synthesis of (*Z*)-**40** by the reduction of 2-phenylethynylbenzene with a copper–zinc couple. The first photochemical *E* \rightarrow *Z* isomerization process was accomplished by Stroemer^[141] in 1909.

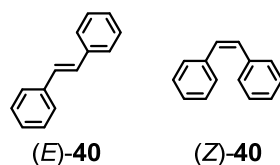


Figure 33 Two isomers of stilbene, (*E*)-**40** and (*Z*)-**40**.

The intensity of the transition band maximum^[142] of (*E*)-**40** at 294 nm is generally higher than that of the transition band maximum^[143] of (*Z*)-**40** at 276 nm. The lower intensity of the transition band maximum in (*Z*)-**40** can be ascribed to steric hindrance of the *ortho* sites of the phenyl moieties and, as a consequence, the phenyl rings are slightly twisted out of the coplanarity. The *E* \rightarrow *Z* isomerization process has a conversion of 54%, whereas the *Z* \rightarrow *E* isomerization process has a conversion of 35%, but it is more troublesome to accomplish.^[144] In general, the photochemical isomerization process happens normally with moderate conversion, meaning the system reaches its equilibrium, also referred to as photostationary state (PSS), which is dependent on (a) the photosensitizer,^[145] (b) the presence of molecular oxygen,^[146] and (c) the geometry of the molecular back-

bone.^[147,148] The $Z \rightarrow E$ isomerization process is more efficient with a triplet photosensitizer (e.g., acetophenone, benzophenone, benzil, to name a few) than upon direct UV light irradiation. A photosensitizer is a molecule, which can initiate a photochemical reaction upon (a) a fast excitation; (b) a subsequent ISC transition to a triplet state; (c) a following collision of the triplet-state photosensitizer with a substrate molecule and, thereby, transfer the exothermic energy and exchange spins; and (d) the photosensitizer finally returns to its ground state and, simultaneously, a triplet state substrate molecule is generated. A triplet photosensitizer is often mandatory because the short-lived singlet-state stilbene has a high probability to return directly back to the ground state without a geometry transformation, whereas the long-lived triplet-state stilbene has more time and, therefore, a higher probability to convert its geometry from $Z \rightarrow E$. Additionally, the singlet state is high in energy and can initiate side reactions. To prevent these side reactions, a photosensitizer (which has a large $S_0 \rightarrow T_1$ excitation energy) can be used because it absorbs at longer wavelengths. In conclusion, the photochemical $Z \rightarrow E$ isomerization of stilbene can either be achieved upon direct irradiation with UV light at the $\pi \rightarrow \pi^*$ transition band wavelength at 294 nm for (*Z*)-**40** or by the use of a triplet photosensitizer.

Hochstrasser et al.^[144] postulated an energy diagram, as illustrated in Figure 34, for the photochemical $Z \rightarrow E$ isomerization process and the possible side reactions which can occur on the basis of the direct excitation into the S_1 state in the gas phase.

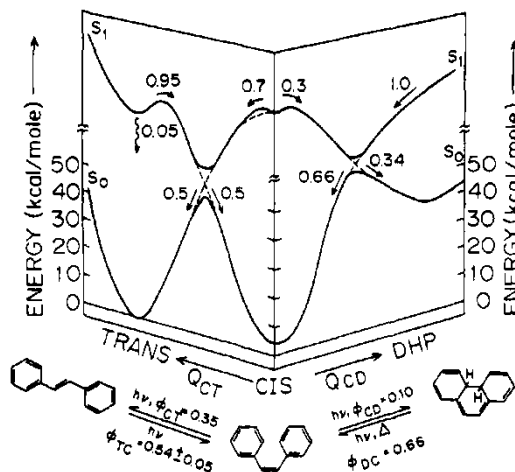
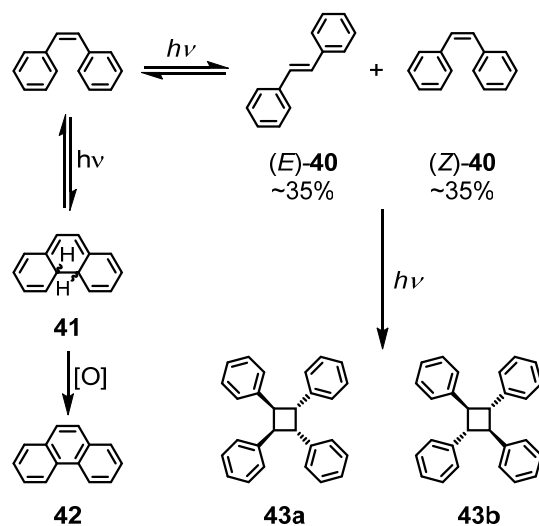


Figure 34 Energy diagram for the photochemical $Z \rightarrow E$ isomerization reaction and the occurring side reactions. Reprinted with permission from Hochstrasser et al.^[144]

The most important findings of the energy diagram in Figure 34 are summarized in the following list:

- The energy barrier (43 kcal/mol) of the photoexcited state must be overcome. Thermal energy in form of heating for the isomerization would require temperatures above 200 °C and the molecule will most probably decompose at this elevated temperature.
- (*Z*)-**40** is 6 kcal/mol less stable than (*E*)-**40**.

- (c) From the (*E*)- S_1 state only 70% of the molecules can relax to the lower-energy twisted S_1 state, which is the transition state. This implies a maximum PSS of 35% for the isomerization of (*Z*)-**40**.
- (d) The remaining 30% will undergo a reversible intramolecular 6π -electrocyclization reaction (Scheme 5) to form an isomeric mixture of 4a,4b-dihydrophenanthrene (DHP) **41** in the S_1 state. Molecules occupying this state either relax to the ground state of DHP (34% of 30%) or the reverse reaction to (*Z*)-**40** (66% of 30%) takes place.
- (e) The isomeric mixture of 4a,4b-dihydrophenanthrene in the S_1 state (Scheme 5) can also be converted slowly but irreversible, through a photooxidative reaction in the presence of an oxidant (such as oxygen or iodine) and a subsequent relaxation (Scheme 5) to the ground-state phenanthrene **42**. Generally, the maximum quantum yield of the photocyclization of (*E*)-**40** to give **42** is 10%. The yield of this reaction is strongly concentration dependent: low concentration ($< 10^{-2}$ M) will disfavor the photodimerization reaction and in the presence of an oxidant **42** can be obtained in high yields.
- (f) The last but very slow reaction is the formation of the stereoisomeric mixture of stilbene dimer, namely, 1,2,3,4-tetraphenylcyclobutane **43a** and **43b** (Scheme 5). **43a** and **43b** are formed by a bimolecular reaction between (*E*)-**40** or (*Z*)-**40** in the electronically excited state S_1 and (*E*)-**40** or (*Z*)-**40** in the ground state S_0 . The yield of this photodimerization reaction is even at high concentration ($< 10^{-1}$ M) inefficient because it competes with the $Z \rightarrow E$ photoisomerization reaction.^[147]



Scheme 5 The side reaction during the photochemical $Z \rightarrow E$ isomerization process.

The two most important mechanisms for the geometric $E \rightarrow Z$ isomerization process (Figure 35) are well described in literature.^[138,149,150,151,152,153,154] (*E*)-**40** has to rotate around the C=C bond (colored in brown), also referred to as one-bond-flip^[155,156] (OBF) mechanism (Figure 35a), to adapt the (*Z*)-conformation. In 1985, Liu and Asato^[157] reported a volume-conserving mechanism, namely,

the hula-twist (HT).^[158,157] The HT mechanism (Figure 35b) occurs in a constrained environment and consists of a concerted rotation of a small C–H moiety (colored in red) about the double bond and an adjacent single bond (both colored in brown). The HT mechanism is disfavored in an unconstrained environment and most probably the OBF mechanism occurs.^[158]

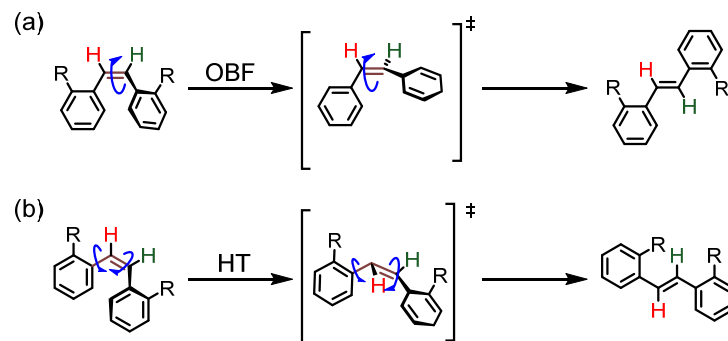


Figure 35 Schematic illustration of the two photochemical $Z \rightarrow E$ isomerization mechanisms in stilbene: (a) the OBF mechanism involves a rotation around a C=C bond (colored in brown), and (b) the HT mechanism consists of a concerted rotation of a small C–H moiety (colored in red) about the double bond and an adjacent single bond (both colored in brown).

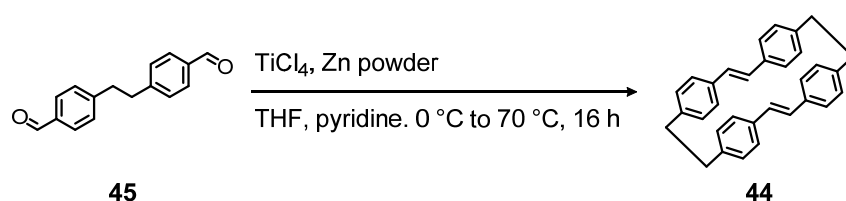
A third isomerization mechanism is possible in polyenes, also referred to as bicycle-pedal^[159,160,161] (BP) mechanism. In 1976, Warshel^[161] reported his work on the BP mechanism. The HT mechanism, however, seems to be more likely to occur than the BP mechanism in the photoisomerization process of biologically important polyenes like calciferol^[162] and rhodopsin.^[160] The BP mechanism does not occur in stilbene moieties and, as a consequence, this mechanism will not be further discussed within this doctoral thesis.

1.5.2 Stilbene Motifs in Highly-Strained Phanes

For the syntheses of stilbene derivatives, the most important methods for the C=C bond formations are:

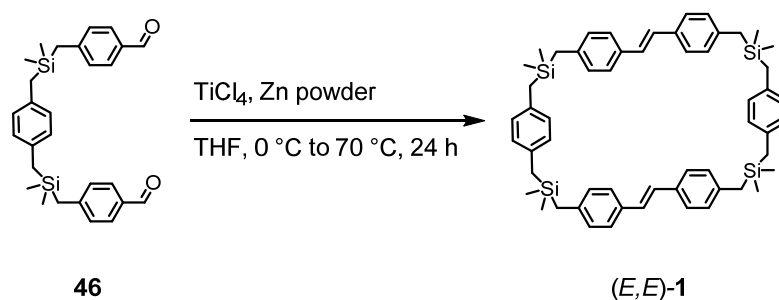
- (a) Aldol-type condensation^[163]
- (b) Barton-Kellogg-Staudinger reaction^[164,165,166]
- (c) Cross-metathesis (CM) with Grubbs' catalyst^[167,70]
- (d) Heck reaction^[168,169,170]
- (e) Negishi–Stille coupling^[171,172]
- (f) McMurry reaction^[173,147]
- (g) Perkin reaction^[174,175]
- (h) Reduction of triple bonds^[176]
- (i) Wittig^[177,178] reaction
- (j) Horner-Wadsworth-Emmons^[179,180,181] (HWE) reaction

Although, there are a lot of synthetic protocols available to create a C=C bond in stilbene derivatives via C=C bond formation, there are only a few examples in literature, where researchers were able to integrate the stilbene motif into a photoswitchable stilbenophane. In 1981, Wennerström et al.^[178] synthesized (*E*)-[2.2](4,4')stilbenophane **44** (Scheme 6) via an intermolecular McMurry reaction of two equivalents of 4,4'-(ethane-1,2-diyl)dibenzaldehyde (**45**) with low-valent titanium species. They were also able to synthesize (*Z*)-[2.2](4,4')stilbenophane **44** by using the same protocol. Furthermore, they studied the photochemical *E* → *Z* isomerization process^[182] in (*E*)-**44**, but not the intramolecular photodimerization, which is a competing side reaction. The group of Wennerström also succeeded in the integration of multiple stilbene motifs into macromolecular structures, such as (a) 6 stilbene units in case of [2₆]paracyclophene,^[183,184,185] (b) 4 stilbene units in case of [2₄]paracyclophene,^[186] and (c) 3 stilbene units in case of [2₃]paracyclophene.^[187] Additionally, they were able to vary the arene moiety from naphthalene in case of [2.2.2.2]paracyclophanetetraene^[188] to biphenyl in case of [2.2.2.2.2]paracyclophanetetraene,^[189] to name a few examples.



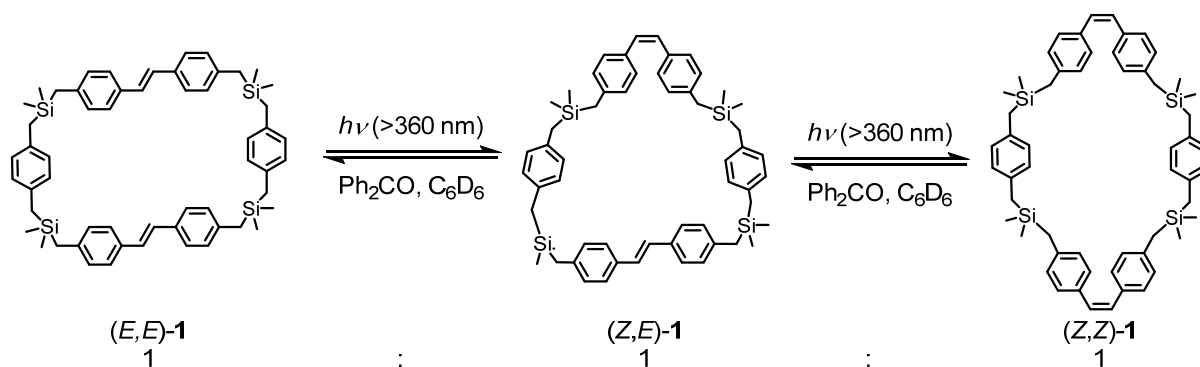
Scheme 6 Synthesis of (*E*)-[2.2](4,4')stilbenophane **44** via an intermolecular McMurry reaction of 4,4'-(ethane-1,2-diyl)dibenzaldehyde (**45**) in 23% yield.

In 2005, Tobita et al.^[147] synthesized, among others, (*E,E*)-**1** (Scheme 7) via an intermolecular McMurry reaction of the bisaldehyde **46**. Subsequently, they irradiated a nuclear magnetic resonance (NMR) sample with light above 360 nm, which contained a 1.17 mM solution of (*E,E*)-**1** in deuterated benzene (C₆D₆) and benzophenone as photosensitizer.



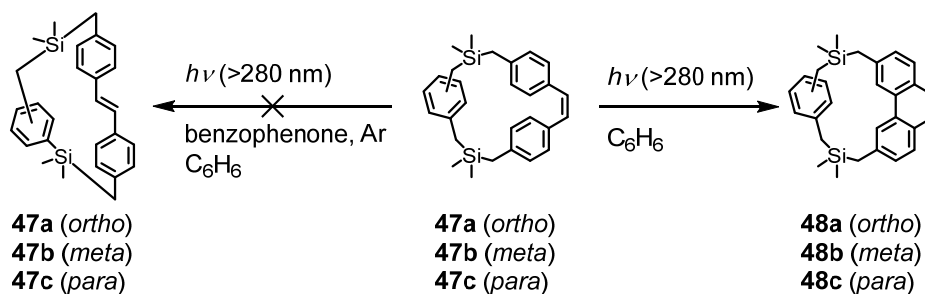
Scheme 7 Synthesis of (*E,E*)-**1** via an intermolecular McMurry reaction of **46** in 14% yield.

After the irradiation for 1 h, they monitored by ¹H-NMR spectroscopy, as seen in Scheme 8, the transformation of (*E,E*)-**1** into two new states. The photostationary state consisted of mixture of (*E,E*)-**1**/(*E,Z*)-**1**/(*Z,Z*)-**1** in a 1:1:1 ratio. The intramolecular dimerization product was prevented due to the use of a photosensitizer.



Scheme 8 The triplet-sensitized photochemical isomerization reaction of $(E,E)\text{-1}$ to yield a PSS mixture of $(E,E)\text{-1}/(E,Z)\text{-1}/(Z,Z)\text{-1}$ in a 1:1:1 ratio. This was achieved by the irradiation of $(E,E)\text{-1}$ with light above 360 nm for 1 h.

In addition, they demonstrated (Scheme 9) that all strained (Z) -stilbenophanes **47a–c** (with *ortho*, *meta*, or *para* substitution pattern on the stilbene benzene rings) did not show any conversion towards the (E) -isomer **47a–c**. They were, however, able to photocyclize them to their corresponding phenanthrenophane derivatives **48a–c**.



Scheme 9 Unsuccessful attempts of the photoisomerization reaction of strained (Z) -stilbenophanes **47a–c** to obtain (E) -stilbenophanes **47a–c**. However, they were able to obtain the phenanthrenophane derivatives **48a–c** in all three cases (**48a**: 12%; **48b**: 43%; **48c**: 43%).

Over the years, different research groups like Medarde et al.^[190] or Darabi et al.^[191] were able to assemble stilbenophanes. The group of Medarde reported the successful synthesis of a stilbenophane analogue of deoxycombretastatin A-4 (Figure 36a) via a McMurry reaction as the final step. Moreover, they also tried to apply a RCM reaction as the final cyclization reaction, but it did not lead to the desired product.

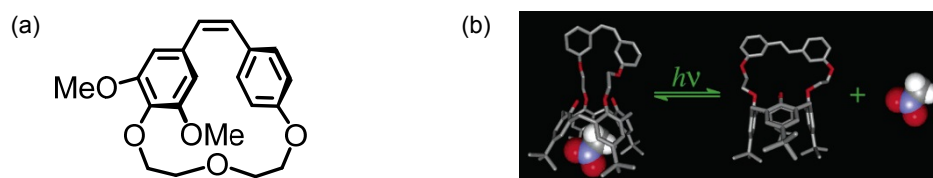


Figure 36 Two examples of stilbenophanes from literature: (a) stilbenophane from Medarde et al., and (b) host-guest system from Sukwattanasinitt et al. Reprinted with permission from Sukwattanasinitt et al.^[192]

The group of Darabi accomplished the synthesis of a cup-shaped (E) -stilbenophane by a final intramolecular McMurry reaction. The cup-shaped stilbenophane showed the ability to complex a silver cation, as a result of the π -acceptor interaction of the alkene groups with the silver cation.

Sukwattanasinitt et al.^[192] demonstrated (Figure 36b) the encapsulation of an electron-deficient guest, namely, nitromethane inside the (*Z*)-isomer of a stilbene-bridged calix[4]arene system, on account of favorable interactions of the guest with the electron-rich cavity of the host. Upon UV light irradiation nitrobenzene was released from the (*E*)-isomer. Additionally, they were able to synthesize derivatives with all four possible substitution patterns (a) *ortho*: 10% yield; (b) *meta*: 85% yield; and (c) *para*: 51% yield.

All the described stilbenophanes were exclusively prepared by an intermolecular McMurry reaction or Wittig reaction in case of Wennerström's stilbenophanes as the final step of the synthetic approach. So far, no examples employing stilbenophanes as the switching unit for molecular electronics are known.

1.5.3 History, Properties, and Isomerization Process Mechanisms of Azobenzene

Another member of the class of photochromic molecular switches is *azobenzene*.^[193] The term *azo* is derived from the French word *azote*, which means *nitrogen*. The IUPAC defines^[194] azobenzene as *diphenyldiazene* but the term azobenzene is still widely used and fully accepted in the chemical community. Diphenyldiazenes are dyes and their derivatives have an orange, red, or yellow color due to the π -extended delocalized system. Nowadays, diphenyldiazene dyes represent approximately 60% of the world production of industrial dyes and are used in all kind of areas, such as food coloring, paints, paper printing, textile dyeing, or as acid–base indicators.^[195,196]

In 1834, Mitscherlich^[197] described the successful synthesis of (*E*)-diphenyldiazene, also referred to as (*E*)-**28**, by reacting nitrobenzene in an ethanolic KOH solution. One century later, Hartley^[198] discovered the photochemical *E* \rightarrow *Z* isomerization process to afford (*Z*)-diphenyldiazene, also referred to as (*Z*)-**28**, by irradiation with light. Two years later, Robertson^[199] confirmed both structures by X-ray diffraction analysis.

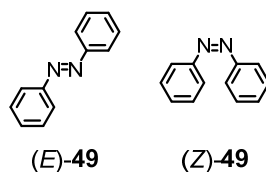


Figure 37 Two isomers, (*E*)-**49** and (*Z*)-**49**, of azobenzene.

The ultraviolet/visible (UV/Vis) absorption spectra (Figure 38) of (*E*)-**49** and (*Z*)-**49** possess two characteristic absorption bands: an intense $\pi \rightarrow \pi^*$ and a much weaker $n \rightarrow \pi^*$ transition band. The $\pi \rightarrow \pi^*$ transition band of (*E*)-**49** is more intense, compared to the $\pi \rightarrow \pi^*$ transition band of (*Z*)-**49**. Whereas, the $n \rightarrow \pi^*$ transition band of (*Z*)-**49** is more intense, compared to the $n \rightarrow \pi^*$ transition band of (*E*)-**49**, which is almost not detectable. The $\pi \rightarrow \pi^*$ transition band is attributed to the azo unit and generally appears in the near UV region (314 nm for (*E*)-**49** and 280 nm for (*Z*)-**49**). The intensity of the $\pi \rightarrow \pi^*$ transition band is significantly weaker for (*Z*)-**49**

than for (*E*)-**49**, which is ascribed to the non-planar geometry of (*Z*)-**49**. The $n \rightarrow \pi^*$ transition band is also attributed to the azo motif (originated from the lone pair of the nitrogen atom) and is observed in the visible region (400 nm for (*E*)-**49** and 430 nm for (*Z*)-**49**). The intensity varies a lot because this transition is symmetry-forbidden for (*E*)-**49** and symmetry-allowed for (*Z*)-**49**, which results in an increased intensity in case of (*Z*)-**49**.

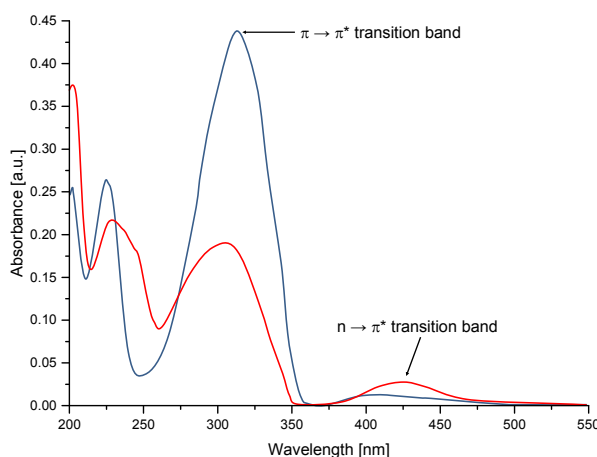


Figure 38 Absorption spectra of (*Z*)-**49** (red line) and (*E*)-**49** (blue line) were recorded in ethanol (EtOH). Adapted from De Maria et al.^[200]

Similarly to stilbene, the *E* → *Z* isomerization process of azobenzene can be achieved upon irradiation with UV light at the $\pi \rightarrow \pi^*$ transition-band wavelength, and the reverse process (*Z* → *E*) either by irradiation with visible light at the $n \rightarrow \pi^*$ transition-band wavelength or thermally in the dark. The energy barrier of the isomerization process is around 23 kcal/mol^[201] and a maximum PSS of 85% for (*Z*)-**49** can be obtained due to the close proximity of the two $\pi \rightarrow \pi^*$ transition bands. This narrow gap causes slow reversion of (*Z*)-**49** to (*E*)-**49**. The steady state depends on the wavelength and the temperature, employed during the irradiation process.^[202] The *E* → *Z* isomerization process occurs usually in the picosecond scale, while the thermal *Z* → *E* back reaction (see Chapter 1.5.4) occurs in the millisecond to days timescale, sometimes years. The energy gap between the $\pi \rightarrow \pi^*$ and $n \rightarrow \pi^*$ transition bands depends on the substituents in the 4 and 4' positions of the azo motif. In this respect, there are three different types,^[203,204] as illustrated in Figure 39, of azo motifs:

- (a) Azobenzene type (Ph–N=N–Ph, **49**): This type is the simplest one and has the above described transition bands. The color of this type of dye is yellow.
- (b) 4-Aminobenzene type (*o*- or *p*-(X)–C₆H₄–N=N–Ph, **50**): X corresponds to an EDG in *ortho* or *para* position. The $\pi \rightarrow \pi^*$ and the $n \rightarrow \pi^*$ transition bands are very close to each other or overlap in the UV/Vis region leading to a shoulder. The color of such dyes is orange, as a result of the red-shift of the two transition bands.

- (c) Pseudo-stilbene type (p -(X)-C₆H₄-N=N-C₆H₄- p -(Y), **51**): X corresponds to an EDG and Y corresponds to an EWG. This configuration results in a push-pull system. The $\pi \rightarrow \pi^*$ and the $n \rightarrow \pi^*$ transition bands appear inversed compared to type 1 meaning the $\pi \rightarrow \pi^*$ causes the red color of these dyes.

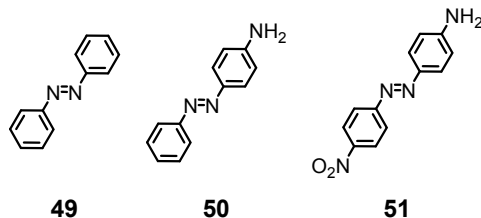


Figure 39 Three different types of azobenzenes **49–51**.

As a consequence of the conformational difference between the (*E*)- and the (*Z*)-isomer, their chemical and physical properties change dramatically, which can be illustrated by an example of (*E*)-**49** and (*Z*)-**49**:

- (*E*)-**49** is ~12 kcal/mol more stable than (*Z*)-**49**.^[205]
- The length of the C–N bond is negligibly shorter (1.41 Å) in (*E*)-**49**, compared to (*Z*)-**49** (1.45 Å).^[199]
- The geometry changes from flat in case of (*E*)-**49** to angular in case of (*Z*)-**49**, because one of the two phenyl rings twists out of the plane to minimize steric repulsion. Therefore, the distance between the two carbon atoms in the positions 4 and 4' of the aromatic rings decreases from 10.0 Å in case of (*E*)-**49** to 5.9 Å in case of (*Z*)-**49** (Figure 40).^[204]
- The dipole moment *D* (*D* corresponds to Debye) increases from 0.0 *D* in the case of (*E*)-**49** to 3.0 *D* in the case of (*Z*)-**49**.^[204]
- The proton signals of the aromatic AB system are upfield shifted in (*Z*)-**49**, compared to (*E*)-**49**. This occurs as a consequence of the anisotropic effect of the π -cloud of the twisted aromatic system.

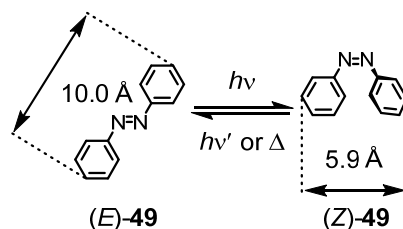


Figure 40 The chemical structure of (*E*)-**49** and (*Z*)-**49**.

Compared to the isomerization of stilbene motifs,^[153, 206] as discussed in Chapter 1.5.1, the exact mechanism of the photochemical isomerization process of azo moieties is still not fully understood and is therefore subject of debate.^[201,207, 206,208,209,210,211,212] The main issue is the presence of the valence electron pair at each nitrogen atom, which has an impact on the mechanistic pathway. Over

the time, two major pathways, as seen in Figure 41, for the photochemical $E \rightarrow Z$ isomerization process have been proposed and are established. One is the rotation mechanism (Figure 41; top) and the other one is the inversion mechanism (Figure 41; bottom). The rotation mechanism, also referred to as OBF mechanism, is similar to the one in stilbene, and involves a $\pi \rightarrow \pi^*$ ($S_0 \rightarrow S_2$) transition leading to a rotation around the N=N bond.

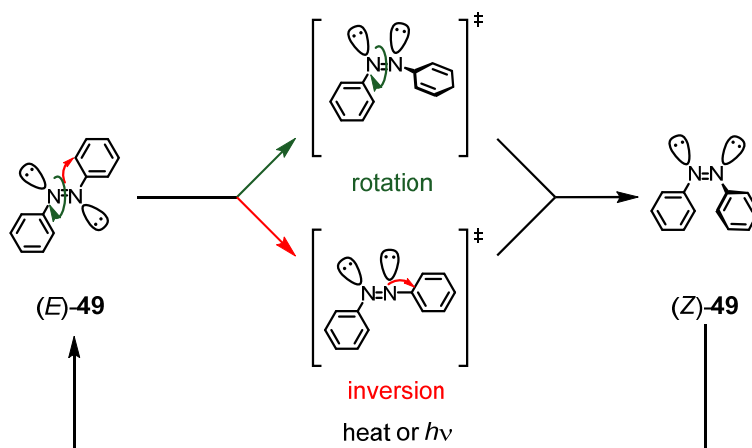
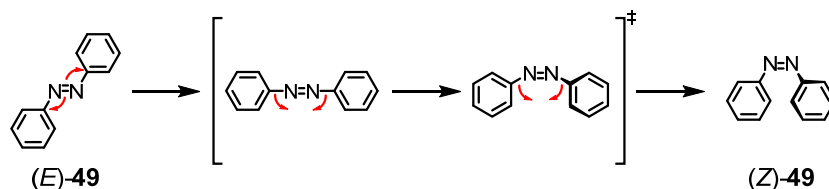


Figure 41 Two possible pathways, rotation (top) and inversion (bottom), for the $E \rightarrow Z$ isomerization process.

The inversion isomerization mechanism involves the lone pairs of both nitrogen atoms and may lead to one $n \rightarrow \pi^*$ ($S_0 \rightarrow S_1$) transition with an inversion at the nitrogen atom (around the N=N–C bond angle). Several parameters, such as the nature of the substituent^[206,209,213] at the aromatic ring, polarity^[206,209] of the solvent and the steric hindrance^[206,210] of the structure determine, which pathway will be favored. The temperature does not influence the efficiency of the $E \rightarrow Z$ isomerization, but significantly decreases the isomerization quantum yield of the reverse reaction, which is 0 at ~ 110 K.^[206] The thermal $Z \rightarrow E$ isomerization reaction occurs via the inversion mechanism which was demonstrated by Rau and Lüddecke^[211] and by Tamaoki and coworkers,^[214] by studying this mechanism in their strained azobenzenophanes which cannot rotate (see Chapter 1.5.4).

Recently, Diau^[215] proposed a new, so-called concerted inversion, photochemical isomerization mechanism, which consists of the simultaneous bend of both C–N=N bond angles (Scheme 10).



Scheme 10 The third mechanism, namely, the concerted inversion mechanism illustrated in (E)-49.

The fatigue resistance factor is for azo compounds high, meaning that the $E \rightarrow Z$ photoisomerization reaction and the reverse $Z \rightarrow E$ isomerization process can occur umpteen times.

1.5.4 Azobenzene Motifs in Highly Strained Phanes

For the syntheses of azobenzene derivatives the most important methods for the N=N bond formations are:

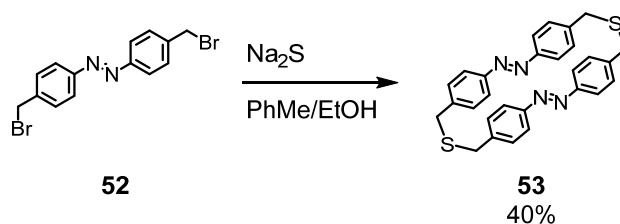
- (a) Electrophilic aromatic substitution reaction of diazonium salts (azo coupling reaction)^[216]
- (b) Mills reaction (condensation of nitrosobenzene with, e.g., aniline)^[217,218,219]
- (c) Oxidative azocoupling (KO^tBu in ^tBuOH/Dimethyl sulfoxide (DMSO) and O₂^[129,220] Pb(OAc)₂ and NEt₃^[221] or NaOCl)^[218]
- (d) Reductive azocoupling (LiAlH₄ in THF;^[222,214,223] Zn/NaOH;^[224] or D/L-glucose in NaOH^[225]
- (e) Pd-catalyzed three-step procedure (1) a Hartwig–Buchwald cross-coupling reaction of an aryl halide with a *N*-Boc protected hydrazine using Cu- or Pd-catalyst, (2) intermolecular Pd-catalyzed cross-coupling reaction yielding a *N*-Boc diaryl hydrazine, and (3) oxidative cleavage of the protective group with a Cu(I) source to yield the desired azobenzene^[226,227,228]
- (f) Schiff base condensation^[229]

Another drawback of azobenzene systems besides the photostationary state is the low stability of the (*Z*)-isomer, which easily isomerizes back to the (*E*)-isomer even at room temperature in the dark. To implement azo motifs as photoswitching unit in macromolecular structures for photochromic molecular switches, several approaches are available to face this problematic issue:

- (a) Stabilization of the (*Z*)-isomer:
 - (1) By the introduction of multiple azo units or introducing strain into the structure (see examples are discussed below).^[230,231,232,233]
 - (2) By the introduction of fluorine atoms in positions *ortho* to the azo moiety.^[234]
- (b) Destabilization of the (*Z*)-isomer:
 - (1) By the introduction of a hydroxyl functionality in the position *ortho* to the azo motif.^[234]

As mentioned in Chapter 1.1.1, there are several strategies to deal with the final intramolecular or intermolecular macrocyclization step either by using the template effect or the high-dilution principle. An additional criterion, which can be taken in account during the final cyclization step, is whether the final target structure bears heteroatoms in the bridging chain or not. If heteroatoms are present in the desired azobenzenophane, one can cyclize two building blocks via a Williamson-type substitution reaction or a condensation reaction, wherein the azo motif is already present in one of the two building blocks. As a result, one building block has to bear a nucleophile and the other one has to bear an electrophile. Benzylic bromide^[235] is the electrophile of choice and, as the nucleophile, amine or thiol^[235] can be used. Examples where a hydroxyl motif is used as nucleophile has not yet been reported in literature.

The first azobenzenophane, as displayed in Scheme 11, was prepared by Rau and Lüddecke^[211] in 1982 by the intermolecular dimerization of 4,4'-di(bromomethyl)azobenzene (**52**) with Na₂S to yield (*E*)-2,19-dithia[3.3](4,4')-diphenyldiazeno(2)phane (**53**) in 40% yield.



Scheme 11 Synthesis of (*E*)-2,19-dithia[3.3](4,4')-diphenyldiazeno(2)phane (**53**) by Rau and Lüddecke.

In their work, Rau et al. demonstrated the conversion of (*E,E*)-**53** through a photoisomerization process to (*Z,Z*)-**53** via (*Z,E*)-**53** and observed a half-life time of 5 days in the dark^[236,211] for (*Z,Z*)-**53**. The aim to prolong the half-life time of the thermally unstable (*Z,Z*)-**53**, resulted in the synthesis of a sterically more hindered azobenzenophane **54**, as seen in Figure 42, which has an improved half-life time of 400 days.^[237] Therefore, this molecule is considered as the first example of an azobenzenophane, where the (*Z,Z*)-isomer is thermodynamically more stable than the (*E,E*)-isomer and, consequently, this azobenzenophane represents a thermally bistable system. Rau's molecule fulfills most of the above-mentioned requirements to be used as an optical storage device, however, it has two drawbacks, namely, the long irradiation time for the photoisomerization process and the instability of both isomers at 313 nm.

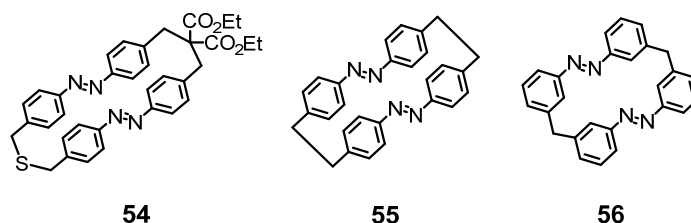


Figure 42 Three different azobenzenophanes **54-56**.

Introduction of strain into a macromolecular structure should in principle help to stabilize the unfavored isomer, but Tamaoki et al. proved the opposite. The authors succeeded in the synthesis of [2.2]parazobenzophane^[214,238,239] **55**, as illustrated in Figure 42, in 0.30% yield and of [1.1]metazobenzophane^[240,241,242] **56**, as seen in Figure 42, in 0.13% yield. The half-life time in the dark of **55** is the same as the one of **49**, namely, 2.6 days.^[214] Compared to the half-life time of **56** with a very high value of 19.7 days.^[240] The prolonged half-life time of **56** is attributed to its lower rigidity compared to **55**. [0.0]Metazobenzophane **57** (Figure 43), also referred to as (*E,E*)-**57**, was first synthesized by Cho et al.,^[227] however, the photochromic properties have not been reported. Tamaoki and coworkers^[243] used this highly strained molecule in their studies and observed a half-life time of 20 days^[243] for (*Z,Z*)-**57**. Therefore, this molecule represents the second example, where the (*Z,Z*)-isomer is the thermally most stable species. The long half-life times of the azobenzenoph-

anes **54** and **57**, both systems can be considered as bistable systems, are caused by the highly distorted (*Z,E*)-isomer and the highly strained (*Z,Z*)-isomer. Within such a system, it is almost impossible to isomerize back to the (*E,E*)-isomer due to the high energy barrier. By changing the biphenyl moiety to a xanthene motif, as seen in (*Z,Z*)-**58** (Figure 43), they were able to beat their own record and increased the half-life time to 6.43 years.^[244,220]

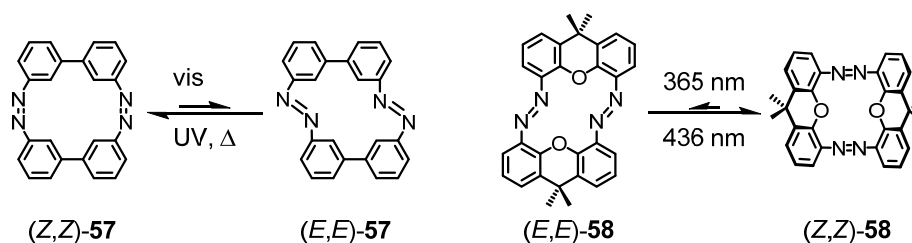


Figure 43 Two examples of azobenzenophanes with very high half-life times for the (*Z,Z*)-isomer.

In contrast to stilbene motifs, azo motifs have found many applications and are used, for example, for the specific ion recognition^[245] (Figure 44), as a molecular hinge,^[220] as a molecular lift,^[246] as a molecular pedal,^[247,248] or as a nanovehicle.^[249,250]

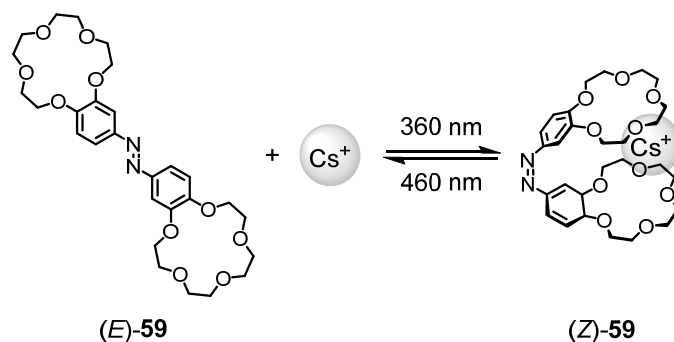


Figure 44 (*E*)-**59** is not able to complex a cesium cation. This behavior changes upon UV light irradiation and isomerization to (*Z*)-**59**, which complex the cesium cation in a sandwich-like structure, and releases it upon irradiation with visible light. The ability of (*Z*)-**59** to remove cations from the aqueous solution decreases in the following order: $\text{Cs}^+ > \text{Rb}^+ > \text{K}^+ > \text{Na}^+$.

A molecular lift is another example of a molecular switch and, therefore, it can be considered as a photooptical storage device.

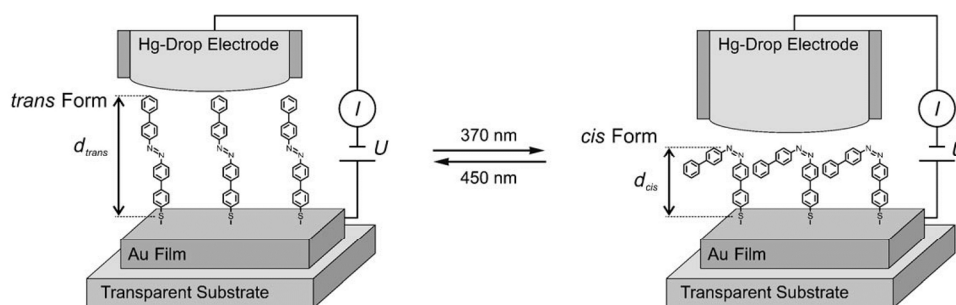


Figure 45 Schematic overview of the experimental setup with different distances between the SAM and the Hg-drop electrode. The experimental setup with the (*E*)-isomer is displayed on the left and with the (*Z*)-isomer on the right. Reprinted with permission from Rampi et al.^[246]

Rampi and coworkers^[246] deposited (*E*)-4'-([1,1'-biphenyl]-4-yl diazenyl)-[1,1'-biphenyl]-4-thiol on a gold surface with the thiol head covalently bonded to the Au(111) substrate (Figure 45) and, thereby, forming a self-assembled monolayer (SAM). The distance between the substrate (SAM_{Azo}) and a mercury drop electrode was subsequently lowered via a photochemical process (*E* → *Z*) upon irradiation with UV light at 370 nm and, vice versa, increased upon irradiation with visible light at 450 nm. The difference in height between the (*E*)- and (*Z*)-isomer is 7 Å, which corresponds to the difference in length between the two geometries. The highly reversible switching mechanism was performed with a 94–100% efficiency.

1.5.5 Dithienylethene—A Third Class of Photochromic Molecular Switches

A third class of photochromic molecular switches is the dithienylethene motif, first reported by Irie et al. This class is considered to be the ideal structure for optoelectronic devices such as optical memories and switches.^[251,252] In general, a dithienylethene motif **60**, as seen in Figure 46, consists of two thiophene rings, which are bridged with an ethene unit in the positions 3 and 3'. The two carbons of the ethene bridge are fused, for example, to a 5- or 6-membered ring with various substitution patterns, to lock the (*Z*) geometry. The positions 4 and 5 of the thiophene moiety can bear a fused aromatic (hetero)cycle or simple aliphatic chains, or even a different molecular backbone. Stability against oxidation is gained by the introduction of methyl groups in the positions 2 and 2' of thiophene and the color in the closed form rises from the extended delocalized π -system of the molecular backbone. The chemical, optical, and physical properties of the two isomers, namely, open form-**61** (which is colorless) and closed form-**61** (which is colored), are very different (Figure 46). The switching mechanism is induced, similarly to the azo and stilbene moiety, with UV light and the reverse reaction is achieved with visible light ($\lambda > 600$ nm).

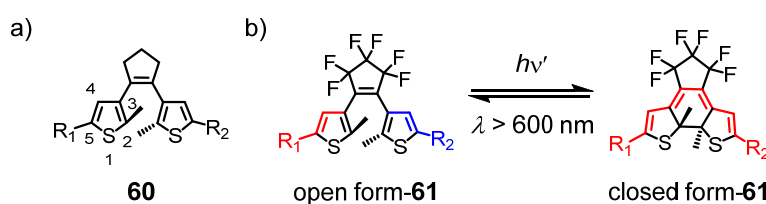


Figure 46 A schematic illustration of: (a) a general chemical structure of a dithienylethene moiety **60**; and (b) an electron transfer is only possible in the closed form-**61** (throughout red), whereas it is impossible in the open form-**61** (indicated by two different colors: the red color corresponds to a possible electron transfer and the blue color to an impossible electron transfer).

The full conjugation can additionally lead to an electron transfer through the molecule, therefore such a system can be, for example, deposited on a gold surface, as demonstrated by Feringa et al.,^[253] or integrated into a MCBJ setup as reported by Feringa and coworkers^[254]. Dithienylethene-containing structures exhibit, likewise to azo compounds, a high fatigue resistance factor.^[255]

However, there is no example known in literature of a dithienylethene-containing phane. Therefore, this subclass of photochromic molecular switch will not be explained in more detail, and for further reading, refer to the literature.^[255,252,251,256,257]

To conclude, owing to the profound research in the field of molecular electronics, fundamental questions and quantum phenomena have been investigated and improved our knowledge on, among others, charge transfers, but still many questions are remain to be answered. Basic applications demonstrated the potential of photochromic molecular switches and, consequently, more research is necessary in this area.

2 Aim of the Work

The work described in this doctoral thesis addresses three objectives. Common themes of all objectives are (a) the backbone of the molecules of interest consists of a chemically inert NDI motif; and (b) upon irradiation a part of the molecule undergoes a transformation, which leads to a reversible change of the molecular geometry. The photoinduced process is studied (1) by fluorescence and transient-absorption spectroscopies, (2) in a break junction setup, or (3) by $^1\text{H-NMR}$ spectroscopy.

Objective 1

To investigate (Figure 47) the influence of the reduced motional freedom of the core substituents in the positions 2 and 6 (IUPAC nomenclature: positions 4 and 9) in a NDI-phanes with two fixed bridges on the photoinduced charge-transfer process. The goal is therefore (a) the design of a collection of three different NDI-phanes, (b) the development of an efficient synthesis of all the members, (c) the investigation of the optical properties of all the members, and (d) the measurement of transient-absorption spectra of all the members.

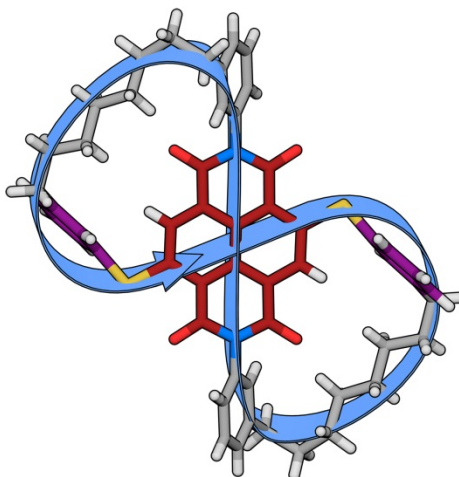


Figure 47 Concept picture of the first objective illustrating the structure of a molecular figure-of-eight.

Objective 2

To probe the photoinduced charge transfer in a linear cNDI integrated into a squeezable break junction setup (Figure 48) and to observe for the first time conductance enhancement on a single-molecule level.

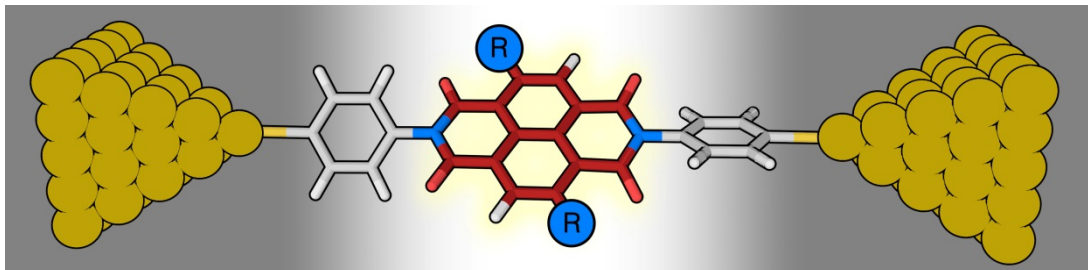


Figure 48 Concept picture of the second objective illustrating the integration of a cNDI into a squeezable break junction setup. R is a short alkyl amino substituent.

The goal is therefore (a) the design of a linear cNDI suitable for this kind of measurements, (b) the development of an efficient synthesis of such a linear cNDI, (c) the investigation of the optical properties of such a linear cNDI, and (d) the conductance measurements of such a linear cNDI in a SBJ setup.

Objective 3

To investigate photoswitchable NDI-phanes (Figure 49) as potential molecular switches. The goal is therefore (a) the design of a photoswitchable NDI-plate, (b) the development of an efficient synthesis of such a NDI-plate, (c) the investigation of the optical properties of such a NDI-plate, (d) the investigation of the photoinduced $E \rightarrow Z$ and $Z \rightarrow E$ isomerization processes in such a NDI-plate, and (e) the deposition of such a NDI-plate on a metallic surface and probe the switching process upon external stimulus.

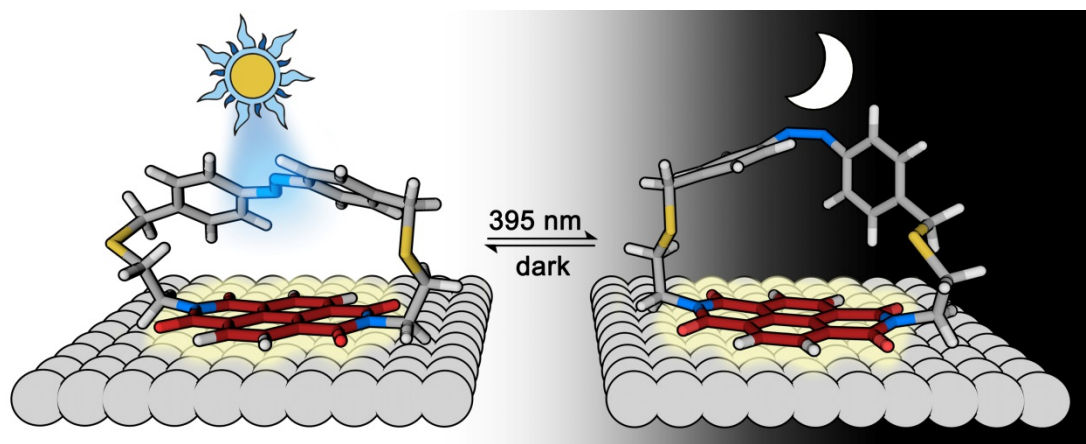


Figure 49 Concept picture of the third objective illustrating a photoswitchable NDI-plate deposited on a surface and its switching process. In this figure, (*E*)-NDI-azobenzenophane (left) is deposited on a silver surface and irradiated with UV light at 395 nm to initiate a photoinduced isomerization process to obtain (*Z*)-NDI-azobenzenophane (right). The reverse reaction occurs in the dark. The two processes are reversible.

3 Synthesis and Properties of Molecular 8 Derivatives

The first objective was to investigate the influence of the reduced motional freedom of the core substituents in the positions 2 and 6 (IUPAC nomenclature: positions 4 and 9) in a NDI-phane (Figure 50a) with two fixed bridges on the photoinduced charge transfer. Therefore, a symmetrical NDI-phane, also referred to as in full *molecular figure-of-eight* and in short *molecular 8*, was designed. In such a NDI derivative by using the IUPAC nomenclature, the phenylsulfanyl substituent in position 4 is bridged with the phenyl substituent in position 7 and the phenylsulfanyl substituent in position 9 is bridged with the phenyl substituent in position 2 and, thereby, forming two loops around the central NDI core. This structure is reminiscent of a figure of eight. The length of the two bridges is designed in such a way that conformational motions are restricted and, thus, leading to a rigid structure.

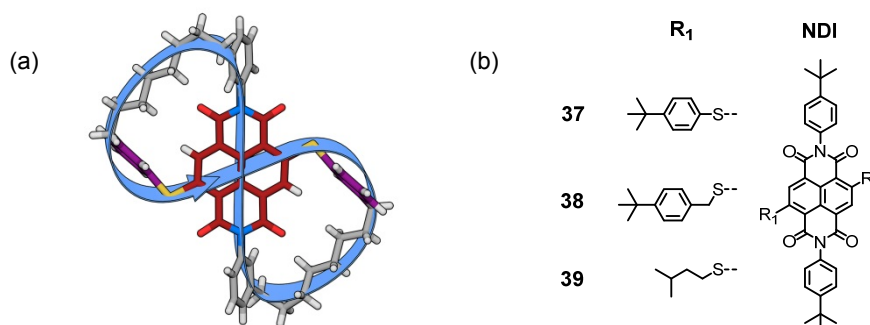


Figure 50 (a) Schematic illustration of a molecular 8 with two fixed bridges and sulfur core substituents in the positions 2 and 6 of the naphthyl core; (b) structures of the model compounds investigated by Pugliesi et al.

This objective is originated from the previous work of Pugliesi et al.,^[77] who reported the first time-resolved study of the rate of charge transfer from sulfanyl core substituents to the NDI motif. In particular, the authors investigated the fluorescence quenching behavior of three symmetrical cNDIs **37–39** bearing different core substituents, as illustrated in Figure 50b (see Chapter 1.3.3), by transient-absorption spectroscopy. In case of a phenylsulfanyl core substituent, they detected an ultrafast fluorescence quenching process. However, in case of a benzylic phenylsulfanyl core substituent, they detect a slower rate of charge transfer and, as a consequence, fluorescence was detected. The quenching process is attributed to conformational changes of the core substituent leading to an electron transfer process. They further supported their proposed mechanism with the help of ab initio calculations.

3.1 General Synthetic Strategy

3.1.1 Molecular Design of Molecular 8 Derivatives

To further probe the postulated quenching mechanism by Pugliesi et al., a collection of NDI-phanes, in which the two phenylsulfanyl substituents are exchanged for phenylamino and phenoxy substituents, were designed. In contrast to the previously studied structures, the phenylsulfanyl core substituent and the phenyl substituent on the imide functionality (Figure 50a) are connected to each other by an aliphatic bridge. As a result, the rotation around the S–C bond of the NDI core substituent in the full-CT state should be restricted. The deceleration of the conformational motion of the core substituent in the full-CT state from a planar orientation to a twisting out of the NDI plane should decrease the fluorescence quenching process and, thereby, an increased FQY should be detected. For the comparison of the obtained FQYs of the molecular 8 derivatives their unbridged derivatives, also referred to as reference compounds, are as well envisioned to be synthesized. Three parameters were considered for the design (Figure 51) of the molecular 8 derivatives:

- The substitution pattern on the two bridged benzene moieties is chosen to be either *meta,meta*, *meta,para*, *para,meta*, or *para,para*.
- The length of the aliphatic bridge is chosen between seven and nine CH₂ repeating units.
- The core substituent heteroatom is chosen to be either oxygen, nitrogen, or sulfur.

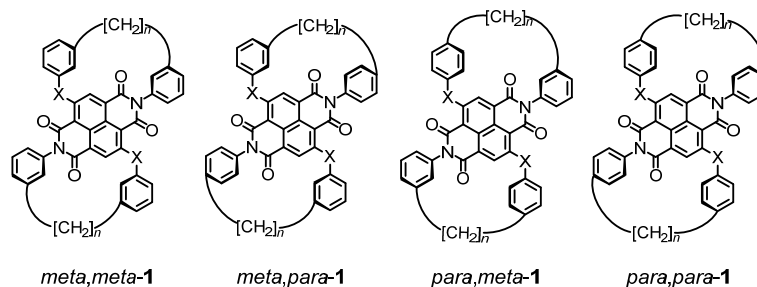


Figure 51 Four possible substitution patterns of the molecular 8. X corresponds to S, NH, or O and $n = 7-9$.

After preliminary studies (Figure 52) a symmetrical *meta,meta*-substitution pattern, two eight-membered aliphatic bridges, and sulfur heteroatoms are chosen.

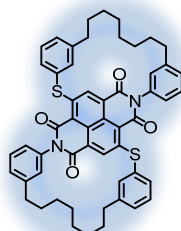


Figure 52 Molecular design of *S,S'*-molecular 8.

A molecular 8 with (a) phenylsulfanyl core substituents is called *S,S'*-molecular 8, (b) phenylamino core substituents is known as *N,N'*-molecular 8, and (c) phenoxy core substituents is denoted by *O,O'*-molecular 8.

3.1.2 Molecular Design of Reference Compounds

The molecular design of the unbridged derivatives **37**, **62**, and **63** is shown in Figure 53. The core substituents and the imide substituents should have in positions 4 and 4', respectively, a *tert*-butyl group to increase the solubility of the pigment. Additionally, at the *para* position the steric influence of the *tert*-butyl group is negligible compared to the *meta* or *ortho* position.

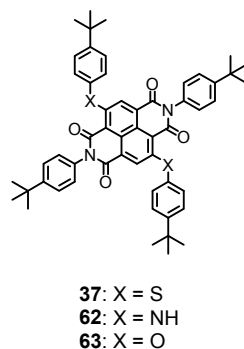
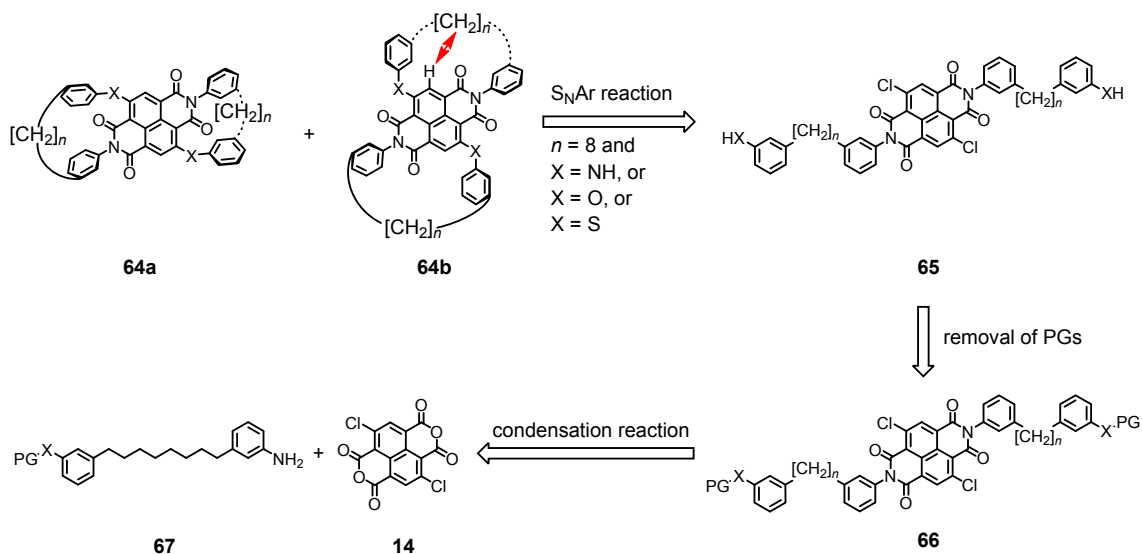


Figure 53 Molecular design of the reference compounds **37**, **62**, and **63**. X corresponds to S, NH, or O.

3.1.3 Retrosynthetic Analysis of Molecular 8 Derivatives

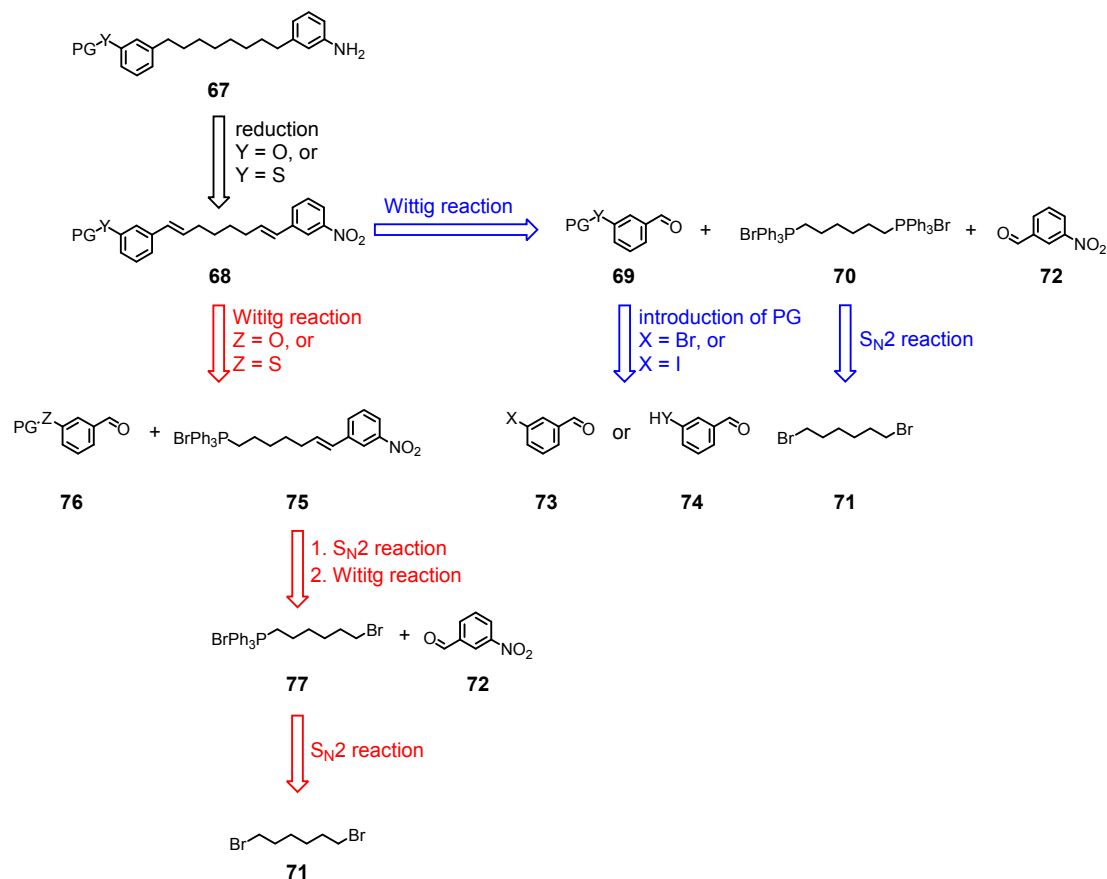
Retrosynthetically, an isomeric mixture of molecular 8 **64a** and **64b** (Scheme 12) can be obtained from an intramolecular nucleophilic aromatic substitution (S_NAr) reaction of linear NDI derivative **65**.



Scheme 12 Retrosynthetic analysis of the synthesis of the isomeric mixture of molecular 8 **64a** and **64b**.

In contrast to isomer **64a**, the aliphatic chain in isomer **64b** is in close proximity to the hydrogen atom of the naphthyl core, which is illustrated by the red up-down arrow in Scheme 12. The linear NDI derivative **65** can be obtained after the cleavage of the protective groups (PGs) in structure **66** and a previous condensation reaction of NDA **14** with the key building block **67**. The asymmetrical key building block **67** containing a protected alcohol motif or a sulfanyl motif can be obtained after applying reductive conditions (Scheme 13) on structure **68**. At this stage, retrosyn-

thetic analysis revealed that there are several methods available (Scheme 13) to afford structure **68**. Structure **68** can be obtained from (a) a Sonogashira cross-coupling reaction route, (b) a Heck cross-coupling reaction type route, (c) a one-pot Wittig reaction pathway, or (d) a stepwise Wittig reaction pathway, to name a few. Here, only the stepwise Wittig reaction (red route) pathway and the one pot Wittig reaction (blue route) pathway are described. The Sonogashira cross-coupling reaction route and the Heck cross-coupling reaction type route are not considered on the basis of the longer linear sequence compared to the routes (c) and (d). The longer linear sequence of each route will ultimately result in a lower overall yield.

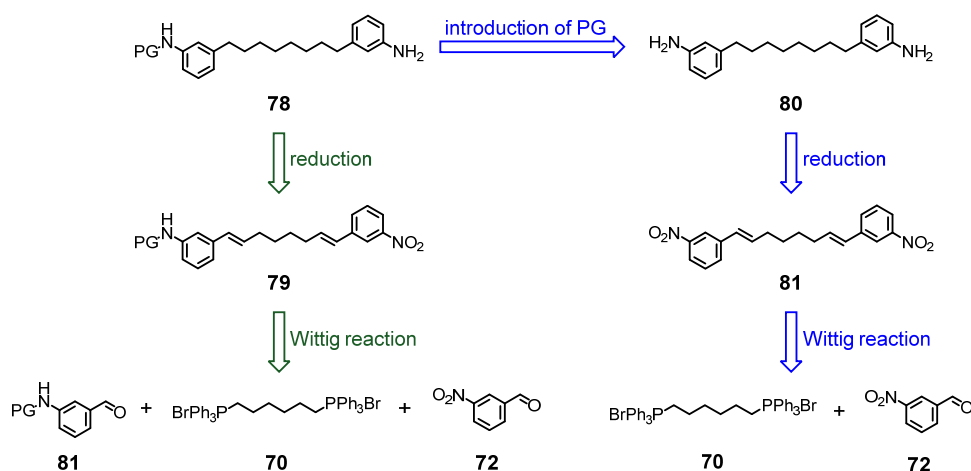


Scheme 13 Retrosynthetic analysis of the synthesis of key building block **67**.

In the one-pot Wittig reaction pathway, the protected benzaldehyde **69**, the corresponding double Wittig ylide **70** of 1,6-dibromohexane (**71**), and 3-nitrobenzaldehyde (**72**) are required. The stepwise Wittig reaction pathway is more selective compared to the one-pot Wittig reaction pathway and, thus, a higher overall yield can be expected. The protected benzaldehyde **69** can be obtained from the successful introduction of an appropriate protective group in structure **73** or **74**. In contrast to that, when a stepwise Wittig approach is applied, structure **68** can be obtained from a single Wittig reaction of Wittig ylide **75** with a protected benzaldehyde **76**. The Wittig ylide **75** can be obtained after a Wittig reaction of mono Wittig ylide **77** with **72** and the subsequent trans-

formation of the Wittig product with triphenylphosphine to the Wittig ylide **75**. The mono Wittig ylide **77** can be obtained after treating **71** with triphenylphosphine.

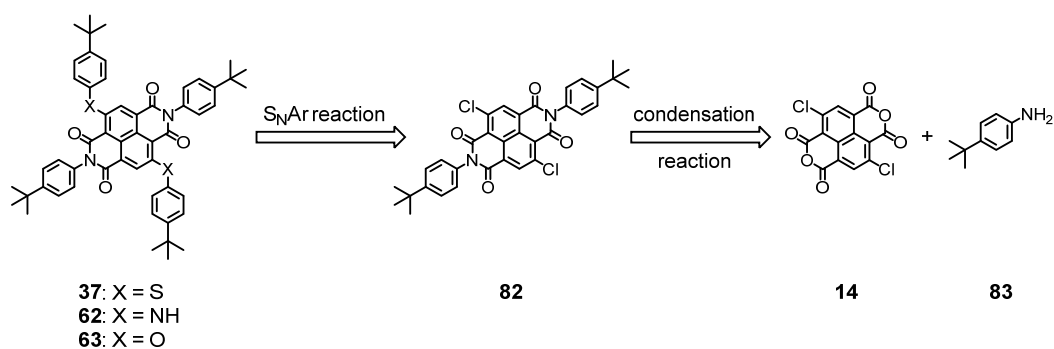
Retrosynthetically, the monoprotected bisamine **78** (Scheme 14) can be obtained by several synthetic methods. However, hereafter only two pathways (blue route and green route) are presented. Similar to the approach towards the sulfur and oxygen nucleophiles, the monoprotected bisamine **78** can be obtained by reduction (green route) of structure **79** or by protection (blue route) of an amine functionality in bisamine **80**. Bisamine **80** (blue route) can be obtained by reduction of compound **81** and a previous one-pot double Wittig reaction of **70** with **72**. In the second route, the monoprotected bisamine **78** (green route) can be obtained by the reduction of structure **79**, and a prior asymmetrical double Wittig reaction of a protected benzaldehyde **81** with **70**, and **72**.



Scheme 14 Retrosynthetic analysis of the synthesis of the monoprotected bisamine **78**.

3.1.4 Retrosynthetic Analysis of Reference Compounds

Retrosynthetically, the unbridged reference compounds **37**, **62**, and **63** (Scheme 15) can be obtained by a final S_NAr reaction of the key building block **82** with the appropriate nucleophile. Structure **82** can be obtained from a condensation reaction of NDA **14** with *tert*-butylaniline (**83**).



Scheme 15 Retrosynthetic analysis of the synthesis of the unbridged reference compounds **37**, **62**, and **63**.

3.2 Results and Discussion

3.2.1 Choice of the Protective Group

From the synthetic point of view, the protective groups (PGs) for the hydroxyl and thiol motifs must be stable against (a) moderate acidic conditions ($pK_A = 4.75$), (b) heat ($130\text{ }^\circ\text{C}$), (c) moderate basic conditions ($pK_A \sim 20$), and (d) hydrogenation using a Pd catalyst. The PGs have to be at the same time labile against (1) strong basic conditions ($pK_B < 0.00$), and (2) acidic conditions ($pK_A = 0.00$) to obtain the free nucleophile in the penultimate step for the final intramolecular ring-closing reaction. In case of a PG for the amine functionality, the PG should be stable under moderate acidic conditions ($pK_A = 4.75$) as well as against heat ($130\text{ }^\circ\text{C}$) and at the same time labile against strong acidic and basic conditions, respectively. After consulting the literature, a series of different possible PGs were on the shortlist. The advantages and disadvantages of these PGs were crucial for the decision, which protecting group had to be utilized in the synthesis of each derivative. Out of this list, the following PGs (Figure 54) were chosen and subsequently investigated (a) the *tert*-butyl (*t*Bu) PG for the thiol nucleophile; (b) the *tert*-butyloxycarbonyl (Boc) PG, carbobenzyloxy (Cbz) PG, and the 9-fluorenylmethyloxycarbonyl (Fmoc) PG for the amine nucleophile; and (c) the β -methoxyethoxymethyl (MEM) PG for the hydroxyl nucleophile.

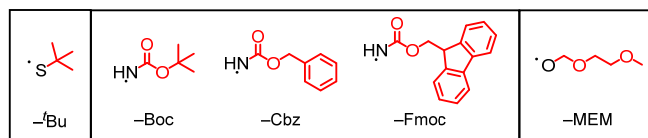


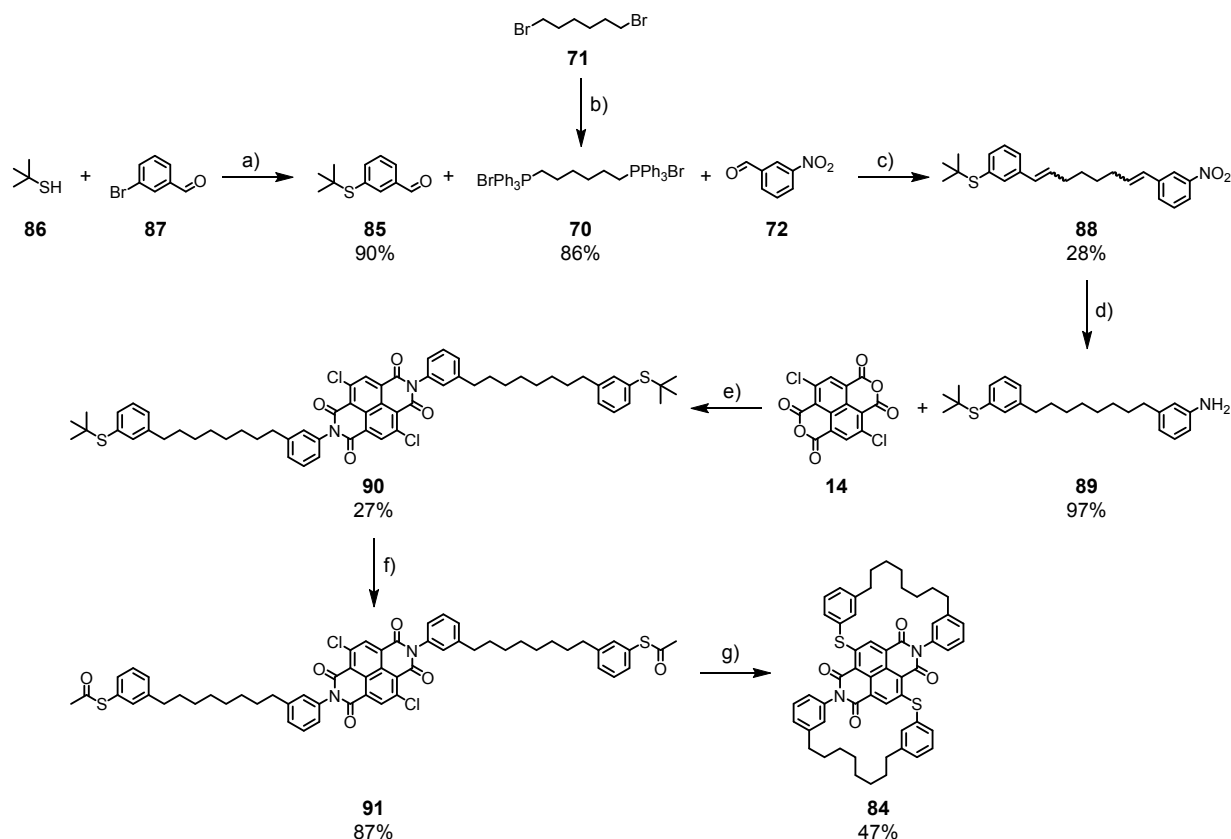
Figure 54 Protective groups used in the synthesis of molecular 8 derivatives.

The synthesis of the unbridged reference compounds **37**, **62**, and **63** did not require the usage of PGs because there was no need to protect the nucleophile as described in Chapter 3.2.5.

3.2.2 Synthesis of *S,S'*-Molecular 8

The synthesis of *S,S'*-molecular 8 **84** (Scheme 16) started with the preparation of 3-(*tert*-butylthio)benzaldehyde (**85**). Initially, **85** was synthesized similar to Mayor et al.^[258] by (1) the protection of the aldehyde functionality of 3-fluorobenzaldehyde in the presence of 4-methylbenzenesulfonic acid with ethane-1,2-diol, (2) the introduction of the sulfanyl functionality with a *t*Bu PG using Na*S**t*Bu, and (3) the final cleavage of the acetal PG under mild acidic conditions (HCl 1 M). The overall yield of this reactions sequence was only 13%. A more attractive route due to the higher overall yield, less steps, and more reliable synthetic procedure was the use of the synthetic protocol developed by Hartwig et al.^[259] starting from commercially available 2-methylpropane-2-thiol (**86**) and 3-bromobenzaldehyde (**87**) which were converted into **85** via a thioetherification reaction in an excellent yield of 90%. The first approach to synthesize *tert*-butyl-(3-(8-(3-nitrophenyl)octa-

1,7-dien-1-yl)phenyl)sulfane (**88**) included a stepwise Wittig reaction pathway. However, this route was very soon dismissed because of the low overall yield (14%) and the long linear sequence.



Scheme 16 Synthesis of *S,S'*-molecular 8 **84** applying: a) Pd(OAc)₂, CyPF-*t*Bu -> 0.005 mol-%, Cs₂CO₃, DME, 110 °C, 20 h; b) PPh₃, DMF, 175 °C, 14 h; c) KO^tBu, THF, rt, 72 h; d) Pd/C (10 %), H₂, 12 bar, EtOAc/EtOH 1:1, 14 h, rt; e) AcOH, 120 °C, 35 min; f) BBr₃ (1 M in CH₂Cl₂), AcCl, PhMe, 0 °C to rt, 3.5 h; g) KOH, DMF, 55 °C, 16 h.

To overcome these drawbacks, the one-pot Wittig reaction route, as displayed in Scheme 16, was designed and started with the transformation^[260] of 1,6-dibromohexane (**71**) to the Wittig ylide, namely, hexa-*P*-phenyl-*P,P'*-octanediy-bis-phosphonium bromide (**70**), in 86% yield. After screening various conditions for the Wittig reaction, tetrahydrofuran (THF) and KO^tBu turned out to be the best solvent and base, respectively. As a result, the asymmetrical, double Wittig reaction was carried out by using 3-nitrobenzaldehyde (**72**), **70**, and **85** in a 1:1:1 ratio. The desired Wittig product **88** was obtained in a good yield of 28% and as a mixture of all four possible isomers, namely, (*E,E*)-**88**, (*Z,E*)-**88**, (*E,Z*)-**88**, and (*Z,Z*)-**88**, as proven by ¹H-NMR analysis. The signals in the ¹H-NMR spectrum (Figure 55) between 8.20 and 8.08 ppm correspond to the protons at the aromatic ring between the nitro group and the olefin of all four possible isomers. The configuration of the four different isomers was determined by a Nuclear Overhauser effect spectroscopy (NOESY) experiment. The NOE contacts between the aromatic protons next to the olefin and the signals at 2.37 and 2.32 ppm, as seen in Figure 55, which were assigned as CH₂ groups next to olefin in (*E*)-position, indicated by a high-field chemical shift of the corresponding carbon shift of

4.42 ppm compared to the carbon shift of the carbon connected to the proton at 2.25 ppm (CH₂ group next to olefin in (*E*)-position).

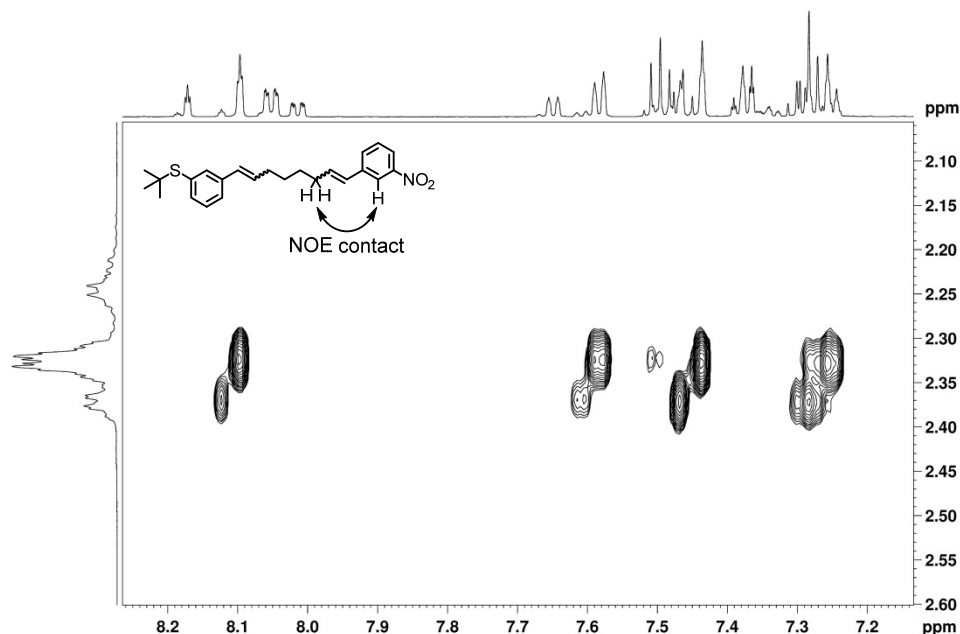


Figure 55 NOESY spectrum of **88** shows the NOE contacts of the aromatic proton with the CH₂ group next to the double bond (indicated by the arrow). The NOESY spectrum was recorded in CD₂Cl₂ at room temperature on a 600 MHz instrument.

From their integrals, the ratio (Figure 56) of the four different isomers was determined:

- 8.10 ppm, 61%: (*Z*)-NO₂, (*Z*)-S^tBu, NOE contacts of 2.32 to 8.10 and 7.58 (both signals of the aromatic ring with the nitro group) and NOE contacts of 2.32 to 7.44 and 7.26 (both signals of the aromatic ring with the thioether)
- 8.12 ppm, 7%: (*Z*)-NO₂, (*E*)-S^tBu, NOE contacts of 2.37 to 8.12 and 7.61 (both signals of the aromatic ring with the nitro group) and no contacts of 2.37 to the aromatic ring with the thioether.
- 8.17 ppm, 28%: (*E*)-NO₂, (*Z*)-S^tBu, NOE contacts of 2.37 to 7.47 and 7.28 (both signals of the aromatic ring with the thioether) and no contacts of 2.37 with aromatic ring with the nitro group.
- 8.19 ppm, 4%: (*E*)-NO₂, (*E*)-S^tBu, only possible isomer left.

After applying reductive conditions on structure **88** to transform the two double bonds into two single bonds and the nitro functionality into an amine functionality using catalytic amounts of Pd/C under a H₂ atmosphere in one step, the desired key building block 3-(8-(3-(*tert*-butylthio)phenyl)octyl)aniline (**89**) was isolated in 97%. The condensation reaction of **14** with **89** under acidic conditions yielded *N,N'*-di-3'-(8'-(3'-(*tert*-butylthio)phenyl)octyl)phenyl-2,6-dichloro-1,4,5,8-naphthalenetetracarboxylic acid diimide (**90**) as a yellow solid in 27% yield. Treatment of **90** with an excess of BBr₃ (1 M in dichloromethane (CH₂Cl₂)) in a mixture of toluene and acetyl chloride

(AcCl) led to the transprotection^[261,262] of the *t*Bu groups into Ac groups, and afforded *N,N'*-di-3'-(8'-(3'-(acetylthio)phenyl)octyl)phenyl-2,6-dichloro-1,4,5,8-naphthalenetetracarboxylic acid diimide (**91**) in 87% yield.

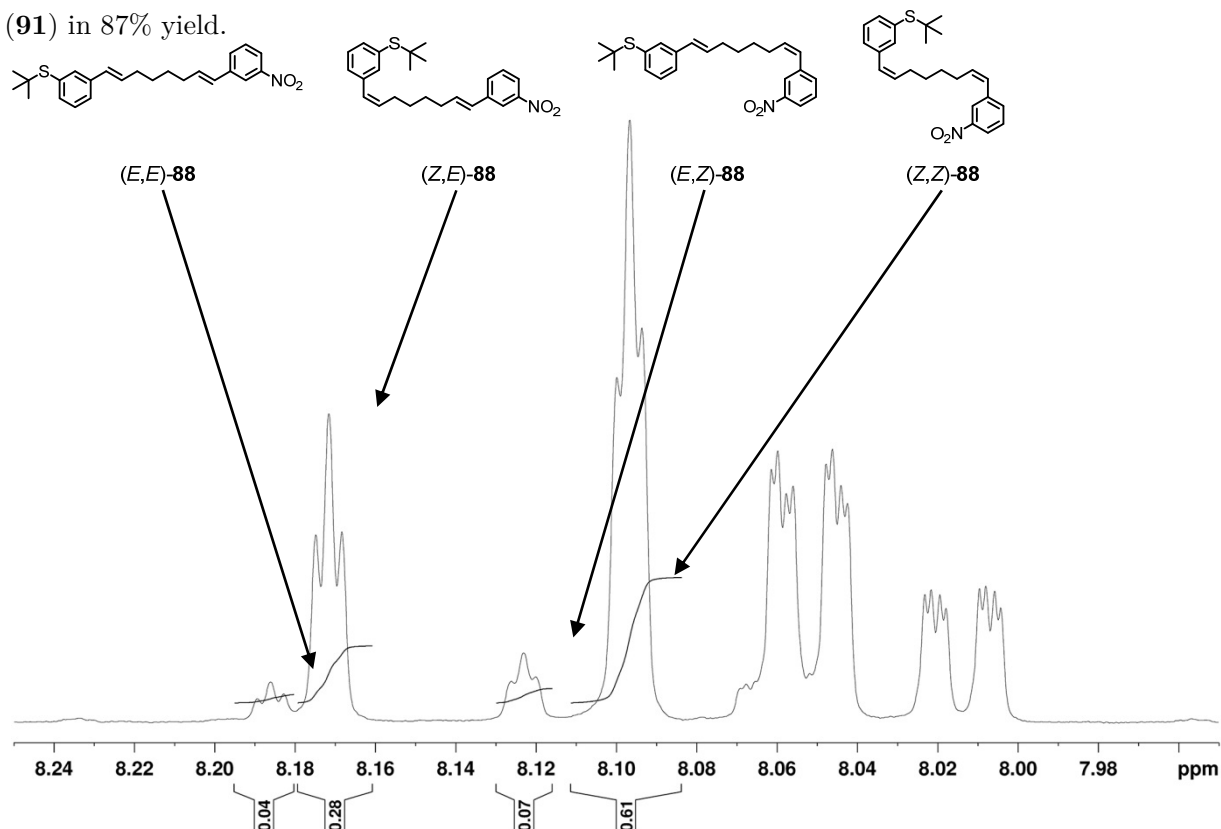


Figure 56 Integration of the signals corresponds to the ratio of the four isomers. ¹H-NMR spectrum was recorded in CD₂Cl₂ at room temperature on a 600 MHz instrument.

The protective groups were subsequently cleaved under basic conditions and, simultaneously, a twofold final intramolecular nucleophilic aromatic substitution reaction occurred to yield the desired *S,S'*-molecular 8 **84**, its correct name being 1((3,3',3'',3''')-2,7-diphenyl-4,9-bis(phenylthio)benzo[*lmn*][3,8]phenanthroline-1,3,6,8(2*H*,7*H*)-tetraona)bicyclo[09.8^{1.1}]heptadecanodane, as an intense red solid in 47%.

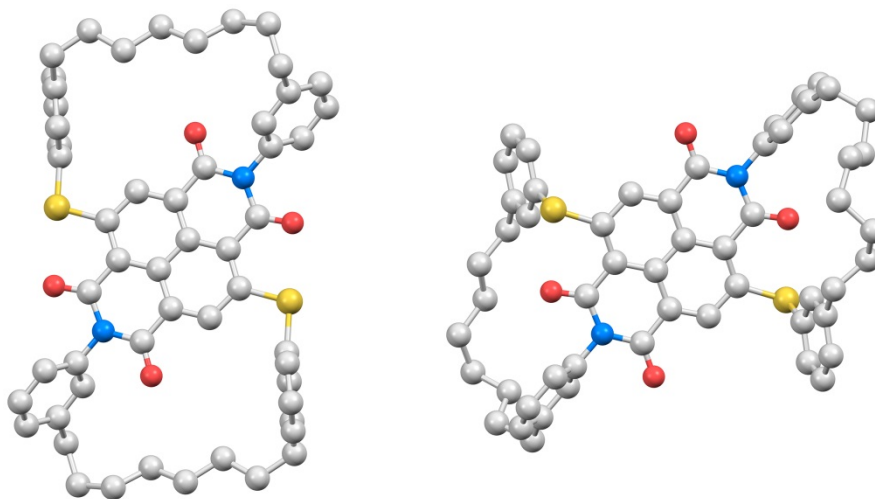


Figure 57 The two possible bridged isomers of **84** (left and right), which can be formed during the final step.

The last reaction step yielded exclusively one of the two possible isomers, as illustrated in Figure 57, because only one signal for the two hydrogen atoms of the naphthyl core was found in the course of the $^1\text{H-NMR}$ analysis. Three NOE contacts, as illustrated in Figure 58a, were found in the NOESY spectrum and the only reasonable explanation is a through space contact of the hydrogen atoms of the aliphatic chain (signals at 1.14, 1.25, and 1.67 ppm) to the hydrogen atom of the naphthyl core (signal at 8.15 ppm) indicated by the red arrows in Figure 58b and, therefore, pointing as well towards the formation of the shown isomer.

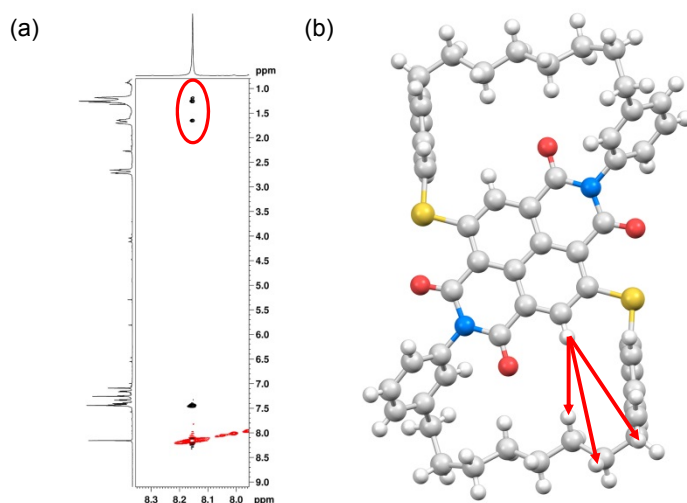


Figure 58 (a) The NOE contacts in the NOESY spectrum of **84** are highlighted in the red box. The NOESY spectrum was recorded in CDCl_3 at room temperature on a 600 MHz instrument; (b) illustration of the three observed NOE contacts in the crystal structure of **84**.

Finally, the proposed structure, as seen in Figure 58b, was confirmed by means of X-ray diffraction analysis. Single crystals suitable for X-ray diffraction analysis were obtained by the use of the solvent diffusion technique in a mixture of CH_2Cl_2 /hexane and these crystals crystallized in the triclinic space-group $P-1$ (2).

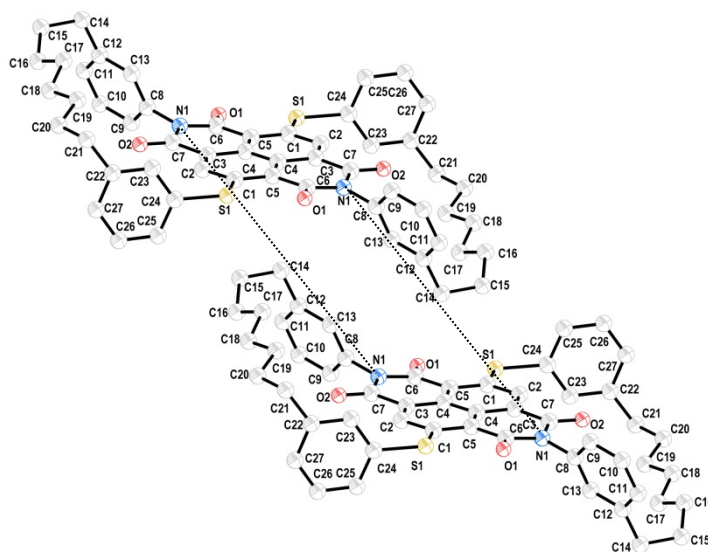
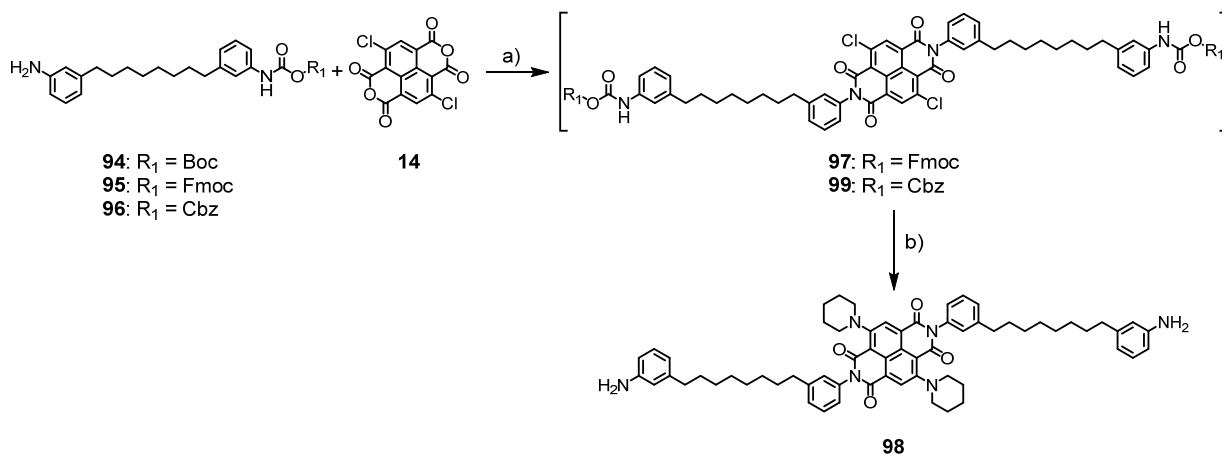


Figure 59 Crystal structure of **84** illustrated in a dimeric arrangement.

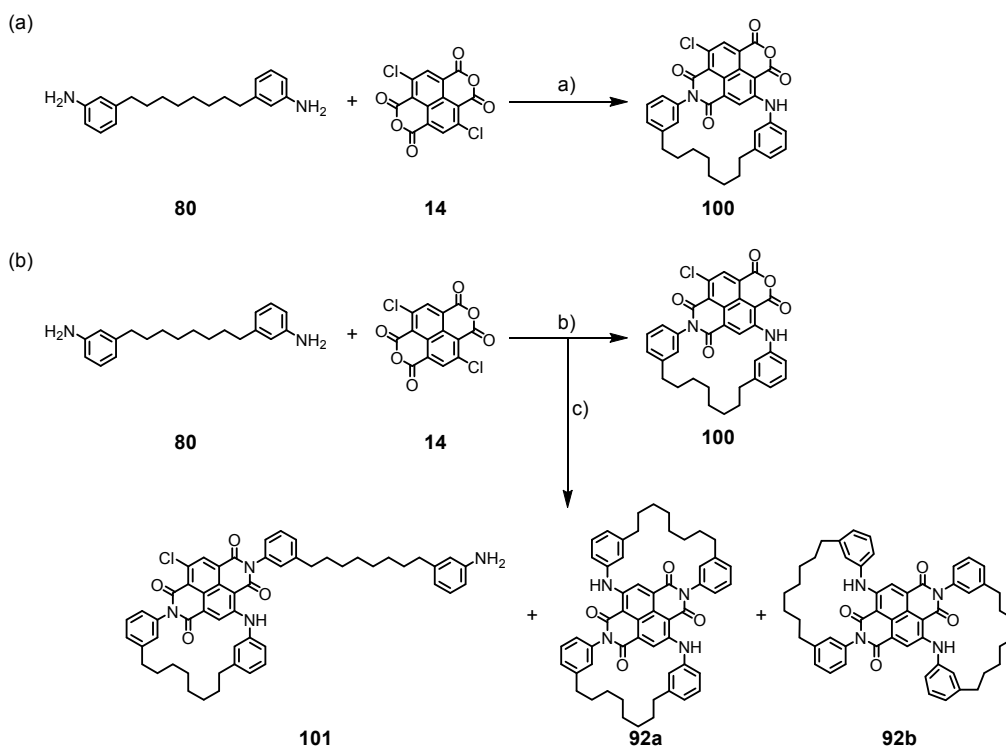
tion (Scheme 19) of **14** with **94** yielded a compound which was attempted to purify by column chromatography with various eluents and different kind of stationary phases, such as (a) silica gel, (b) aluminum oxide (alox), and (c) reversed-phase silica gel (C8), but all attempts failed to get a clean $^1\text{H-NMR}$ spectrum and a mass spectrum (electrospray ionization (ESI) and matrix assisted laser desorption ionization time of flight (MALDI-TOF)). The condensation reaction of **14** with **95** yielded the desired linear NDI **97** (Scheme 19) but unfortunately the removal of the PGs with DMF/piperidine 5:1,^[263] resulted in the simultaneous nucleophilic attack of piperidine to exchange the chlorine atoms of the NDI motif and, as a result, cNDI **98** was isolated according to MALDI-TOF-MS analysis. The condensation reaction of **14** with **96** yielded the desired linear NDI **99** (Scheme 19) according to MALDI-TOF-MS analysis, but all attempts to subsequently remove the two PGs failed. The cleavage of the PGs was attempted under acidic and reductive conditions, such as (1) (pH = 1)^[264]; (2) Pd/C (10%), H_2 (10 bar)^[265]; and (3) Pd/C (10%)/Pd(OH)₂ (20%) 1:1, H_2 (5 bar).^[266]



Scheme 19 Failed attempts towards the synthesis of *N,N'*-molecular 8 **92a** and **92b** applying: a) AcOH, 135 °C, 35 min; b) DMF/piperidine 5:1, rt, 2 h.

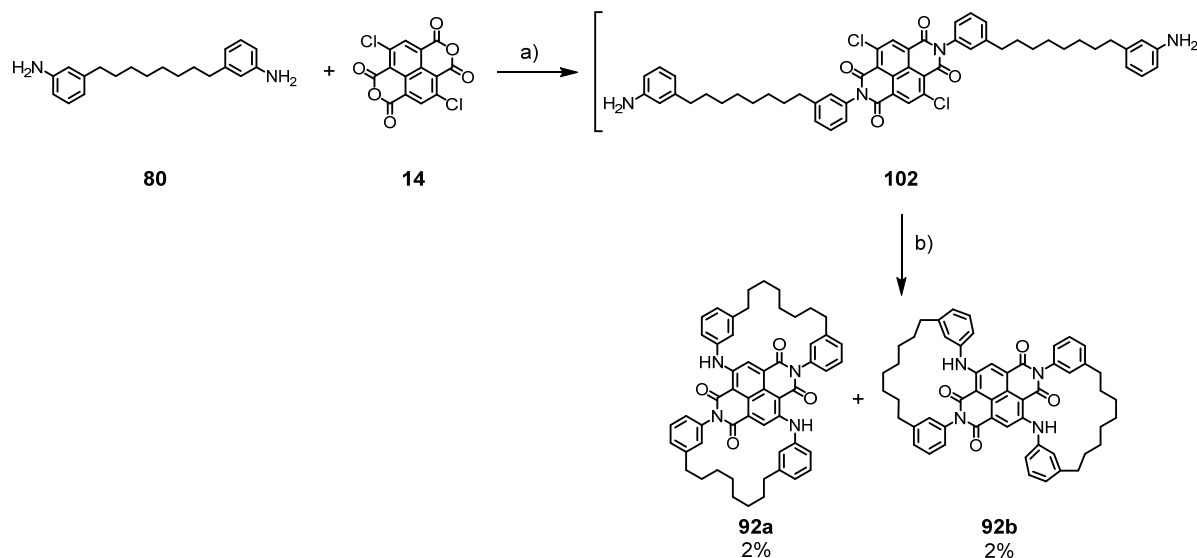
The approach of using PGs was tried to overcome by a new synthetic approach, namely, a two-fold condensation reaction and, simultaneously, a twofold nucleophilic aromatic substitution reaction to yield the target structure *N,N'*-molecular 8 in one step. Therefore, **80** (2 equiv) and **14** (1 equiv) were heated in DMF at 124 °C for 18 h. The outcome of this reaction (Scheme 20a) was the formation of the mono-bridged compound **100** in traces but no formation of **92a** and **92b** was observed according to thin-layer chromatography (TLC) analysis. The main spots on the TLC on silica gel were not migrating with the eluent and, as a result, indicated polymerization or decomposition of the starting material. In 1974, Bonnet et al.^[267] reported the synthesis of *N,N'*-di-4'-(aminophenyl)-2,6-dichloro-1,4,5,8-naphthalenetetracarboxylic acid diimide by refluxing 1,4-diaminobenzene and **14** in AcOH at 120 °C for 2 h. Inspired by their success, similar conditions were applied to our system and the reaction time for the condensation reaction was in a next step investigated. Thus, a mixture of **14** and **80** in AcOH was heated at 125 °C for (a) 4 h, and (b) 35 min. In

both cases, the solvent was evaporated under reduced pressure after the indicated reaction time, the residue diluted with DMF (equal concentration), and finally stirred at 120 °C for 14 h.



Scheme 20 Approaches to synthesize *N,N'*-molecular 8 **92a** and **92b** applying: a) DMF, 124 °C, 18 h; b) AcOH, 125 °C, 4 h, then DMF, 120 °C, 14 h; c) AcOH, 125 °C, 35 min, then DMF, 120 °C, 14 h.

In contrast to case (a) where only the formation of **100** (Scheme 20b) was observed, in case (b) traces of the monobridged cNDI **101** and *N,N'*-molecular 8 **92a** and **92b** were detected. After improving all the reaction conditions and purification methods, the NDI with two free amines **102** was prepared, as illustrated in Scheme 21, by stirring a mixture of **80** and **14** in AcOH at 135 °C for 35 min. After the purification of the crude product by column chromatography on silica gel, **102** was isolated as a purple solid. No yield is indicated for this reaction step, because the product was not completely pure. Additionally, it must be emphasized that the molecular mass of **102** was only detectable by direct analysis at real time mass spectroscopy (DART-MS) and not with all the other common mass spectrometer, such as ESI-MS and MALDI-TOF-MS. The crude free amine **102** was finally added with a syringe pump over 3 h to preheated DMF (120 °C), and the reaction mixture was stirred at 120 °C for 14 h after the complete addition. The purification (Figure 60, top) of the blue residue afforded 1((3,3',3'',3''')-2,7-diphenyl-4,9-bis(phenylamino)benzo[*lmn*][3,8]-phenanthroline-1,3,6,8(2*H*,7*H*)-tetraona)bicyclo[09.8^{1,1}]heptadecanodane, also referred to as *N,N'*-molecular 8, as an isomeric mixture, **92a** and **92b**.



Scheme 21 Synthesis of *N,N'*-molecular 8 **92a** and **92b** applying: a) AcOH, 135 °C, 35 min; b) DMF, 130 °C, 14 h.

In the $^1\text{H-NMR}$ spectrum, the isomeric mixture has two signals with the same multiplicity for the hydrogen atoms (Figure 60, middle and bottom) of the naphthyl core (framed in the blue box) and two signals with the same multiplicity for the hydrogen atoms attached to the amine functionality (framed in the red box). The separation of this isomeric mixture was achieved by preparative normal-phase high-performance liquid chromatography (NP HPLC) and yielded each isomer in an overall yield of 2% over two steps.

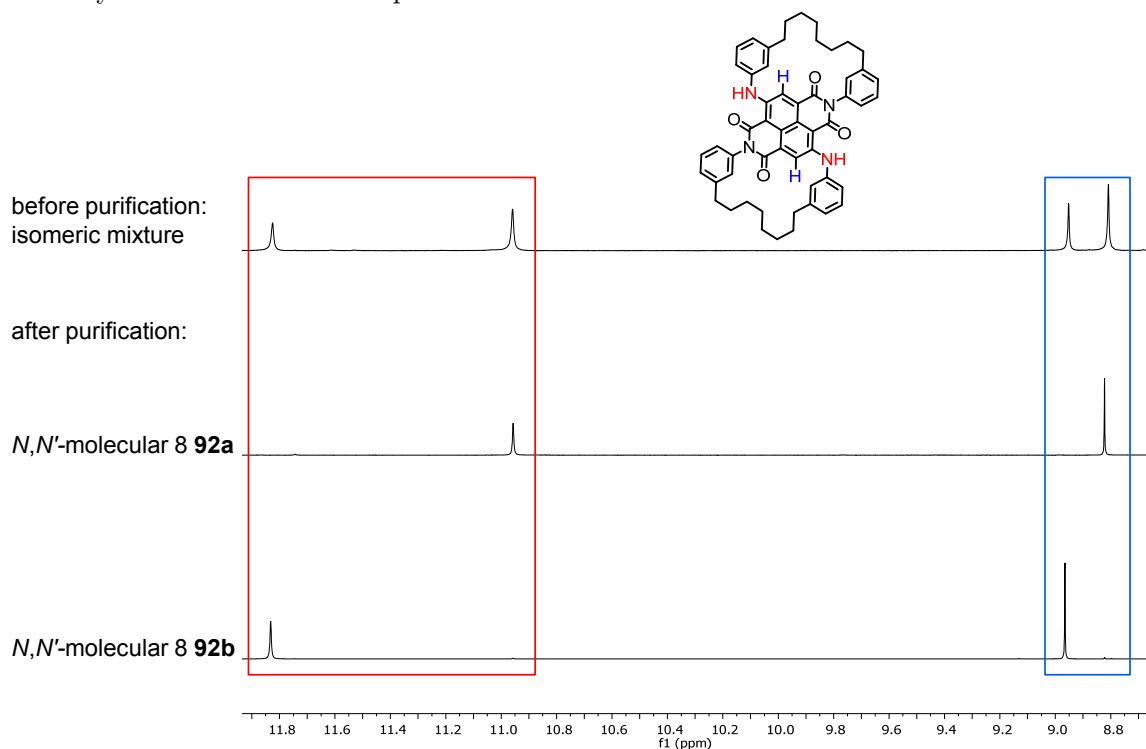


Figure 60 $^1\text{H-NMR}$ spectra were recorded before (top) and after purification (middle and bottom) by preparative NP-HPLC to yield the two isomers **92a** and **92b**. All spectra were in CDCl_3 at room temperature on a 400 MHz instrument

The NOE contacts in the NOESY experiment of the hydrogen atom of the naphthyl core (signal at 8.82 ppm) to the hydrogen atoms of the aliphatic chain (signals between 1.75–1.27 ppm) strongly indicated the formation of the shown structure in case of **92a** (Figure 61a) and, vice versa, in case of **92b** (Figure 61b) with missing NOE contacts.

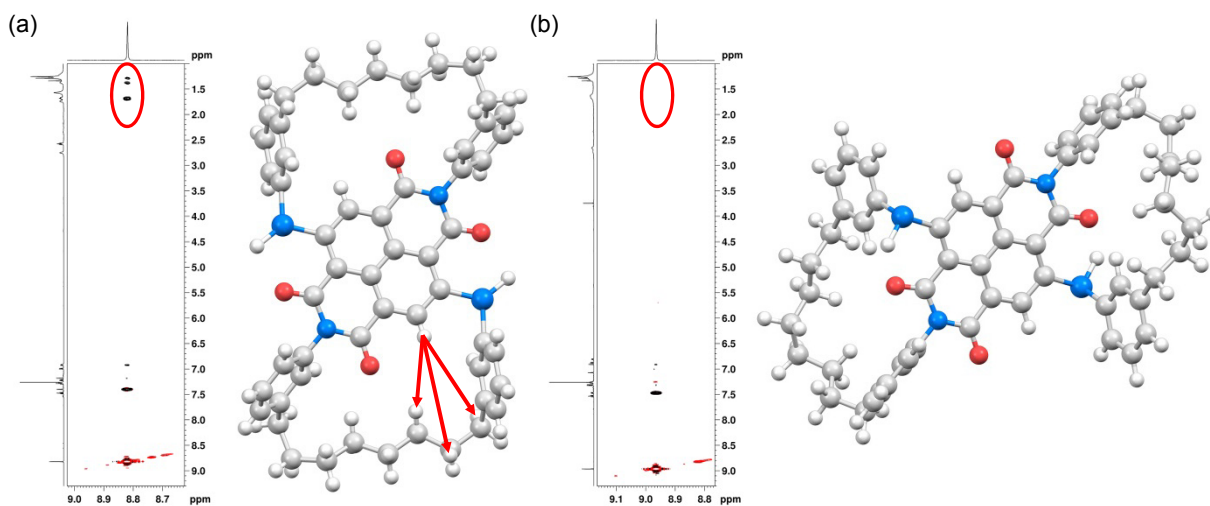


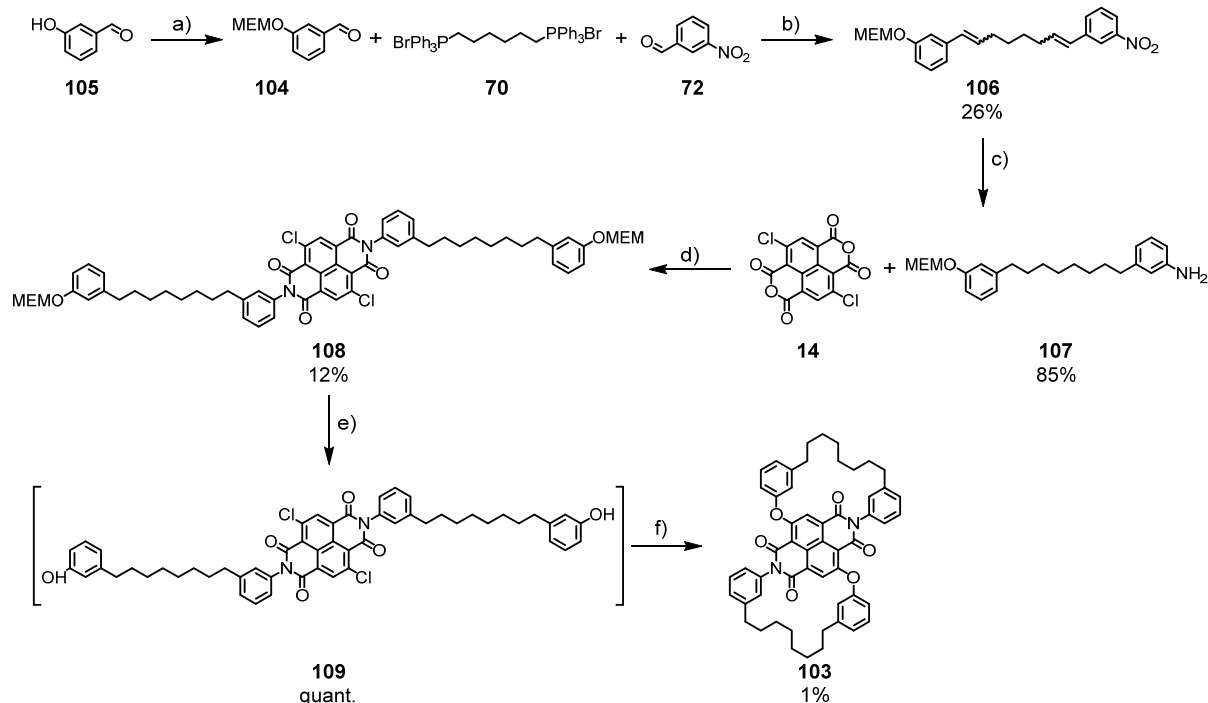
Figure 61 (a) The observed NOE contacts are highlighted in the NOESY spectrum of **92a** and illustrated by red arrows in the chemical structure of **92a**; (b) no NOE contacts in the NOESY spectrum of **92b** were observed. Both spectra were recorded in CDCl_3 at room temperature on a 600 MHz instrument.

High-resolution mass spectroscopy confirmed for both isomers the calculated molecular mass. In **92a** by using the IUPAC nomenclature, the substituents in the positions 2 and 9, and the substituents in the positions 4 and 9 are bridged to each other. In case of **92b**, the substituents in the positions 2 and 4 and the substituents in positions 7 and 9 are bridged to each other. As a result, **92a** and **92b** are structural isomers.

3.2.4 Synthesis of *O,O'*-Molecular 8

The first step of the synthetic approach to synthesize *O,O'*-molecular 8 **103** (Scheme 22) was the preparation of the protected benzaldehyde, namely, 3-((2-methoxyethoxy)methoxy)benzaldehyde (**104**).^[268] The preparation was achieved by dissolving 3-hydroxybenzaldehyde (**105**) and *N,N*-diisopropylethylamine (DIPEA) in CH_2Cl_2 , and followed by the dropwise addition of MEM-Cl to the reaction mixture. The desired product was obtained as a yellow liquid in 86% yield. A subsequent Wittig reaction of **104**, **70**, and **72** in a 1:1:1 ratio using the same reaction conditions (base, solvent, and temperature) as in the previous two cases, afforded 1-((2-methoxyethoxy)methoxy)-3-(8-(3-(3-nitrophenyl)octa-1,7-dien-1-yl)benzene (**106**) in 26% yield. The isolated olefin **106** consisted of four different isomers and once more the ratio was not determined by $^1\text{H-NMR}$ spectroscopy. **106** was subsequently exposed to reductive conditions using catalytic amounts of Pd/C and a H_2 atmosphere to obtain 3-(8-(3-((2-methoxyethoxy)methoxy)phenyl)octyl)aniline (**107**) as a yellow oil in 85% yield. The condensation reaction of **107** with **14** under

standard conditions afforded the double MEM-protected NDI **108**, namely, *N,N'*-di-3'-(8'-(3'-(2'-methoxyethoxy)methoxy)phenyl)octyl)phenyl-2,6-dichloro-1,4,5,8-naphthalenetetracarboxylic acid diimide, the mono MEM-protected NDI, and the double deprotected NDI **109**. The mixture was purified by preparative gel permeation chromatography (GPC) to yield **108** as a red solid in 12%.



Scheme 22 Synthesis of *O,O'*-molecular 8 **103** applying: a) DIPEA, MEM-Cl, CH₂Cl₂, 0 °C to rt; b) KO^tBu, THF, rt, 74 h; c) Pd/C (10%), H₂ (10 bar), EtOAc/EtOH, rt, 14 h; d) AcOH, 120 °C, 35 min; e) TFA/ CH₂Cl₂ 4:1, rt, 4 h, and f) KOH, DMF, 80 °C, 14 h.

The cleavage of the two protective groups in **108** was subsequently investigated (Table 1), and the progress of the deprotection reaction was monitored by MALDI-TOF-MS analysis. Applying the deprotecting reagents listed in entries 1 and 2 of Table 1 did not lead to the desired result. The removal of the two protective groups was only achieved by stirring the starting material in a 3:1 mixture of TFA/CH₂Cl₂ at room temperature for 5 h.

Entry	Reagent	Solvent	Temp.	Time	MALDI-TOF-MS
1	CeCl ₃ · 7H ₂ O ^[269]	MeCN	90 °C	2 h	only starting material
2	HCl (4 M in 1,4-dioxane) ^[270]	none	rt	2 h	only starting material
3	TFA/CH ₂ Cl ₂ 3:1	none	rt	5 h	only product

Table 1 Three different deprotection reaction conditions were investigated for the cleavage of the protective groups in **108** to obtain **109**.

In a next step, the crude product **109** of the deprotection reaction was dissolved in DMF and added dropwise to a hot solution (85 °C) of KOH in DMF. The reaction mixture was stirred at the indicated temperature for 14 h, and after purification the desired product 1((3,3',3'',3''')-2,7-diphenyl-4,9-bis(phenoxy)benzo[*lmn*][3,8]phenanthroline-1,3,6,8(2*H*,7*H*)-tetraona)bicyclo[09.8¹⁻¹]hep-

tadecanodane (**103**), also referred to as *O,O'*-molecular 8, was isolated as a yellow solid in 1% yield over two steps. The unsatisfying low yield of the final cyclization reaction led to the investigation of the reaction conditions and, as a consequence, different parameters were investigated:

- (a) the nature of the base (KOH, KO^tBu, Cs₂CO₃, K₂CO₃, and NaH)
- (b) the equivalents of base (3.9–18.0 equiv)
- (c) the influence of additives (proton sponge[®] and 18-crown-6-ether)
- (d) the choice of solvent (DMSO and DMF)
- (e) the amount of solvent (15–220 mL)
- (f) the concentration of the starting material (SM; 2.4–38.3 mM)
- (g) the addition time of the starting material (no addition time to addition over 1440 min)

Entry	SM Conc. [mM]	Additive [equiv]	Base [equiv]	Solvent [mL]	Temp [°C]	Addition time [min]	MALDI-TOF-MS
1	5.5	none	KOH (15)	DMF (15)	85	40	product
2	8.1	none	K ₂ CO ₃ (10)	DMF (20)	80	120	no product
3	11.6	none	KOH (10)	DMF (20)	80	120	product
4	17.3	none	KOH (8.3)	DMF (40)	80	960	no product
5	44.1	none	NaH (10)	DMF (200)	70	240	product
6	12.9	8-crown-6-ether (0.5)	KOH (3.9)	DMF (100)	94C	0	no product
7	3.0	none	NaH (4.5)	DMF (200)	91	1080	no product
8	5.4	none	KOH (5.1)	DMF (230)	94	120	no product
9	7.3	none	KOH (4.3)	DMF (230)	94	120	no product
10	3.3	none	NaH (15)	DMF (200)	90	120	no product
11	1.4	none	NaH (18)	DMF (15)	90	60	monocycle (841 <i>m/z</i>)
12	2.9	proton-sponge [®] (8.1)	none	DMF (200)	90	100	traces of product
13	2.5	proton-sponge [®] (8.1)	none	DMF (200)	90	100	no product
14	2.3	none	KOH (8.2)	DMF (220)	85	100	no product

15	38.3	none	KOH (9.3)	DMF (20)	85	120	no product
16	4.7	none	KOH (10)	DMF (20)	85	120	no product
17	2.4	none	KOH (9.7)	DMF (40)	80	120	no product
18	12.7	none	KOH (10)	DMF (40)	80	200	monocycle (841 <i>m/z</i>)
19	8.4	none	NaH (10)	DMF (40)	80	100	no product
20	7.1	none	KO ^t Bu (5.0)	DMF (40)	80	500	(854 <i>m/z</i>)
21	3.3	none	KOH (7.6)	DMF (60)	80	360	no product
22	6.33	none	NaH (6.3)	DMF (60)	70	480	no product
23	5.3	none	KOH (5.4)	DMF (100)	80	720	no product
24	9.2	none	NaH (5.0)	DMF (40)	60	1440	no product
25	8.4	none	Cs ₂ CO ₃ (5.1)	DMF (40)	80	720	no product
26	4.5	none	Cs ₂ CO ₃ (12.5)	DMF (40)	140	1080	no product
27	7.5	none	KOH (4.5)	DMF (40)	85	50	no product
28	5.2	Cu(I) (0.50)	K ₂ CO ₃ (11.1)	DMSO (200)	90	480	no product (798 <i>m/z</i>)

Table 2 A series of investigated reaction conditions for the intramolecular cyclization reaction of **109** to yield **103**.

The synthesis of **103** was twice achieved with KOH as base and DMF as solvent (Table 2; entries 1 and 3), but all further attempts to resynthesize the target structure under the same or similar conditions (Table 2; entries 4, 8, 9, 14–18, 21, 23, and 27) failed. Additionally, **103** was once synthesized with NaH as base and DMF as solvent (Table 2; entry 5), here as well all further approaches to resynthesize **103** with the same or similar conditions (Table 2; entries 7, 10–12, 19 and 24) were not successful. A possible explanation why KOH and NaH were not the best choice is their ability to substitute the two chloride atoms of the naphthyl moiety nucleophilically by attacking with the hydroxyl and the hydride functionality, respectively. In entries 11 and 18 of Table 2 an orange solid was isolated for which a molecular mass of 841 *m/z* was found by MALDI-TOF MS analysis. This particular mass, as shown in Figure 62, might correspond to the mono-closed *O,O'*-molecular 8 with a hydroxyl group attached to the naphthyl core. As a result, other non-nucleophilic bases,^[271,272] such as proton sponge[®], KO^tBu, and alkali metal carbonate salts (Na₂CO₃,

K_2CO_3 , and Cs_2CO_3) were investigated. In 1968, Alder and coworkers^[273] reported the synthesis of 1,8-bis(ethylamino)naphthalene, also referred to as proton sponge[®], and attributed a remarkable high basicity to this molecule.^[274,275,276]

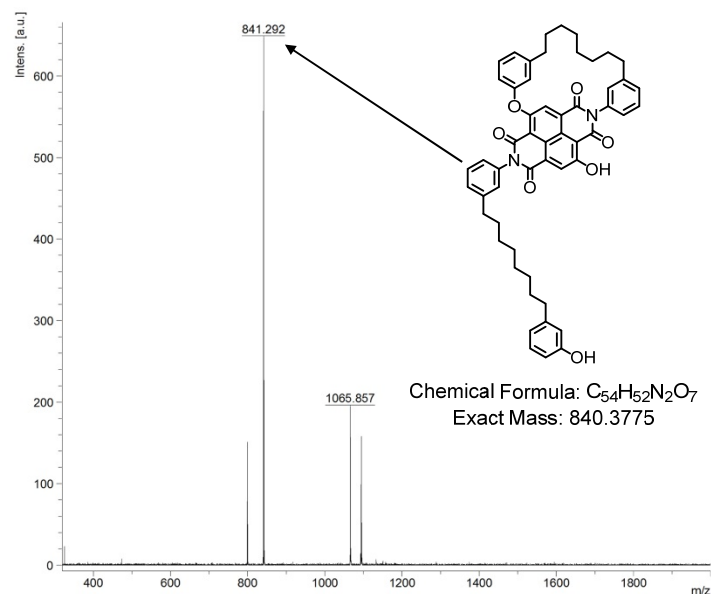


Figure 62 An overlay of the MALDI-TOF-MS spectrum of the isolated orange compound in entries 11 and 18 with a mass of 840 m/z and the possible chemical structure.

Indeed, the conjugated acid of proton sponge[®] has a pK_a of 12.34 and, therefore, proton sponge[®] is known to be one of the strongest amine bases available (e.g., conjugated acid of NEt_3 has a pK_a of 10.2^[271]). The ability of proton sponge[®] to act as a suitable base for the final reaction was investigated and the desired product could be obtained in traces (Table 2; entry 12). However, when the same experimental conditions were applied again in entry 13, no product was detected according to TLC analysis. A second investigated additive was 18-crown-6-ether. It is literature^[277,278] known that 18-crown-6-ether is able to complex potassium cations with a high efficiency and, therefore, this additive (Table 2; entry 6) was investigated. Unfortunately, the target structure was not formed according to TLC analysis. The last class on the list of non-nucleophilic bases were the alkali metal carbonates, such as K_2CO_3 and Cs_2CO_3 . All approaches (Table 2; entries 25, 26, and 28) to obtain the desired product failed in these cases. Moreover, the solvent was changed from DMF to DMSO (Table 2; entry 28) and the base to $KOtBu$ (Table 2; entry 20) but still no product could be isolated.

To conclude, all attempts failed to reproduce the successful synthesis of **103**. Nevertheless, enough substance was available to (a) do mass analysis of O,O' -molecular 8; (b) measure 2D NMR spectra and prove the structure of O,O' -molecular 8; and (c) investigate the optical properties of O,O' -molecular 8.

In the $^1\text{H-NMR}$ spectrum only one signal was found for the hydrogen atom of the naphthyl core (Figure 63a) and, as a result, the formation of only one isomer can be assumed like in the case of **84**. Additionally, a NOESY experiment strongly indicated the formation of the structure drawn in Figure 60b, which was the only logical explanation for the NOE contacts of the hydrogen atoms of the aliphatic chain (signals between 1.58 and 1.22 ppm) to the hydrogen atom of the naphthyl core (signal at 8.39 ppm) as indicated by the red arrows.

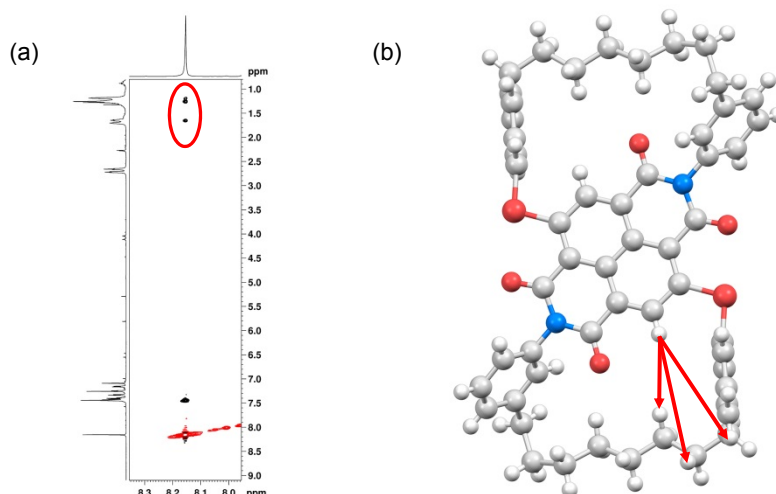


Figure 63 (a) NOESY spectrum of *O,O'*-molecular **8** with three NOE contacts; (b) the NOE contacts in *O,O'*-molecular **8** are indicated by red arrows. NOESY spectrum was recorded in CDCl_3 at room temperature on a 600 MHz instrument.

In general, an increase of the atomic size goes along with an increase of nucleophilicity and, simultaneously, the nucleophilicity increases across a row from right to left in the periodic table. Therefore, a very reasonable explanation for the difficulties to obtain *N,N'*-molecular **8** and *O,O'*-molecular **8** can be attributed to the low nucleophilicities of nitrogen and oxygen, respectively, if compared to sulfur. This observation is reflected in the very low yields in the formation of both derivatives.

3.2.5 Synthesis of Reference Compounds

The synthesis of the three unbridged derivatives, as illustrated in Scheme 23, was initiated with the preparation of the literature known^[279] key building block, *N,N'*-di-(4'-*tert*-butylphenyl)-2,6-dichloro-1,4,5,8-naphthalenetetracarboxylic acid diimide (**82**) and was accomplished by heating **14** and **83** in AcOH at 120 °C for 30 min in a good yield of 56%. The conversion of **82** to *N,N'*-di-(4'-*tert*-butylphenyl)-2,6-di-(4-*tert*-butylphenylsulfanyl)-1,4,5,8-naphthalenetetracarboxylic acid diimide (**37**) was achieved by heating a mixture of **82**, 4-*tert*-butylthiophenol (**156**), and K_2CO_3 in DMF at 60 °C for 1 h. This synthetic protocol was first reported by Mayor et al.^[279] and afforded **37** as an intense red solid in 68% yield. The second reference compound, namely, *N,N'*-di-(4'-*tert*-butylphenyl)-2,6-di(4-*tert*-butylphenylamino)-1,4,5,8-naphthalenetetracarboxylic acid diimide (**62**),

3.2.6 Overlay of Two Crystal Structures

The overlay of the crystal structures of **37** and **84**, as shown in Figure 65, revealed that in the crystal structure of **84** (carbon atoms are colored in orange) the phenyl substituent at the *N*-terminus of each imide functionality is slightly twisted compared to the phenyl substituent at the *N*-terminus of each imide functionality of **37** (carbon atoms are colored in green), which is perfectly perpendicular. This twist is attributed to the eight-membered aliphatic bridge in **84**, which causes to a certain extent rigidity in the structure. However, the aliphatic bridge did not create a very constrained environment.

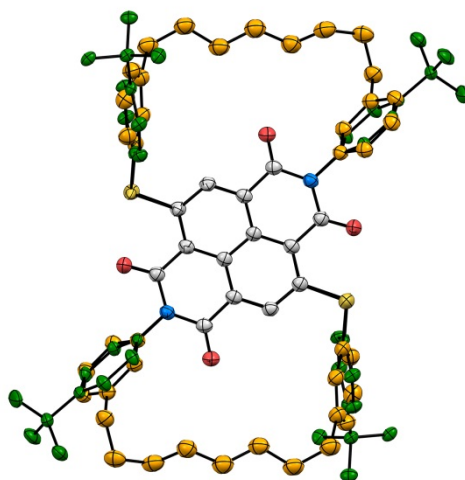


Figure 65 Overlay of the crystal structure of **37** and **84**.

3.2.7 Optical Properties of Molecular 8

The absorption and fluorescence spectra, as well as the fluorescence quantum yields, for all molecular 8 derivatives and the reference compounds were measured and analyzed.

The ground-state optical absorption spectra (Figure 66) of **37** (blue line) and **84** (red line), recorded in CHCl_3 , show absorption bands between 340 and 400 nm, which were attributed to the $\pi \rightarrow \pi^*$ transition of the NDI chromophore, as well as transitions at a lower energy (450–550 nm), which were attributed to the intramolecular charge transfer from the electron-rich phenylsulfanyl substituents to the NDI core. These absorption profiles are in excellent agreement with those of the previously described^[57,75,76] naphthalene diimide derivatives. The absorption band maximum of the charge-transfer transition in **84** is at 516 nm and is slightly hypsochromically shifted compared to that of **37** (522 nm). Apart from this difference, both absorption spectra (Figure 66) have almost identical profiles at almost the same concentration.

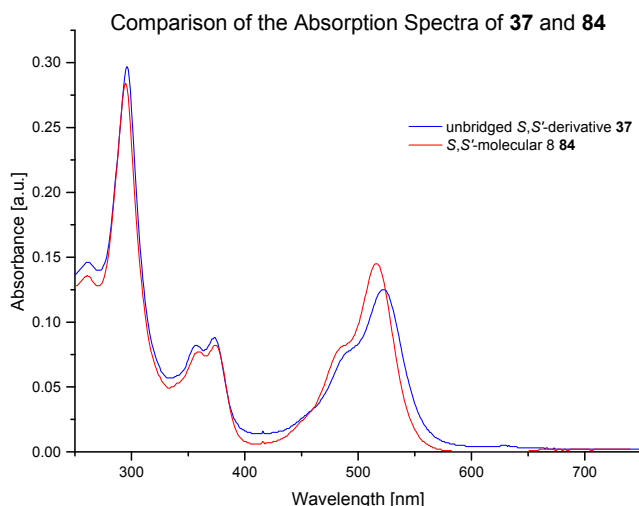


Figure 66 Absorption spectra of the unbridged derivative **37** (blue line; $c = 7.41 \mu\text{M}$) and S,S' -molecular **8 84** (red line; $c = 7.89 \mu\text{M}$) recorded in CHCl_3 at room temperature.

The emission spectra of **84** (excitation at 359 and 374 nm) are shown in Figure 67. The weak emission band at 544 nm is caused by the phenylsulfanyl core substituent. Upon excitation at 516 nm, the emission of the core substituent at 548 nm was observed. In all three cases, the excitation led to a very weak fluorescence signal as shown in Figure 67.

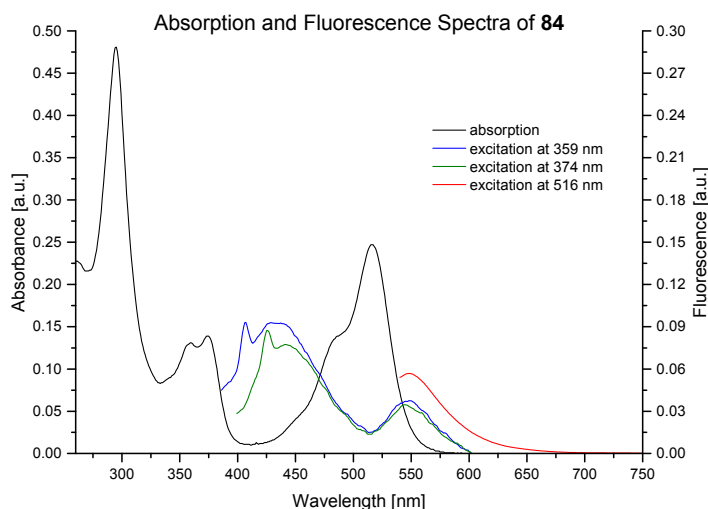


Figure 67 Absorption (black line; $c = 13.4 \mu\text{M}$) and fluorescence (colored lines: excitation at 359 (blue line), 374 (green line), 516 nm (red line)) spectra of **84** recorded in CHCl_3 at room temperature.

The fluorescence quantum yields (FQYs) for compounds **37** and **84** were measured in CHCl_3 and determined to be below 1% ($\Phi_{\text{fl}} < 0.01$) in each case. As a result, it was not necessary to show the emission spectra of **37** and compare it with the emission spectra of **84**. In addition, the low values of the FQY did not allow it to verify the proposed hypothesis at this stage of the study.

The absorption spectra of the three NDI derivatives **62**, **92a**, and **92b** bearing phenylamino core substituents are shown in Figure 68. All three spectra show the two absorption bands between 340 and 400 nm, which were ascribed to $\pi \rightarrow \pi^*$ transitions of the NDI chromophore. By compari-

son of the three absorption spectra, it becomes evident that a less resolved broad absorption band in the range 340–400 nm is found in the case of **92b**, compared to **92a** and **62** (Figure 68). Gabutti et al.,^[75,76] who studied a 2,6-dipiperidinyl-core-substituted NDI derivative (Figure 23c), observed a similar broad band in their absorption spectrum but did not describe the origin of this band. Two other amino-core-substituted NDI derivatives, as described in Chapter 4.2.4, that were also studied do not exhibit such broadening effect. It is known in the literature^[281] that steric hindrance of substituents can cause broadening of the absorption bands. In this respect, the broadening of the absorption band in the case of **92b** (Figure 61b) can be most probably ascribed to the steric effects of the core substituent that are negligible in the case of **92a** (Figure 61a) and **62**. An almost identical shape for the absorption spectra of **62** (blue line; $c = 13.4 \mu\text{M}$) and **92a** (red line; $c = 21.8 \mu\text{M}$) at different concentrations, as shown in Figure 68, was found.

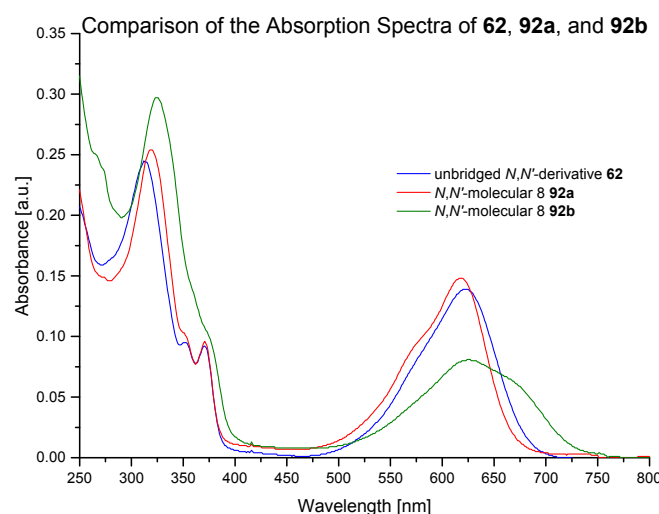


Figure 68 Absorption spectra of the unbridged derivative **62** (blue line; $c = 13.4 \mu\text{M}$), and the isomeric N,N' -molecular 8 **92a** (red line; $c = 21.8 \mu\text{M}$) and **92b** (green line; $c = 52.8 \mu\text{M}$). All spectra were recorded in CHCl_3 at room temperature.

In the emission spectrum of **92a** (Figure 69; red solid line) upon excitation at 617 nm, an emission band with a maximum at 668 nm was observed. In case of **92b**, upon excitation at 648 nm (Figure 69; red dashed line), the emission of the core substituent at 716 nm was detected. However, the fluorescence band signal was weaker than the one of **92a**. The excitation spectra of **92a–b** were as well recorded. In this operating mode, the variations in fluorescence intensity (emission intensity) are recorded at a fixed emission wavelength, while varying the excitation wavelength. In general, the fixed emission wavelength corresponds to the longest wavelength band maximum in the emission spectrum. This set-up minimizes possible decomposition of the measured sample caused by high-energy (short wavelength) irradiation.^[282] Only if one fluorescent compound is present, the excitation spectrum is identical to the shape of the absorption spectrum. If there is more than one light-absorbing species present, the absorption and the excitation spectra are not superimposable. The excitation spectra for **92a** (blue solid line) and **92b** (blue dashed line) measured at

668 and 716 nm, respectively, are shown in Figure 69. Both excitation spectra are superimposable with their absorption spectrum and, therefore, indicated the presence of one light-absorbing species. The peak at 358 nm in the excitation spectrum of **92b** was ascribed to Rayleigh scattering (half of the value of the emission wavelength). The fluorescence quantum yields for compounds **62**, **92a**, and **92b** were determined in CHCl_3 and the obtained values are below 1% ($\Phi_{\text{fl}} < 0.01$) for **62** and **92b**. For compound **92a**, a FQY of 1.2% ($\Phi_{\text{fl}} = 0.012$) was measured.

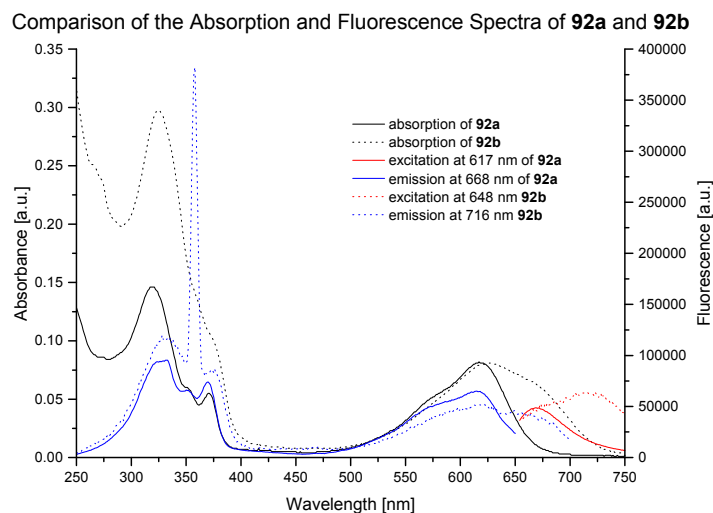


Figure 69 Absorption (**92a**: black solid line; **92b**: black dotted line) and fluorescence spectra (**92a**: colored solid lines for excitation at 617 nm (red solid line) and emission at 668 nm (blue solid line); **92b**: colored dashed lines for excitation at 648 nm (red dashed line) and emission at 716 nm (blue dashed line)) recorded in CHCl_3 at room temperature.

The absorption spectra, as displayed in Figure 70, of **63** (blue line; $c = 13.1 \mu\text{M}$) and **103** (red line; $c = 40.3 \mu\text{M}$) have the same profile, observation similar to the comparison of the phenylamino derivatives **62** and **92a**.

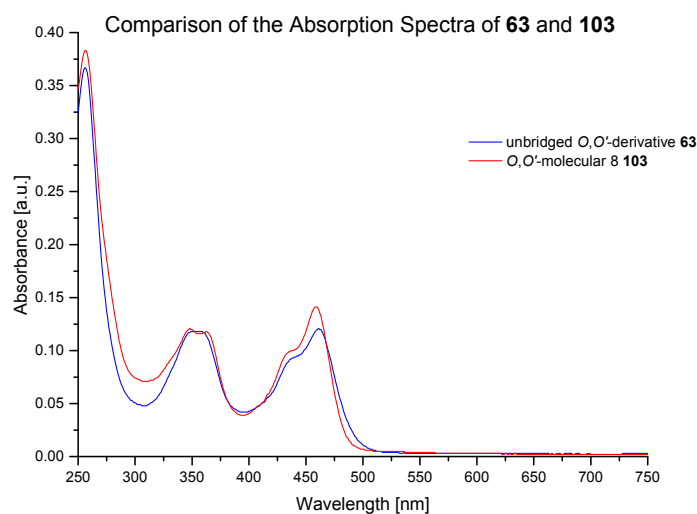


Figure 70 Absorption spectra of **63** (blue line; $c = 13.1 \mu\text{M}$,) and **103** (red line; $c = 40.3 \mu\text{M}$) recorded in CHCl_3 at room temperature.

Both structures have absorption bands between 300 and 400 nm, which were attributed to the $\pi \rightarrow \pi^*$ transition of the NDI chromophore. The presence of an oxygen core substituent causes a significant blue shift of the absorption band (400–500 nm) compared to a phenylamino or a phenylsulfanyl core substituent. The emission spectrum of **103** (excitation at 459 nm), emission band with a maximum at 529 nm was observed. The excitation spectrum at 529 nm was also measured and is shown in Figure 71. The excitation spectrum is superimposable with the absorption spectrum, an observation, which indicates that only one light-absorbing component is present.

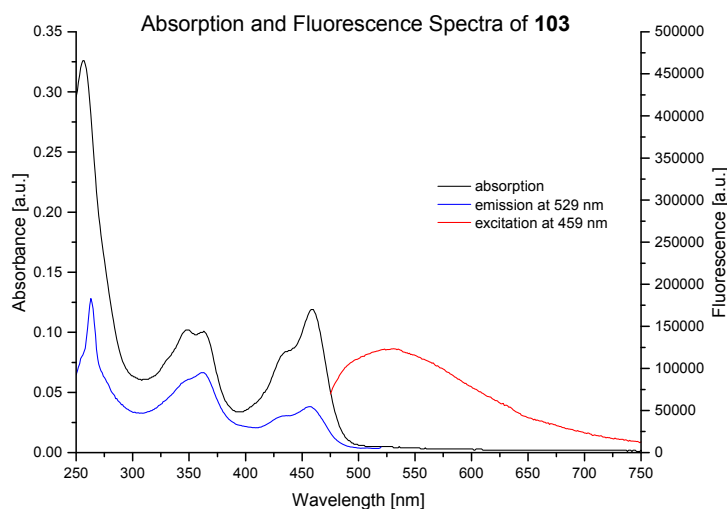


Figure 71 Absorption (black line; $c = 40.3 \mu\text{M}$) and fluorescence (colored lines; emission at 529 nm (blue line), and excitation at 459 nm (red line)) spectra of **103** recorded in CHCl_3 at room temperature.

The FQYs for compounds **103** and **63** were determined in CHCl_3 and the values are below 1% ($\Phi_{\text{fl}} < 0.01$) and 1% ($\Phi_{\text{fl}} = 0.01$) for **63** and **103**, respectively.

As discussed in Chapter 1.3.1, the core substituent can significantly change the absorption band maximum.

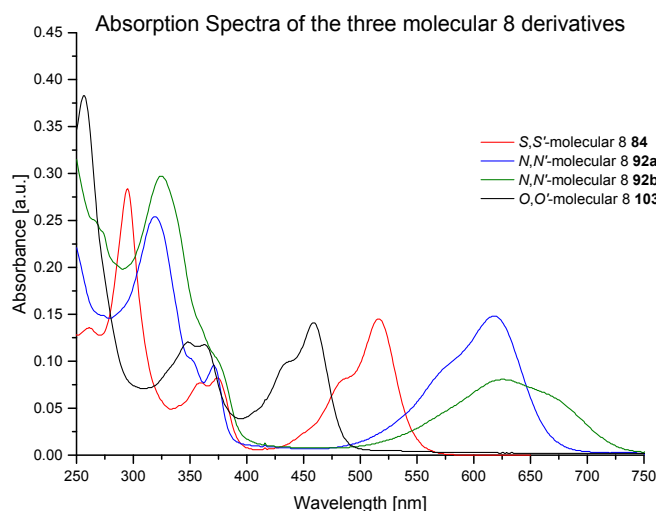


Figure 72 Absorption spectra of **84** (red line; $c = 7.89 \mu\text{M}$), **92a** (blue line; $c = 21.8 \mu\text{M}$), **92b** (green line; $c = 52.8 \mu\text{M}$), and **103** (black line; $c = 40.3 \mu\text{M}$) recorded in CHCl_3 at room temperature.

A bathochromic shift of the charge-transfer band, as displayed in Figure 72, was observed when the phenylsulfanyl core substituent (red line; 450–550 nm) was exchanged for the phenylamino core substituent (blue and green lines; 500–750 nm). Whereas, the introduction of a phenoxy core substituent (black line; 400–500 nm) led to a hypsochromic shift of the charge-transfer band. Table 3 gives an overview of the optical properties of the NDIs presented in this section.

Name	λ_{abs} [nm]	ϵ_{max} [$\text{mol}^{-1} \cdot \text{dm}^3 \cdot \text{cm}^{-1}$]	λ_{em} [nm]	FQY [%]	Stokes Shift [nm]
37	357	10017			
	373	10947			
	522	16626	605	< 1	83
84	359	9886			
	374	10554			
	516	18635	548	< 1	32
62	352	7769			
	371	7552			
	621	10811	707	< 1	86
92a	320	11877			
	371	4390			
	617	6697	668	1.2	51
92b	325	5700			
	625	1155	716	< 1	51
63	356	9387			
	461	9651	536	< 1	75
103	348	2944			
	363	2892			
	459	2943	529	1.0	70

Table 3 Optical properties of **37**, **62**, **63**, **84**, **92a**, **92b**, and **103** recorded in CHCl_3 at room temperature.

3.2.8 Transient-Absorption Spectra

All molecular 8 derivatives displayed FQY values of around 1% or below 1%. *S,S'*-Molecular 8 **84** was investigated in more detailed in collaboration with Dr. Igor Pugliesi from the research group of Prof. Dr. Eberhard Riedle at the LMU. Time-resolved absorption spectra after excitation at 522 nm of **37** (Figure 73; left) and **84** (Figure 73; right) were measured and lifetimes of the full-CT state of 6.50 and 8.39 ps, respectively, were found using the model function for stable fits as described in Equation 2. By the comparison of the transient-absorption spectra of **37** and **84**, it becomes evident that **84** features an extended lifetime of the full-CT state. The transient-absorption spectra of **84** collected after 0.3 ps (red lines) and 1.0 ps (black line) have almost identical profiles, whereas in the case of **37**, the decay still progresses after 1 ps, which is indicated by the different shapes of the absorption band maximum at 684 nm. The transient-absorption spectrum of **84** collected after 5 ps (purple line) has still a small absorption band maximum at 648 nm. Such a small absorption band maximum is not observed in the transient-absorption spectrum of **37** and is therefore an indication of the progressed decay of the full-CT state in the case of **37**.

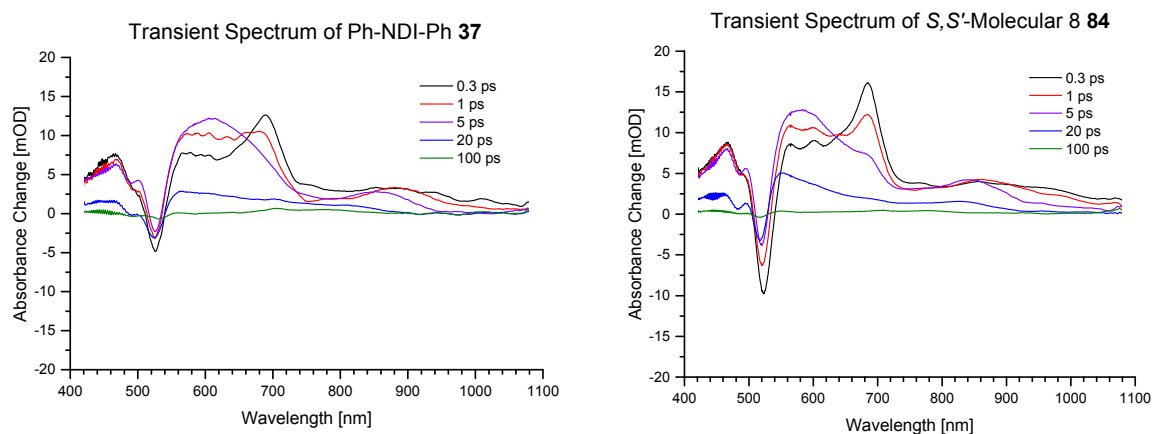


Figure 73 Transient-absorption (excitation at 522 nm) spectra of **37** (left) and **84** (right). After 5 ps a small peak (purple line at 684 nm) was still visible in case of **84**, whereas, in **37** such a peak shape was not detectable. Therefore, this indicated an extended lifetime of the full CT state.

The measured value of 8.39 ps indicates that bridging of the core substituents has an influence on the full-CT rate and, thus, proves the proposed hypothesis. Unfortunately, the effect is not as distinct as expected but the observed tendency points in the right direction.

4 Synthesis and Properties of Linear cNDIs

The second objective of this thesis was (a) to design and synthesize two core-substituted NDIs with a protected sulfur anchoring group and short alkylamino substituents, (b) to study a next step the optical properties of these two linear cNDIs, and (c) to attach these linear cNDIs to two gold electrodes in a SBJ setup and measure for the first time conductance enhancement on the single molecule level. The origin of the enhancement effect should arise from the excitation of electrons from the HOMO to the LUMO state of the cNDI by irradiation with a laser beam.

4.1 General Synthetic Strategy

4.1.1 Molecular Design

For the purposes of our investigation, cNDIs must have the following characteristics:

- Absorb visible light above 530 nm to prevent light absorption by gold electrodes.
- Possess small HOMO–LUMO band gap of approximately 2 eV. A band gap larger than 2 eV will require the use of energetically stronger light sources and, consequently, the use of shorter wavelength, which will ultimately lead to absorption of light by gold electrodes.
- Be conductive by an order of magnitude higher compared to no molecule in the gap. If this requirement is fulfilled, the electronic device limitation, also referred to as amplification limitation, can be excluded and reliable data are obtained.
- Be equipped with two anchoring groups, which can bind covalently to the two gold electrodes in the SBJ setup.

To fulfill the first three requirements, cNDIs (Figure 74) with short aliphatic amine-core-substituents, namely, ethylamine (**110**) and dimethylamine (**111**), were chosen for the investigation.

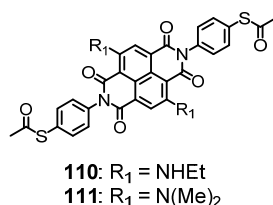
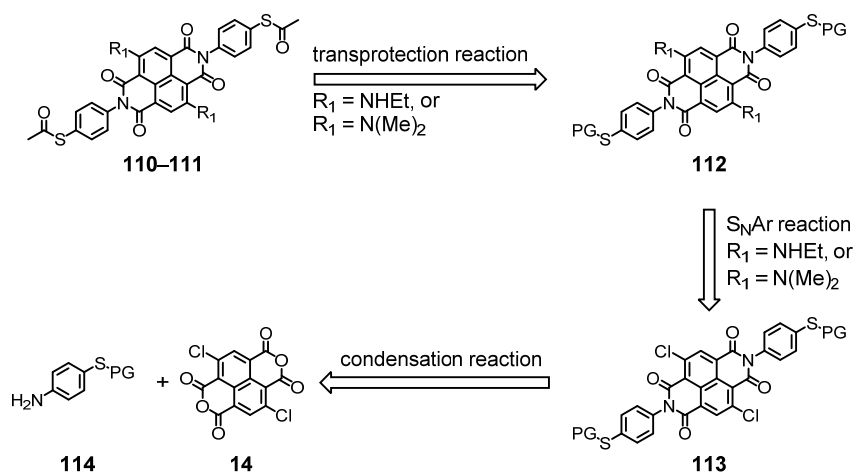


Figure 74 Structure of cNDIs **110** and **111**.

cNDIs **110** and **111** absorb red light at around 620–650 nm and possess a small HOMO–LUMO band gap of about 2 eV. As described in Chapter 1.4.3, a thiol substituent is the anchoring group of choice in molecular junctions. The thiol group is usually introduced as thioester, which can be easily cleaved to obtain the free thiol.^[283]

4.1.2 Retrosynthetic Analysis

Retrosynthetically, the acetyl-protected cNDIs **110** and **111**, as illustrated in Scheme 24, can be obtained in the final step by a transprotection reaction of cNDI **112**. Structure **112** can be obtained from a S_NAr reaction of **113**, which introduces the aliphatic amine (dimethylamine and ethylamine) on the NDI core. The key building block **113** can be obtained by a condensation reaction of the protected amine **114** with compound **14**. Last but not least, the thiol-protected amine **114** must be synthesized using a suitable protocol.



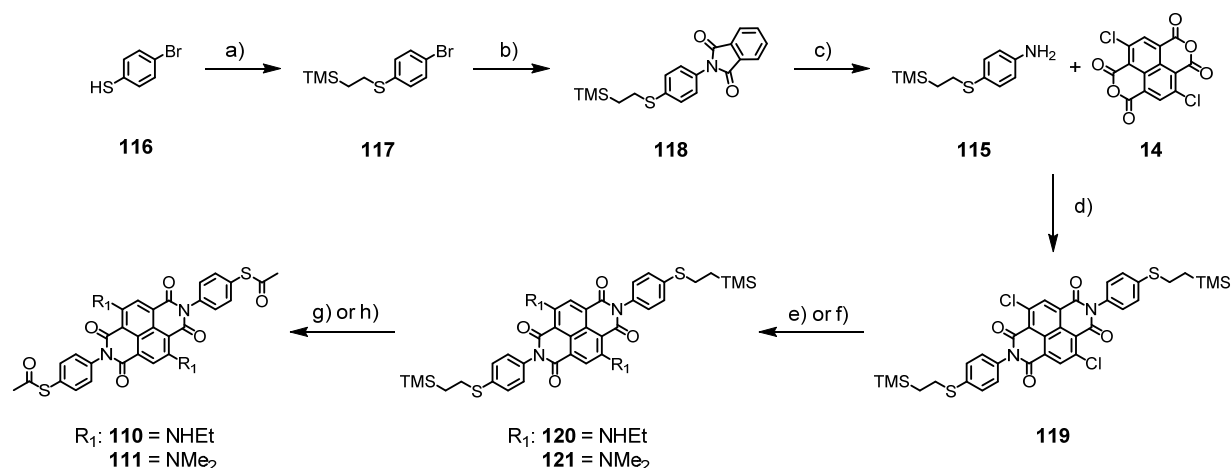
Scheme 24 Retrosynthetic analysis of the synthesis of cNDIs **110** and **111**.

4.2 Results and Discussion

4.2.1 Synthesis of Linear cNDIs

The synthetic approach to assemble 4-((2-(trimethylsilyl)ethyl)thio)aniline (**115**) started with the introduction (Scheme 25) of the 2-(trimethylsilyl)ethyl (TMSE) protective group in 4-bromothiophenol (**116**) via a radical reaction^[284] to obtain 2-((4-bromophenyl)thio)ethyltrimethylsilane (**117**) as a colorless liquid in 91% yield. The following two steps of the synthetic approach were developed by Reinders^[285] in our research group. The first step included a copper(I)-mediated introduction of phthalimide into **117** to yield *N*-((4-(2-(trimethylsilyl)ethyl)thio)phenyl)-phthalimide (**118**) as a yellow solid in 85%. A subsequent work-up by the Ing–Manske procedure with hydrazine afforded **115** as a colorless liquid in 94% yield. The condensation reaction of **118** with **14** in AcOH at 124 °C afforded the key building block, *N,N'*-di-((4'-(2'-trimethylsilyl)ethyl)thio)phenyl)-2,6-dichloro-1,4,5,8-naphthalenetetracarboxylic acid diimide (**119**), as a yellow solid in 21% yield. The key building block **119** was on the one hand converted to *N,N'*-di-((4'-(2'-trimethylsilyl)ethyl)thio)phenyl)-2,6-bis(ethylamino)-1,4,5,8-naphthalenetetracarboxylic acid diimide (**120**) in 54% yield and on the other hand to *N,N'*-di-((4'-(2'-trimethylsilyl)ethyl)thio)phenyl)-2,6-bis(dimethyl-

amino)-1,4,5,8-naphthalenetetracarboxylic acid diimide (**121**) in 63% yield. Both compounds were isolated as blue solids.



Scheme 25 Synthesis of cNDIs **110** and **111** applying: a) vinyltrimethylsilane, cat. DTBP, 105 °C, 24 h; b) phthalimide, Cu₂O, 2,4,6-collidine, 175 °C, 60 h; c) H₂NNH₂ · H₂O, CH₂Cl₂/THF/MeOH 6:1:1, 50 °C, 30 min; d) AcOH, 124 °C, 35 min; e) EtNH₂ (2 M in THF), DMF, 125 °C, 12 h; f) NH(Me)₂ (2 M in THF), DMF, 125 °C, 11 h; g) 1) **120**, TBAF (1 M in THF), THF, rt, 1.2 h, 2) AcCl, 0 °C, 20 min to yield **110**; h) **121**, AgBF₄, AcCl, CH₂Cl₂, rt, 15 h to yield **111**.

The transprotection reaction of **120** to afford *N,N'*-di-(4'-(acetylsulfanyl)phenyl)-2,6-bis(ethylamino)-1,4,5,8-naphthalenetetracarboxylic acid diimide (**110**) was successfully performed by stirring **120** in a solution of tetra-*n*-butylammonium fluoride (TBAF; 1 M in THF) and THF^[286,287] at room temperature for 1.2 h, before AcCl was added. After several chromatographic purification steps, **110** was obtained as a blue solid in 51% yield. The transprotection reaction yielded as side product the dealkylated structure **122** (Figure 75), which was proved by ESI-MS analysis. Both compounds, **110** and **122**, were successfully separated by column chromatography on silica gel. A further drawback of this transprotection reaction was the decreasing yield with increasing reaction scale and, therefore, the transprotection reagent was changed to AgBF₄ in CH₂Cl₂.^[288,289] Unfortunately, this approach did not lead to the desired success and only starting material was reisolated.

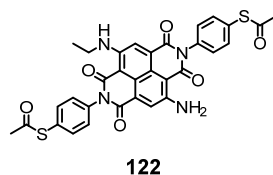


Figure 75 The dealkylated side product **122** of the transprotection reaction of **120**.

The transprotection reaction of **121** to yield *N,N'*-di-(4'-(acetylsulfanyl)phenyl)-2,6-bis(dimethylamino)-1,4,5,8-naphthalenetetracarboxylic acid diimide (**111**) was accomplished by using AgBF₄ in CH₂Cl₂ and afforded the pure product as a blue solid in 79% yield.

4.2.2 Investigation of the Cleavage of the Protective Groups

The cleavage of the *o* thioester PGs in **111** was investigated with four different deprotection reagents (Table 4).

Entry	Reagent	Solvent	Temp.	Time	MALDI-TOF-MS
1	MeOH, AcCl	CH ₂ Cl ₂	0 °C to rt	2.5 h	only starting material
2	KOH	CH ₂ Cl ₂ and MeOH	45 °C	2 h	cleavage of PG
3	NEt ₃	TFA/CH ₂ Cl ₂ 3:1	rt	5 h	only starting material
4	TBAH (40% in H₂O)	THF	rt	16 h	only product

Table 4 Different investigated deprotection reagents to cleave the thioester PGs in **111**.

Entry 1 in Table 4 is a deacetylation method developed by Teweri et al.^[290] using acetyl chloride in methanol to create in-situ HCl which initiate the cleavage of the protective groups. In our case, however, this approach did not lead to the desired success. In entry 2 of Table 4, the starting material was added to a mixture of KOH, CH₂Cl₂, and MeOH. This solution was stirred at 45 °C for 2 h and subsequently neutralized with HCl (1 M). After the work-up, the crude reaction mixture was analyzed by MALDI-TOF MS. The signal for the molecular mass of the starting material disappeared, but no signal corresponding to the desired product was observed. Therefore, decomposition of the starting material can be assumed. Hummelen et al.^[283] investigated the formation of high-quality SAMs with the help of no base, triethylamine, tetrabutylammonium hydroxide (TBAH), KOH, and pyrrolidine as deprotection reagent. They reported the best results with triethylamine and good results with Bu₄NOH. In the latter case, the quality of the SAMs had a concentration dependency. These two deprotection reagents were subsequently investigated for the removal of the PGs in **111**. The successful cleavage of the PGs was only achieved with TBAH (Table 4; entry 4) and not with NEt₃ (Table 4; entry 3) as deprotection reagent.

4.2.3 Origin of the High Efficiency of the TMSE Protective Group Cleavage

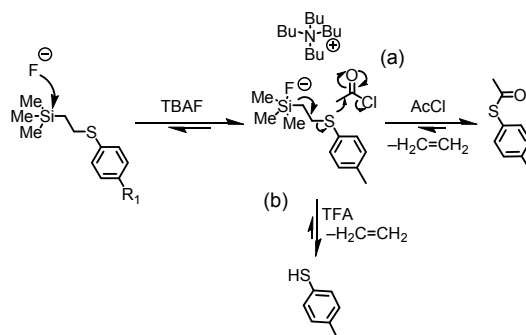
The high efficiency of the cleavage (Scheme 26) of the TMSE-PG from the thiol moiety via a β -elimination with a fluorine source is as a result of (a) the rapid attack of the hard nucleophilic fluorine anion, (b) the formation of the strong Si–F bond, and (c) the β -effect.

The length of the C–Si bond (1.89 Å) is longer than the one of the C–C bond (1.53 Å) and, therefore, the attack of the nucleophile is facilitated.^[272] Moreover, the electronegativity value of silicon (1.9 χ^P) is lower than the one for carbon (2.6 χ^P) and, as a consequence, the C–Si bond is polarized. This makes the silicon atom more accessible to be attacked by the nucleophile^[291] and, thus, this marks the first driving force of the efficient deprotection reaction.

The strength of a homonuclear Si–Si bond (226 kJ/mol) is lower than the one of a homonuclear C–C bond (346 kJ/mol). The opposite is the case of heteronuclear bonds, namely, the strength of a Si–O bond (466 kJ/mol) is higher than the one of the C–O σ -bond (359 kJ/mol).^[291] The same tendency is observed when the strength of a Si–F bond (582 kJ/mol) and a C–F bond (485 kJ/mol) are compared. The formation of the strong Si–F bond, which is more stable (97 kJ/mol) than the C–F bond, marks the second driving force of this reaction.

The third driving force, namely, the β -effect, arises from the stabilization of the positive charge of a carbocation in β -position to silicon by donation of electron density from the filled σ -orbital of silicon to the empty p-orbital of carbon, also referred to as Si–C hyperconjugation.^[292] The maximum overlap of the two orbitals occurs only if the empty p-orbital and the filled σ -orbital are in the same plane, which is more likely in case of acyclic systems and, consequently, its efficiency decreases from acyclic to cyclic systems.

Mechanistically, the β -elimination reaction (Scheme 26) starts with the nucleophilic attack of a fluorine anion (e.g. from a fluorine source like TBAF) to form a pentavalent silicon center. As a result of the β -elimination, Si(CH₃)₃F, ethene, and the TBAF salt are formed. The TBAF salt can be in-situ (a) converted to the thioester (transprotection) by the addition of AcCl, or (b) transformed to the free thiol (deprotection) with a strong acid such as TFA.



Scheme 26 Main mechanism of the TMSE PG cleavage and the subsequent trapping of the TBAF salt with (a) AcCl to perform a transprotection reaction (upper pathway), or (b) TFA to conduct a deprotection reaction (lower pathway).

4.2.4 Optical Properties

A comparison of the absorption spectra of 2,6-bis(ethylamino)-cNDI **110** (Figure 76; blue line; $c = 11.5 \mu\text{M}$) and 2,6-bis(dimethylamino)-cNDI **111** (Figure 76; red line; $c = 10.8 \mu\text{M}$) shows a red-shift of the core-substituent transition band (620 nm) and a blue-shift of the $\pi \rightarrow \pi^*$ transition bands (363 nm and 346 nm) of the NDI chromophore in the case of **110** compared to **111** (608 nm, 368 nm, and 352 nm, respectively).

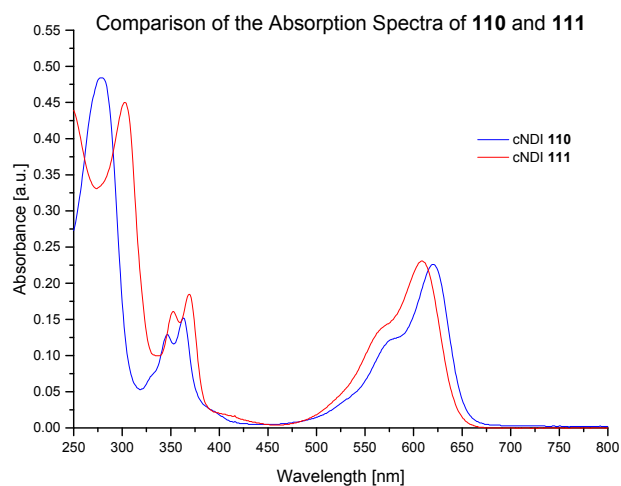


Figure 76 Absorption spectra of **110** (blue line; $c = 11.5 \mu\text{M}$) and **111** (red line; $c = 10.8 \mu\text{M}$) recorded in CHCl_3 at room temperature.

Other than these two shifts, both spectra have almost identical profile. Both compounds have similar molar absorption coefficients. The FQYs of both compounds were determined. A high FQY of 45% ($\Phi_{\text{fl}} = 0.45$) was observed in case of **110**. For **111**, a FQY of less than 1% ($\Phi_{\text{fl}} < 0.01$) was measured. This finding can be clearly attributed to the fact that there is no hydrogen atom available at the amine functionality of structure **111**, which can be used for hydrogen bonding with the oxygen atom of the carbonyl functionality (see Chapter 1.3.1).

Table 5 gives an overview of the optical properties of **110** and **111**.

Name	λ_{abs} [nm]	ϵ_{max} [$\text{mol}^{-1} \cdot \text{dm}^3 \cdot \text{cm}^{-1}$]	λ_{em} [nm]	FQY [%]	Stokes shift [nm]
110	346	11013			
	363	12979			
	620	19604	644	45	24
111	352	14379			
	368	16565			
	608	21210	636	< 1	28

Table 5 Optical properties of **110**, and **111** recorded in CHCl_3 at room temperature.

4.2.5 Physical Properties

Each synthesized cNDI fulfills the requirement (a) to have the core-substituent absorption band maximum above 530 nm, and (b) to bear sulfur protected anchoring groups. The cleavage of the protecting groups was successfully probed and squeezable break junction measurements of these cNDIs were thus performed in collaboration with the research group of Dr. Selzer at the Tel Aviv University (TAU; carried out by Michal Vadai). In the SBJ setup base-line conductance (Figure 77) of $0.40 \text{ m}G_0$ was measured for **110** without illuminating the sample with light. Therefore, the two requirements (c) and (d) described in Chapter 4.1.1 were fulfilled.

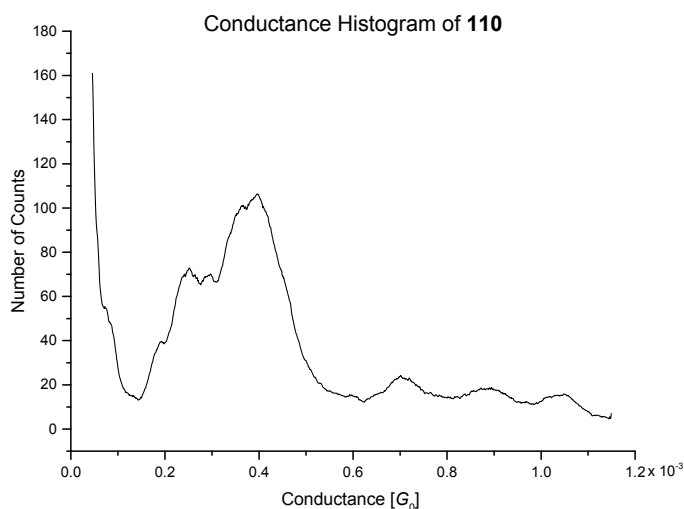


Figure 77 The measured conductance histogram of cNDI **110** in a SBJ setup with a conductance maximum of $0.40 \text{ m}G_0$. The measurement was performed without illuminating the sample with light.

Conductance measurements of **110** and **111** (Figure 78) in the SBJ setup upon laser illumination were cumbersome because heat formation occurred as a side effect.

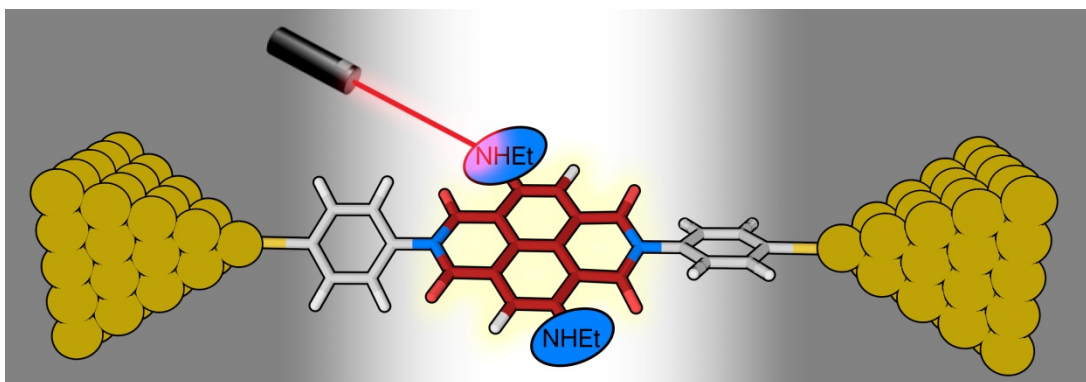


Figure 78 Schematic drawing of cNDI **110** attached to two gold electrodes in a SBJ setup and being illuminated with a laser beam.

This side effect caused expansion of the metallic electrodes and, as a consequence, the measured conductivities were higher. There were also issues with detecting small electrical signals during the measurements and, therefore, more data cannot be provided in this doctoral thesis.

5 Synthesis and Properties of Photoswitchable NDI-Phanes

The third objective of this thesis was (a) to design and synthesize two rigid NDI-phanes containing either a stilbene or an azobenzene moiety; (b) to study in a next step the photoinduced $E \rightarrow Z$ isomerization process as well as the reverse ($Z \rightarrow E$) isomerization reaction in both systems; (c) to deposit such NDI-phanes on a metallic surface upon electrospray ionization; and (f) to investigate the isomerization processes upon external stimuli, such as application of current or irradiation with light.

5.1 General Synthetic Strategy

5.1.1 Molecular Design

The following requirements were considered during the design of photoswitchable NDI-phanes to allow for their immobilization on a metallic surface:

- Be stable against thermal evaporation under ultrahigh vacuum (UHV) or be ionizable with electrospray ionization (ESI) to immobilize the photoswitchable NDI-phere on a silver surface.
- Possess a photoswitchable moiety, which can undergo photoinduced $E \rightarrow Z$ and $Z \rightarrow E$ isomerization processes.
- Be equipped with a platform, which can be deposited on a metallic surface.
- Interlinking of the platform and the photoswitchable unit is necessary to (1) create strain into the molecule and, thus, disfavor the reverse $Z \rightarrow E$ isomerization reaction; and (2) decouple the photoswitchable unit from the metallic surface and, thereby, avoid quenching of the excited state by the metallic surface.

To fulfill the requirements (b–d), a phane-like structure with a NDI platform and a stilbene or an azobenzene unit as photoswitchable moiety (Figure 79a; X corresponds to carbon atom in case of stilbene, or X corresponds to nitrogen atom in case of azobenzene) is preferred. A NDI platform is envisioned to be used on the basis of its ability to self-assemble on metallic surfaces as shown by Mayor et al.^[293] The self-assembly process is caused by (a) the planarity of the NDI core, and (b) intermolecular hydrogen bondings.

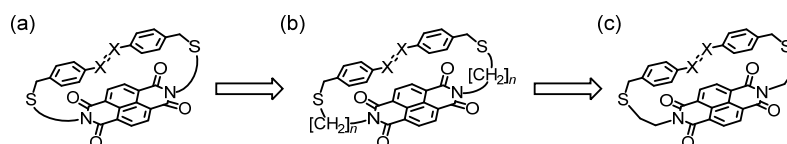


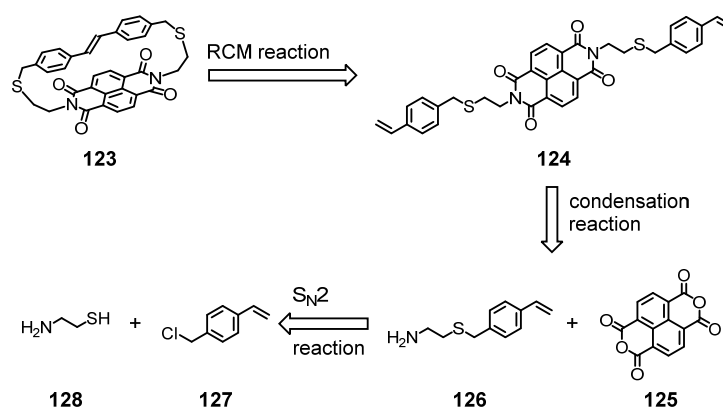
Figure 79 Fulfilment of the above-described requirements results in a structure as shown in (c). X corresponds either to carbon atom in case of a stilbene moiety or to nitrogen atom in case of an azobenzene moiety.

Stilbene and azobenzene moieties are chosen because of (1) their accessibility via established synthetic methods, and (2) the various examples of their successful integration into molecular

switches as described in Chapter 1.5. The interlinking (Figure 79b) of the two moieties can be achieved by a bridge. To keep the molecular structure of the bridge as simple as possible, an alkyl chain is chosen to connect the NDI platform to the switching moiety. For this purpose, the shortest commercially available amine-(CH₂)_n-thiol, 2-aminoethanethiol, is selected (Figure 79c).

5.1.2 First Generation Retrosynthetic Analysis of a NDI-Stilbenophane

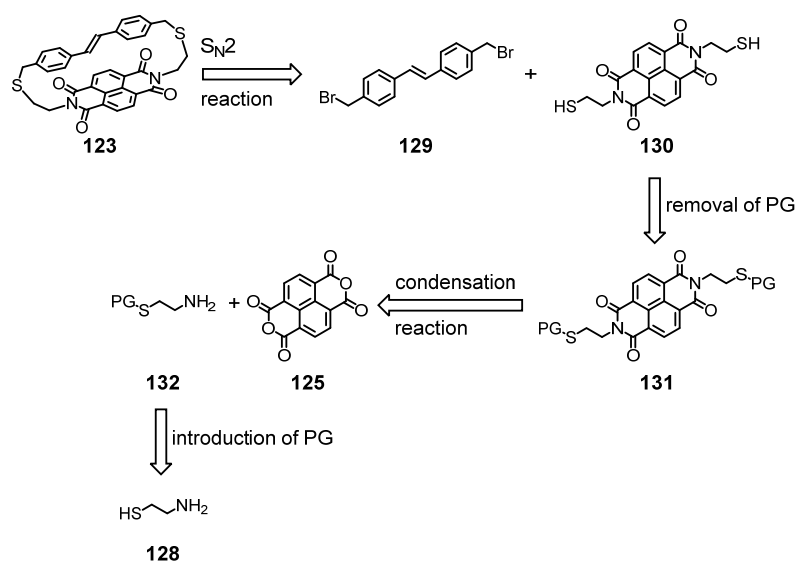
Retrosynthetically, NDI-stilbenophane **123** (Scheme 27) can be obtained by a ring-closing metathesis (RCM) reaction of vinylic NDI **124**. The vinylic NDI **124** can be obtained from a condensation reaction of 1,4,5,8-naphthalenetetracarboxylic dianhydride (**125**) with 2-((4-vinylbenzyl)thio)ethan-1-amine (**126**). Compound **126** can be obtained by a bimolecular nucleophilic substitution (S_N2) reaction of 1-(chloromethyl)-4-vinylbenzene (**127**) with 2-aminoethanethiol (**128**).



Scheme 27 Retrosynthetic analysis of the 1st generation synthesis of stilbenophane **123**.

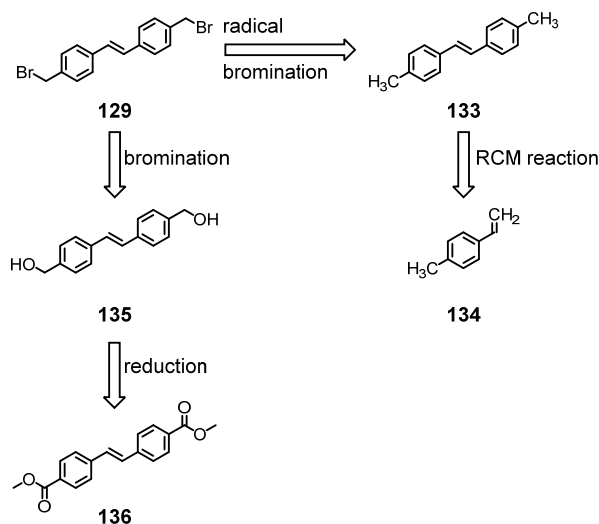
5.1.3 Second Generation Retrosynthetic Analysis of a NDI-Stilbenophane

Retrosynthetically, NDI-stilbenophane **123** (Scheme 28) can be obtained by a S_N2 reaction of (*E*)-1,2-bis(4-(bromomethyl)phenyl)ethane (**129**) with the bisthiol NDI **130**.



Scheme 28 Retrosynthetic analysis of the 2nd generation synthesis of stilbenophane **123**.

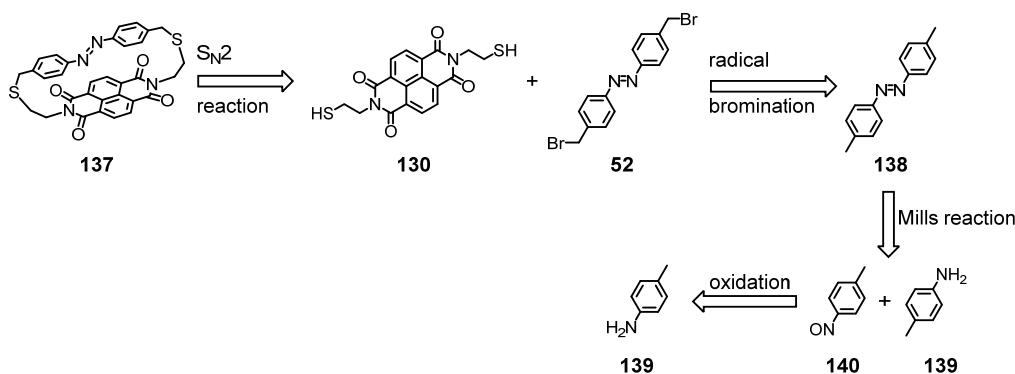
The bisthiol **130** can be obtained from the removal of the protective groups in NDI **131** and a prior condensation reaction of NDA **125** with a *S*-protected 2-aminoethanethiol **132**. Structure **132** can be obtained after the introduction of an appropriate PG into structure **128**. The second building block (Scheme 29) **129** can be obtained (a) by radical bromination of (*E*)-1,2-di-*p*-tolylethene (**133**) and a prior cross metathesis (CM) reaction of 4-vinyltoluene (**134**) with an appropriate Grubbs catalyst, or (b) by bromination of (*E*)-(ethene-1,2-diylbis(4,1-phenylene))dimethanol (**135**) and a previous reduction of dimethyl 4,4'-(ethene-1,2-diyl)(*E*)-dibenzoate (**136**).



Scheme 29 Retrosynthetic analysis of the synthesis of **129** revealed two possible routes.

5.1.4 Retrosynthetic Analysis of NDI-Azobenzenophane

Retrosynthetically, NDI-azobenzenophane **137** (Scheme 30) can be obtained from a S_N2 reaction of (*E*)-1,2-bis(4-(bromomethyl)phenyl)diazene (**52**) with the bisthiol **130**. The retrosynthetic analysis of the bisthiol **130** corresponds to the one discussed in Chapter 5.1.3. The key building block **52** can be obtained after radical bromination of (*E*)-1,2-di-*p*-tolyl-diazene (**138**).



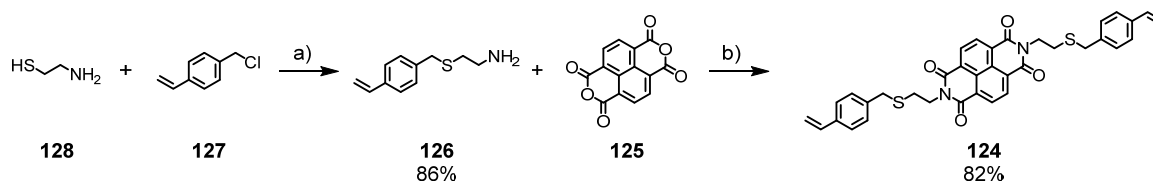
Scheme 30 Retrosynthetic analysis of the synthesis of azonbenzenophane **137**.

Compound **138** is afforded after a Mills reaction of 4-aminotoluene (**139**) with the corresponding nitroso derivative of **139**. The nitroso derivative **140** can be obtained by oxidation of **139**.

5.2 Results and Discussion

5.2.1 First Generation Synthesis of a NDI-Stilbenophane

The initial reaction (Scheme 31) of the first generation approach was the preparation^[294] of **126** by stirring **127** and **128** under basic conditions at room temperature for 16 h and was accomplished in a yield of 86%. The following microwave-assisted condensation reaction of **125** with **126** in DMF at 120 °C afforded *N,N'*-di-(2-((4-vinylbenzyl)thio)ethyl)-1,4,5,8-naphthalenetetracarboxylic acid diimide (**124**) as a yellow solid in 82% yield.



Scheme 31 Towards the synthesis of NDI-Stilbenophane **123** applying: a) KOH, H₂O/MeOH, 0 °C to rt, 16 h; b) DMF, MW, 120 °C, 4 h.

Subsequently, different reaction conditions for the RCM reaction were investigated, such as (a) solvent (CHCl₃, EDC, and PhMe); (b) reaction temperature (40 °C, 60 °C, and 105 °C); (c) catalyst (first generation Grubbs catalyst and second generation Grubbs catalyst); and (d) concentration (2 to 100 mM). In all cases, however, no product formation was observed. Beside the reisolation of the starting material the side product **141**, as displayed in Figure 80, was isolated as well, which was confirmed by HR-ESI-TOF-MS analysis and ¹H-NMR spectroscopy.

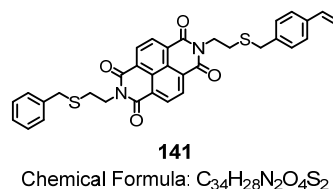
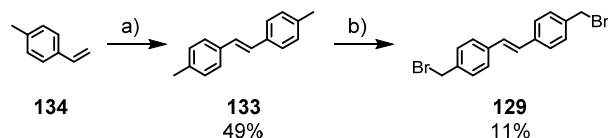


Figure 80 Structure of the side product **141** of the RCM reaction of **124** obtained under various conditions.

5.2.2 Second Generation Synthesis of a NDI-Stilbenophane

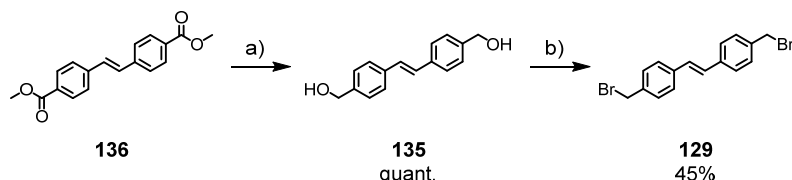
Two synthetic protocols for the preparation of **129** were literature known. The first approach (Scheme 32) to synthesize **129** started with a CM reaction^[295] of **134** to yield **133** and was achieved in 49% yield using second generation Grubbs catalyst. The subsequent radical bromination^[296] of **133** to yield **129** as a white solid was carried out by using CCl₄ as solvent and azobisisobutyronitrile (AIBN) as radical initiator. The separation of the product from the over brominated side product and starting material was performed by repeated column chromatography on silica gel and not by recrystallization because the purity of the desired product after recrystallization was not sufficient. A milder method, which should prevent over-bromination of the starting material, is the use of a halogen lamp (500 W) as energy source and methyl formate as solvent. By

using this method, however, no conversion towards **129** was observed according to TLC analysis, and mainly starting material was reisolated after the purification by column chromatography on silica gel. In conclusion, all attempts to increase the yield above 11% (lit.^[297] 17%) were unsuccessful.



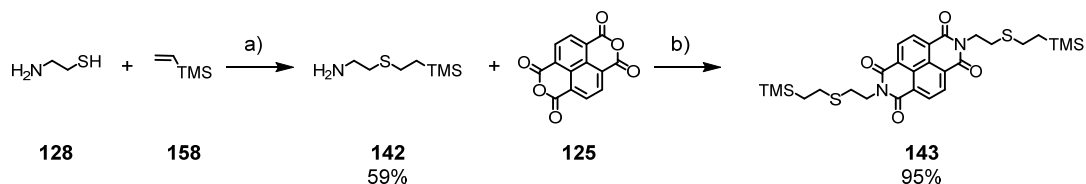
Scheme 32 1st approach of the synthesis of **129** applying: a) 2nd generation Grubbs catalyst, CH₂Cl₂, 50 °C, 17 h; b) NBS, AIBN, CCl₄, 85 °C, 16 h.

The problem of the low overall yield and the difficult purification procedure was overcome by changing the synthetic strategy (Scheme 33). Initially, **136** was reduced^[296] with LiAlH₄ in THF to **135** in 99% yield and, subsequently, converted^[296] to the key building block **129** with *N*-bromosuccinimide (NBS) and PPh₃ in THF in 45% yield.



Scheme 33 2nd approach of the synthesis of **129** applying: a) LiAlH₄, THF, 0 °C to rt, 20 h; b) NBS, PPh₃, THF, rt, 36 h.

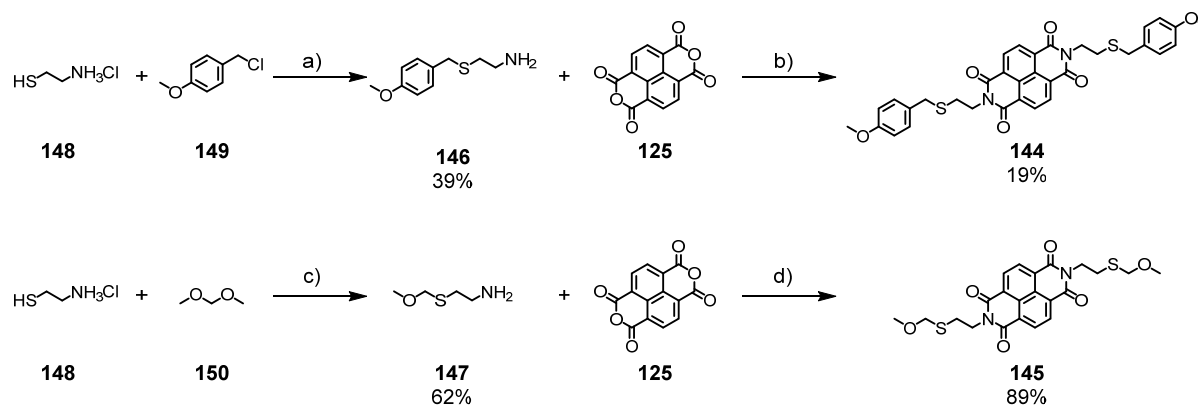
The assembly (Scheme 34) of the second building block, *N,N'*-di-(2'-thioethyl)-1,4,5,8-naphthalenetetracarboxylic acid diimide (**130**), started with the introduction^[298] of the TMSE PG into **128** by heating **158** and benzophenone in a 15:1 mixture of THF/H₂O for 20 h with a halogen lamp (500 W). The product of this reaction, 2-((2-(trimethylsilyl)ethyl)thio)ethan-1-amine (**142**), was obtained as a yellow liquid after fractional distillation. The subsequent condensation reaction of **142** with **125** in DMF was carried out in a microwave reactor and yielded the desired product, namely, *N,N'*-di-((2'-((2-(trimethylsilyl)ethyl)thio)ethyl)-1,4,5,8-naphthalenetetracarboxylic acid diimide (**143**) as yellow solid in 95%.



Scheme 34 Synthesis of **143** applying: a) Ph₂CO, THF/H₂O, 500 W, 20 h; b) DMF, MW, 120 °C, 4 h.

The cleavage of the protective groups in **143** to afford **130** under highly acidic conditions (standard deprotection conditions), such as trifluoroacetic acid (TFA), could unfortunately not be achieved. Therefore, two other protective groups were investigated, namely, PMB and MOM. The synthesis (Scheme 35) of *N,N'*-di-((2'-((4'-methoxybenzyl)thio)ethyl)-1,4,5,8-naphthalenetetracarbo-

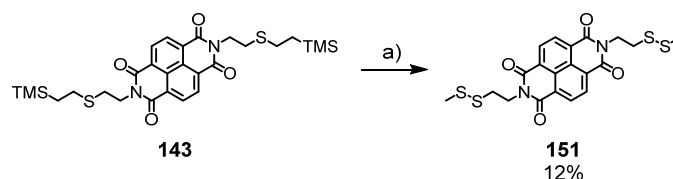
xylic acid diimide (**144**) started with the preparation of 2-((4-methoxybenzyl)thio)ethan-1-amine (**146**) and the synthesis of *N,N'*-di-(2'-((methoxymethyl)thio)ethyl)-1,4,5,8-naphthalenetetracarboxylic acid diimide (**145**) with the preparation of 2-((methoxymethyl)thio)ethan-1-amine (**147**). **146** was synthesized^[299] by stirring a mixture of LiOH, 2-aminoethanethiol hydrochloride (**148**), and 4-methoxybenzylchloride (**149**) in a 4:1 solution of EtOH/H₂O at 35 °C for 2 h and yielded the pure product as a white solid in 39%. A following condensation reaction of **125** with **146** in DMF at 130 °C was carried out in a microwave reactor and afforded **144** as a yellow solid in a moderate yield of 19%. After stirring a mixture of **148** and dimethoxymethane (**150**) at room temperature for 4 h, **147** was afforded^[300] as a colorless solid in 62% yield. The subsequent condensation reaction of **147** with **125** in DMF at 125 °C for 4 h in a microwave reactor yielded **145** as a white solid in a high yield of 89%. Having both target structure in hand, the removal of the PMP PGs in **145** and the MOM PGs in **146** under highly acidic conditions (TFA) was investigated, but in each case no cleavage of the PGs was detected by MALDI-TOF-MS analysis.



Scheme 35 Synthesis of **144** and **145** applying: a) LiOH, EtOH/H₂O, 35 °C, 2 h; b) DMF, MW, 130 °C, 2.5 h; c) rt, 4 h; d) DMF, MW, 125 °C, 4 h.

Moreover, the cleavage of the TMSE PG in **143** was attempted by using the two other standard conditions, namely, (a) AgBF₄ in CH₂Cl₂, and (b) TBAF (1 M) in THF, but no product formation was detected in both cases according to MALDI-TOF-MS analysis. It is known in the literature^[301,302] that the removal of the alkyl TMSE protective group is cumbersome and it can be overcome by using the method developed by Fuchs et al.^[301,303] In their synthetic approach, they first added dimethyl(methylthio)sulfonium tetrafluoroborate ([Me₃S₂]⁺BF₄⁻) to the TMSE protected starting material in the presence of an excess of dimethyl disulfide (Me₂S₂). The resulting reaction mixture was stirred at room temperature over night to yield the desired disulfide in a high yield. In a second step, the authors reduced the disulfide moiety with tributylphosphane to the free thiol in a quantitative yield. Consequently, the same synthetic method (Scheme 36) was applied on **143**. The transprotection reaction in THF as solvent to obtain *N,N'*-di-(2'-((methylthio)ethyl)-1,4,5,8-naphthalenetetracarboxylic acid diimide (**151**) was accomplished in a moderate yield of 12%.

Compared to the use of THF as solvent, a mixture of CH₂Cl₂/THF or pure CH₂Cl₂, did not afford the desired product in acceptable yields.



Scheme 36 Synthesis of **151** applying: a) [Me₃S₂]BF₄, Me₂S₂, THF, rt, 16 h.

The purification of the transprotection reaction turned out to be challenging for mainly two reasons (a) the substance is not detectable with a UV lamp, and (b) no functional groups are present in the molecule that can be stained with a TLC staining solution. Therefore, the yellow residue was first purified by a so-called column-chromatographic filtration over a plug of silica gel to isolate **151** and the monotransprotected side product **152** as a mixture. This mixture was subsequently separated by GPC (Figure 81) to obtain **151** purely as a yellow solid.

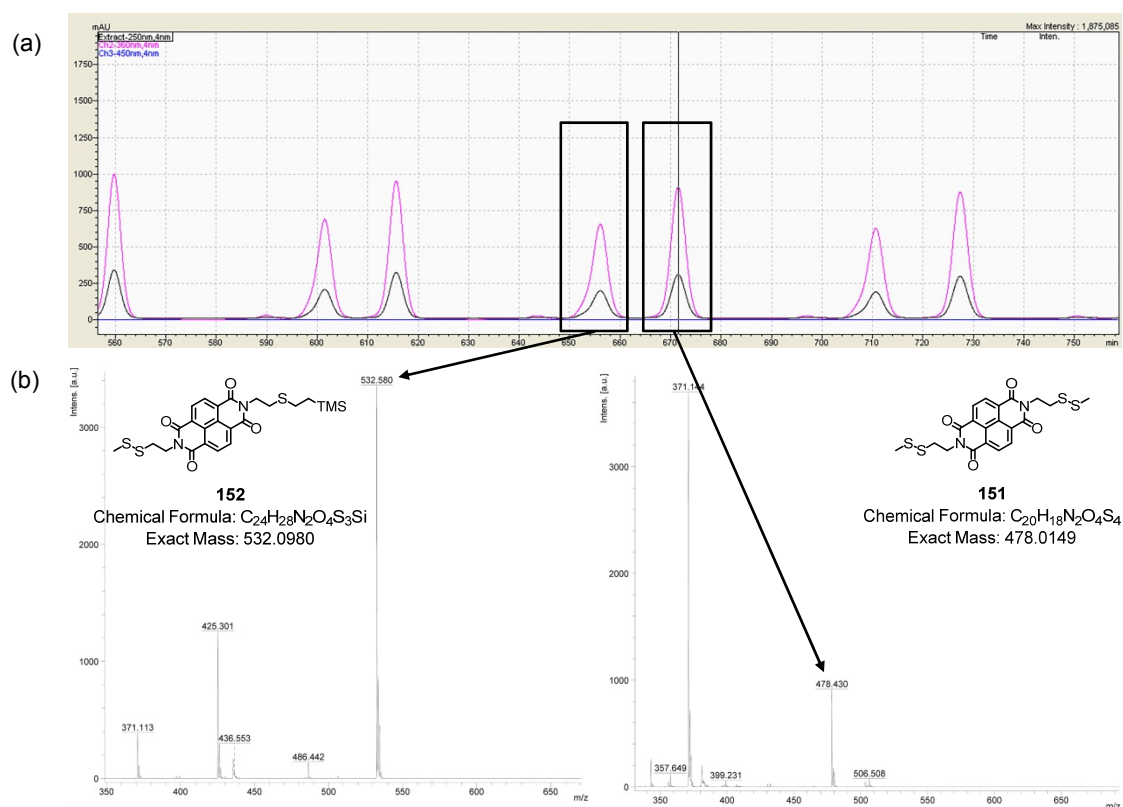
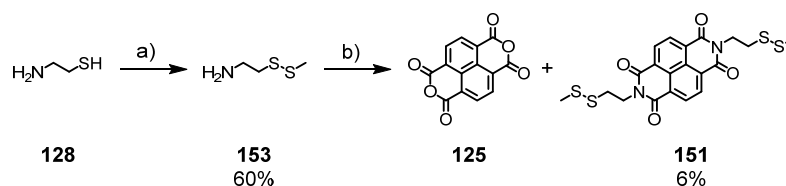


Figure 81 Successful isolation of **151** by GPC: (a) the UV/Vis absorption (top) spectrum at 250 (black line) and 360 nm (red line) of the purification run shows the successful separation of the **151** and **152**. The 1st fraction contained **152** and the 2nd fraction contained **151**; and (b) MALDI-TOF-MS analysis of both fractions was performed and verified the mass of **152** (left) and **151** (right) as displayed in the recorded mass spectra.

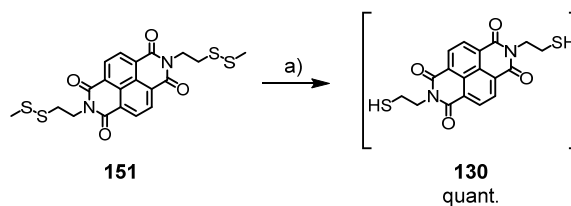
It was tried to improve the yield of this reaction sequence and, therefore, a second approach (Scheme 37) of the synthesis of **151** was developed. The synthesis started with the assembly of 2-(methyldisulfanyl)ethan-1-amine (**153**), which was prepared by stirring **128**, dimethyl disulfide,

and NEt_3 at 105 °C in a pressure vial. The literature known procedure^[304] yielded **153** as a colorless liquid in 60% yield.



Scheme 37 Synthesis of **151** applying: a) Me_2S_2 , NEt_3 , 105 °C, 15 h; b) DMF, 120 °C, 13 h.

The condensation reaction of **125** with **151** in DMF at 120 °C afforded **151** in low yield of 6% after using the same purification procedure as in the previous approach. Unfortunately, an improvement of the yield was not achieved and, consequently, this synthetic route was no longer considered. The reduction (Scheme 38) of the disulfide moiety in **151** was performed similar to Fuchs et al.^[301,303] with tributylphosphane in a 1:1 mixture of MeOH/THF to yield **130**. The progress of the reaction was monitored by MALDI-TOF-MS analysis and showed complete conversion after stirring the reaction mixture at room temperature for 2 h. The crude product was used without further purification in the final cyclization reaction.



Scheme 38 Synthesis of **130** applying: a) PBu_3 , MeOH/THF, rt 2 h.

The first approach to perform the final cyclization reaction (Scheme 39) consisted of the addition of **129** in DMF to a solution of DMF, **130**, and K_2CO_3 applying the so-called pseudo-high-dilution principle. Unfortunately, no product was isolated neither by using a fresh bottle of dry DMF nor by changing the base to Cs_2CO_3 . In each case, only **129** was reisolated, whereas **130** was not reisolated most likely due to decomposition of **130** in the course of the reaction or work-up.



Scheme 39 Unsuccessful synthesis of **123** applying: K_2CO_3 , DMF.

Generally, the rate r of an $\text{S}_{\text{N}}2$ reaction (Figure 82) is increased in polar aprotic solvents compared to polar protic solvents. Polar protic solvents, such as MeOH, will form hydrogen bondings to nucleophile and, as a result, lower its reactivity. Whereas, in case of polar aprotic solvents only weak interactions between the solvent molecules and the nucleophile occur and, thus, the nucleophile is more reactive. This effect is illustrated in Figure 82 by the comparison of the relative rate

of the S_N2 reaction in a polar protic solvent (MeOH) and different polar aprotic solvents, such as methanamide, DMF, and *N,N*-dimethylacetamide (DMA).

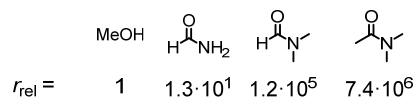
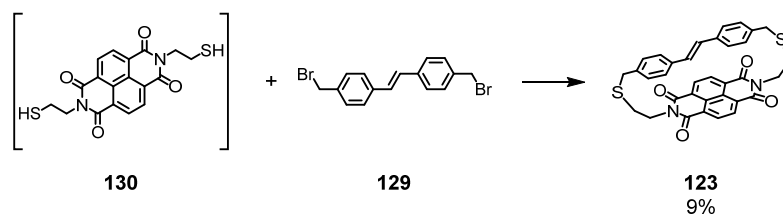


Figure 82 Comparison of the relative rate of the S_N2 reaction in different solvents. The lowest relative reaction rate was detected in case of MeOH (is set to 1) and the highest in case of DMA.^[305]

The lowest relative reaction rate was detected in case of MeOH (is set to 1) and the highest in case of DMA. An even more increased reaction rate compared to DMA should be observed in 1,3-dimethyl-2-imidazolidinone (DMI) according to Figure 82. Thus, DMI was investigated as solvent of choice and, indeed, the application of the same reaction conditions resulted in the isolation of **123**. In detail, K_2CO_3 and **130** in deoxygenated DMI (Scheme 40) were heated at 60 °C, and **129** was added in one portion to the reaction mixture. This mixture was stirred at 60 °C for 17 h, before the crude product was purified by column chromatography on silica gel and GPC to yield (*E*)-1((2,7)-benzo[*lmn*][3,8]phenanthroline-1,3,6,8(2*H*,7*H*)-tetraona)-6((4,4')-1,2-diphenylethene)-4,8-dithiadecanodane (**123**), also referred to as NDI-stilbenophane, as an orange solid in a yield of 9%.

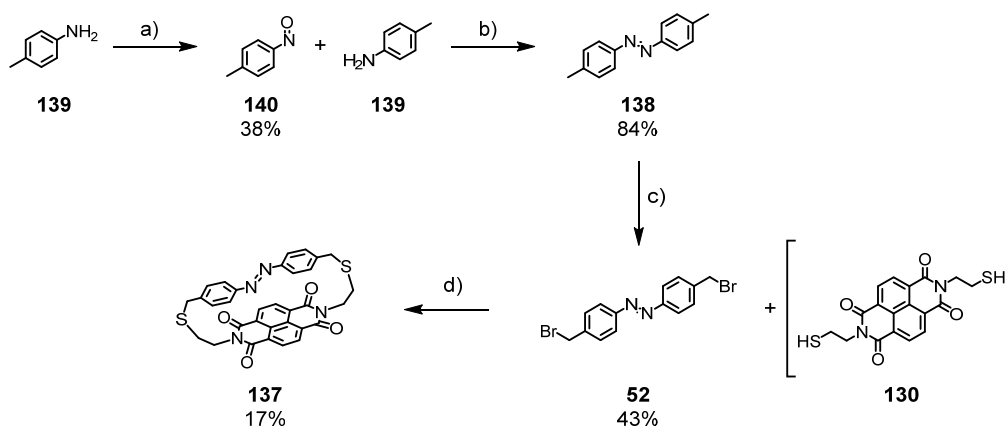


Scheme 40 Successful synthesis of **123** applying: K_2CO_3 , DMI, 60 °C, 17 h.

By considering the low solubility of **129** and the low probability of a cyclization reaction to yield a monomeric structure like **123** instead of dimeric or even oligomeric structures, the yield was considered as good.

5.2.3 Synthesis of a NDI-Azobenzenophane

The assembly (Scheme 41) of **52** was accomplished by using the synthetic method developed by Feringa et al.^[219] The first step of the synthetic strategy was the oxidation of **139** with Oxone[®] in a 3:1 mixture of CH₂Cl₂/H₂O to afford 1-methyl-4-nitrosobenzene (**140**) as a green solid in 59% yield. Oxone[®] and Caroat[®] are the trade names for a mild and stable oxidizing agent, which is the triple salt with the formula “2KHSO₅ · KHSO₄ · K₂SO₄”. KHSO₅ is the potassium salt of peroxy-monosulfuric acid (H₂SO₅), also referred to as Caro’s acid, which is not only one of the strongest oxidants known ($E^0 = 1.81$ V), but also highly explosive. In a second step, **139** and **140** were converted via a Mills reaction to **138** and the pure product was isolated as an orange solid in 84%. The third and last step of the synthetic procedure was the radical bromination by stirring a mixture of **138**, NBS, and AIBN in CCl₄ at 85 °C for 16 h. The purification of the crude product was cumbersome because the recrystallization, as described in literature, did not yield the pure product. Instead, repeated purification by column chromatography on silica gel was performed to separate the over-brominated side product from **52**. Finally, the pure product was afforded as an orange solid in 43% yield.



Scheme 41 Synthesis of NDI-azobenzenophane **137** applying: a) Oxone[®], CH₂Cl₂/H₂O 3:1, rt, 40 min; b) AcOH, rt, 14 h; c) NBS, AIBN, CCl₄, 85 °C, 16 h; d) K₂CO₃, DMF, 75 °C, 16 h.

The last step of the synthetic approach, namely, the cyclization reaction, was done by using DMF as solvent, K₂CO₃ as base, and applying a pseudo-high-dilution principle. In detail, K₂CO₃ and **130** in deoxygenated DMF (319 μM solution) were heated at 75 °C, and **52** in deoxygenated DMF (8.0 mM solution) was added to the reaction mixture via a syringe pump over 1 h. After the complete addition, the solution was stirred at 75 °C for 16 h. The purification was accomplished by column chromatography on silica gel and GPC to yield (*E*)-1-((2,7)-benzo[*lmn*][3,8]phenanthroline-1,3,6,8(2*H*,7*H*)-tetraona)-6-((4,4′)-1,2-diphenyldiazena)-4,8-dithiadecanodane (**137**), also referred to as NDI-azobenzenophane, as an orange solid in 17% yield.

5.2.4 Optical Properties

After the successful assembly of both NDI-phanes, the absorption spectra of **123** (Figure 83; blue line; $c = 9.57 \mu\text{M}$) and **137** (Figure 83; red line; $c = 10.5 \mu\text{M}$) were recorded. The absorption spectrum of NDI-stilbenophane **123** possessed more defined absorption bands compared to NDI-azobenzenophane **137**. The absorption spectrum of **123** featured a maximum transition band at 331 nm and two shoulders at 317 and 349 nm. Additionally, a big absorption band maximum was found at 234 nm and small absorption band maximum at 381 nm. In contrast to that the absorption spectrum of NDI-azobenzenophane **137** possessed one major broad peak from 238 to 390 nm with a shoulder at 348 nm.

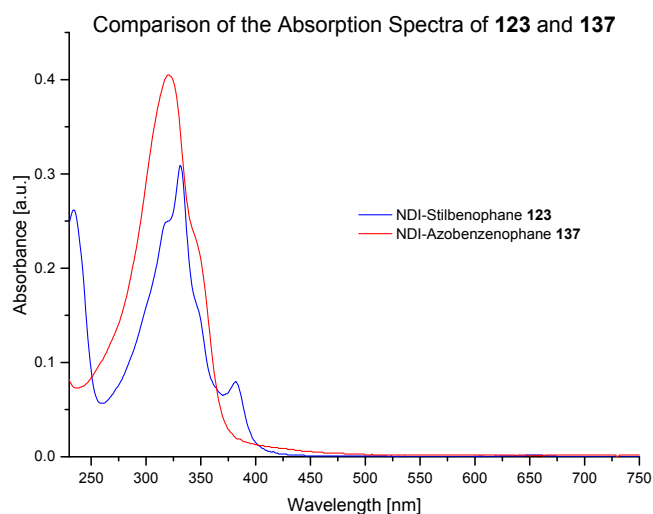


Figure 83 Comparison of the absorption spectra of **123** (blue line; $9.57 \mu\text{M}$) and **137** (red line; $10.5 \mu\text{M}$) showed refined absorption bands in **123** and one broad band in **137**. Both spectra were recorded in CH_2Cl_2 and room temperature.

Table 6 gives an overview of the optical properties of NDI-stilbenophane **123** and NDI-azobenzenophane **137**.

Name	λ_{abs} [nm]	ϵ_{max} [$\text{mol}^{-1} \cdot \text{dm}^3 \cdot \text{cm}^{-1}$]
123	235	27244
	330	32500
	382	8414
137	350	39721

Table 6 Optical properties of **123** and **137** recorded in CH_2Cl_2 at room temperature.

5.2.5 UV/Vis Study of Isomerization

The photoinduced $E \rightarrow Z$ isomerization process of **123** was first probed (Figure 84; left, $c = 24.3 \mu\text{M}$) by UV/Vis spectroscopy. Upon irradiation at 382 nm for 2 min (red line) of a solution of **123** in CH_2Cl_2 , a decrease of intensity of the absorption band at 331 nm and an increase of intensity of the absorption bands at 234 nm and 382 nm were observed, indicating that the conversion of the (E)- to the (Z)-isomer occurred. After irradiating the same sample for 7 min (blue line), no further change in the shape of the absorption bands could be observed, suggesting that the isomerization process was completed. The same sample was then left in the dark and absorption spectra were measured after 3 min (pink line) and 12 min (green line) but, again, no further change in the shape of the absorption bands could be observed. The irradiation at 331 nm resulted in a similar behavior compared with irradiation at 382 nm, however, the decrease of intensity of the absorption band at 331 nm and the increase of intensity of the absorption bands at 234 nm and 382 nm were not as distinct as in the previous case, meaning that the wavelength of 382 nm is better suited for the isomerization process than 331 nm. In addition, the photoisomerization study revealed that the overlapped set of absorption spectra of **123** possessed three isosbestic points (black circles) at 291, 356, and 386 nm. An isosbestic point is defined^[306] “as the wavelength at which the total absorbance of a sample does not change during a chemical reaction. [...] The existence of an isosbestic point only indicates that the stoichiometry of the reaction remains unchanged during the chemical reaction, and that no secondary reactions occur during the considered time range”. This finding did not come as a surprise and can be attributed to the single $E \rightarrow Z$ isomerization process without dimer or phenanthrenophane formation as these side reactions are normally favored in more concentrated solution (Chapter 1.5.1).

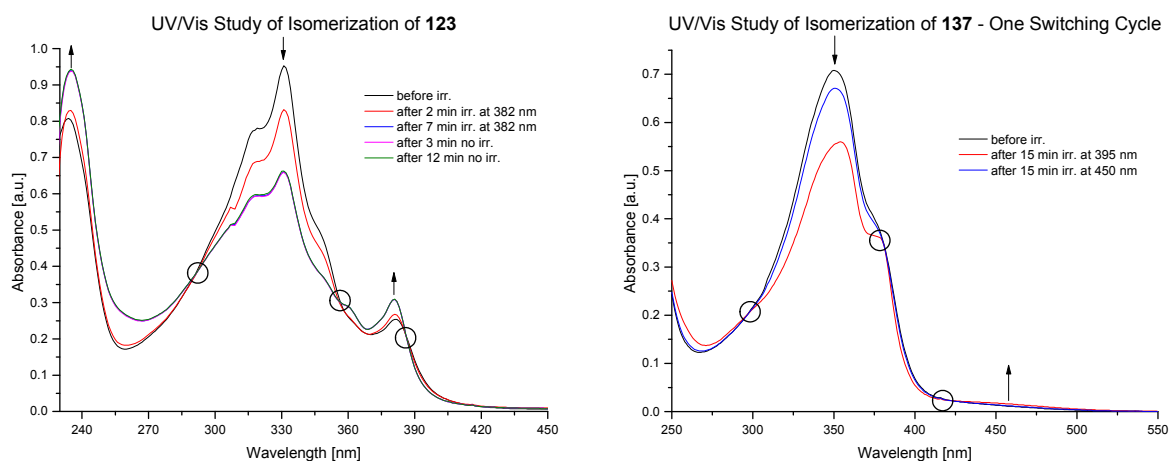


Figure 84 Absorption spectra of NDI-stilbenophane **123** (left; $c = 24.3 \text{ mM}$) and NDI-azobenzenophane **137** (right; $c = 16.1 \text{ mM}$) at different stages of the photoinduced processes upon irradiation with UV light. All spectra were recorded in CH_2Cl_2 at room temperature.

The photoinduced isomerization study was also probed by $^1\text{H-NMR}$ spectroscopy experiments as described in Chapter 5.2.6. The UV/Vis study of the photoinduced $Z \rightarrow E$ isomerization process with or without a triplet photosensitizer, however, was not done yet because of limited time. It will be done in near future.

In case of NDI-azobenzenophane **137**, the photoisomerization study revealed that the overlapped set of absorption spectra of **137** possessed three isosbestic points (black circles) at 298, 380, and 418 nm. The wavelengths used for the $E \rightarrow Z$ and $Z \rightarrow E$ isomerization processes were 395 and 450 nm, respectively. The absorption spectra (Figure 84; right) of a diluted solution of **137** in CH_2Cl_2 ($c = 16.1 \mu\text{M}$) were measured (a) before irradiation (black line), (b) after irradiation of the same sample at 395 nm (red line) for 15 min, and (c) after irradiation of the same sample at 450 nm (blue line) for 15 min. After irradiation at 395 nm for 15 min, a significant decrease of intensity of the broad absorption band at 320 nm was observed, indicating that the conversion of the (E)- to the (Z)-isomer occurred, and no further decrease upon extended irradiation at this wavelength was observed. Then, the same sample was irradiated at 450 nm for 15 min and the intensity of the broad absorption band at 320 nm increased, but did not reach the initial absorption band shape even after 30 min of irradiation. This indicated that the reverse reaction occurred, but not with a full conversion. This observation suggests that the photoinduced isomerization processes $E \rightarrow Z$ and $Z \rightarrow E$ are not 100% reversible. This hypothesis was further supported by the performed $^1\text{H-NMR}$ study as discussed in Chapter 5.2.6.

5.2.6 $^1\text{H-NMR}$ Study of Isomerization

In the studies of the photoinduced $E \rightarrow Z$ and the reverse $Z \rightarrow E$ isomerization processes, a monochromator, as described in Chapter 7.2.19, with an optical fiber, which was dipped into a NMR sample containing **123** or **137** in CD_2Cl_2 , was used.

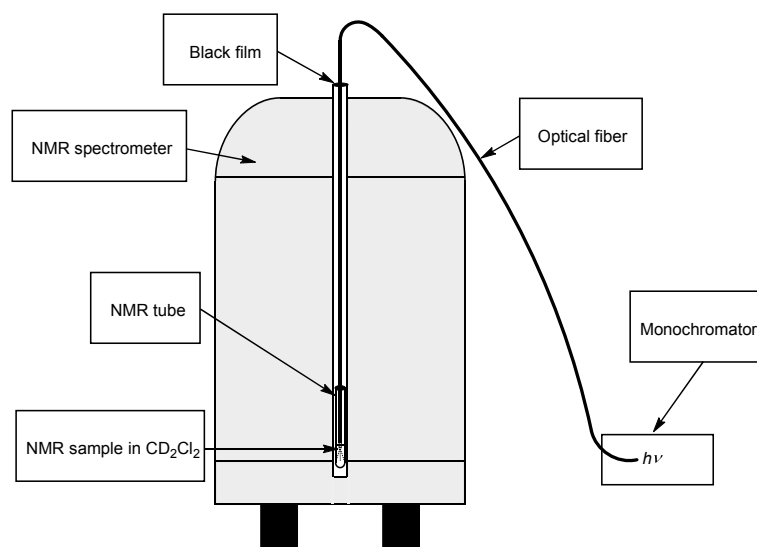


Figure 85 Schematic drawing of the experimental setup for measuring the photoinduced $E \rightarrow Z$ and $Z \rightarrow E$ isomerization processes of **123** and **137** by $^1\text{H-NMR}$ spectroscopy.

The NMR sample and the optical fiber were wrapped with Parafilm[®] and placed, as shown in Figure 85, into an NMR spectrometer. The top of the shim system was covered with a black film to prevent interferences arising from the ambient light, and the sample was subsequently irradiated at a specific wavelength.

To investigate the efficiency of the photoinduced $E \rightarrow Z$ isomerization process of NDI-stilbenophane **123**, the singlet signal, which belongs to the two core hydrogen atoms of the NDI moiety, as illustrated in Figure 86, was followed. This signal appears at 8.57 ppm (red dot) in the case of (*E*)-**123** and at 8.65 ppm (blue dot) in the case of (*Z*)-**123**. The ratio of these two singlet signals, obtained by the integration of the two signals, represents the ratio of (*E*)-**123** and (*Z*)-**123** in the mixture.

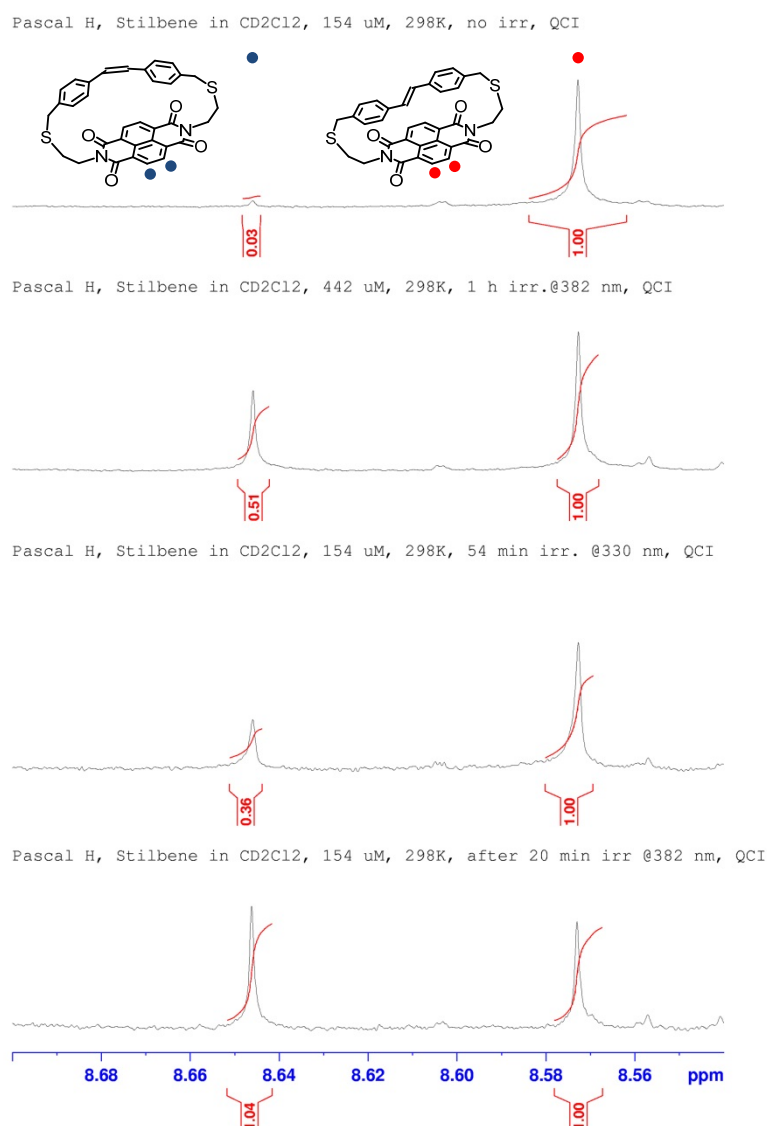


Figure 86 Different PSSs were obtained for the photoinduced $E \rightarrow Z$ isomerization process of **123** at different concentrations. The maximum PSS was obtained in the case when a 154 μM solution of (*E*)-**123** in CD_2Cl_2 was used. The ^1H -NMR spectrum on the top was recorded before irradiation and the ^1H -NMR spectra below after irradiation. All ^1H -NMR spectra were recorded in CD_2Cl_2 at room temperature on a 600 MHz instrument.

Firstly, the wavelength dependency of the photoinduced $E \rightarrow Z$ isomerization process was investigated (Figure 86) on irradiation at 382 nm of a 442 μM solution of (E)-**123** in CD_2Cl_2 and irradiation at 330 nm of a 154 μM solution of (E)-**123** in CD_2Cl_2 . In the former case, a PSS of 34% was found after 60 min of irradiation, and in the latter case, a PSS of 26% after 54 min of irradiation. By extending the time of irradiation at 330 nm to 5 h, decomposition of both (E)-**123** and (Z)-**123** was observed.

Secondly, the concentration dependency of the photoinduced $E \rightarrow Z$ isomerization process was probed (Figure 86) on irradiation at 382 nm of a 154 μM solution of (E)-**123** in CD_2Cl_2 . Compared to the 442 μM solution with a PSS of 26%, the diluted sample showed an increased PSS of 51%. The higher efficiency of the isomerization process in the diluted samples can be ascribed to a deeper penetration of the UV light into the solution. As mentioned in Chapter 1.5.1, a maximum PSS of 54% for the $E \rightarrow Z$ isomerization process can be obtained and, therefore, the observed PSS of 51% almost reached its maximum. In Figure 87, the initial $^1\text{H-NMR}$ spectrum of (E)-**123** before irradiation is compared with the $^1\text{H-NMR}$ spectrum after irradiation at 382 nm for 60 min at its PSS state. For each proton signal present in the spectrum measured before irradiation, a second signal with the same multiplicity appeared and, therefore, these signals were attributed to (Z)-**123** and not to the products of decomposition of (E)-**123**.

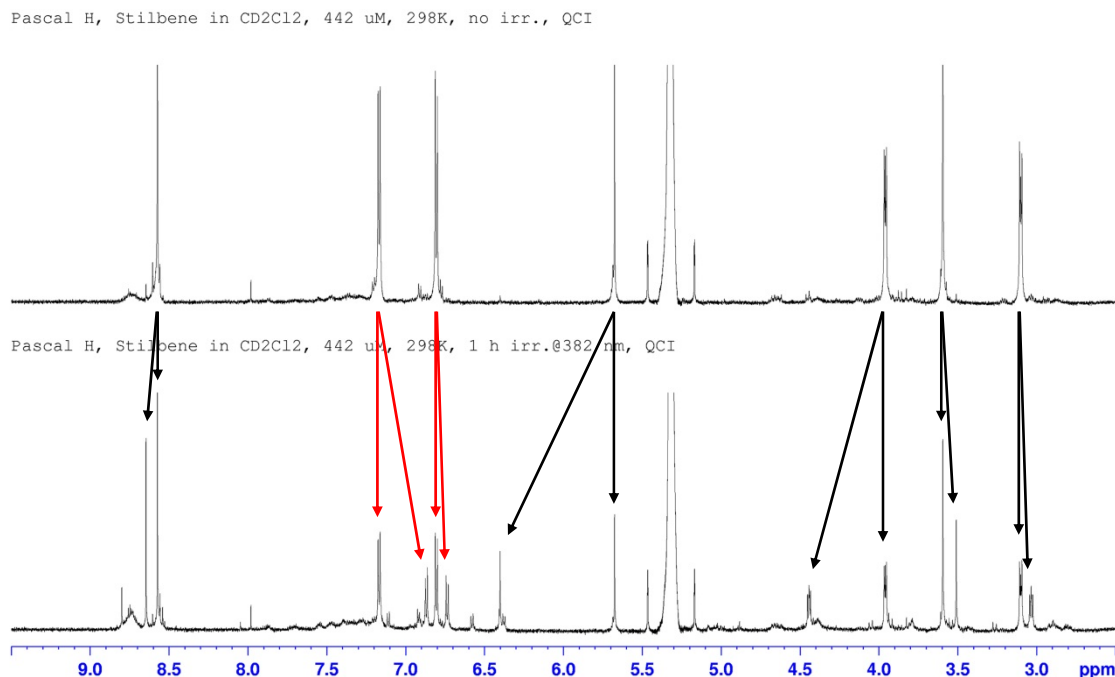


Figure 87 $^1\text{H-NMR}$ Spectra of (E)-**123** before (top) and after (bottom) irradiation at 382 nm for 60 min, a period, after which the process reached its steady state. In the steady state, a pair of signals for each proton was present in the spectrum, which indicates the formation of a mixture of (E)-**123** and (Z)-**123**. All $^1\text{H-NMR}$ spectra were recorded in CD_2Cl_2 at room temperature on a 600 MHz instrument.

Unfortunately, the decay of the PSS via a reverse $Z \rightarrow E$ isomerization process could not be observed, not even after 120 min in the dark. The $^1\text{H-NMR}$ study of the photoinduced $Z \rightarrow E$

isomerization process with or without a triplet photosensitizer was not done yet because of limited time. It will be done in near future.

To investigate the efficiency of the photoinduced $E \rightarrow Z$ isomerization process of NDI-azobenzophane **137**, the singlet signal, which belongs to the two core hydrogen atoms of the NDI moiety, as seen in Figure 88, was followed. This signal appears at 8.53 ppm in the case of (*E*)-**137** (red dot) and at 8.73 ppm in the case of (*Z*)-**137** (blue dot). The ratio of these two singlet signals, obtained by integration of the two signals, represents the ratio of (*E*)-**137** and (*Z*)-**137** in the mixture. As described in Chapter 5.2.5, the wavelengths used for the $E \rightarrow Z$ and $Z \rightarrow E$ isomerization processes were 395 and 450 nm, respectively.

Firstly, the temperature dependency of the photoinduced $E \rightarrow Z$ isomerization process was investigated on irradiation at 395 nm of a solution of (*E*)-**137** in CD_2Cl_2 at 298 K and 278 K. However, no dependency on the temperature was found.

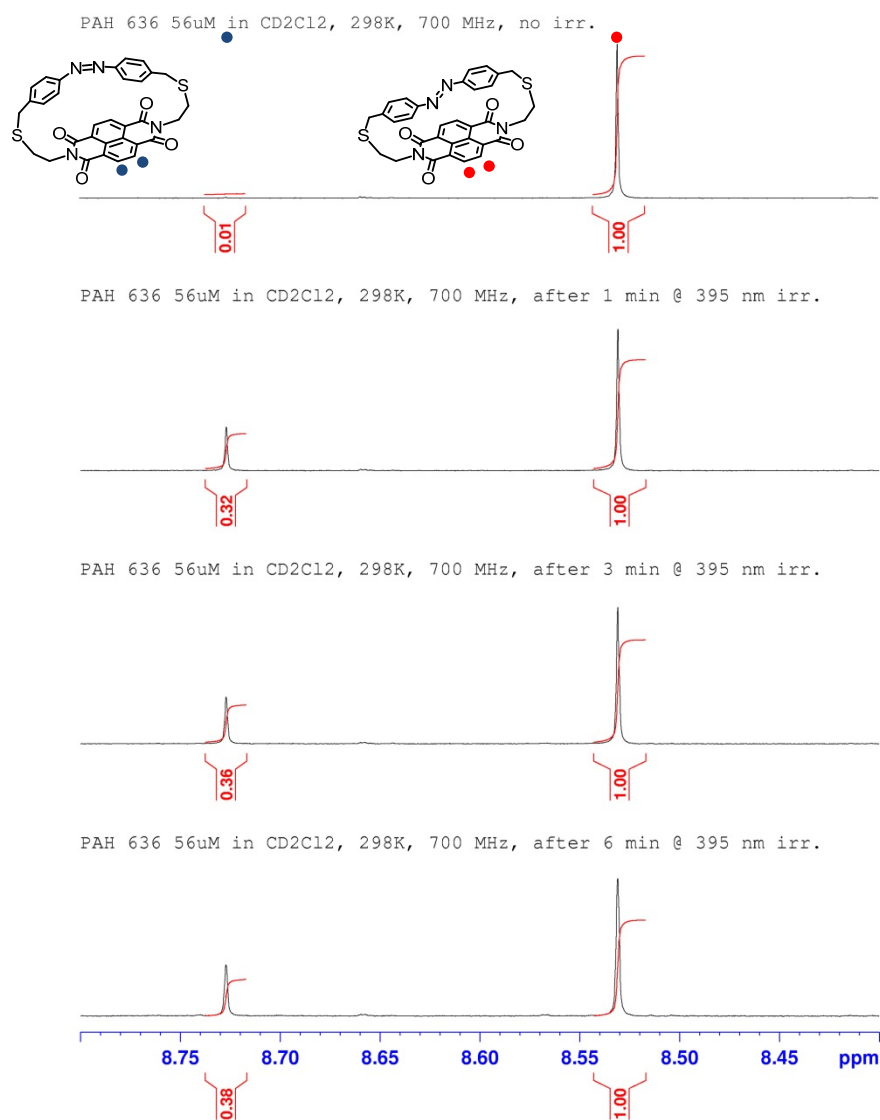


Figure 88 A maximum PSS was obtained in the case when 56 μM solution of (*E*)-**137** in CD_2Cl_2 was used. The ^1H -NMR spectrum on the top was recorded before irradiation and the three ^1H -NMR spectra below after different irradiation times. All ^1H -NMR spectra were recorded in CD_2Cl_2 at room temperature on a 700 MHz instrument.

Secondly, the concentration dependency of the photoinduced $E \rightarrow Z$ isomerization process was probed on irradiation at 395 nm of a 56 μM solution of (E)-**137** in CD_2Cl_2 . Compared to the 472 μM solution with a PSS of 13%, the diluted sample showed an increased PSS of 28%. The higher efficiency of the isomerization process in the diluted samples can be ascribed to a deeper penetration of the UV light into the solution. This finding was similar to the $^1\text{H-NMR}$ study of isomerization of NDI-stilbenophane **123**. As displayed in Figure 88, the initial $^1\text{H-NMR}$ spectrum of (E)-**137** before irradiation is compared with the $^1\text{H-NMR}$ spectrum after irradiation at 395 nm for 1, 3, and 6 min. After 6 min the system reached its PSS state as clearly seen in Figure 88 and Figure 89.

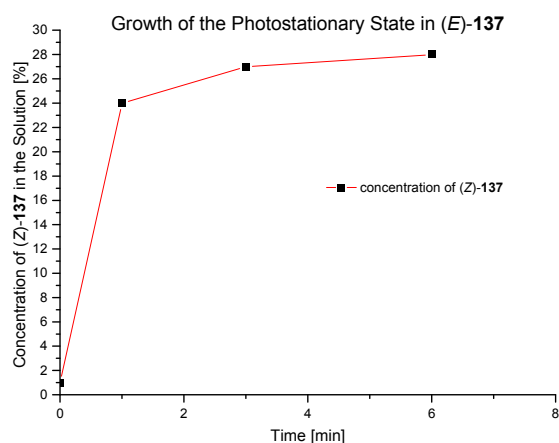


Figure 89 The data of this graph are taken from Figure 88 and the concentration of (Z)-**137** in a 56 μM solution of (E)-**137** in CD_2Cl_2 is plotted as a function of time. After 6 min the photostationary state is reached.

Thirdly, the reversibility of the photoinduced $E \rightarrow Z$ and $Z \rightarrow E$ isomerization processes, as illustrated in Figure 90, was investigated on irradiation at 395 nm of a 56 μM solution of (E)-**137** in CD_2Cl_2 for 5 min to obtain a PSS of 28%. This sample was subsequently irradiated at 450 nm for 1 min to induce the $Z \rightarrow E$ isomerization process, and a 9:91 mixture of (Z)-**137**/ (E) -**137** was calculated. This indicated that the reverse reaction occurred, but not with a full conversion. Therefore, the irradiation time at 450 nm was extended to 5 min. Instead of a decreased ratio of the (Z)-**137**/ (E) -**137** mixture, increased intensities of the signals at 8.74 and 8.57 ppm were detected. These signals were attributed to decomposition of **137**. The same sample was exposed to a second photoinduced switching cycle (bottom) and after the final $Z \rightarrow E$ isomerization process, the signals at 8.74 and 8.57 ppm were increased compared to the first switching cycle. This indicated that again the reverse reaction occurred, however, the signals of decomposition of **137** increased simultaneously. Thereby, this study supported the UV/Vis study and it can be concluded that the photoinduced $Z \rightarrow E$ isomerization process of (Z)-**137** upon irradiation at 450 nm led not only to the formation of (E)-**137** but also to decomposition of **137**.

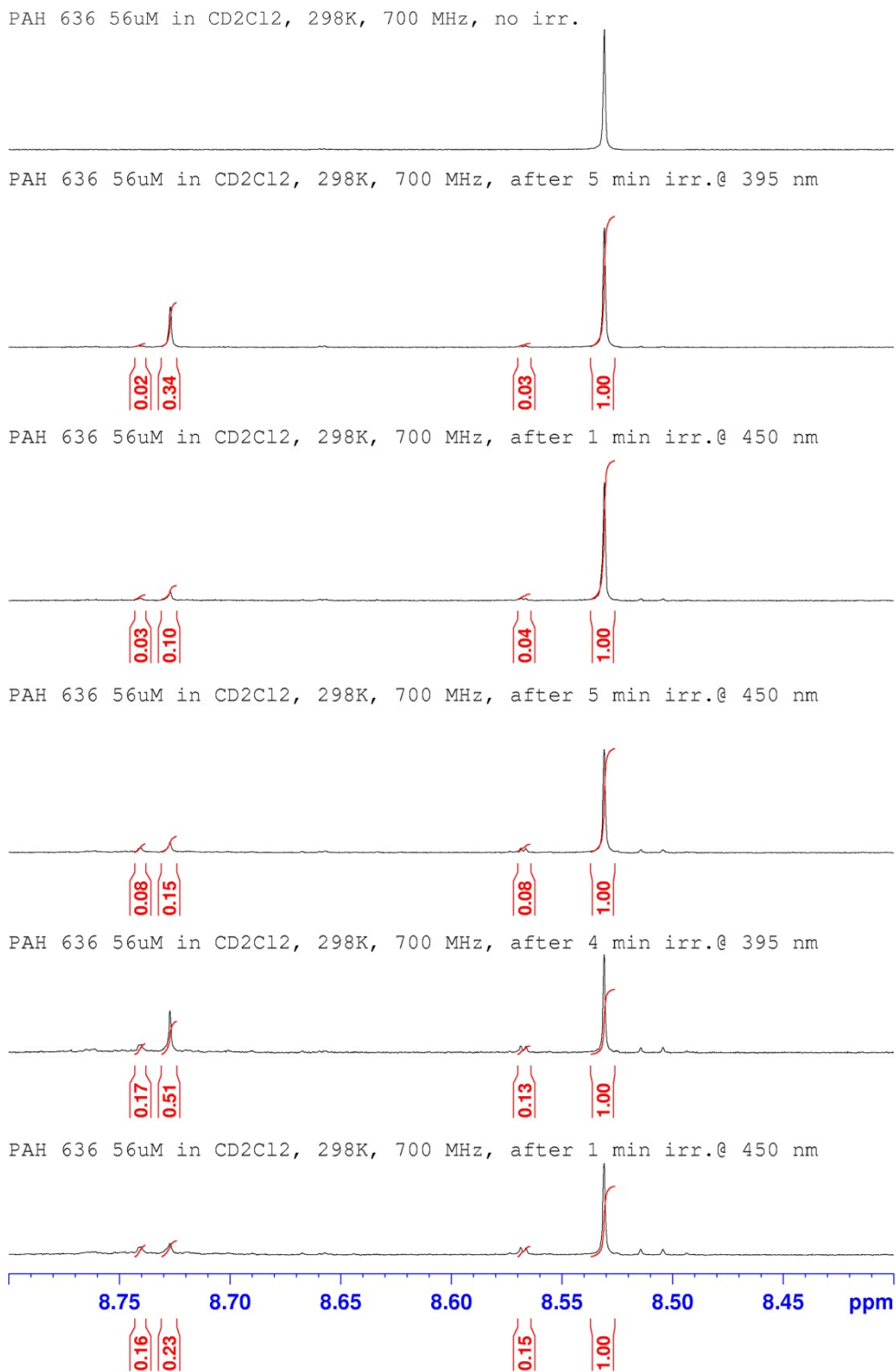


Figure 90 ¹H-NMR spectrum on the top was recorded before irradiation of a 56 μM solution of (*E*)-**137** and the ¹H-NMR spectra below after irradiations at 395 or 450 nm. An increasing decomposition was observed after each cycle and, as a consequence, indicated the inefficiency of the photoinduced reverse *Z* → *E* isomerization reaction upon irradiation at 450 nm. All ¹H-NMR spectra were recorded in CD₂Cl₂ at room temperature on a 700 MHz instrument.

Fourthly, the reversibility of the photoinduced *E* → *Z* and *Z* → *E* isomerization processes, as displayed Figure 91, was investigated on the thermal reverse reaction in the dark. Therefore, at

different stages of the process $^1\text{H-NMR}$ spectra of a $56\ \mu\text{M}$ solution of (*E*)-**137** in CD_2Cl_2 were measured (a) before irradiation (top), (b) after irradiation of the sample at $395\ \text{nm}$ for $6\ \text{min}$ at the PSS of **137** (middle), and (c) after leaving the same sample in the dark for $261\ \text{min}$ (bottom).

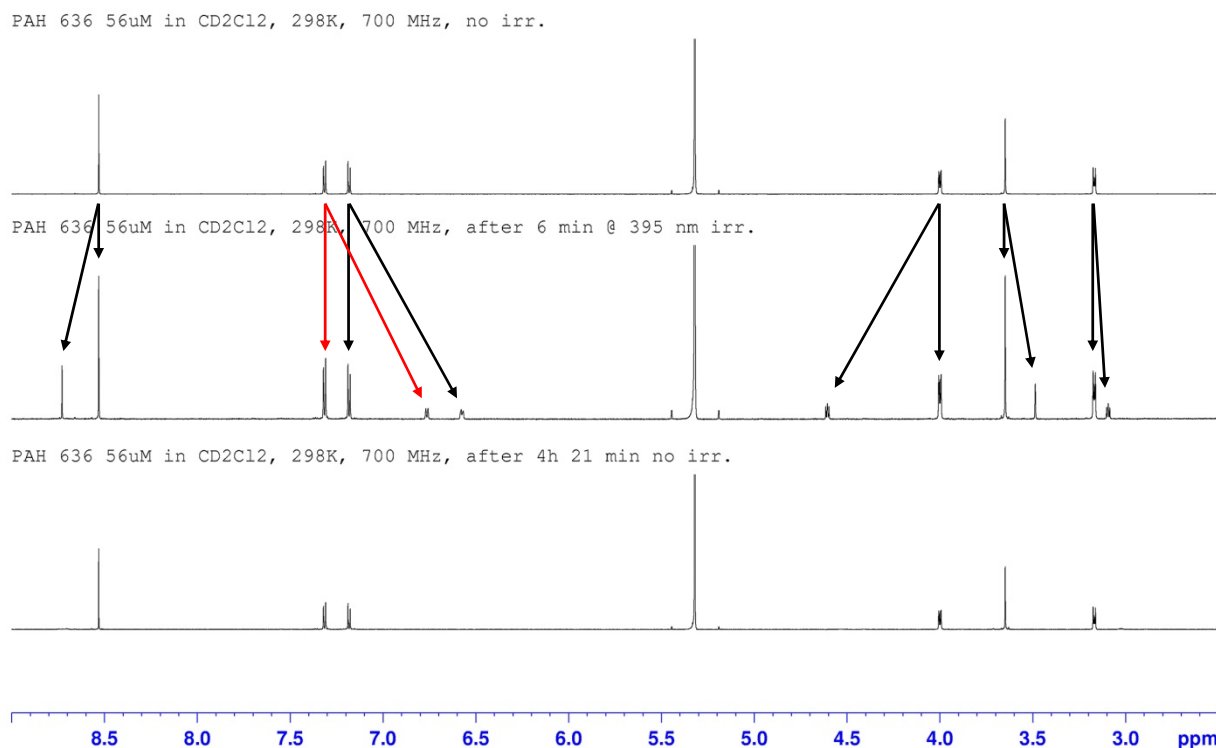


Figure 91 Prove of the reversible photoinduced $E \rightarrow Z$ isomerization reaction and the thermal reverse $Z \rightarrow E$ isomerization reaction in the dark: (a) $^1\text{H-NMR}$ spectrum on the top was recorded before irradiation, (b) $^1\text{H-NMR}$ spectrum in the middle was recorded at its PSS, and (c) $^1\text{H-NMR}$ spectrum at the bottom was recorded after the thermal back reaction in the dark. All $^1\text{H-NMR}$ spectra were recorded in CD_2Cl_2 at room temperature on a $700\ \text{MHz}$ instrument.

As shown in Figure 91, the initial $^1\text{H-NMR}$ spectrum of (*E*)-**137** before irradiation (top) is compared with the $^1\text{H-NMR}$ spectrum after irradiation at $395\ \text{nm}$ at its PSS state (middle). For each proton signal present in the spectrum measure before irradiation, a second signal with the same multiplicity appeared and, therefore, these signals were attributed to (*Z*)-**137**. After leaving the same sample in the dark for $261\ \text{min}$, a $^1\text{H-NMR}$ spectrum was recorded and the signals of (*Z*)-**137** disappeared almost 100%. Therefore, it indicated that the reverse $Z \rightarrow E$ isomerization reaction occurred thermally in the dark without any decomposition.

Last but not least, the lifetime of (*Z*)-**137** (Figure 92) in the dark was probed by first irradiation at $395\ \text{nm}$ of a $56\ \mu\text{M}$ solution of (*E*)-**137** in CD_2Cl_2 for $6\ \text{min}$ to reach its PSS. Subsequently, this sample was left in the NMR instrument and the top of the shim system was covered with a black film to prevent interferences arising from the ambient light. Over $261\ \text{min}$ five $^1\text{H-NMR}$ spectra were measured. The investigation revealed by applying an interpolation on the recorded data

that the reverse $Z \rightarrow E$ isomerization reaction to obtain (Z)-**137** would be completed in the time-scale of 354 min.

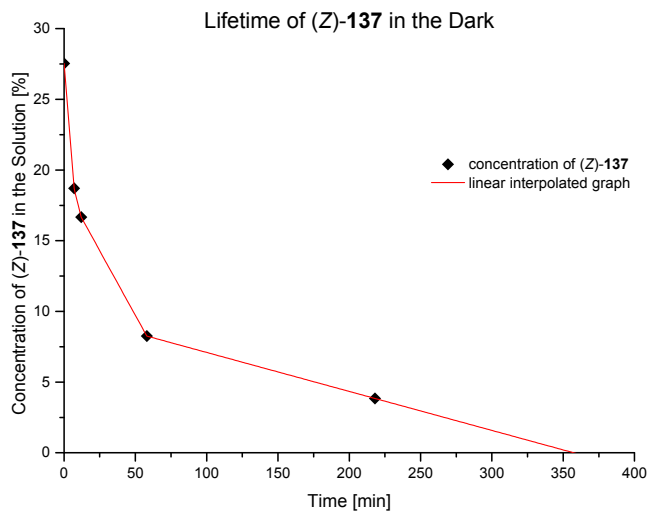


Figure 92 Lifetime of (Z)-**137** was investigated by recording five $^1\text{H-NMR}$ spectra at different stages of the thermal decay of (Z)-**137** to obtain five data points (indicated by black squares). By applying a linear interpolation on the graph (red line), a lifetime of 354 min was found for (Z)-**137**. All $^1\text{H-NMR}$ spectra were recorded in CD_2Cl_2 at room temperature on a 700 MHz instrument.

5.2.7 Immobilization of NDI-Azobenzenophane on a Metallic Surface

NDI-azobenzenophane **137** fulfills the requirements (a) to be stable against thermal evaporation and electrospray ionization (mass spectra of **137** were successfully measured by MALDI-TOF-MS and ESI-MS), and (b) to possess a reversible switching process ($^1\text{H-NMR}$ study). Therefore, **137** was deposited under UHV on a Ag(111) surface and STM images were taken. This was performed in close collaboration with the research group of Prof. Dr. Berndt in Kiel (carried out by Katharina Scheil). As shown in Figure 93, the molecules formed ordered islands. The picture was taken while measuring in the constant current mode and applying 600 mV and 57 pA. A constant current STM image depends, as described in Chapter 1.4.1, on two major influences (1) the density of state of the surface, which means the ability of electrons to tunnel from the metallic tip to the sample surface, and (2) the topography of the surface. If a part of the molecule is closer to the STM tip than the rest of the molecule, the STM tip is consequently retracted and, thereby, a bright spot results. The combination of both influences results in the formation of a self-assembled array as shown in Figure 93. The bright spots, highlighted with a black circle, correspond to a deposited NDI-azobenzenophane which pulls back the STM tip and the dark spots corresponds to a gap where no NDI-azobenzenophane is located. Additionally, the formation of such an array is favored based on the fact that NDI-phanes are able to self-assemble on metallic surfaces as reported by inter alia Mayor et al.^[293] The high efficiency of this self-assembly process can be ascribed to possible intermolecular hydrogen bondings between the NDI-phanes (the dotted lines are showing possible hydrogen bondings).

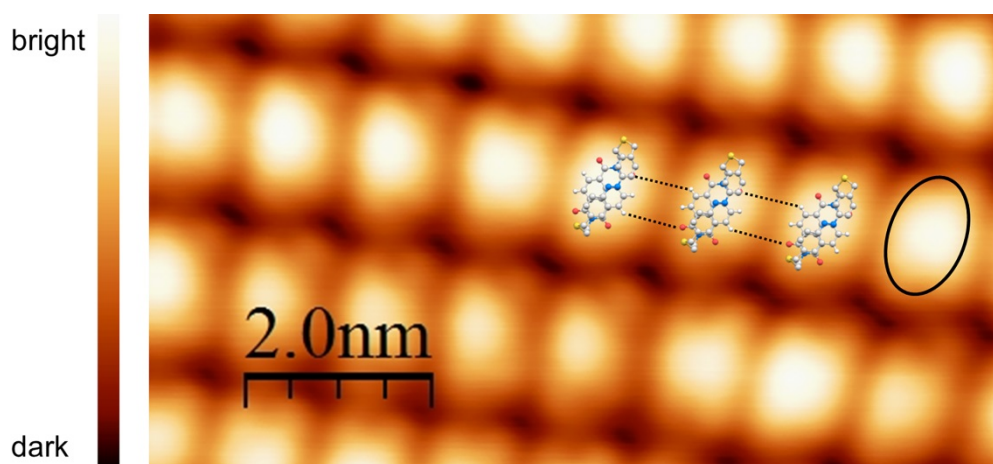


Figure 93 STM picture of **137** deposited on a Ag(111) surface. The picture was taken at 600 mV and 57 pA.

It must be pointed out that such an arrangement was not proven by the time this doctoral thesis was written and, as a result, it represents only a hypothesis of the possible arrangement of **137** on the Ag(111) surface. In addition, the switching process upon applying current is still under investigation and, therefore, more data cannot be provided in this doctoral thesis.

6 Summary and Outlook

All three proposed objectives of this doctoral thesis were successfully completed.

In the first project, the photoinduced processes in molecular figure-of-eight (8) NDI derivatives were investigated, namely, charge transfer from the core substituent to the naphthyl moiety. In the case of 2,6-diphenylsulfanyl-core-substituted NDI **37**, an ultrafast fluorescence quenching upon irradiation was observed. The applied approach to restrict the rotation around the S–C bond of the NDI core substituent and, thus, prevent the fluorescence quenching, was successful. The rotation around the S–C was suppressed by connecting the core substituent with the substituent at the *N*-terminus of the imide moiety by an aliphatic bridge. The photophysical studies were carried out in collaboration with Igor Pugliesi from the research group of Prof. Dr. Riedle at the LMU Munich.

Prior to performing the photophysical measurements, synthetic strategy towards the synthesis of *S,S'*-molecular 8 **84** was developed. This compound was synthesized in seven steps and isolated as a bright red solid. The *tert*-butyl group proved to be a versatile protective group for the thiol functionality throughout the entire synthesis. Moreover, single crystals of **84** suitable for X-ray diffraction analysis were grown and the obtained solid-state structure revealed that the phenylsulfanyl core substituents were slightly twisted out of the NDI plane compared to the phenylsulfanyl core substituents in an unbridged analogue **37**, which indicated the rigid character of **84**. The optical properties, such as absorption, fluorescence, and the fluorescence quantum yield, were almost identical for compounds **37** and **84**. Therefore, transient-absorption spectra of **37** and **84** were measured at LMU. It was found that compound **84** had an extended lifetime (8.39 ps) of the excited state compared to that (6.50 ps) of **37**. This result proved that the proposed hypothesis was correct, although the observed effect was not as distinct as expected. Additionally, two molecular 8 derivatives, namely, *N,N'*-molecular 8 **92a** and **92b**, and *O,O'*-molecular 8 **103**, were therefore synthesized and studied.

In the case of *N,N'*-molecular 8 derivatives, various protective groups (Boc, Cbz, and Fmoc) for the amino functionality were tested, however, the desired product could not be isolated in all cases. Finally, it was found that when no amino-protecting group was used, the desired product was formed. The lower overall yield can be ascribed to the lower nucleophilicity of the nitrogen atom compared to the sulfur atom. The final step of the synthesis of *N,N'*-molecular 8 **92** yielded two structural isomers, **92a** and **92b**, both as bright blue solids. Optical studies showed that in the case of the more strained isomer **92b**, the absorption band maximum was broader compared to that of **92a**. The optical properties of **92a** were compared to those of the unbridged analogue **62** but no significant difference was observed. The transient-absorption spectra of the two isomers are not yet measured, but the measurements will be conducted very soon in close collaboration with our collaborators.

The third molecular 8 derivative, *O,O'*-molecular 8 **103**, was synthesized by employing the same synthetic strategy as in the case of *S,S'*-molecular 8 derivative. The MEM protecting group proved to be a versatile oxygen-protecting group throughout the entire synthesis. All synthetic steps, apart from the final aromatic nucleophilic substitution reaction, yielded the desired products in good to excellent reproducible yields. The last step of the synthesis was performed reproducibly three times to obtain *O,O'*-molecular 8 **103** as a yellow solid. The optical properties of **103** were investigated and, similarly to the case of **92**, the optical properties of **103** and the unbridged analogue **63** were similar. Identical to the two *N,N'*-molecular 8 derivatives, here as well the transient-absorption spectra are not yet recorded, but the measurements will be conducted very soon in close collaboration with our collaborators.

The transient-absorption spectra of the last two molecular 8 derivatives must be measured to further support the proposed hypothesis, which was already proved in case of *S,S'* molecular 8. The extension of the full-CT state could be achieved by shortening the aliphatic bridge from eight CH₂ units to six or seven and, thereby, suppressing the rotational freedom around the S–C bond even further. This would ultimately lead to a decreased decay of the full-CT state and a higher fluorescence quantum yield should be measured.

In the second project, the photoinduced charge-transfer process of a linear cNDI placed in a squeezable break junction setup was investigated, in collaboration with Dr. Yoram Selzer at the Tel Aviv University. The aim was to observe for the first time conductance enhancement on a single-molecule level. For this purpose, a series of symmetrical 2,6-amino-core-substituted NDIs were designed and synthesized. The target cNDI compounds featured a protected thiolphenol on the imide functionality to allow for a linkage of the thiols to the gold electrodes in the squeezable break junction setup, as well as ethylamino or dimethylamino core substituents. The synthesis of the both cNDIs employed the key building block **119**. This key building block was then converted either to the 2,6-diethylamino-core-substituted NDI **120** or to the 2,6-bisdimethylamino-core-substituted NDI **121**. The target cNDI was in each case isolated as a bright blue solid in six steps. The optical properties of compounds **120** and **121** were completely different on account of the fact that cNDI **120** can form two intramolecular hydrogen bondings whereas cNDI **121** cannot. As a consequence of the hydrogen-bonding abilities, cNDI **120** is highly fluorescent while cNDI **121** is not. Because both target compounds fulfilled all requirements, namely, to have to core-substituent absorption band maximum above 530 nm, and bearing a protected thiol moiety, they were investigated in a squeezable break junction setup in collaboration with Michal Vadai from the research group of Dr. Yoram Selzer at the Tel Aviv University.

Although the conductance of cNDI **120** in this setup could be measured without illuminating with light (base line conductance of 0.4 mG₀), the conductance measurements upon irradiation

with a laser beam were not successful yet. Attempts to observe the conductance enhancement on a single-molecule level are ongoing.

In the third project, the switching process in photoswitchable NDI-phanes was first investigated in solution, possessing either a stilbene or an azobenzene moiety as the switching unit, before depositing NDI-azobenzenophane on a Ag(111) surface to study the switching process by $^1\text{H-NMR}$ spectroscopy and UV/Vis absorption spectroscopy. For the synthesis of strained NDI-stilbenophane **123** and a strained NDI-azobenzenophane **137**, the precursors, namely, (*E*)-1,2-bis(4-(bromomethyl)phenyl)ethene and (*E*)-1,2-bis(4-(bromomethyl)phenyl)diazene, were in each case previously described in the literature. The main task was therefore to develop synthetic strategy for the synthesis of the key building block **130**, which was successfully accomplished. After the isolation of pure NDI-stilbenophane **123** and NDI-azobenzenophane **137**, the photoinduced *E* \rightarrow *Z* isomerization process in these compounds was investigated.

Both NDI-phanes **123** and **137** were able to undergo a photoinduced *E* \rightarrow *Z* isomerization photostationary states of 51% and 28%, respectively, were obtained by means of $^1\text{H-NMR}$ spectroscopy. In the case of **123**, the decay of the (*Z*)-isomer in the dark was not observed. In the case of **137**, however, the almost 100% decay of the (*Z*)-isomer in the dark was observed after 4.4 h. Subsequently, NDI-azobenzenophane **137** was deposited on a Ag(111) surface, which was done in collaboration with Katharina Scheil from the research group of Prof. Dr. Berndt at the Christian-Albrechts-Universität zu Kiel. The switching process upon applying current is still under investigation and, therefore, no further data are available at this time.

Future work will focus on increasing the yield for the preparation of **130**, as well as yields for compound **123** and **137**. For this purpose, the reaction condition of each procedure must be investigated in more detail and subsequently optimized. Additionally, the real arrangement of the deposited NDI-azobenzenophane on the silver surface must be investigated, before the influence of an external stimulus, such as current and UV light, on the isomerization process is probed.

7 Experimental Section

7.1 General Information

7.1.1 Reagents and Solvents

All chemicals were used as received from ABCR GmbH & Co. KG (Karlsruhe, Germany), Acros Organics™ (Basel, Switzerland), Alfa Aesar® (Karlsruhe, Germany), Fluka AG (Buchs, Switzerland), fluorochem Ltd (Hadfield, United Kingdom), or Sigma-Aldrich® (Buchs, Switzerland) unless stated otherwise. 2,3,6,7-Tetrabromo-1,4,5,8-naphthalenetetracarboxylic acid dianhydride (**206**) and 2,6-dichloronaphthalene-1,4,5,8-tetracarboxylic acid dianhydride (**14**) were synthesized by Mathias Fischer at Karlsruhe Institute of Technology (KIT). Dry solvents were purchased from Fluka AG or were dried using standard procedures^[307] and stored over 4 Å molecular sieves. Technical-grade solvents used for extractions and chromatographies were distilled once before usage.

7.1.2 Sensitive Reactions

Air- and water-sensitive reactions were performed under a deoxygenated atmosphere using Argon 4.8 from PanGas AG (Damarsellen, Switzerland). For water-sensitive reactions, glassware was heated (90 °C) and then cooled under argon before use.

7.2 Instrumentation

7.2.1 Elemental Analysis (EA)

Elemental analysis was measured on a Perkin-Elmer® Analysator 240 or a Vario Micro Cube from Elementar and values are given in mass percentage (calcd vs. measured abundance). In most cases, the NMR pure product was purified by GPC and dried at 40 °C for several days before the EA was measured.

7.2.2 Fourier-Transform Infrared (FT-IR) Spectroscopy

FT-IR spectra were recorded on a Bruker Platinum ATR instrument. The compounds were measured neat through an ATR attachment and the wavenumbers of transmission maxima are reported in cm⁻¹.

7.2.3 Gel Permeation Chromatography (GPC)

GPC was recorded on a Shimadzu Prominence System with SDV preparative columns from Polymer Standards Service (two columns in series, 60 cm each, operating range: 100–30000 g/mol)

and measurements were performed at room temperature with CHCl_3 as eluent and a flow rate of 4 mL/min.

7.2.4 ^1H -Nuclear Magnetic Resonance (^1H -NMR)

All ^1H -NMR spectra were recorded on an Oxford NMR spectrometer operating at 400 MHz, a Bruker Avance III with a BBFO⁺ probe head spectrometer operating at 400 MHz, a Bruker BZH-NMR with a QNP probe head spectrometer operating at 250 MHz, a Bruker Ultra Shield Avance III with a BBO probe head spectrometer operating at 500 MHz, or on a Bruker Avance III NMR spectrometer operating at 700 MHz equipped with a ^1H - $^{13}\text{C}/^{15}\text{N}$ - ^2D TCI cryoprobe head with z -axis pulsed field gradients. Chemical shifts (δ) are reported in parts per million (ppm) relative to residual solvent signals or trimethylsilane (TMS), and coupling constants (J) are reported in Hertz (Hz). Deuterated solvents were obtained from Cambridge Isotope Laboratories, Inc. (Andover, MA, USA) or from Armar AG (Döttingen, Switzerland). The measurements were performed at room temperature. The multiplicities are described as: s = singlet, d = doublet, t = triplet, q = quartet, p = pentet, h = hextet, hept = heptet and m = multiplet. For multiplets, the range of chemical shifts (ppm) of the signal is reported.

7.2.5 ^{13}C -Nuclear Magnetic Resonance (^{13}C -NMR)

All ^{13}C -NMR spectra were recorded on an Oxford NMR spectrometer operating at 101 MHz, a Bruker Avance III 400 with a BBFO⁺ probe head spectrometer operating at 101 MHz, a Bruker Ultra Shield Avance III spectrometer with a BBO probe head with z -gradients operating at 126 MHz, or a Bruker Avance III HD NMR spectrometer operating at 151 MHz equipped with a 5 mm $^1\text{H}/^{19}\text{F}$ - $^{13}\text{C}/^{15}\text{N}$ -D QCI cryoprobe head with z -axis pulsed field gradients. Chemical shifts (δ) are reported in parts per million (ppm) relative to residual solvent signals. Deuterated solvents were obtained from Cambridge Isotope Laboratories, Inc. (Andover, MA, USA) or from Armar AG (Döttingen, Switzerland). The measurements were performed at room temperature. All two-dimensional NMR experiments required to assign the ^1H - and ^{13}C -signals, namely, ^1H - ^1H -COSY, ^1H - ^{13}C -HMQC, ^1H - ^{13}C -HMBC and ^1H - ^1H -NOESY were recorded on a Bruker 500 MHz Ultra Shield Avance III spectrometer equipped with a BBO probe head with z -gradients at 500 and 126 MHz, respectively, a Bruker 600 MHz Ultra Shield Avance III spectrometer with a BBFO⁺ probe head at 600 and 151 MHz, respectively, a Bruker Avance III HD NMR spectrometer operating at 600 and 151 MHz, respectively, equipped with a 5 mm $^1\text{H}/^{19}\text{F}$ - $^{13}\text{C}/^{15}\text{N}$ - ^2D QCI cryoprobe head with z -axis pulsed field gradients, or a Bruker Avance III NMR spectrometer operating at 700 and 176 MHz, respectively, equipped with a ^1H - $^{13}\text{C}/^{15}\text{N}$ - ^2D TCI cryoprobe head with z -axis pulsed field gradients.

7.2.6 Melting point (MP)

MPs were measured on a Will Wetzlar apparatus. The measured temperatures are not corrected.

7.2.7 Microwave (MW) Reactions

All MW reactions were performed in a Biotage[®] Initiator 8.0 microwave reactor.

7.2.8 Direct Analysis at Real Time Mass Spectroscopy (DART-MS)

The DART-SVP source (IonSense[®], MA, USA) was equipped with a Shimadzu LCMS-2020. The distance between the source orifice and the ceramic transfer tube was approximately 10 mm. The DART source was operated in either a positive or a negative mode with helium gas (5.0) and the substances were desorbed from a glass capillary. The other parameters, including the gas temperature, were optimized for the best performance in the experiments.

7.2.9 Gas Chromatography Mass Spectrometry (GC-MS)

A Shimadzu GCMS-QP2010 SE gas chromatography system with a ZB-5HT inferno column (30 m × 0.25 mm × 0.25 mm) at 1 mL/min He-flow rate (split = 20:1) with a Shimadzu electron ionization (EI 70 eV) mass detector was used to record the GC-MS spectra.

7.2.10 Electrospray Ionization Mass Spectrometry (ESI-MS)

All ESI-MS spectra were recorded on a Bruker amaZon[™] X.

7.2.11 Matrix Assisted Laser Desorption Ionization Time of Flight Mass Spectrometry (MALDI-TOF-MS)

All MALDI-TOF mass spectra were recorded on a Bruker microflex[™] using as calibrant CsI₃ and (*E*)-2-[3-(4-*tert*-butylphenyl)-2-methyl-2-propenylidene]malononitrile (DCTB) as matrix.

7.2.12 High-Resolution Mass Spectroscopy (HRMS)

High-resolution mass spectra were either recorded as HR-ESI-TOF-MS on a maXis[™] 4G from Bruker or as HR-ESI/MALDI-FTICR-MS on a Bruker solariXR[™].

7.2.13 Column Chromatography (CC)

Silica gel 60 (40–63 μm) from Sigma Aldrich[®] or SilicaFlash P60 (40–63 μm) from Silicycle[®] was used for CC.

7.2.14 Preparative Thin-Layer Chromatography (PTLC)

Silica gel glass plates with a thickness of 2.0 mm from Merck KGaA were used for PTLC.

7.2.15 Thin-Layer Chromatography (TLC)

Silica gel 60 F₂₅₄ glasses plates with a thickness of 0.25 mm from Merck KGaA or Polygram[®] Alox N/UV254 aluminum oxide plates with a thickness of 0.2 mm from Macherey-Nagel were used for TLC. The detection was carried out under a UV lamp at 253 nm, 302 nm or 366 nm. Compounds were visualized by vanillin, KMnO₄, or ninhydrin in some cases.

7.2.16 High-Performance Liquid Chromatography (HPLC)

Analytical reversed-phase HPLC-ESI-MS measurements were performed on a Shimadzu LC-20AD instrument using a Reprospher 100 C18-Aqua, 5 µm column (125 mm × 2 mm) from Maisch GmbH. Furthermore, analytical normal-phase measurements were performed by using a Reprosil 100 Si, 5 µm column (240 mm × 4.6 mm) from Maisch GmbH on a Shimadzu LC-20AT instrument. Finally, preparative normal-phase HPLC separations were performed on a Dionex P680 HPLC instrument using a Reprosil 100 Si, 5 µm column (250 mm × 40 mm) from Maisch GmbH with solvent gradients specified in detail for the corresponding separation issues at a flow rate of 20 mL/min.

7.2.17 Fluorescence Spectroscopy and Fluorescence Quantum Yield (FQY)

The fluorescence spectra were recorded on a Horiba Scientific FluoroMax[®]-4 spectrofluorometer using 1115F-QS Hellma[®] cuvettes (10 mm light path). All measurements were performed at room temperature and in the presence of air. The wavelength of the absorption band maxima (λ_{\max}) are reported in nm. FQY measurements were recorded on a Quantaury-QY from Hamamatsu using PLQY software and CHCl₃ as solvent.

7.2.18 Ultraviolet/Visible (UV/Vis) Absorption Spectroscopy

The UV/Vis spectra were recorded on a Shimadzu UV spectrophotometer UV-1800 using 1115F-QS Hellma[®] cuvettes (10 mm light path). All measurements were performed at room temperature and the wavelength of the emission band maxima (λ_{\max}) are reported in nm.

7.2.19 Monochromator

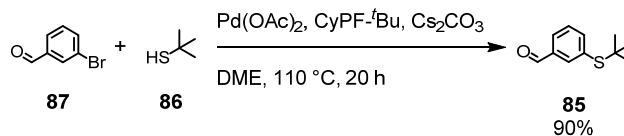
Polychrome V device from TILL Photonics GmbH with a 150 W xenon high-stability lamp (output power > 10 mW at 470 nm) and a half-power bandwidth of 14 nm was used to measure the switching process of the photoswitchable NDI-phanes. The insulation of the optical fiber was

removed at the rear part of the fiber. This part was subsequently dipped into the solution (deuterated solvent and probe) to a depth of about 4 mm and finally the NMR tube was sealed with Parafilm[®]. For the switching experiments, the NMR samples were irradiated with monochromatic light via an optical fiber (length 6 m) directly in a 5 mm ^1H - $^{13}\text{C}/^{15}\text{N}$ - ^2D TCI cryoprobe head with z -axis pulsed field gradients and operating at 700 MHz (Bruker Avance III NMR spectrometer) The measurements were performed at the indicated temperature.

7.3 Synthesis of Molecular 8 Derivatives and Reference Compounds

7.3.1 3-(*tert*-Butylthio)benzaldehyde (**85**)

Reaction Scheme



Experimental Procedure

Preparation of the stock solution

Pd(OAc)₂ (3.58 mg) and CyPF-^tBu (4.22 mg) were dissolved in DME (1.0 mL) and the mixture was stirred at room temperature for 1 min.

Coupling Conditions

To an oven-dried microwave vial were added 3-bromobenzaldehyde (**87**; 1.67 g, 8.75 mmol, 1.0 equiv), Cs₂CO₃ (5.49 g, 16.7 mmol, 1.1 equiv), and DME (11 mL), followed by the addition of the stock solution (50.0 μL, 0.005%) and 2-methylpropane-2-thiol (**86**; 1.00 mL, 8.80 mmol, 1.0 equiv). The microwave vial was sealed and heated at 110 °C for 20 h. The reaction mixture was diluted with H₂O (40 mL) and EtOAc (80 mL). The organic layer was separated and the aqueous layer was extracted with EtOAc (2 × 50 mL). The combined organic layers were dried over Na₂SO₄, filtered, and the solvent was removed under reduced pressure. The residue was purified by column chromatography (SiO₂, cyclohexane/EtOAc 15:1 to 9:1) to yield the pure product (1.53 g, 7.86 mmol, 90%, lit.^[259] 90%) as a colorless liquid.

GC–MS (EI), *m/z* (% relative intensity, ion): 194.2 (10.2, [M]⁺), 137.2. (15.0, [M – C₄H₉]⁺).

¹H-NMR (400 MHz, CDCl₃, δ): 10.02 (s, 1H), 8.02 (t, ³*J*_{HH} = 1.7 Hz, 1H), 7.88 (dt, ³*J*_{HHn} = 7.6 Hz, ⁴*J*_{HH} = 1.4 Hz, 1H), 7.79 (dt, ³*J*_{HH} = 7.6 Hz, ⁴*J*_{HH} = 1.6 Hz, 1H), 7.51 (t, ³*J*_{HH} = 7.6 Hz, 1H), 1.31 (s, 9H).

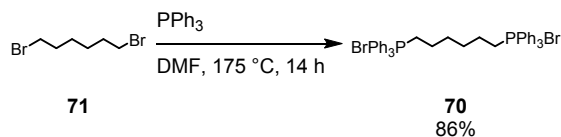
¹³C-NMR (101 MHz, CDCl₃, δ): 191.9, 143.3, 138.7, 136.9, 134.6, 129.7, 129.3, 46.6, 31.1.

TLC (SiO₂, cyclohexane/EtOAc 10:1, UV): *R*_f = 0.31.

The characterization data are in agreement with the literature.^[259]

7.3.2 Hexa-*P*-phenyl-*P,P'*-octanediyl-bis-phosphonium bromide (**70**)

Reaction Scheme



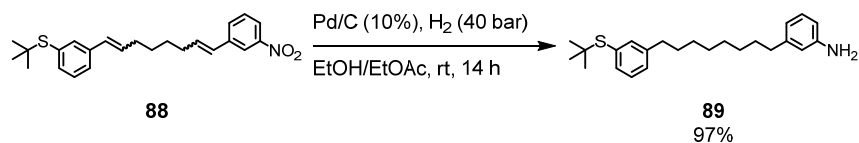
Experimental Procedure

To a two-necked round-bottom flask were added triphenylphosphine (61.8 g, 236 mmol, 2.0 equiv), 1,6-dibromohexane (**71**; 18.0 mL, 116 mmol, 1.0 equiv), and DMF (100 mL). The reaction mixture was stirred at 175 °C for 14 h, before it was cooled to room temperature. The supernatant was filtered off and the residue was washed with acetone (100 mL) and Et₂O (200 mL). The precipitate was dried under high-vacuum to obtain the pure product (76.9 g, 100 mmol, 86%, lit.^[260] 88%) as a white solid.

¹H-NMR (400 MHz, CDCl₃, δ): 7.85–7.62 (m, 30H), 3.80–3.68 (m, 4H), 1.86–1.73 (m, 4H), 1.71–1.55 (m, 4H).

¹³C-NMR (101 MHz, CDCl₃, δ): 135.0 (d, ⁴J_{PC} = 3.0 Hz), 133.7 (d, ³J_{PC} = 10.0 Hz), 130.5 (d, ²J_{PC} = 12.5 Hz), 118.3 (d, ¹J_{PC} = 85.9 Hz), 29.1 (d, ²J_{PC} = 17.0 Hz), 22.5 (d, ¹J_{PC} = 50.2 Hz), 22.3 (d, ³J_{PC} = 4.4 Hz).

The characterization data are in agreement with the literature.^[308]

7.3.4 3-(8-(3-(*tert*-Butylthio)phenyl)octyl)aniline (**89**)Reaction SchemeExperimental Procedure

To a reaction vial were added **88** (532 mg, 1.34 mmol), Pd/C (10%, 55.0 mg, 3.84 mol-%), and a 1:4 mixture of EtOH/EtOAc (10 mL). The vial was placed in an autoclave and the reaction was performed under H₂ atmosphere (40 bar) at room temperature over 14 h. The suspension was filtered through a Celite® pad and washed with CH₂Cl₂ (120 mL) and EtOAc (100 mL). The solvents were evaporated and the residue was purified by column chromatography (SiO₂, cyclohexane/CH₂Cl₂ 1:2 with 1% NEt₃ to 1:4 with 1% NEt₃) to yield the pure product (480 mg, 1.30 mmol, 97%) as a yellow oil.

EA (%): calcd for C₂₄H₃₅NS: C, 77.99; H, 9.54; N, 3.79;
 found: C, 78.36; H, 9.53; N, 3.78.

GC-MS (EI), *m/z* (% relative intensity, ion): 369.5 (17.4, [M]⁺), 313.4 (29.5, [M - C₄H₈]⁺).

HRMS (ESI): [M + H]⁺ calcd for C₂₄H₃₅NS: 370.2563; found: 370.2565.

IR (cm⁻¹): 3459 (w), 3367 (w), 2923 (s), 2852 (s), 1619 (m), 1589 (m), 1459 (m), 1165 (m), 780 (m), 695 (s).

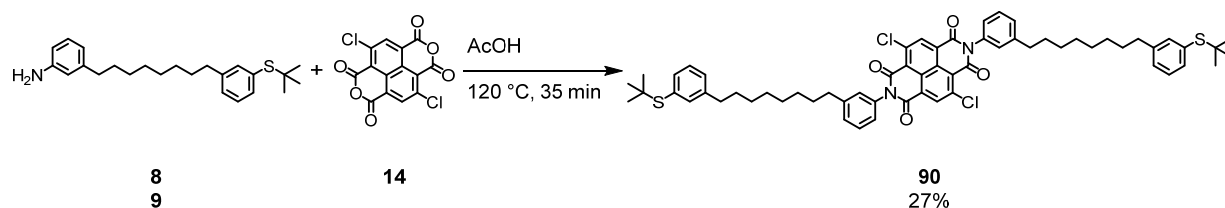
¹H-NMR (400 MHz, CDCl₃, δ): 7.37–7.32 (m, 2H), 7.25–7.20 (m, 1H), 7.19–7.14 (m, 1H), 7.08–7.02 (m, 1H), 6.61–6.56 (m, 1H), 6.54–6.48 (m, 2H), 3.59 (s, 2H, NH₂), 2.63–2.55 (m, 2H), 2.54–2.45 (m, 2H), 1.62–1.52 (m, 4H), 1.32–1.31–1.26 (m, 16H).

¹³C-NMR (101 MHz, CDCl₃, δ): 146.4, 144.3, 143.3, 137.7, 134.8, 132.4, 129.3, 129.0, 128.4, 119.0, 115.4, 112.7, 45.9, 36.1, 35.8, 31.5, 31.5, 31.1, 29.6, 29.5, 29.5, 29.3.

TLC (SiO₂, cyclohexane/CH₂Cl₂ 1:1, UV and ninhydrin): *R_f* = 0.24.

7.3.5 *N,N'*-Di-3'-(8'-(3'-(*tert*-butylthio)phenyl)octyl)phenyl-2,6-dichloro-1,4,5,8-naphthalenetetracarboxylic acid diimide (**90**)

Reaction Scheme



Experimental Procedure

To a round-bottom flask were added **89** (459 mg, 1.24 mmol, 4.0 equiv), 2,6-dichloronaphthalene-1,4,5,8-tetracarboxylic acid dianhydride (**14**; 106 mg, 314 μ mol, 1.0 equiv), and AcOH (70 mL). The resulting suspension was stirred at 120 °C for 35 min, before it was cooled to room temperature and concentrated under reduced pressure. The residue was purified by column chromatography (1st: SiO₂, cyclohexane/CH₂Cl₂ 1:40 to 1:20; 2nd: SiO₂, CH₂Cl₂) and GPC to obtain the pure product (86.0 mg, 82.7 μ mol, 27%) as a yellow solid.

EA (%): calcd. for C₆₂H₆₈Cl₂N₂O₄S₂: C, 71.59; H, 6.59; N, 2.69;

found: C, 71.95; H, 6.69; N, 2.83.

HRMS (ESI): [M + Na]⁺ calcd for C₆₂H₆₈Cl₂N₂O₄S₂: 1061.3890; found: 1061.3878.

IR (cm⁻¹): 2919 (m), 2851 (m), 1721 (m), 1670 (s), 1562 (m), 1425 (m), 1359 (m), 1323 (m), 1228 (s), 888 (m), 789 (s), 736 (s), 688 (s).

MP: 174–176 °C.

MS (MALDI-TOF), *m/z*: 1038.8 ([M]⁻).

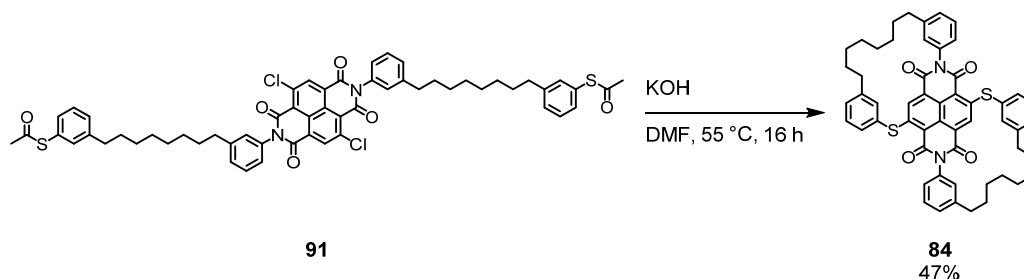
¹H-NMR (400 MHz, CDCl₃, δ): 8.81 (s, 2H), 7.52–7.46 (m, 2H), 7.38–7.29 (m, 6H), 7.25–7.19 (m, 2H), 7.18–7.12 (m, 6H), 2.74–2.67 (m, 4H), 2.63–2.57 (m, 4H), 1.72–1.57 (m, 9H), 1.39–1.32 (m, 15H), 1.28 (s, 18H).

¹³C-NMR (101 MHz, CDCl₃, δ): 161.2, 160.8, 144.8, 143.3, 140.7, 137.6, 136.3, 134.7, 134.2, 132.3, 129.6, 129.6, 128.9, 128.3, 128.3, 127.7, 126.5, 125.6, 122.8, 45.8, 35.8, 35.8, 31.5, 31.2, 31.1, 29.4, 29.4, 29.4, 29.3.

TLC (SiO₂, CH₂Cl₂, UV): *R_f* = 0.38.

7.3.7 1((3,3',3'',3''')-2,7-Diphenyl-4,9-bis(phenylthio)benzo[*lmn*][3,8]phenanthroline-1,3,6,8(2*H*,7*H*)-tetraona)bicyclo[09.8^{1,1}]heptadecanodane (84)

Reaction Scheme



Experimental Procedure

To an oven-dried two-necked round-bottom flask were added KOH (38.0 mg, 677 μmol , 10.0 equiv) and dry DMF (20 mL). The resulting solution was deoxygenated with argon for 15 min and then heated at 55 °C. A solution of **91** (69.0 mg, 68.1 μmol , 1.0 equiv) dissolved in dry DMF (30 mL) was added via a syringe pump over 2.5 h to the reaction mixture. The resulting mixture was stirred at 55 °C for 16 h before the solvent was removed under reduced pressure, and the residue was purified repeatedly by column chromatography (SiO_2 , CH_2Cl_2) to yield the pure product (27.0 mg, 41.6 μmol , 47%) as a red solid.

FQY (%): $\Phi_{\text{fl}} < 0.01$.

HRMS (ESI): $[\text{M} + \text{H}]^+$ calcd for $\text{C}_{54}\text{H}_{50}\text{N}_2\text{O}_4\text{S}_2$: 855.3285; found: 855.3282.

IR (cm^{-1}): 2921 (m), 2849 (m), 1708 (m), 1667 (s), 1551 (m), 1427 (m), 1318 (s), 1225 (s), 785 (m), 739 (s), 670 (m).

MP: above 280 °C.

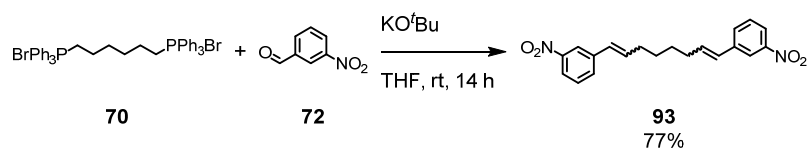
MS (MALDI-TOF), m/z : 854.0 ($[\text{M}]^-$).

$^1\text{H-NMR}$ (400 MHz, CDCl_3 , δ): 8.15 (s, 2H), 7.46–7.38 (m, 8H), 7.35–7.32 (m, 2H), 7.26–7.24 (m, 2H), 7.18–7.14 (m, 2H), 7.09 (t, $^4J_{\text{HH}} = 1.8$ Hz, 2H), 2.74–2.69 (m, 4H), 2.66 (t, $^3J_{\text{HH}} = 6.8$ Hz, 4H), 1.75–1.59 (m, 8H), 1.25–1.14 (m, 16H).

$^{13}\text{C-NMR}$ (101 MHz, CDCl_3 , δ): 163.8, 162.3, 150.6, 145.7, 143.8, 136.2, 134.3, 133.2, 131.2, 130.7, 130.4, 130.0, 129.9, 129.4, 128.9, 125.8, 125.7, 124.3, 118.8, 36.2, 34.8, 32.5, 31.3, 29.5, 29.1, 28.6, 28.0.

TLC (SiO_2 , CH_2Cl_2 , UV): $R_f = 0.58$.

UV/Vis (CDCl_3): λ_{max} (ϵ_{max}): 359 (9886), 374 (10554), 516 (18635) nm ($\text{mol}^{-1} \cdot \text{dm}^3 \cdot \text{cm}^{-1}$).

7.3.8 1,8-Bis(3-nitrophenyl)octa-1,7-diene (**93**)Reaction SchemeExperimental Procedure

To an oven-dried flask were added **70** (18.4 g, 24.0 mmol, 1.0 equiv), KO^tBu (5.95 g, 53.0 mmol, 2.2 equiv), and dry THF (250 mL). The resulting mixture was deoxygenated with argon for 10 min, followed by the addition of **72** (7.25 g, 48.0 mmol, 2.0 equiv) in one portion. The resulting mixture was stirred at room temperature for 14 h. Brine (30 mL) and EtOAc (20 mL) were added. The organic phase was separated and the aqueous layer was extracted with EtOAc (3 × 40 mL). The organic layers were combined, washed with brine (30 mL), dried over MgSO₄, filtered, and concentrated under reduced pressure. The residue was purified by column chromatography (1st, short one: SiO₂, cyclohexane/CH₂Cl₂ 1:3 to 1:20; 2nd: cyclohexane/CH₂Cl₂ 1:2 to 1:3) to yield the pure product (6.53 g, 18.5 mmol, 77%) as a yellow oil.

EA (%): calcd. for C₂₀H₂₀N₂O₄: C, 68.17; H, 5.72; N, 7.95;

found: C, 68.10; H, 5.64; N, 7.98.

HRMS (ESI): [M + Na]⁺ calcd for C₂₀H₂₀N₂O₄: 375.1315; found: 375.1319.

IR (cm⁻¹): 2930 (w), 2847 (s), 1521 (s), 1461 (w), 1343 (s), 1093 (w), 969 (m), 707 (m), 666 (m).

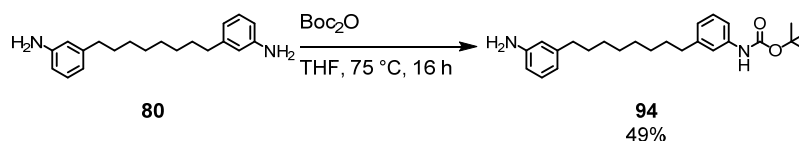
MP: 68–70 °C.

¹H-NMR and the ¹³C-NMR spectra contained a mixture of all four isomers, but the ratio was not determined.

¹H-NMR (400 MHz, CDCl₃, δ): 8.22–7.98 (m, 4H), 7.66–7.39 (m, 4H), 6.51–6.29 (m, 2.4H), 5.89–5.75 (m, 1.6H), 2.40–2.22 (m, 4H), 1.60–1.48 (m, 4H).

¹³C-NMR (101 MHz, CDCl₃, δ): 148.7, 148.3, 139.6, 139.3, 139.3, 135.7, 135.6, 134.8, 134.8, 134.3, 134.2, 132.0, 132.0, 129.5, 129.2, 129.2, 128.2, 128.1, 127.1, 123.5, 123.4, 121.6, 121.5, 121.5, 120.6, 33.0, 32.9, 29.3, 28.8, 28.7, 28.5, 28.4.

TLC (SiO₂, cyclohexane/CH₂Cl₂ 1:1, UV): R_f = 0.27.

7.3.9 *tert*-Butyl (3-(8-(3-aminophenyl)octyl)phenyl)carbamate (**94**)Reaction SchemeExperimental Procedure

To an oven-dried flask were added **80** (5.23 g, 17.6 mmol, 1.0 equiv), dry THF (175 mL), and di-*tert*-butyldicarbonate (3.84 g, 17.6 mmol, 1.0 equiv). The resulting mixture was heated at 75 °C for 16 h, before it was cooled to room temperature. The solvent was evaporated under reduced pressure and the residue was purified by column chromatography (SiO₂, cyclohexane/EtOAc 2:1 with NEt₃ 1% to 1:1 with NEt₃ 1%) to obtain the pure product (3.41 g, 8.59 mmol, 49%) as a brown solid.

HRMS (ESI): [M +H]⁺ calcd for C₂₅H₃₆N₂O₂: 397.2850; found: 397.2848.

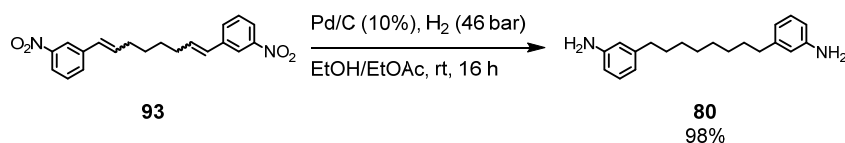
IR (cm⁻¹): 2922 (m), 2849 (m), 1720 (s), 1543 (m), 1238 (s), 1154 (s), 692 (s).

MP: 80–82 °C.

¹H-NMR (500 MHz, CDCl₃, δ): 7.24–7.15 (m, 2H), 7.16–7.10 (m, 1H), 7.06 (td, ³J_{HH} = 7.4 Hz, ⁴J_{HH} = 1.0 Hz, 1H), 6.85 (dt, ³J_{HH} = 7.4 Hz, ⁴J_{HH} = 1.4 Hz, 1H), 6.59 (dt, ³J_{HH} = 7.6 Hz, ⁴J_{HH} = 1.1 Hz, 1H), 6.54–6.49 (m, 2H), 6.48–6.42 (m, 1H), 3.60 (s, 2H, NH₂), 2.60–2.53 (m, 2H), 2.54–2.47 (m, 2H), 1.62–1.56 (m, 4H), 1.52 (s, 9H), 1.34–1.28 (m, 8H).

¹³C-NMR (101 MHz, CDCl₃, δ): 152.9, 146.4, 144.4, 144.1, 138.4, 129.2, 128.9, 123.3, 119.0, 118.6, 115.9, 115.4, 112.6, 80.5, 36.2, 36.1, 31.6, 31.5, 29.6, 29.5, 29.5, 28.5.

TLC (SiO₂, cyclohexane/EtOAc 3:1, UV): R_f = 0.26.

7.3.10 3,3'-(Octane-1,8-diyl)dianiline (80)Reaction SchemeExperimental Procedure

To a reaction vial were added **93** (826 mg, 2.35 mmol), Pd/C (10%, 47.0 mg, 1.88 mol-%), and a 1:5 mixture of EtOH/EtOAc (12 mL). The vial was placed in an autoclave and the reaction was performed under H₂ atmosphere (46 bar) at room temperature over 16 h. The suspension was filtered through a Celite[®] pad and washed with CH₂Cl₂ (140 mL) and EtOAc (100 mL). The solvents were evaporated and the residue was purified by column chromatography (SiO₂, cyclohexane/EtOAc 3:2 to 1:1 with 1% NEt₃) to afford the pure product (680 mg, 2.29 mmol, 98%) as a colorless solid.

EA (%): calcd. for C₂₀H₂₈N₂: C, 81.03; H, 9.52; N, 9.45;

 found: C, 80.87; H, 9.40; N, 9.38.

HRMS (ESI): [M + H]⁺ calcd for C₂₀H₂₈N₂: 297.2325; found: 297.2329.

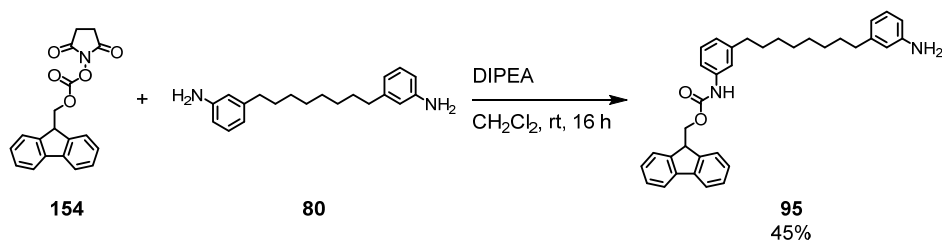
IR (cm⁻¹): 3419 (m), 3333 (m), 2918 (s), 2847 (s), 1587 (s), 1489 (m), 1461 (m), 1298 (m), 1168 (m), 781 (s), 696 (s).

MP: 75–77 °C.

¹H-NMR (400 MHz, (CD₃)₂SO, δ): 6.88 (t, ³J_{HH} = 7.6 Hz, 2H), 6.40–6.25 (m, 6H), 4.88 (s, 4H, NH₂), 2.39 (t, ³J_{HH} = 7.5 Hz, 4H), 1.55–1.44 (m, 4H), 1.29–1.22 (d, 8H).

¹³C-NMR (101 MHz, (CD₃)₂SO, δ): 148.4, 142.8, 128.6, 115.9, 113.9, 111.4, 35.4, 30.9, 28.9, 28.7.

TLC (SiO₂, cyclohexane/EtOAc 2:1, UV): R_f = 0.17.

7.3.11 (9*H*-Fluoren-9-yl)methyl (3-(8-(3-aminophenyl)octyl)phenyl)carbamate (**95**)Reaction SchemeExperimental Procedure

N-(9-Fluorenylmethoxycarbonyloxy)succinimide (**154**; 331 mg, 981 μmol , 1.0 equiv), **80** (300 mg, 990 μmol , 1.0 equiv), DIPEA (340 μL , 2.06 mmol, 2.1 equiv), and dry CH_2Cl_2 (35 mL) were added to an oven-dried flask and stirred at room temperature for 16 h. After the addition of CH_2Cl_2 (50 mL) and brine (60 mL), the aqueous layer was separated. The organic layer was dried over Na_2SO_4 , filtered, and the solvent was evaporated under reduced pressure. The residue was purified by column chromatography (SiO_2 , cyclohexane/EtOAc 3:1) to afford the pure product (230 mg, 443 μmol , 45%) as a white solid.

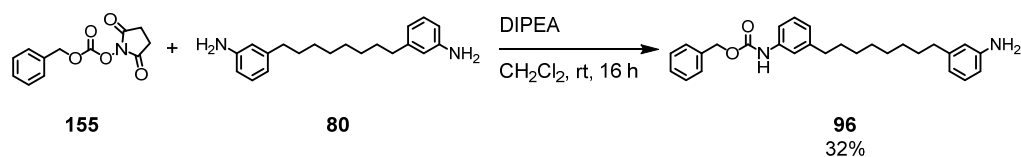
EA (%): calcd. for $\text{C}_{35}\text{H}_{38}\text{N}_2\text{O}_2$: C, 81.05; H, 7.38; N, 5.40;
 found: C, 80.95; H, 7.36; N, 5.33.

HRMS (ESI): $[\text{M} + \text{H}]^+$ calcd for $\text{C}_{35}\text{H}_{38}\text{N}_2\text{O}_2$: 519.3006; found: 519.3008.

$^1\text{H-NMR}$ (400 MHz, CDCl_3 , δ): 7.79 (d, $^3J_{\text{HH}} = 7.5$ Hz, 2H), 7.62 (d, $^3J_{\text{HH}} = 7.4$ Hz, 2H), 7.42 (t, $^3J_{\text{HH}} = 7.4$ Hz, 2H), 7.33 (td, $^3J_{\text{HH}} = 7.4$ Hz, $^4J_{\text{HH}} = 1.2$ Hz, 2H), 7.20 (d, $^3J_{\text{HH}} = 6.1$ Hz, 2H), 7.06 (td, $^3J_{\text{HH}} = 7.3$ Hz, $^4J_{\text{HH}} = 1.2$ Hz, 1H), 6.92–6.86 (m, 1H), 6.66 (s, 1H), 6.59 (d, $^3J_{\text{HH}} = 7.6$ Hz, 1H), 6.53–6.47 (m, 2H), 4.55 (d, $^3J_{\text{HH}} = 6.6$ Hz, 2H), 4.29 (t, $^3J_{\text{HH}} = 6.6$ Hz, 1H), 3.57 (s, 2H, NH_2), 2.60–2.54 (m, 2H), 2.53–2.48 (m, 2H), 1.62–1.52 (m, 4H), 1.33–1.28 (m, 8H).

$^{13}\text{C-NMR}$ (101 MHz, CDCl_3 , δ): 146.4, 144.4, 144.2, 143.9, 141.5, 129.2, 129.0, 127.9, 127.3, 125.1, 123.9, 120.2, 119.0, 115.5, 112.7, 66.9, 47.3, 36.1, 36.1, 31.5, 31.4, 29.5, 29.4, 29.4.

TLC (SiO_2 , cyclohexane/EtOAc 1:3, UV): $R_f = 0.50$.

7.3.12 Benzyl (3-(8-(3-aminophenyl)octyl)phenyl)carbamate (96)Reaction SchemeExperimental Procedure

N-(Benzyloxycarbonyloxy)succinimide (**155**; 1.37 g, 5.50 mmol, 1.0 equiv), **80** (1.71 g, 5.78 mmol, 1.1 equiv), DIPEA (910 μ L, 5.51 mmol, 1.0 equiv), and dry CH₂Cl₂ (40 mL) were added to an oven-dried flask and stirred at room temperature for 16 h. After the addition of sat. aq. NH₄Cl, the organic layer was separated and the aqueous layer was extracted with CH₂Cl₂ (2 \times 30 mL). The combined organic layers were dried over Na₂SO₄, filtered, and the solvent was evaporated under reduced pressure. The residue was purified twice by column chromatography (SiO₂, cyclohexane/EtOAc 4:1) to afford the pure product (758 mg, 1.76 mmol, 32%) as a white solid.

HRMS (ESI): [M + H]⁺ calcd for C₂₈H₃₄N₂O₂: 431.2693; found: 431.2695.

MP: 46–48 °C.

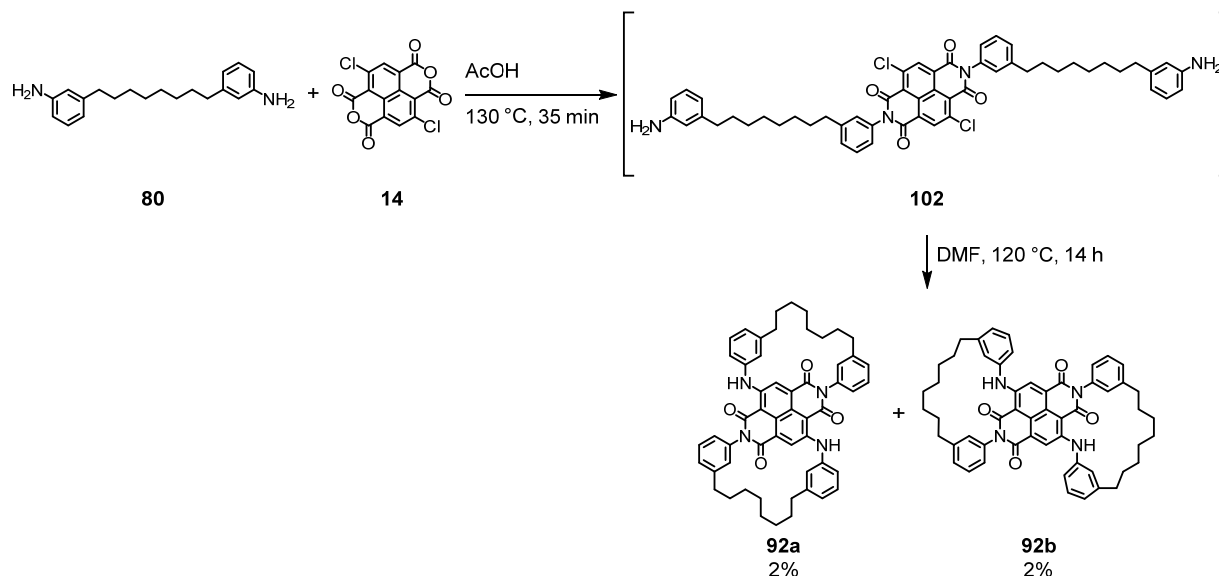
¹H-NMR (400 MHz, CDCl₃, δ): δ 7.45–7.31 (m, 5H), 7.24–7.16 (m, 3H), 7.09–7.03 (m, 1H), 6.91–6.86 (m, 1H), 6.69–6.56 (m, 2H), 6.54–6.48 (m, 2H), 5.20 (s, 2H), 3.59 (s, 2H, NH₂), 2.57 (dd, ³J_{HH} = 8.7 Hz, ³J_{HH} = 6.8 Hz, 2H), 2.50 (t, ³J_{HH} = 7.7 Hz, 2H), 1.61–1.54 (m, 4H), 1.32–1.28 (m, 8H).

¹³C-NMR (101 MHz, CDCl₃, δ): 153.4, 146.4, 144.4, 144.3, 137.8, 136.3, 129.3, 129.0, 128.8, 128.5, 128.4, 123.9, 119.0, 116.1, 115.5, 112.7, 67.1, 36.1, 36.1, 31.5, 31.5, 29.6, 29.5, 29.4.

TLC (SiO₂, cyclohexane/EtOAc 3:1, UV): R_f = 0.22.

7.3.13 1((3,3',3'',3''')-2,7-Diphenyl-4,9-bis(phenylamino)benzo[*lmn*][3,8]phenanthroline-1,3,6,8(2*H*,7*H*)-tetraona)bicyclo[09.8^{1,1}]heptadecanodane (92a and 92b)

Reaction Scheme



Experimental Procedure

80 (566 mg, 1.91 mmol, 4.7 equiv) and **14** (138 mg, 409 μmol , 1.0 equiv) were dissolved in AcOH (150 mL) and the resulting mixture was stirred at 130 °C for 35 min. The solvent was removed under reduced pressure and the residue was purified by column chromatography (SiO_2 , $\text{CH}_2\text{Cl}_2/\text{EtOAc}$ 10:1) to obtain the free amine **102** (59.0 mg) as a violet solid, which was dried under high vacuum. The crude product was used without further purification. **102** (59.0 mg) was dissolved in dry DMF (10 mL) and this solution was added over 3 h to a hot solution (120 °C) of dry DMF (250 mL). After the addition, the reaction mixture was stirred at 130 °C for 14 h. The solvent was evaporated under reduced pressure and the residue was purified by column chromatography (SiO_2 , cyclohexane/ EtOAc 2:1) to obtain the pure product as an isomeric mixture. A final purification on preparative NP HPLC (CH_2Cl_2 to $\text{CH}_2\text{Cl}_2/2\text{-propanol}$ 94:6 over 60 min) yielded the two isomers **92a** (5.7 mg, 6.94 μmol , 2%) **92b** (7.5 mg, 9.13 μmol , 2%) as blue solids.

102

MS (DART-EI), m/z (% relative intensity, ion): 891.2 (100, $[\text{M} - \text{H}]^-$).

TLC (SiO_2 , $\text{CH}_2\text{Cl}_2/\text{EtOAc}$ 10:1, UV): $R_f = 0.70$.

92a (with NOE signal)

FQY (%): $\Phi_{\text{fl}} = 0.012$.

HRMS (MALDI/ESI): $[M]^+$ calcd for $C_{54}H_{52}N_4O_4$: 820.3983; found: 820.3984.

IR (cm^{-1}): 2922 (m), 2851 (m), 1693 (m), 1637 (m), 1581 (s), 1225 (s), 786 (m), 692 (m).

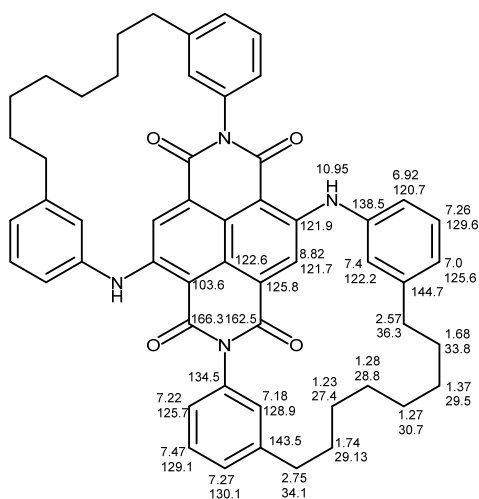
MP: above 360 °C.

MS (MALDI-TOF), m/z : 821.4 ($[M]^+$).

$^1\text{H-NMR}$ (600 MHz, CDCl_3 , δ): 10.95 (s, 2H, NH), 8.82 (s, 2H), 7.47 (t, $^3J_{\text{HH}} = 7.7$ Hz, 2H), 7.40 (s, 2H), 7.30–7.26 (m, 4H), 7.24–7.21 (m, 2H), 7.18 (s, 2H), 6.99 (d, $^3J_{\text{HH}} = 7.6$ Hz, 2H), 6.92 (d, $^3J_{\text{HH}} = 7.9$ Hz, 2H), 2.75 (t, $^3J_{\text{HH}} = 6.3$ Hz, 4H), 2.58 (t, $^3J_{\text{HH}} = 7.8$ Hz, 4H), 1.75–1.66 (m, 8H), 1.38–1.28 (m, 16H).

$^{13}\text{C-NMR}$ (151 MHz, CDCl_3 , δ): 166.3, 162.5, 144.7, 143.5, 138.5, 134.5, 130.1, 129.6, 129.1, 128.9, 125.8, 125.7, 125.6, 122.6, 122.2, 121.9, 121.7, 120.7, 103.6, 36.3, 34.1, 33.8, 30.7, 29.5, 29.1, 28.8, 27.4.

Assignment of hydrogen and carbon atoms was done by 2D-NMR.



TLC (SiO_2 , cyclohexane/EtOAc 2:1, UV): $R_f = 0.69$.

UV/Vis (CDCl_3): λ_{max} (ϵ_{max}): 320 (11877), 371 (4390), 617 (6697) nm ($\text{mol}^{-1} \cdot \text{dm}^3 \cdot \text{cm}^{-1}$).

92b (without NOE signal)

FQY (%): $\Phi_{\text{fl}} < 0.01$.

HRMS (MALDI/ESI): $[M]^+$ calcd for $C_{54}H_{52}N_4O_4$: 820.3983; found: 820.3984.

IR (cm^{-1}): 2922 (m), 2851 (m), 1693 (w), 1637 (m), 1581 (s), 1322 (w), 1225 (s), 786 (m), 691 (m).

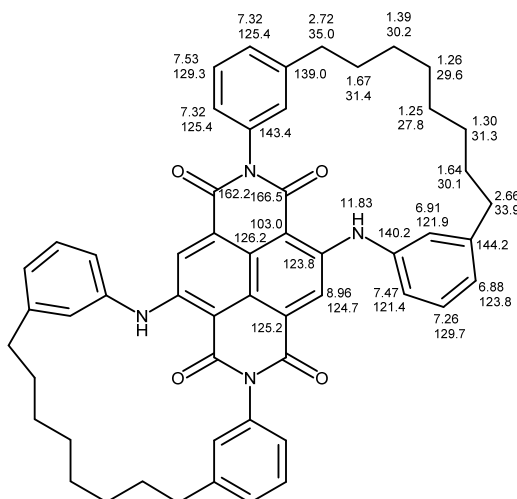
MS (MALDI-TOF), m/z : 821.4 ($[M]^+$).

MP: above 360 °C.

$^1\text{H-NMR}$ (600 MHz, CDCl_3 , δ): 11.83 (s, 2H), 8.96 (s, 2H), 7.53 (t, $^3J_{\text{HH}} = 7.7$ Hz, 2H), 7.49–7.46 (m, 2H), 7.33–7.30 (m, 4H), 7.27–7.26 (m, 2H), 7.07 (s, 2H), 6.91 (s, 2H), 6.88 (d, $^3J_{\text{HH}} = 7.5$ Hz, 2H), 2.83–2.60 (m, 8H), 1.68–1.62 (m, 8H), 1.30–1.26 (m, 16H).

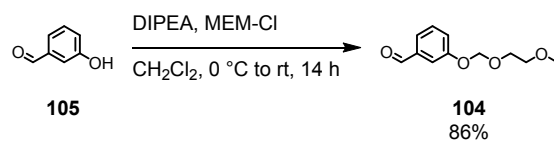
$^{13}\text{C-NMR}$ (151 MHz, CDCl_3 , δ): 166.5, 162.2, 144.3, 144.2, 143.4, 140.2, 139.0, 129.7, 129.3, 129.2, 126.2, 125.4, 125.2, 124.7, 123.8, 121.9, 121.4, 103.0, 35.0, 33.9, 31.4, 31.3, 30.2, 30.1, 29.6, 27.8.

Assignment of hydrogen and carbon atoms was done by 2D-NMR.



TLC (SiO_2 , cyclohexane/EtOAc 2:1, UV): $R_f = 0.68$.

UV/Vis (CDCl_3): λ_{max} (ϵ_{max}): 325 (5700), 625 (1155) nm ($\text{mol}^{-1} \cdot \text{dm}^3 \cdot \text{cm}^{-1}$).

7.3.14 3-((2-Methoxyethoxy)methoxy)benzaldehyde (**104**)Reaction SchemeExperimental Procedure

3-Hydroxybenzaldehyde (**105**; 4.52 g, 36.5 mmol, 1.0 eq) was dissolved in dry CH_2Cl_2 (50 mL) and cooled to 0 °C. DIPEA (12.7 mL, 72.9 mmol, 2.0 equiv) was added in one portion, followed by the dropwise addition of MEM-Cl (5.36 mL, 43.0 mmol, 1.18 eq) in dry CH_2Cl_2 (50 mL). After the complete addition, the reaction mixture was warmed to room temperature and stirred for 3 h. The solution was quenched with aq. HCl (1 M, 30 mL). The organic layer was separated and the aqueous layer was extracted with CH_2Cl_2 (2 \times 40 mL). The combined organic phases were dried over Na_2SO_4 , filtered, and concentrated under reduced pressure. The residue was purified by column chromatography (SiO_2 , cyclohexane/EtOAc 2:1 to 3:2) to afford the pure product (6.55 g, 31.2 mmol, 86%, lit.^[268] 86%) as a slightly yellow liquid.

GC-MS (EI), m/z (% relative intensity, ion): 135.2 (3.6, $[\text{M} - \text{OCH}_2\text{OCH}_3]^+$), 121.2 (2.5, $[\text{M} - \text{CH}_2\text{OCH}_2\text{OCH}_3]^+$).

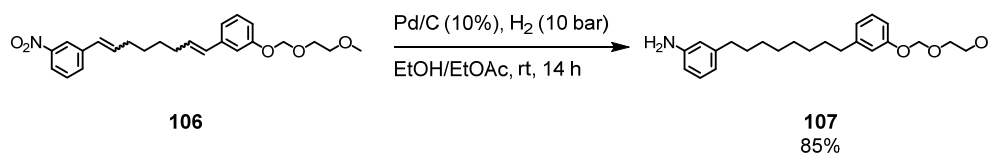
$^1\text{H-NMR}$ (400 MHz, CDCl_3 , δ): 9.97 (s, 1H), 7.58–7.48 (m, 2H), 7.45 (t, $^3J_{\text{HH}} = 7.8$ Hz, 1H), 7.35–7.27 (m, 1H), 5.32 (s, 2H), 3.86–3.80 (m, 2H), 3.58–3.52 (m, 2H), 3.37 (s, 3H).

$^{13}\text{C-NMR}$ (101 MHz, CDCl_3 , δ): 192.1, 157.9, 138.0, 130.3, 123.8, 122.9, 116.5, 93.6, 71.70, 68.1, 59.2.

TLC (SiO_2 , cyclohexane/EtOAc 3:2, UV, KMnO_4): $R_f = 0.39$.

TLC (SiO_2 , cyclohexane/EtOAc 4:1, UV, KMnO_4): $R_f = 0.17$.

The characterization data are in agreement with the literature.^[268]

7.3.16 3-(8-(3-((2-Methoxyethoxy)methoxy)phenyl)octyl)aniline (107)Reaction SchemeExperimental Procedure

To a reaction vial with a stir bar were added **106** (1.24 g, 3.01 mmol), Pd/C (10%, 43.0 mg, 1.35 mol-%), and a 2:3 mixture of EtOH/EtOAc (14 mL). The vial was placed in an autoclave and the reaction was performed under H₂ atmosphere (10 bar) at room temperature over 14 h. The suspension was filtrated through a Celite[®] pad and washed with CH₂Cl₂ (40 mL) and EtOAc (50 mL). The solvents were evaporated and the residue was purified by column chromatography (SiO₂, cyclohexane/EtOAc 2:1 to 1:1 with 1% NEt₃) to obtain the pure product (990 mg, 2.57 mmol, 85%) as yellow oil.

HRMS (ESI): [M + H]⁺ calcd for C₂₄H₃₅NO₃: 386.2690; found: 386.2693.

IR (cm⁻¹): 2922 (m), 2852 (m), 1585 (m), 1487 (m), 1015 (s), 781 (m), 696 (m).

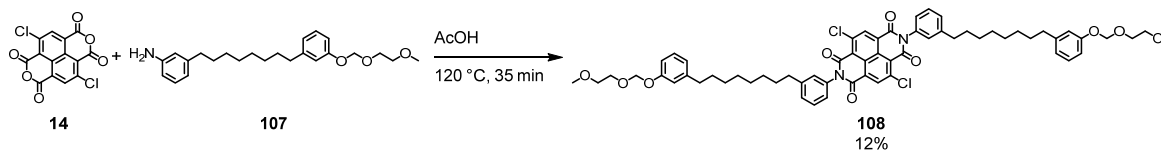
¹H-NMR (400 MHz, CDCl₃, δ): 7.22–7.14 (m, 1H), 7.09–7.02 (m, 1H), 6.91–6.79 (m, 3H), 6.64–6.45 (m, 3H), 5.26 (s, 2H), 3.86–3.80 (m, 2H), 3.62–3.53 (m, 4H), 3.38 (s, 3H), 2.62–2.53 (m, 2H), 2.54–2.46 (m, 2H), 1.63–1.54 (m, 4H), 1.33–1.25 (m, 8H).

¹³C-NMR (101 MHz, CDCl₃, δ): 157.4, 146.4, 144.8, 144.4, 129.3, 129.3, 122.2, 119.0, 116.5, 115.4, 113.5, 112.6, 93.6, 71.8, 67.7, 59.2, 36.1, 31.5, 31.5, 29.6, 29.6, 29.5, 29.5.

TLC (SiO₂, cyclohexane/EtOAc 2:1, UV and ninhydrin): R_f = 0.30.

7.3.17 *N,N'*-Di-3'-(8'-(3'-((2'-methoxyethoxy)methoxy)phenyl)octyl)phenyl-2,6-dichloro-1,4,5,8-naphthalenetetracarboxylic acid diimide (108)

Reaction Scheme



Experimental Procedure

14 (89.4 mg, 265 μmol , 1.0 equiv) and **107** (304 mg, 789 μmol , 3.0 equiv) in AcOH (90 mL) were heated at 120 $^\circ\text{C}$. The resulting mixture was stirred at 120 $^\circ\text{C}$ for 35 min, before it was cooled to room temperature. The solvent was removed under reduced pressure and the residue was purified by column chromatography (SiO_2 , cyclohexane/EtOAc 1:1) and GPC to yield the pure product (35.5 mg, 32.6 μmol , 12%) as a red solid.

MS (MALDI-TOF), m/z : 1071.6 ($[\text{M}]^-$).

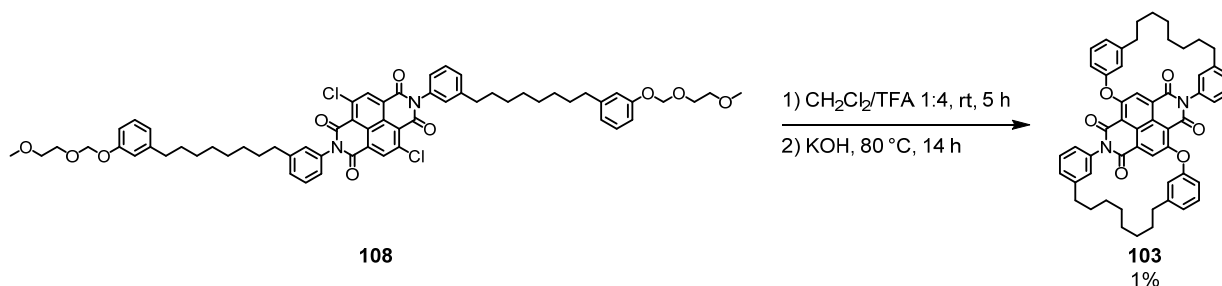
$^1\text{H-NMR}$ (400 MHz, CDCl_3 , δ): 8.83 (s, 2H), 7.51–7.47 (m, 2H), 7.37–7.33 (m, 2H), 7.20–7.15 (m, 2H), 7.14 – 7.12 (m, 4H), 6.86–6.80 (m, 6H), 5.25 (s, 4H), 3.84–3.80 (m, 4H), 3.58–3.53 (m, 4H), 3.37 (s, 6H), 2.72–2.67 (m, 4H), 2.59–2.52 (m, 4H), 1.71–1.56 (m, 12H), 1.40–1.33 (m, 12H).

$^{13}\text{C-NMR}$ (125 MHz, CDCl_3 , δ): 161.2, 160.9, 157.4, 144.9, 144.8, 140.8, 136.4, 134.2, 129.6, 129.6, 129.3, 128.3, 127.7, 126.5, 125.6, 122.8, 122.1, 116.4, 113.4, 93.6, 71.7, 67.7, 59.1, 36.1, 35.9, 31.5, 31.2, 29.5, 29.5, 29.5, 29.4.

TLC (SiO_2 , cyclohexane/EtOAc 1:1, UV): $R_f = 0.43$.

7.3.18 1((3,3',3'',3''')-2,7-Diphenyl-4,9-bis(phenoxy)benzo[*lmn*][3,8]phenanthroline-1,3,6,8(2*H*,7*H*)-tetraona)bicyclo[09.8^{1,1}]heptadecanodane (103)

Reaction Scheme



Experimental Procedure

108 (225 mg, 210 μmol, 1.0 equiv) was dissolved in a 1:4 mixture of CH₂Cl₂/TFA (20 mL) and stirred at room temperature for 5 h (the course of the deprotection reaction was monitored by MALDI-TOF-MS analysis). The reaction mixture was quenched with H₂O (50 mL) and extracted with CH₂Cl₂ (3 x 30 mL). The combined organic layers were dried over Na₂SO₄, filtered, and the solvent evaporated under reduced pressure. The residue was dissolved in dry DMF (18 mL) and added dropwise (0.5 mm/min) to a solution of dry DMF (20 mL) and KOH (118 mg, 2.10 mmol, 10.0 equiv) at 80 °C. After the complete addition, the reaction mixture was stirred at 80 °C for 14 h and was cooled to room temperature. H₂O (40 mL) and CH₂Cl₂ (100 mL) were added and the organic layer was separated. The aqueous phase was extracted with CH₂Cl₂ (3 x 40 mL), dried over Na₂SO₄, filtered, and the solvent was evaporated under reduced pressure. The residue was purified by column chromatography (SiO₂, cyclohexane/EtOAc 3:1) to yield the pure product (2.0 mg, 2.43 μmol, 1%) as a yellow solid.

FQY (%): $\Phi_{\text{H}} = 0.01$.

IR (cm⁻¹): 2921 (s), 2851 (m), 1673 (w), 1223 (w).

HRMS (ESI): [M + H]⁺ calcd for C₅₄H₅₀N₂O₆ 823.3742; found: 823.3738.

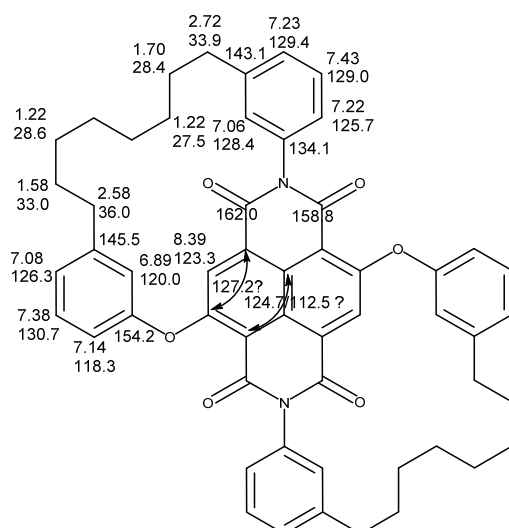
MP: above 340 °C.

¹H-NMR (600 MHz, CDCl₃, δ): 8.39 (s, 2H), 7.43 (t, ³J_{HH} = 7.7 Hz, 2H), 7.38 (t, ³J_{HH} = 7.8 Hz, 2H), 7.25–7.20 (m, 4H), 7.16–7.12 (m, 2H), 7.10–7.04 (m, 4H), 6.91–6.88 (m, 2H), 2.76–2.69 (m, 4H), 2.58 (t, ³J_{HH} = 6.7 Hz, 2H).

24 aliphatic protons were underneath the grease signal; therefore this range was not considered.

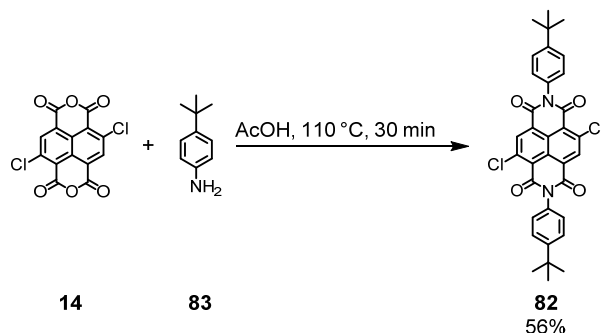
¹³C-NMR (151 MHz, CDCl₃, δ): 162.0, 158.8, 154.2, 145.5, 143.1, 134.1, 130.7, 129.4, 129.0, 128.1, 127.2, 126.3, 125.7, 124.7, 123.3, 120.0, 118.3, 112.5, 36.0, 33.9, 33.0, 28.6, 28.4, 27.5.

Assignment of hydrogen and carbon atoms was done by 2D-NMR. Signals at 127.2, 124.7 and 112.5 ppm cannot be clearly assigned, they have the same ²J_{HC} and ³J_{HC} coupling to the signal at 8.39 ppm.



TLC (SiO₂, cyclohexane/EtOAc 3:1, UV): R_f = 0.30.

UV/Vis (CDCl₃): λ_{max} (ε_{max}): 363 (2892), 459 (2943) nm (mol⁻¹ · dm³ · cm⁻¹).

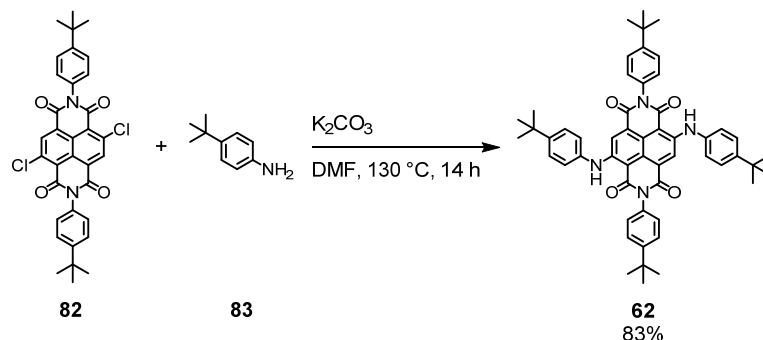
7.3.19 *N,N'*-Di-(4'-*tert*-butylphenyl)-2,6-dichloro-1,4,5,8-naphthalenetetracarboxylic acid diimide (82**)**Reaction SchemeExperimental Procedure

14 (50.0 mg, 149 μmol , 1.0 equiv) was suspended in AcOH (40 mL) and heated at 120 °C. 4-*tert*-Butylaniline (**83**; 0.2 mL, 1.23 mmol, 8.3 equiv) was added to the hot solution and the resulting mixture was kept at 110 °C for 30 min. Immediately after the addition of the amine, a violet precipitation started to form. The reaction mixture was cooled to room temperature, the precipitate was filtered off, and washed with AcOH (60 mL) and MeOH (40 mL) to afford the pure product (50.0 mg, 83.4 μmol , 56%, lit.^[77] 70%).

¹H-NMR (400 MHz, CD₂Cl₂, δ): 8.84 (s, 2H), 7.65–7.60 (m, 4H), 7.27–7.24 (m, 4H), 1.42 (s, 18H).

No **¹³C-NMR** spectrum was measured due to solubility problem.

The characterization data is in agreement with the literature.^[77]

7.3.21 *N,N'*-Di-(4'-*tert*-butylphenyl)-2,6-di(4-*tert*-butylphenylamino)-1,4,5,8-naphthalenetetracarboxylic acid diimide (62**)**Reaction SchemeExperimental Procedure

82 (28.0 mg, 46.7 μmol , 1.0 equiv), K_2CO_3 (34.0 mg, 244 μmol , 5.4 equiv), and **83** (70.0 μL , 432 μmol , 9.2 equiv) were suspended in dry DMF (10 mL) and deoxygenated with argon for 10 min. The reaction mixture was heated at 130 $^\circ\text{C}$ for 14 h. After filtration through a silica gel plug and washing with CH_2Cl_2 (200 mL), the solvents were removed under reduced pressure. The yellow residue was purified by column chromatography (SiO_2 , CH_2Cl_2) to provide the pure product (32.0 mg, 38.8 μmol , 83%) as a blue solid.

FQY (%): $\Phi_{\text{fl}} < 0.01$.

HRMS (ESI): $[\text{M} + \text{H}]^+$ calcd for $\text{C}_{54}\text{H}_{56}\text{N}_4\text{O}_6$: 825.4374; found: 825.4363.

IR (cm^{-1}): 2956 (w), 2922 (w), 2853 (w), 1693 (m), 1639 (s), 1588 (s); 1470 (s), 1322 (s), 1232 (s), 1112 (m), 832 (m), 787 (s), 561 (s).

MP: above 360 $^\circ\text{C}$.

MS (MALDI-TOF), m/z : 825.0 ($[\text{M}]^-$).

$^1\text{H-NMR}$ (400 MHz, CDCl_3 , δ): 10.96 (s, 2H, NH), 8.62 (s, 2H), 7.60–7.57 (m, 4H), 7.41–7.37 (m, 4H), 7.27–7.26 (m, 4H), 7.24–7.21 (m, 6H), 1.38 (s, 18H), 1.31 (s, 18H).

$^{13}\text{C-NMR}$ (126 MHz, CDCl_3 , δ): 166.8, 163.3, 152.0, 149.2, 147.9, 135.7, 132.3, 127.9, 126.8, 126.7, 126.3, 123.9, 122.7, 121.1, 103.2, 35.0, 34.7, 31.5, 31.5, 22.9.

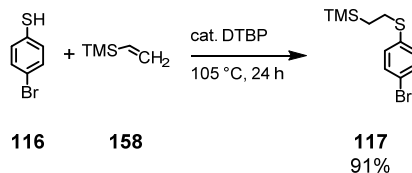
TLC (SiO_2 , CH_2Cl_2 , UV): $R_f = 0.90$.

UV/Vis (CDCl_3): λ_{max} (ϵ_{max}): 352 (7769), 371 (7552), 621 (10811) nm ($\text{mol}^{-1} \cdot \text{dm}^3 \cdot \text{cm}^{-1}$).

7.4 Synthesis of Linear cNDIs

7.4.1 2-((4-Bromophenyl)thio)ethyltrimethylsilane (**117**)

Reaction Scheme



Experimental Procedure

4-Bromothiophenol (**116**; 11.4 g, 60.3 mmol, 1.0 equiv), vinyltrimethylsilane (**158**; 11.0 mL, 74.6 mmol, 1.2 equiv), and di-*tert*-butyl peroxide (1.60 mL, 8.75 mmol, 0.15 equiv) were added to a Schlenk tube. The Schlenk tube was deoxygenated with argon for 5 min, sealed, and heated at 105 °C for 24 h. The reaction mixture was cooled to room temperature, before it was diluted with cyclohexane (50 mL). After washing with aq. NaOH (1 M, 40 mL), the organic layer was separated and the aqueous layer was extracted with cyclohexane. The combined organic layers were dried over Na₂SO₄, filtered, and the solvent was removed under reduced pressure to obtain a liquid, which was purified by vacuum distillation. The pure product (15.9 g, 54.9 mmol, 91%, lit.^[309] 99%) was isolated as a colorless liquid.

Bp: 125 °C at 2.0 mbar.

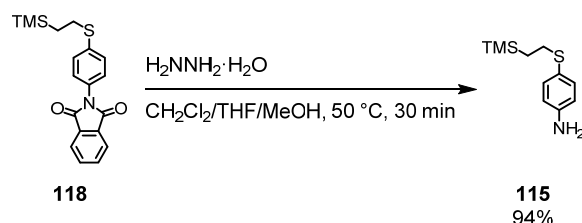
GC–MS (EI), *m/z* (% relative intensity, ion): 288.0 (2.6, [M]⁺), 101.2 (9.3, [EtTMS]⁺).

¹H-NMR (400 MHz, CDCl₃, δ): 7.45–7.34 (m, 2H), 7.20–7.11 (m, 2H), 2.98–2.88 (m, 2H), 0.95–0.88 (m, 2H), 0.04 (s, 9H).

¹³C-NMR (101 MHz, CDCl₃, δ) 136.6, 132.0, 130.6, 119.5, 29.8, 16.9, – 1.6.

TLC (SiO₂, EtOAc/hexane 1:2, UV): R_f = 0.40.

The characterization data are in agreement with the literature.^[309,284,310]

7.4.3 4-((2-(Trimethylsilyl)ethyl)thio)aniline (**115**)Reaction SchemeExperimental Procedure

118 (4.30 g, 12.1 mmol, 1.0 equiv) and hydrazine monohydrate (64%, 6.00 mL, 124 mmol, 10.2 equiv) were added to a 6:1:1 mixture of dry $\text{CH}_2\text{Cl}_2/\text{THF}/\text{MeOH}$ (80 mL). The resulting solution was stirred at room temperature for 30 min and then at 50 °C for 30 min. The formed, white precipitate was filtered off and washed with CH_2Cl_2 (80 mL). The filtrate was washed with aq. NaOH (1 M, 50 mL) and the organic layer was separated. The aqueous phase was extracted with CH_2Cl_2 (3 \times 40 mL) and the combined organic layers were washed with brine (50 mL). The organic phase was dried over MgSO_4 , filtered, and the solvent was evaporated under reduced pressure to obtain a colorless liquid. The liquid was purified by column chromatography (SiO_2 , EtOAc/cyclohexane 1:2) to isolate the pure product (2.56 g, 11.4 mmol, 94%) as a colorless liquid.

GC-MS (EI), m/z (% relative intensity, ion): 225.2 (10.3, $[\text{M}]^+$), 124.1 (8.5, $[\text{M} - \text{EtTMS}]^+$).

HRMS (ESI): $[\text{M} + \text{H}]^+$ calcd for $\text{C}_{11}\text{H}_{19}\text{NSSi}$: 226.1080; found: 226.1081.

IR (cm^{-1}): 2950 (w), 1619 (m), 1597 (m), 1494 (s), 1248 (s), 1176 (w), 839 (s), 517 (w).

$^1\text{H-NMR}$ (400 MHz, $(\text{CD}_3)_2\text{SO}$, δ): 7.08–7.04 (m, 2H), 6.53–6.49 (m, 2H), 5.19 (s, 2H, NH_2), 2.75–2.69 (m, 2H), 0.79–0.72 (m, 2H), –0.03 (s, 9H).

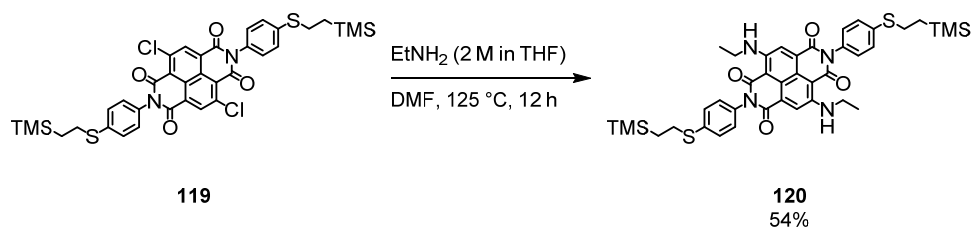
$^{13}\text{C-NMR}$ (101 MHz, $(\text{CD}_3)_2\text{SO}$, δ): 148.3, 133.6, 119.3, 114.4, 31.7, 16.8, –1.7.

TLC (SiO_2 , EtOAc/hexane 1:2, UV and ninhydrin): $R_f = 0.48$.

The characterization data are in agreement with the literature.^[285]

7.4.5 *N,N'*-Di-((4'-(2'-trimethylsilyl)ethyl)thio)phenyl)-2,6-bis(ethylamino)-1,4,5,8-naphthalenetetracarboxylic acid diimide (**120**)

Reaction Scheme



Experimental Procedure

To a microwave vial were added **119** (378 mg, 503 μ mol, 1.0 equiv), ethylamine (2 M in THF, 12.0 mL, 24.0 mmol, 47.7 equiv), and dry DMF (7.0 mL). The vial was sealed and stirred at 125 $^{\circ}$ C for 12 h. After cooling to room temperature, the solvent was removed under reduced pressure and the residue was purified twice by column chromatography (SiO_2 , $\text{CH}_2\text{Cl}_2/\text{EtOAc}$ 20:1) to afford the pure product (207 mg, 269 μ mol, 54%) as a blue solid.

EA (%): calcd. for $\text{C}_{40}\text{H}_{48}\text{N}_4\text{O}_4\text{S}_2\text{Si}_2$: C, 62.46; H, 6.29; N, 7.28;
 found: C, 62.41; H, 6.61; N, 7.51.

HRMS (ESI): $[\text{M} + \text{H}]^+$ calcd for $\text{C}_{40}\text{H}_{48}\text{N}_4\text{O}_4\text{S}_2\text{Si}_2$: 769.2728; found: 769.2732.

IR (cm^{-1}): 2951 (w), 1696 (m), 1654 (s), 1573 (s), 1496 (m), 1245 (m), 1207 (m), 1166 (m), 839 (m).

MS (MALDI-TOF), m/z : 768.2 ($[\text{M}]^-$).

MP: 297–299 $^{\circ}$ C.

$^1\text{H-NMR}$ (400 MHz, CD_2Cl_2 , δ): 9.08 (s, 2H, NH), 7.97 (s, 2H), 7.43 (d, $^3J_{\text{HH}} = 8.3$ Hz, 4H), 7.25 (d, $^3J_{\text{HH}} = 8.3$ Hz, 4H), 3.43–3.33 (m, 4H), 3.14–3.04 (m, 4H), 1.34 (t, $^3J_{\text{HH}} = 7.2$ Hz, 6H), 1.09–1.01 (m, 4H), 0.10 (s, 18H).

$^{13}\text{C-NMR}$ (126 MHz, CD_2Cl_2 , δ): 166.7, 163.4, 149.6, 139.6, 133.2, 129.7, 128.8, 126.6, 121.8, 118.7, 102.0, 38.4, 29.5, 17.2, 14.9, -1.5 .

TLC (SiO_2 , $\text{CH}_2\text{Cl}_2/\text{EtOAc}$ 20:1, UV): $R_f = 0.75$.

7.4.6 *N,N'*-Di-((4'-(2'-trimethylsilyl)ethyl)thio)phenyl)-2,6-bis(dimethylamino)-1,4,5,8-naphthalenetetracarboxylic acid diimide (**121**)

Reaction Scheme



Experimental Procedure

119 (131 mg, 174 μmol , 1.0 equiv), dimethylamine (2 M in THF, 8.00 mL, 16.0 mmol, 92.0 equiv), and dry DMF (10 mL) were added to a microwave vial and sealed. The reaction mixture was stirred at 125 $^{\circ}\text{C}$ for 11 h. After cooling to room temperature, the solvent was removed under reduced pressure and the residue was purified by column chromatography (SiO_2 , $\text{CH}_2\text{Cl}_2/\text{EtOAc}$ 20:1) to obtain the pure product (84.0 mg, 109 μmol , 63%) as a blue solid.

EA (%): calcd. for $\text{C}_{40}\text{H}_{48}\text{N}_4\text{O}_4\text{S}_2\text{Si}_2$: C, 62.46; H, 6.29; N, 7.28;

 found: C, 62.03; H, 6.40; N, 7.64.

HRMS (ESI): $[\text{M} + \text{H}]^+$ calcd for $\text{C}_{40}\text{H}_{48}\text{N}_4\text{O}_4\text{S}_2\text{Si}_2$: 769.2728; found: 769.2738.

IR (cm^{-1}): 3431 (w), 3320 (w), 2950 (w), 1688 (m), 1637 (s), 1584 (s), 1488 (m), 1318 (m), 1216 (m), 827 (s), 753 (s).

MP: above 360 $^{\circ}\text{C}$.

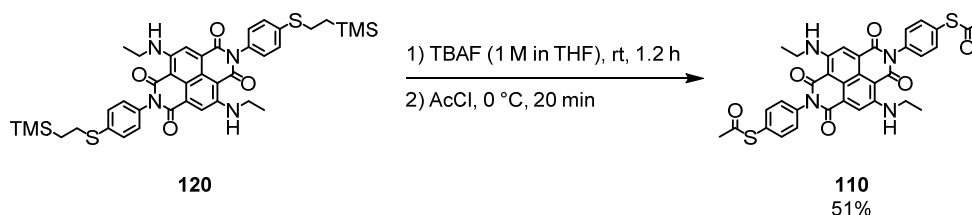
$^1\text{H-NMR}$ (400 MHz, CD_2Cl_2 , δ): 8.46 (s, 2H), 7.47–7.43 (m, 4H), 7.23–7.19 (m, 4H), 3.14 (s, 12H), 3.11–3.06 (m, 4H), 1.07–1.01 (m, 4H), 0.09 (s, 18H).

$^{13}\text{C-NMR}$ (101 MHz, CD_2Cl_2 , δ): 164.1, 162.3, 152.0, 139.1, 134.2, 129.8, 129.0, 126.1, 124.5, 123.9, 107.7, 44.5, 29.7, 17.3, –1.5.

TLC (SiO_2 , $\text{CH}_2\text{Cl}_2/\text{EtOAc}$ 20:1, UV): $R_f = 0.58$.

7.4.7 *N,N'*-Di-(4'-(acetysulfanyl)phenyl)-2,6-bis(ethylamino)-1,4,5,8-naphthalene-tetracarboxylic acid diimide (**110**)

Reaction Scheme



Experimental Procedure

To an oven-dried flask were added **120** (35.0 mg, 45.5 μmol , 1.0 equiv) and dry THF (40 mL) and the resulting solution was deoxygenated with argon for 5 min. TBAF (1 M in THF, 400 μL , 400 μmol , 8.8 equiv) was added dropwise over 30 min and the solution was stirred at room temperature for 1.2 h. The reaction mixture was cooled to 0 $^\circ\text{C}$ and AcCl (500 μL , 7.01 mmol, 154 equiv) was added. The reaction mixture was stirred at 0 $^\circ\text{C}$ for 20 min and warmed to room temperature. It was quenched with H_2O (30 mL) and diluted with CH_2Cl_2 (110 mL). The organic layer was separated and the aqueous phase was extracted with CH_2Cl_2 (3 \times 50 mL). The combined organic layers were washed with brine (40 mL), dried over MgSO_4 , filtered, and the solvent was evaporated under reduced pressure. The residue was purified by column chromatography (1st: SiO_2 , EtOAc/ CH_2Cl_2 1:10; 2nd: SiO_2 , cyclohexane/EtOAc 1:3 to CH_2Cl_2 /EtOAc 10:1) to yield the pure product (15.0 mg, 23.0 μmol , 51%) as a blue solid.

FQY (%): $\Phi_{\text{fl}} = 0.45$.

HRMS (ESI): $[\text{M} + \text{H}]^+$ calcd for $\text{C}_{34}\text{H}_{29}\text{N}_4\text{O}_6\text{S}_2$: 653.1523; found: 653.1525.

IR (cm^{-1}): 2924 (w), 1692 (m), 1640 (s), 1587 (s), 1488 (m), 1231 (m).

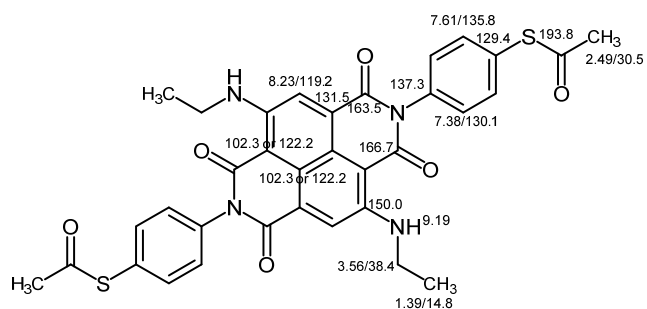
MS (MALDI-TOF), m/z : 652.7 ($[\text{M}]^-$).

MP: above 300 $^\circ\text{C}$.

$^1\text{H-NMR}$ (700 MHz, CD_2Cl_2 , δ): 9.19 (s, 2H), 8.23 (s, 2H), 7.61 (d, $^3J_{\text{HH}} = 7.6$ Hz, 4H), 7.38 (d, $^3J_{\text{HH}} = 7.9$ Hz, 4H), 3.56 (q, $^3J_{\text{HH}} = 6.8$ Hz, 4H), 2.49 (s, 6H), 1.39 (t, $^3J_{\text{HH}} = 6.9$ Hz, 6H).

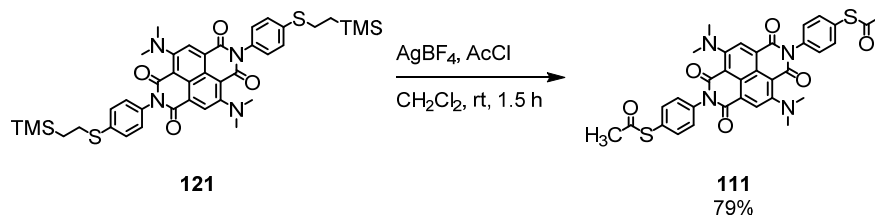
$^{13}\text{C-NMR}$ (176 MHz, CD_2Cl_2 , δ): 193.8, 166.7, 163.5, 150.0, 137.3, 135.8, 131.5, 130.1, 129.4, 122.2, 119.2, 102.3, 38.4, 30.5, 14.8.

Assignment of hydrogen and carbon atoms was done by 2D-NMR. Signals at 122.2 and 102.3 ppm cannot be clearly assigned, they have the same $^3J_{\text{HC}}$ coupling to the signal at 8.23 ppm.



TLC (SiO₂, CH₂Cl₂/EtOAc 10:1, UV,): R_f = 0.59.

UV/Vis (CDCl₃): λ_{max} (ε_{max}): 346 (11013), 363 (12979), 620 (19604) nm (mol⁻¹ · dm³ · cm⁻¹).

7.4.8 *N,N'*-Di-(4'-(acetysulfanyl)phenyl)-2,6-bis(dimethylamino)-1,4,5,8-naphthalene-tetracarboxylic acid diimide (111)Reaction SchemeExperimental Procedure

To an oven-dried flask were added **121** (78.0 mg, 102 μmol , 1.0 equiv), dry CH_2Cl_2 (30 mL), AgBF_4 (200 mg, 1.01 mmol, 9.9 equiv), and AcCl (3.00 mL, 42.0 mmol, 414 equiv). The reaction mixture was stirred at room temperature for 1.5 h. During the course of the reaction the color changed from blue to orange and finally to yellow. After quenching with sat. aq. NaHCO_3 (40 mL) and diluting with CH_2Cl_2 (60 mL), the color changed back to blue. The organic phase was separated and the aqueous layer was extracted with CH_2Cl_2 (3×30 mL). The combined organic layers were dried over MgSO_4 , filtered, and the solvent was evaporated under reduced pressure. The blue residue was purified by column chromatography (SiO_2 , $\text{CH}_2\text{Cl}_2/\text{EtOAc}$ 10:1) and the pure product (53.0 mg, 81.2 μmol , 79%) was isolated as a blue solid.

FQY (%): $\Phi_{\text{H}} < 0.01$.

HRMS (ESI): $[\text{M} + \text{H}]^+$ calcd for $\text{C}_{34}\text{H}_{28}\text{N}_4\text{O}_6\text{S}_2$: 653.1523; found: 653.1529.

IR (cm^{-1}): 2854 (w), 1688 (m), 1649 (s), 1570 (m), 1494 (m), 1400 (m), 1324 (m), 1203 (s), 1164 (m), 1127 (m), 1064 (m), 906 (m), 746 (m).

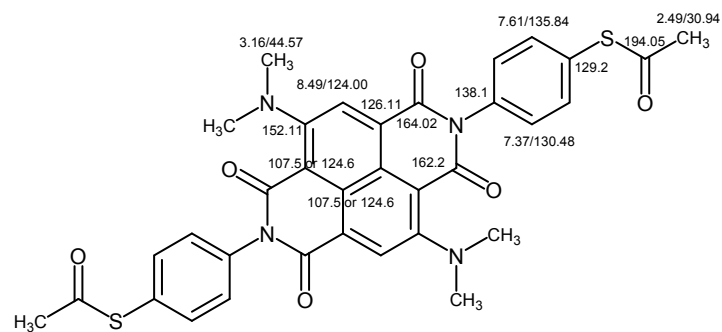
MS (MALDI-TOF), m/z : 652.5 ($[\text{M}]^-$).

MP: above 360 $^\circ\text{C}$.

$^1\text{H-NMR}$ (600 MHz, CD_2Cl_2 , δ): 8.48 (s, 2H), 7.60 (d, $^3J_{\text{HH}} = 7.8$ Hz, 4H), 7.37 (d, $^3J_{\text{HH}} = 7.8$ Hz, 4H), 3.16 (s, 12H), 2.49 (s, 6H).

$^{13}\text{C-NMR}$ (151 MHz, CD_2Cl_2 , δ): 194.1, 164.0, 162.2, 152.1, 138.1, 135.8, 130.5, 129.2, 126.1, 124.6, 124.0, 107.5, 44.6, 30.9.

Assignment of hydrogen and carbon atoms was done by 2D-NMR. Signals at 124.0 and 107.54 ppm cannot be clearly assigned, they have the same $^3J_{\text{HC}}$ coupling to the signal at 8.49 ppm.



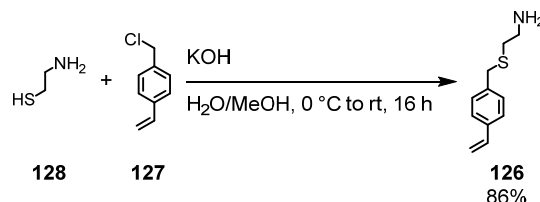
TLC (SiO₂, CH₂Cl₂/EtOAc 10:1, UV): R_f = 0.20.

UV/Vis (CDCl₃): λ_{max} (ε_{max}): 352 (14379), 368 (16565), 608 (21210) nm (mol⁻¹ · dm³ · cm⁻¹).

7.5 Synthesis of Photoswitchable NDI-Phanes

7.5.1 2-((4-Vinylbenzyl)thio)ethan-1-amine (**126**)

Reaction Scheme



Experimental Procedure

2-Aminoethanethiol (**128**; 1.08 g, 13.3 mmol, 1.1 equiv) was dissolved in MeOH (30 mL) and after 10 min KOH (876 mg, 13.4 mmol, 1.1 equiv) in H₂O (20 mL) was added. The resulting mixture was cooled to 0 °C and 1-(chloromethyl)-4-vinylbenzene (**127**; 1.9 mL, 12.1 mmol, 1.0 equiv) was added dropwise over 30 min. The suspension was stirred at 0 °C for 1.5 h, warmed to room temperature overnight, and stirred for 14.5 h. The mixture was diluted with EtOAc (50 mL) and brine (40 mL), and the organic phase was separated. The aqueous phase was extracted with EtOAc (2 × 60 mL), the combined organic layers were dried over MgSO₄, filtered, and the solvent was removed under reduced pressure. The yellow residue was purified by column chromatography (SiO₂, CH₂Cl₂/MeOH 10:1) to yield the pure product (2.22 g, 11.5 mmol, 86%, lit.^[294] 75%) as a yellow liquid.

GC-MS (EI), *m/z* (% relative intensity, ion): 193.1 (51.7, [M]⁺), 166.1 (9.8, [M - C₂H₃]⁺) 149.1 (25.3, [M - EtNH₂]⁺), 117.8 (100, [M - SEtNH₂]⁺).

¹H-NMR (400 MHz, (CD₃)₂SO, δ): 7.46–7.38 (m, 2H), 7.34–7.25 (m, 2H), 6.71 (dd, ³J_{HH} = 17.7 Hz, ³J_{HH} = 10.9 Hz, 1H), 5.85–5.76 (m, 1H), 5.27–5.21 (m, 1H), 3.71 (s, 2H), 2.70–2.61 (m, 2H), 2.44–2.38 (m, 2H), 1.77 (s, 2H, NH₂).

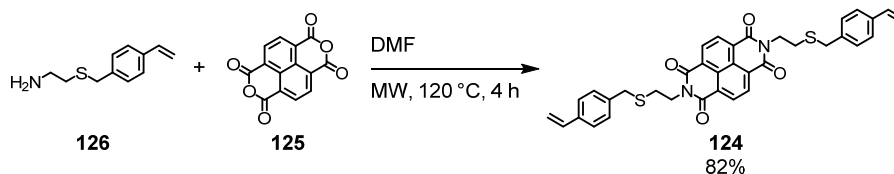
¹³C-NMR (101 MHz, (CD₃)₂SO, δ): 138.7, 136.3, 129.1, 126.1, 113.9, 41.2, 34.7, 34.6.

¹³C-NMR (101 MHz, CDCl₃, δ): 138.1, 136.6, 136.5, 129.2, 126.5, 113.9, 41.0, 35.8, 35.5.

TLC (SiO₂, CH₂Cl₂/MeOH 10:1, UV): R_f = 0.05.

7.5.2 *N,N'*-Di-2-((4-vinylbenzyl)thio)ethane-1,4,5,8-naphthalenetetracarboxylic acid diimide (**124**)

Reaction Scheme



Experimental Procedure

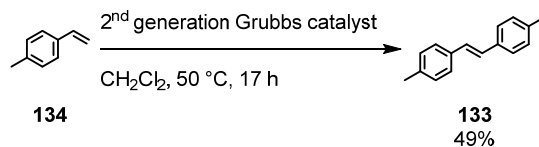
To a microwave vial were added **126** (457 mg, 2.36 mmol, 4.4 equiv), 1,4,5,8-naphthalenetetracarboxylic dianhydride (**125**; 44 mg, 537 μ mol, 1.0 equiv), and dry DMF (15 mL). The vial was sealed and heated in the microwave reactor at 120 °C for 4 h. The solvent was removed under reduced pressure and the residue was purified twice by column chromatography (CH₂Cl₂/EtOAc 10:1) to obtain the pure product (273 mg, 441 μ mol, 82%) as a yellow solid.

HRMS (ESI): [M + H]⁺ calcd for C₃₆H₃₀N₂O₄S₂: 619.1720; found: 619.1716.

¹H-NMR (400 MHz, CD₂Cl₂, δ): 8.73 (s, 4H), 7.35–7.27 (m, 8H), 6.64 (dd, ³J_{HH} = 17.6 Hz, ³J_{HH} = 10.9 Hz, 2H), 5.72–5.66 (m, 2H), 5.21–5.16 (m, 2H), 4.41–4.37 (m, 4H), 3.82 (s, 4H), 2.83–2.79 (m, 4H).

¹³C-NMR (101 MHz, CDCl₃, δ): 162.9, 138.0, 136.5, 136.5, 131.2, 129.3, 126.9, 126.7, 126.5, 113.8, 39.7, 36.0, 29.0.

TLC (SiO₂, CH₂Cl₂/EtOAc 10:1, UV): R_f = 0.72.

7.5.3 (*E*)-1,2-Di-*p*-tolylethene (133**)**Reaction SchemeExperimental Procedure

To an oven-dried flask were added 4-methylstyrene (**134**; 1.30 mL, 9.87 mmol, 1.0 equiv), 2nd generation Grubbs catalyst (27.0 mg, 0.30 mol-%), and dry CH₂Cl₂ (25 mL). The reaction mixture was heated at 50 °C and stirred for 17 h. The solvent was removed under reduced pressure and the residue was purified by column chromatography (SiO₂, cyclohexane/CH₂Cl₂ 10:1) to yield the pure product (1.01 g, 4.85 mmol, 49%, lit.^[295] 100%) as a white solid.

GC-MS (EI), *m/z* (% relative intensity, ion): 208.2 (100, [M]⁺), 193.2 (68.5, [M - CH₃]⁺), 179.2 (15.1, [M - 2 x CH₃]⁺).

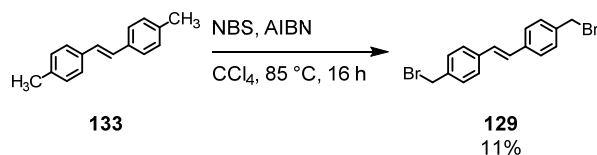
¹H-NMR (400 MHz, CDCl₃, δ): 7.40 (d, ³*J*_{HH} = 8.0 Hz, 4H), 7.16 (d, ³*J*_{HH} = 7.8 Hz, 4H), 7.04 (s, 2H), 2.36 (s, 6H).

¹³C-NMR (101 MHz, CDCl₃, δ): 137.4, 134.9, 129.5, 127.8, 126.5, 21.4.

The characterization data are in agreement with the literature.^[295]

7.5.4 (*E*)-1,2-Bis(4-(bromomethyl)phenyl)ethane (**129**)

Reaction Scheme



Experimental Procedure

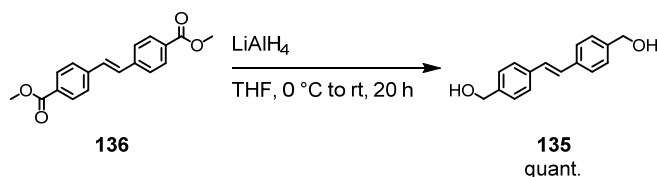
To a deoxygenated solution of **133** (540 mg, 2.59 mmol, 1.0 equiv) in CCl₄ (40 mL) were added NBS (971 mg, 5.46 mmol, 2.1 equiv) and AIBN (6.0 mg, 35.8 μmol, 13.8 mol-%). The resulting mixture was stirred at 85 °C for 16 h before the solvent was removed under reduced pressure. The residue was purified by column chromatography (SiO₂, cyclohexane/CH₂Cl₂ 3:1), recrystallized from EtOH, and again purified twice by column chromatography (SiO₂, cyclohexane/CH₂Cl₂ 3:1) to afford the pure product (102 mg, 27.9 μmol, 11%, lit.^[297] 17%) as a white solid.

¹H-NMR (400 MHz, CDCl₃, δ): 7.51–7.47 (m, 4H), 7.42–7.36 (m, 4H), 7.10 (s, 2H), 4.51 (s, 4H).

¹³C-NMR (101 MHz, CDCl₃, δ): 137.5, 137.4, 129.6, 128.8, 127.1, 33.6.

TLC (SiO₂, cyclohexane/EtOAc 6:1, UV): R_f = 0.53.

The characterization data are in agreement with the literature.^[296]

7.5.5 (*E*)-(Ethene-1,2-diylbis(4,1-phenylene))dimethanol (135**)**Reaction SchemeExperimental Procedure

To an oven-dried two-necked flask were added dimethyl 4,4'-(ethene-1,2-diyl)(*E*)-dibenzoate (**136**; 420 mg, 1.42 mmol, 1.0 equiv) and dry THF (20 mL). The resulting suspension was cooled to 0 °C and LiAlH₄ (118 mg, 3.12 mmol, 2.2 equiv) dissolved in THF (20 mL) was added carefully in three portions. The reaction mixture was stirred at 0 °C for 3 h, before it was stirred at room temperature for 19 h. After quenching the reaction mixture with aq. NaOH (1 M, 1 mL), the biphasic mixture was diluted with EtOAc (40 mL) and brine (30 mL). The organic layer was separated and the aqueous phase was extracted with EtOAc (2 × 30 mL). The combined organic layers were dried over MgSO₄, filtered, and the solvents were removed under reduced pressure. The residue was purified twice by column chromatography (SiO₂, CH₂Cl₂/MeOH 10:1) to yield the pure product (340 mg, 1.41 mmol, 99%, lit.^[296] 99%) as a white solid.

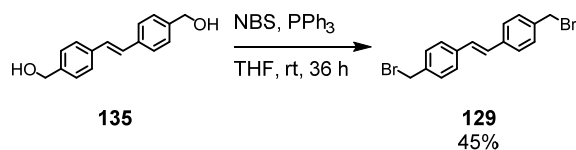
HRMS (ESI): [M + Na]⁺ calcd for C₁₆H₁₆O₂: 263.1043; found: 263.1040.

¹H-NMR (400 MHz, (CD₃)₂SO, δ): 7.55 (d, ³J_{HH} = 8.2 Hz, 4H), 7.31 (d, ³J_{HH} = 8.2 Hz, 4H), 7.21 (s, 2H), 5.18 (t, ³J_{HH} = 5.7 Hz, 2H), 4.50 (d, ³J_{HH} = 5.7 Hz, 4H).

¹³C-NMR (101 MHz, (CD₃)₂SO, δ): 142.0, 135.6, 127.7, 126.8, 126.1, 62.7.

TLC (SiO₂, CH₂Cl₂/MeOH 10:1, UV [302 nm]): R_f = 0.42.

The characterization data are in agreement with the literature.^[296]

7.5.6 (*E*)-1,2-Bis(4-(bromomethyl)phenyl)ethane (129)Reaction SchemeExperimental Procedure

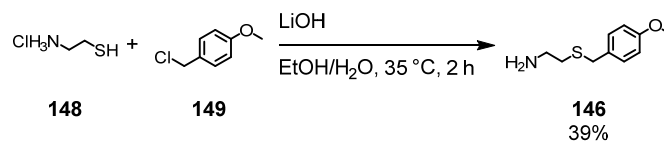
To an oven-dried two-necked flask were added **135** (295 mg, 1.23 mmol, 1.0 equiv), dry THF (40 mL), triphenylphosphine (716 mg, 2.70 mmol, 2.2 equiv), and NBS (479 mg, 2.66 mmol, 2.2 equiv). The resulting mixture was stirred at room temperature for 36 h, before it was quenched with sat. aq NaHCO₃ (40 mL) and diluted with CH₂Cl₂ (80 mL) and H₂O (30 mL). The organic phase was separated and the aqueous layer was extracted with CH₂Cl₂ (2 × 30 mL). The organic phase was dried over MgSO₄, filtered, and the solvent was evaporated under reduced pressure. The residue was purified twice by column chromatography (SiO₂, cyclohexane/EtOAc 6:1) to obtain the pure product (204 mg, 557 μmol, 45%, lit.^[296] 74%) as a white solid.

¹H-NMR (400 MHz, CDCl₃, δ): 7.51–7.47 (m, 4H), 7.42–7.36 (m, 4H), 7.10 (s, 2H), 4.51 (s, 4H).

¹³C-NMR (101 MHz, CDCl₃, δ): 137.5, 137.4, 129.6, 128.8, 127.1, 33.6.

TLC (SiO₂, cyclohexane/EtOAc 6:1, UV): R_f = 0.53.

The characterization data are in agreement with the literature.^[296]

7.5.9 2-((4-Methoxybenzyl)thio)ethan-1-amine (146)Reaction SchemeExperimental Procedure

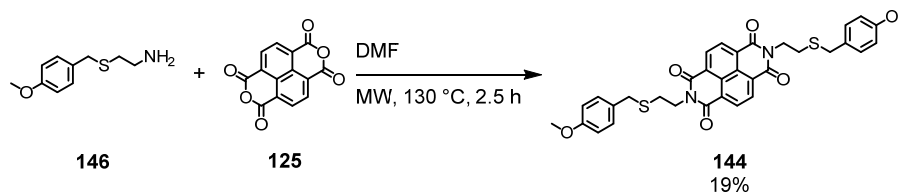
LiOH (364 mg, 21.3 mmol, 2.1 equiv) was dissolved in a 4:1 mixture of EtOH/H₂O (50 mL) and 2-aminoethanethiol hydrochloride (**148**; 1.14 g, 10.0 mmol, 1.0 equiv) was added in one portion. After stirring the reaction mixture for 30 min, 4-methoxybenzylchloride (**149**; 1.60 g, 10.0 mmol, 1.0 equiv) was added, and the resulting solution was stirred at 35 °C for 2 h. EtOH was removed under reduced pressure and the suspension was diluted with H₂O (50 mL) and CH₂Cl₂ (70 mL). The organic phase was separated and the aqueous layer was extracted with CH₂Cl₂ (2 × 50 mL). The combined organic layers were dried over Na₂SO₄, filtered, and the solvent was removed under reduced pressure. The residue was purified by column chromatography (SiO₂, CH₂Cl₂/MeOH 10:1) to yield the pure product (764 mg, 3.87 mmol, 39%, lit.^[299] 94%) as white solid.

¹H-NMR (400 MHz, (CD₃)₂SO, δ): δ 7.26–7.20 (m, 2H), 6.91–6.84 (m, 2H), 3.73 (s, 3H), 3.67 (s, 2H), 2.82–2.64 (m, 4H), 2.45–2.39 (m, 2H).

¹³C-NMR (101 MHz, (CD₃)₂SO, δ): 158.1, 130.5, 129.9, 113.7, 55.0, 40.9, 34.3, 33.9.

TLC (SiO₂, CH₂Cl₂/MeOH 10:1, UV): R_f = 0.44.

The characterization data are in agreement with the literature.^[299]

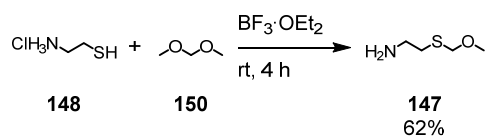
7.5.10 *N,N'*-Di-(2'-((4'-methoxybenzyl)thio)ethyl)-1,4,5,8-naphthalenetetracarboxylic acid diimide (144)Reaction SchemeExperimental Procedure

To a microwave vial were added **146** (743 mg, 3.77 mmol, 4.0 equiv), **125** (266 mg, 942 μ mol, 1.0 equiv), and dry DMF (15 mL). The vial was sealed and heated in the microwave reactor at 130 °C for 2.5 h. After cooling to room temperature, the solvent was removed under reduced pressure and the residue was purified by column chromatography (SiO₂, CH₂Cl₂/MeOH 20:1) to yield the pure product as a dark yellow solid (113 mg, 180 μ mol, 19%).

MS (MALDI-TOF), m/z : 626.7 ($[M]^-$).

¹H-NMR (400 MHz, CDCl₃, δ): 8.77 (s, 4H), 7.32–7.25 (m, 4H), 6.83–6.76 (m, 4H), 4.46–4.37 (m, 4H), 3.80 (s, 4H), 3.76 (s, 6H), 2.81 (t, ³ J_{HH} = 7.1 Hz, 4H).

TLC (SiO₂, CH₂Cl₂/MeOH 20:1, UV): R_f = 0.88.

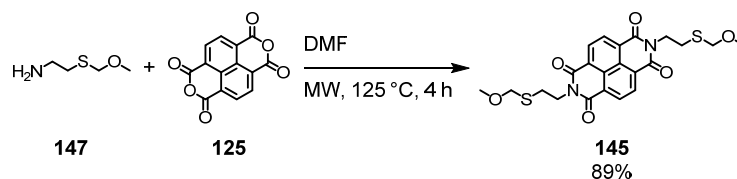
7.5.11 2-((Methoxymethyl)thio)ethan-1-amine (**147**)Reaction SchemeExperimental Procedure

To an oven-dried flask were added **148** (4.55 g, 40.0 mmol, 1.0 equiv), $\text{BF}_3 \cdot \text{OEt}_2$ (1.00 mL, 7.89 mmol, 0.2 equiv), and dimethoxymethane (**150**; 25.0 mL, 280 mmol, 7.0 equiv). The resulting mixture was stirred at room temperature for 4 h, before it was quenched by the addition of an ice cold aq. KOH (1 M, 100 mL) and diluted with CH_2Cl_2 (80 mL). The organic layer was separated and the aqueous layer was extracted with CH_2Cl_2 (3×60 mL). The combined organic phases were dried over MgSO_4 , filtered, and the solvent was removed under reduced pressure. The residue was purified by vacuum distillation to yield the pure product (3.01 g, 24.8 mmol, 62%, lit.^[300] 60%) as a colorless liquid.

Bp: 41–42 °C at 1 mbar

$^1\text{H-NMR}$ (250 MHz, CDCl_3 , δ): 4.63 (s, 2H), 3.36 (s, 3H), 2.95–2.85 (m, 2H), 2.73–2.66 (m, 2H), 1.27 (s, 2H, NH_2).

$^{13}\text{C-NMR}$ (101 MHz, CDCl_3 , δ): 75.7, 55.9, 42.0, 35.8.

7.5.12 *N,N'*-Di-(2'-((methoxymethyl)thio)ethyl)-1,4,5,8-naphthalenetetracarboxylic acid diimide (145)Reaction SchemeExperimental Procedure

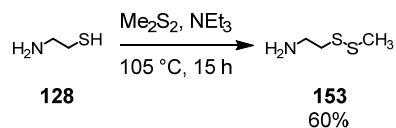
To a microwave vial were added **147** (262 mg, 2.16 mmol, 4.0 equiv), **125** (145 mg, 540 μ mol, 1.0 equiv), and dry DMF (15 mL). The microwave vial was sealed and heated in the microwave reactor at 125 °C for 4 h. The solvent was removed under reduced pressure and the residue was purified by column chromatography (SiO₂, CH₂Cl₂/EtOAc 10:1) to yield the pure product (229 mg, 483 μ mol, 89%) as a white solid.

MS (MALDI-TOF), m/z : 474.1 ($[M]^-$).

¹H-NMR (400 MHz, CDCl₃, δ): 8.78 (s, 4H), 4.72 (s, 4H), 4.50–4.45 (m, 4H), 3.31 (s, 6H), 3.03–2.98 (m, 4H).

¹³C-NMR (101 MHz, CDCl₃, δ): 162.9, 131.2, 126.9, 126.8, 75.8, 56.2, 40.3, 28.8.

TLC (SiO₂, CH₂Cl₂/EtOAc 10:1, UV, KMnO₄): R_f = 0.14.

7.5.13 2-(Methyldisulfanyl)ethan-1-amine (153)Reaction SchemeExperimental Procedure^[311]

To a microwave vial were added **128** (942 mg, 12.2 mmol, 1.0 equiv), dimethyl disulfide (4.8 mL, 54.1 mmol, 4.4 equiv), and NEt₃ (0.25 mL, 1.76 mmol, 0.14 equiv). The vial was sealed and heated at 105 °C for 15 h. The reaction mixture cooled to room temperature, toluene was added, and the unreacted dimethyl disulfide was evaporated under reduced pressure. The colorless residue was purified by column chromatography (SiO₂, CH₂Cl₂/MeOH 10:1 with 1% NEt₃ to 8:1 with 1% NEt₃) to afford the pure product (906 mg, 7.35 mmol, 60%) as a colorless liquid.

¹H-NMR (400 MHz, CDCl₃, δ): 3.02 (t, ³J_{HH} = 6.2 Hz, 2H), 2.77 (t, ³J_{HH} = 6.2 Hz, 2H), 2.41 (s, 3H), 1.35 (s, 2H, NH₂).

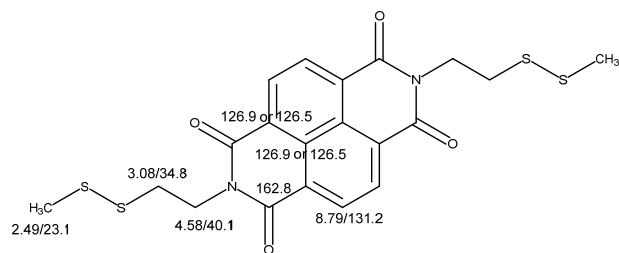
¹³C-NMR (101 MHz, CDCl₃, δ): 42.0, 40.8, 23.4.

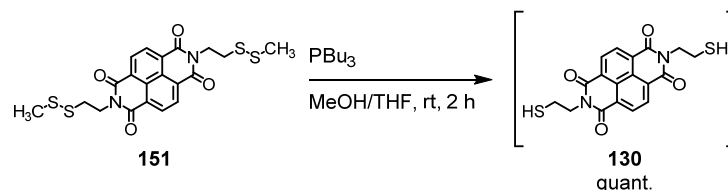
TLC (SiO₂, CH₂Cl₂/MeOH 10:1, ninhydrin): R_f = 0.07.

The characterization data are in agreement with the literature.^[304]

$^{13}\text{C-NMR}$ (126 MHz, CDCl_3 , δ): 162.8, 131.2, 126.9, 126.5, 40.1, 34.8, 23.1.

Assignment of hydrogen and carbon atoms was done by 2D-NMR. Signals at 126.9 and 126.5 ppm cannot be clearly assigned, they have the same $^3J_{\text{HC}}$ coupling to the signal at 8.79 ppm.



7.5.15 *N,N'*-Di-(2'-thioethyl)-1,4,5,8-naphthalenetetracarboxylic acid diimide (**130**)Reaction SchemeExperimental Procedure

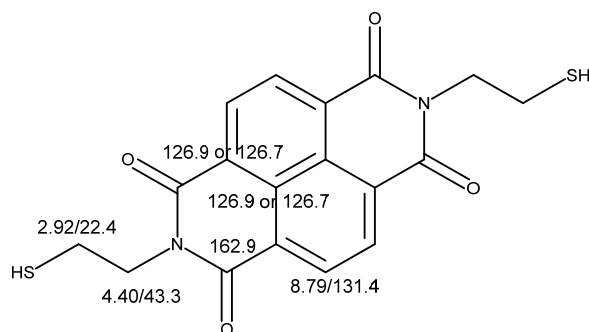
To an oven-dried round-bottom flask were added **151** (8.32 mg, 17.4 μmol , 1.0 equiv) and a 1:1 mixture of MeOH/THF (10 mL). After the reaction mixture was deoxygenated with argon for 5 min, tributylphosphane (80.0 μL , 272 μmol , 15.7 equiv) was added. The progress of the reaction was monitored by MALDI-TOF-MS analysis and after stirring at room temperature for 2 h complete conversion was observed. The solvents were removed under reduced pressure to yield the crude product as an oil which was used without further purification (product contained tributylphosphine oxide).

MS (MALDI-TOF), m/z : 386.0 ($[\text{M}]^-$). (MALDI-TOF-MS analysis showed full conversion)

$^1\text{H-NMR}$ (500 MHz, CDCl_3 , δ): 8.78 (s, 4H), 4.46–4.38 (m, 4H), 2.94–2.86 (m, 4H).

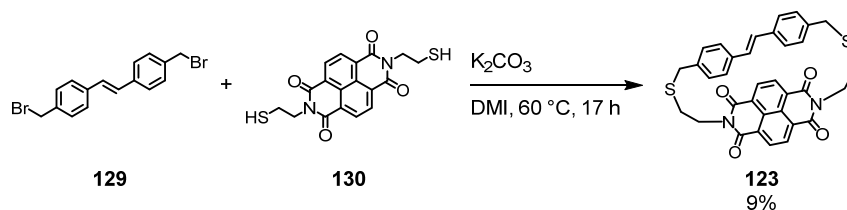
$^{13}\text{C-NMR}$ (126 MHz, CDCl_3 , δ): 162.9, 131.4, 126.9, 126.7, 43.3, 22.4.

Assignment of hydrogen and carbon atoms was done by 2D-NMR. Signals at 126.9 and 126.7 ppm cannot be clearly assigned, they have the same $^3J_{\text{HC}}$ coupling to the signal at 8.79 ppm.



7.5.16 (*E*)-1((2,7)-Benzo[*lmn*][3,8]phenanthroline-1,3,6,8(2*H*,7*H*)-tetraona)-6((4,4')-1,2-diphenylethene)-4,8-dithiadecanodane (**123**)

Reaction Scheme



Experimental Procedure

To a flame-dried two-necked round-bottom flask was added dry DMI (200 mL) and deoxygenated with argon for 15 min. K_2CO_3 (158 mg, 1.13 mmol, 10.8 equiv, dried for one day at 200 °C by bulb-to-bulb distillation) was added to the solvent and stirred for 10 min. **130** (40.6 mg, 105.0 μ mol, 1.0 equiv) in dry and deoxygenated DMI (10 mL) was added in one portion, followed by the addition of **129** (38.4 mg, 105.0 μ mol, 1.0 equiv) in one portion. The resulting reaction mixture was heated at 60 °C and stirred for 17 h. After cooling to room temperature, the mixture was diluted with CH_2Cl_2 (50 mL), repeatedly washed with aq. HCl (2 M, 6 \times 200 mL), dried over $MgSO_4$, and filtered. The solvents were removed under reduced pressure, the residue was purified by column chromatography (SiO_2 , $CH_2Cl_2/EtOAc$ 10:1) and GPC to afford the pure product (5.70 mg, 9.65 μ mol, 9%) as a neon orange solid.

HRMS (ESI): $[M + Na]^+$ calcd for $C_{34}H_{26}N_2O_4S_2$: 613.1226; found: 613.1226.

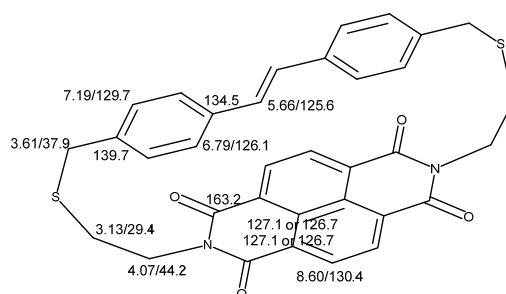
IR (cm^{-1}): 2920 (m), 2852 (w), 1703 (m), 1662 (s), 1452 (w), 1327 (s), 1243(s), 766 (m).

MP: above 340 °C.

1H -NMR (400 MHz, $CDCl_3$, δ): 8.60 (s, 4H), 7.18 (d, $^3J_{HH} = 8.2$ Hz, 4H), 6.79 (d, $^3J_{HH} = 8.2$ Hz, 4H), 5.66 (s, 4H), 4.05–3.98 (m, 4H), 3.60 (s, 1H), 3.16–3.09 (m, 4H).

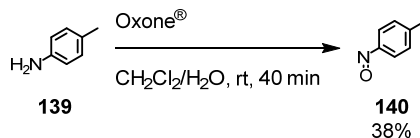
^{13}C -NMR (151 MHz, $CDCl_3$, δ): 163.2, 139.7, 134.5, 130.4, 129.7, 127.1, 126.7, 126.1, 125.6, 44.2, 37.9, 29.4.

Assignment of hydrogen and carbon atoms was done by 2D-NMR. Signals at 127.1 and 126.7 ppm cannot be clearly assigned, they have the same $^3J_{HC}$ coupling to the signal at 8.53 ppm.



TLC (SiO_2 , $CH_2Cl_2/EtOAc$ 10:1, UV): $R_f = 0.40$.

UV/Vis (CD_2Cl_2): λ_{max} (ϵ_{max}): 235 (27244), 330 (32500), 382 (8414) nm ($mol^{-1} \cdot dm^3 \cdot cm^{-1}$).

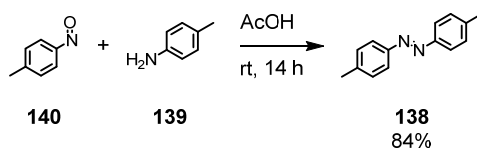
7.5.17 1-Methyl-4-nitrosobenzene (140)Reaction SchemeExperimental Procedure

4-Methylaniline (**139**; 4.29 g, 40.0 mmol, 1.0 equiv) was dissolved in CH₂Cl₂ (100 mL) and a solution of Oxone[®] (18.4 g, 60.0 mmol, 1.5 equiv) in H₂O (300 mL) was added. The resulting reaction mixture was stirred at room temperature for 40 min. The organic layer was separated and the aqueous layer was extracted with CH₂Cl₂ (2 × 30 mL). The combined organic layers were washed with aq. HCl (1 M, 80 mL), sat. aq. NaHCO₃ (60 mL), and brine (50 mL). The organic phase was dried over MgSO₄, filtered, and the solvent was evaporated under reduced pressure to obtain the pure product (1.83 g, 15.1 mmol, 38%, lit.^[219] 59%) as a light green solid.

¹H-NMR (400 MHz, CDCl₃, δ): 7.81 (d, ³J_{HH} = 8.3 Hz, 4H), 7.42–7.37 (m, 4H), 2.45 (s, 6H).

TLC (SiO₂, cyclohexane/EtOAc 1:2, UV): R_f = 0.55.

The characterization data are in agreement with the literature.^[219]

7.5.18 (*E*)-1,2-Di-*p*-tolylidiazene (**138**)Reaction SchemeExperimental Procedure

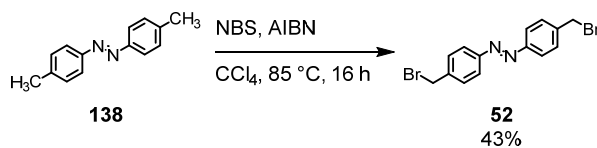
To a round-bottom flask were added **140** (321 mg, 2.65 mmol, 1.3 equiv), **139** (214 mg, 2.00 mmol, 1.0 equiv), and AcOH (20 mL). The reaction mixture was stirred at room temperature for 14 h. The solvent was evaporated under reduced pressure and the residue was purified by column chromatography (1st, short one: SiO₂, cyclohexane/EtOAc 6:1; 2nd: SiO₂, cyclohexane/EtOAc 5:1) to yield the pure product (351 mg, 1.67 mmol, 84%, lit.^[219] 86%) as an orange solid.

¹H-NMR (400 MHz, CDCl₃, δ): 7.85–7.78 (m, 4H), 7.35–7.27 (m, 4H), 2.44 (s, 6H).

¹³C-NMR (101 MHz, CDCl₃, δ): 151.0, 141.3, 129.8, 122.9, 21.6.

TLC (SiO₂, cyclohexane/EtOAc 5:1, UV): R_f = 0.57.

The characterization data are in agreement with the literature.^[219]

7.5.19 (*E*)-1,2-Bis(4-(bromomethyl)phenyl)diazene (52**)**Reaction SchemeExperimental Procedure

To a solution of compound **138** (667 mg, 3.17 mmol) in CCl_4 (60 mL) were added NBS (1.31 g, 7.36 mmol, 2.3 equiv) and AIBN (39.0 mg, 233 μmol , 7.30 mol-%). The resulting mixture was stirred at 85 $^\circ\text{C}$ for 16 h and the solvent was removed under reduced pressure. The residue was dissolved in CH_2Cl_2 , washed with sat. aq. NaHCO_3 (40 mL), brine (60 mL), dried over MgSO_4 , and filtered. After evaporation of the solvent, the orange solid was purified repeatedly by column chromatography (SiO_2 , cyclohexane/ CH_2Cl_2 1:1) to afford the pure product (503 mg, 1.37 mmol, 43%, lit.^[219] 42%) as an orange solid.

$^1\text{H-NMR}$ (400 MHz, CDCl_3 , δ): 7.91–7.88 (m, 4H), 7.57–7.52 (m, 4H), 4.56 (s, 4H).

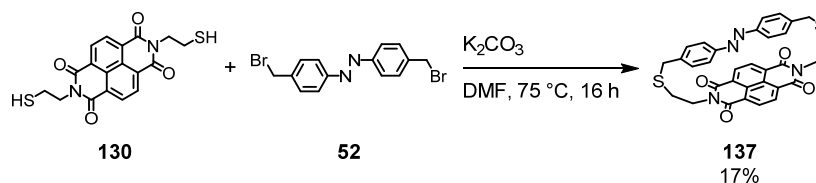
$^{13}\text{C-NMR}$ (101 MHz, CDCl_3 , δ): 152.4, 140.9, 130.1, 123.5, 32.8.

TLC (SiO_2 , cyclohexane/ CH_2Cl_2 1:1, UV): $R_f = 0.82$.

The characterization data are in agreement with the literature.^[219]

7.5.20 (*E*)-1((2,7)-Benzo[*lmn*][3,8]phenanthroline-1,3,6,8-(2*H*,7*H*)-tetraona)-6((4,4')-1,2-diphenyldiazena)-4,8-dithiadecanodane (**137**)

Reaction Scheme



Experimental Procedure

To an oven-dried two-necked flask was added dry DMF (230 mL) and deoxygenated with argon for 5 min. After the addition of **130** (30.8 mg, 79.7 μmol , 1.0 equiv) and K_2CO_3 (146 mg, 1.05 mmol, 13.1 equiv), the resulting mixture was heated at 75 °C. **52** (29.3 mg, 79.7 μmol , 1.0 equiv) in dry DMF (10 mL) was added to the hot solution over 1 h and the solution was stirred at 75 °C for 16 h. The solution was cooled to room temperature and the solvent was removed under reduced pressure. The crude product was purified by column chromatography (1st, short one: SiO_2 , EtOAc/ CH_2Cl_2 1:5; 2nd: SiO_2 , EtOAc/ CH_2Cl_2 1:10 to 1:5) and GPC to yield the pure product (8.00 mg, 13.5 μmol , 17%) as a yellow solid.

HRMS (ESI): $[\text{M} + \text{H}]^+$ calcd for $\text{C}_{32}\text{H}_{24}\text{N}_4\text{O}_4\text{S}_2$: 593.1312; found: 593.1310.

IR (cm^{-1}): 2908 (w), 1702 (m), 1658 (s), 1579 (m), 1324 (s), 1242 (s), 851 (m), 765 (s).

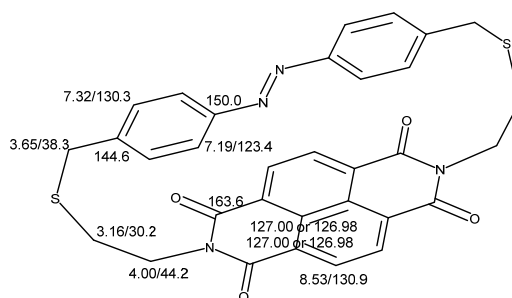
MP: above 360 °C.

MS (MALDI-TOF), m/z : 592.7 ($[\text{M}]^-$).

$^1\text{H-NMR}$ (600 MHz, CD_2Cl_2 , δ): 8.53 (s, 4H), 7.33–7.30 (m, 4H), 7.21–7.15 (m, 4H), 4.01–3.98 (m, 4H), 3.65 (s, 4H), 3.19–3.15 (m, 4H).

$^{13}\text{C-NMR}$ (151 MHz, CD_2Cl_2 , δ): 163.6, 150.0, 144.6, 130.9, 130.3, 127.0, 127.0, 123.4, 44.2, 38.3, 30.2.

Assignment of hydrogen and carbon atoms was done by 2D-NMR. Signals at 127.00 and 126.98 ppm cannot be clearly assigned, they have the same $^3J_{\text{HC}}$ coupling to the signal at 8.53 ppm.



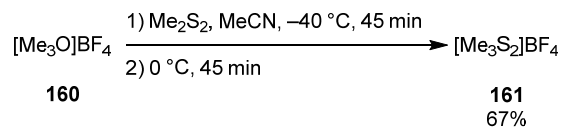
TLC (SiO_2 , $\text{CH}_2\text{Cl}_2/\text{EtOAc}$ 10:1, UV (365 nm)): $R_f = 0.33$.

TLC (SiO_2 , $\text{CH}_2\text{Cl}_2/\text{MeOH}$ 10:1, UV (365 nm)): $R_f = 0.90$.

UV/Vis (CD_2Cl_2): λ_{max} (ϵ_{max}): 350 (39721) nm ($\text{mol}^{-1} \cdot \text{dm}^3 \cdot \text{cm}^{-1}$).

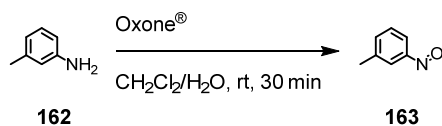
7.5.21 Thiomethyldimethyl Sulfonium Fluoroborate (**161**)

Reaction Scheme



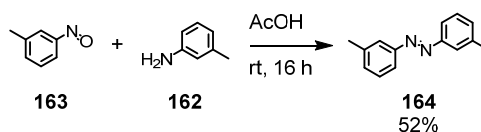
Experimental Procedure

To an oven-dried two-necked round-bottom flask were added trimethyloxonium tetrafluoroborate (**160**; 3.32 g, 22.4 mmol, 1.0 equiv) and dry MeCN (15 mL). The resulting mixture was cooled to $-40\text{ }^\circ\text{C}$ and dimethyl disulfide (2.00 mL, 22.6 mmol, 1.1 equiv) was added. The reaction mixture was stirred at $-40\text{ }^\circ\text{C}$ for 45 min, before it was warmed to $0\text{ }^\circ\text{C}$ and stirred for 45 min. After the addition of Et_2O (30 mL), a white powder was formed and the precipitate was filtered off. The white solid (2.94 g, 15.0 mmol, 67%, lit.^[312] 82%) was stored in the freezer and used without further purification.

7.5.22 1-Methyl-3-nitrosobenzene (163)Reaction SchemeExperimental Procedure

To a two-necked round-bottom flask were added 3-methylaniline (**162**; 1.05 g, 9.74 mmol, 1.0 equiv) and CH₂Cl₂ (40 mL). A solution of Oxone[®] (9.96 g, 32.4 mmol, 3.3 equiv) in H₂O (80 mL) was added and the resulting biphasic mixture was stirred at room temperature for 30 min. The organic layer was separated and the aqueous layer was extracted with CH₂Cl₂ (2 × 40 mL). The combined organic layers were washed with aq. HCl (1 M, 30 mL), sat. aq. NaHCO₃ (70 mL), and brine (50 mL). The organic phase was dried over MgSO₄, filtered, and the solvent was evaporated under reduced pressure. The crude product was purified by column chromatography (SiO₂, EtOAc/pentane 1:5) to yield the pure product (518 mg, lit.^[219] 59%) as a green solid.

The product was not clean according to ¹H-NMR analysis and, as a result, no yield was indicated.

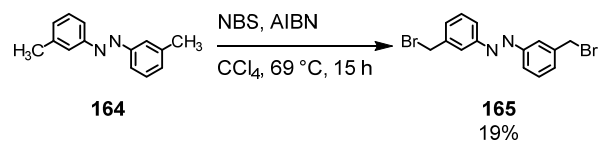
7.5.23 (E)-1,2-Di-*m*-tolylidiazene (164)Reaction SchemeExperimental Procedure

To a one-necked round-bottom flask were added **163** (518 mg, 4.27 mmol, 1.2 equiv), **162** (392 mg, 3.62 mmol, 1.0 equiv), and AcOH (40 mL). The resulting mixture was stirred at room temperature for 16 h, diluted with H₂O, and extracted with EtOAc. The aqueous phase was separated. The organic phase was washed with H₂O (2 × 30 mL), brine (40 mL), dried over MgSO₄, and filtered. After evaporating the solvent under reduced pressure, the crude product was filtered through a silica gel plug and washed with CH₂Cl₂ (200 mL). A final purification by column chromatography (SiO₂, CH₂Cl₂) afforded the pure product (393 mg, 1.87 mmol, 52%, lit.^[219] 55%) as an orange solid.

¹H-NMR (400 MHz, CDCl₃, δ): 7.74–7.70 (m, 4H), 7.43–7.38 (m, 2H), 7.29 (d, ³J_{HH} = 7.5 Hz, 2H), 2.46 (s, 6H).

TLC (SiO₂, CH₂Cl₂, UV): R_f = 0.85.

The characterization data are in agreement with the literature.^[219]

7.5.24 (*E*)-1,2-Bis(3-(bromomethyl)phenyl)diazene (**165**)Reaction SchemeExperimental Procedure

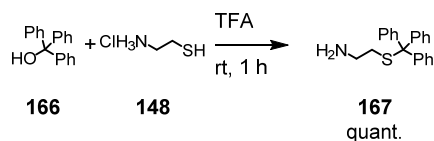
To a deoxygenated solution of **164** (393 mg, 1.87 mmol, 1.0 equiv) in CCl₄ (20 mL) were added NBS (669 mg, 3.76 mmol, 2.0 equiv) and AIBN (27.0 mg, 161 μmol, 8.6 mol-%). The resulting mixture was stirred at 69 °C for 15 h and the solvent was removed under reduced pressure. The residue was purified by column chromatography (1st: SiO₂, CH₂Cl₂; 2nd: SiO₂, cyclohexane/CH₂Cl₂ 2:1) to obtain the pure product (131 mg, 356 μmol, 19%, lit.^[219] 35%) as a bright orange solid.

¹H-NMR (400 MHz, CDCl₃, δ): 7.98–7.93 (m, 2H), 7.90–7.86 (m, 2H), 7.55–7.50 (m, 4H), 4.59 (s, 4H).

¹³C-NMR (101 MHz, CDCl₃, δ): 152.9, 139.1, 131.8, 129.8, 123.6, 123.1, 32.9.

TLC (SiO₂, cyclohexane/CH₂Cl₂ 1:1, UV): R_f = 0.83.

The characterization data are in agreement with the literature.^[219]

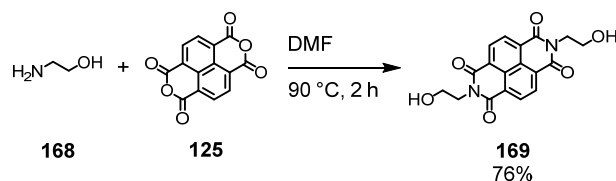
7.5.25 2-(Tritylsulfanyl)ethanamine (167)Reaction SchemeExperimental Procedure

Triphenylmethanol (**166**; 2.42 g, 9.00 mmol, 1.0 equiv) was added to a solution of **148** (1.03 g, 9.08 mmol, 1.0 equiv) in TFA (10 mL). The resulting solution was stirred at room temperature for 1 h and the solvent was removed under reduced pressure. The residue was dissolved in EtOAc (60 mL), washed with aq. NaOH (1 M, 2 × 30 mL), brine (40 mL), dried over MgSO₄, and filtered. The solvent was evaporated under reduced pressure and the pure product (3.09 g, 9.67 mmol, quant., lit.^[313] 85%) was obtained as a white solid.

¹H-NMR (400 MHz, CD₃OD, δ): 7.47–7.42 (m, 6H), 7.36–7.29 (m, 6H), 7.28–7.23 (m, 3H), 2.62–2.53 (m, 2H), 2.54–2.45 (m, 2H).

¹³C-NMR (126 MHz, CD₃OD, δ): 145.6, 130.7, 129.2, 128.2, 68.4, 39.6, 30.1.

The characterization data are in agreement with the literature.^[314]

7.5.26 *N,N'*-Di-(2'-hydroxyethyl)-1,4,5,8-naphthalenetetracarboxylic acid diimide (169)Reaction SchemeExperimental Procedure

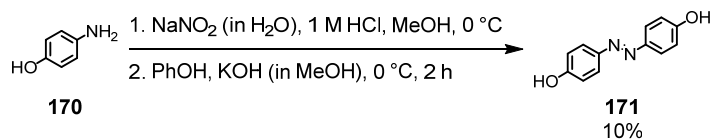
Ethanolamine (**168**; 5.0 mL, 82.8 mmol, 8.8 equiv) was added to a solution of **125** (2.51 g, 9.37 mmol, 1.0 equiv) in dry DMF (40 mL). The reaction mixture was heated at 90 °C for 2 h. The formed precipitate was filtered off, cooled to room temperature, and washed with acetone (40 mL). The pure product (2.52 g, 7.13 mmol, 76%, lit.^[315] 81%) was obtained as a brown solid.

¹H-NMR (400 MHz, (CD₃)₂SO, δ): 8.61 (s, 4H), 4.85 (t, ³J_{HH} = 6.0 Hz, 2H), 4.16 (t, ³J_{HH} = 6.4 Hz, 4H), 3.65 (q, ³J_{HH} = 6.2 Hz, 4H).

¹³C-NMR (101 MHz, (CD₃)₂SO, δ): 162.7, 130.3, 126.2, 126.0, 57.7, 42.3.

The characterization data are in agreement with the literature.^[315]

7.5.27 4,4'-Dihydroxyazobenzene (171)

Reaction SchemeExperimental Procedure

4-Hydroxyaniline (**170**; 6.39 g, 58.0 mmol, 1.0 equiv) was dissolved in aq. HCl (1 M, 100 mL) and cooled to 0 °C. An aqueous solution of sodium nitrite (4.08 g, 58.0 mmol, 1.0 equiv) in H₂O (20 mL) was added dropwise over 20 min to this solution. The mixture was diluted by adding pre-cooled (4 °C) MeOH (200 mL). To a second flask phenol (5.51 g, 58.0 mmol, 1.0 equiv), KOH (6.53 g, 116 mmol, 2.0 equiv) and MeOH (40 mL) were added and cooled to 0 °C. The phenolate solution was added dropwise over 30 min under constant stirring to the first reaction mixture. The red solution was stirred at 0 °C for 2 h before the reaction was quenched with aq. HCl (1 M) and the mixture was acidified until the pH value reached 7. CH₂Cl₂ was added, the separated aqueous layer acidified (pH = 1) with aq. HCl (3 M), and diluted with CH₂Cl₂ (100 mL). The aqueous phase was separated, the organic layers were combined, dried over MgSO₄, filtered, and the solvent was removed under reduced pressure. The residue was purified three times by column chromatography (SiO₂, cyclohexane/EtOAc 1:1). The mixed fractions were combined and recrystallized from AcOH.

Filter cake: black solid; mother liquor: filtrated after cooling to room temperature and the formed orange filter cake was isolated. Both filter cakes (both contained pure product) were combined and yielded the pure product (1.21 g, 5.65 mmol, 10%, lit.^[316] 36%) as an orange/black solid.

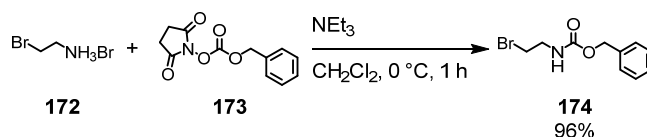
MS (ESI), *m/z*: 215.0 ([M + H]⁺).

¹H-NMR (400 MHz, (CD₃)₂SO, δ): 10.11 (s, 2H), 7.74–7.68 (m, 4H), 6.93–6.88 (m, 4H).

¹³C-NMR (101 MHz, (CD₃)₂SO, δ): 159.9, 145.2, 124.1, 115.7.

TLC (SiO₂, cyclohexane/EtOAc 1:1, UV): R_f = 0.38.

The characterization data are in agreement with the literature.^[316]

7.5.28 *N*-Benzyloxycarbonyl-2-bromoethylamine (**174**)Reaction SchemeExperimental Procedure^[317]

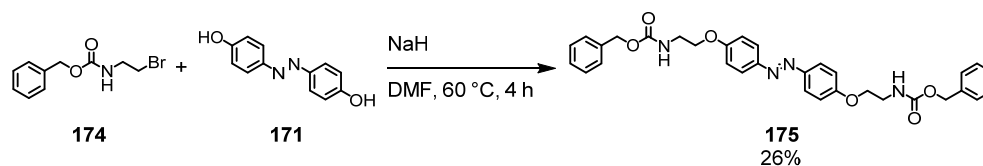
To a two-necked round-bottom flask were added 2-bromoethylamine hydrobromide (**172**; 1.23 g, 6.00 mmol, 1.2 equiv), *N*-(benzyloxycarbonyloxy)succinimide (**173**; 1.37 g, 5.22 mmol, 1.0 equiv), and CH₂Cl₂ (50 mL). The reaction mixture was cooled to 0 °C and NEt₃ (0.75 mL, 5.28 mmol, 1.0 equiv) was slowly added while keeping the temperature at 0 °C. After stirring for 1 h, the solvent was removed under reduced pressure, and the residue white solid was purified by column chromatography (SiO₂, cyclohexane/EtOAc 3:1) to yield the pure product (1.29 g, 5.00 mmol, 96%) as a white solid.

¹H-NMR (400 MHz, CDCl₃, δ/ppm): 7.40–7.31 (m, 5H), 5.12 (s, 2H), 3.61 (q, ³J_{HH} = 5.9 Hz, 2H), 3.47 (t, ³J_{HH} = 5.9 Hz, 2H).

¹³C-NMR (101 MHz, CDCl₃, δ/ppm): 156.3, 136.4, 128.7, 128.4, 128.3, 67.1, 42.9, 32.6.

TLC (SiO₂, cyclohexane/EtOAc 2:1, UV, KMnO₄): R_f = 0.35.

The characterization data are in agreement with the literature.^[318]

7.5.29 4,4'-Di[γ -(*N*-benzyloxycarbonyl)aminoethoxy]azobenzene (**175**)Reaction SchemeExperimental Procedure

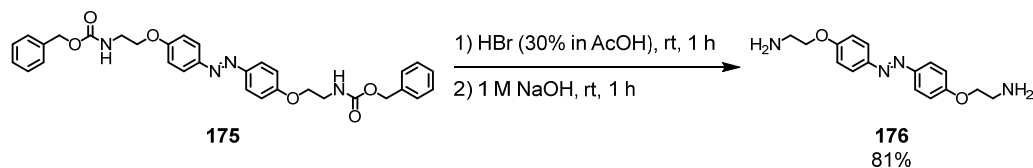
To an oven-dried two-necked round-bottom flask were added NaH (60%, 113 mg, 2.82 mmol, 2.9 equiv) and dry DMF (10 mL). **171** (206 mg, 962 μ mol, 1.0 equiv) dissolved in dry DMF (10 mL) was added dropwise to the previous solution. The resulting mixture was stirred at room temperature for 20 min and **174** (575 mg, 2.23 mmol, 2.3 equiv) was added in one portion. After stirring at 60 °C for 16 h, the solvent was evaporated under reduced pressure. The residue was recrystallized from a 1:1 mixture of 2-butanol/EtOH (40 mL) and the obtained crystals were purified by column chromatography (SiO₂, cyclohexane/EtOAc 2:1 to 1:2) to afford the pure product (141 mg, 248 μ mol, 26%, lit.^[319] 65%) as a yellow solid.

¹H-NMR (400 MHz, (CD₃)₂SO, δ): 7.83 (d, ³*J*_{HH} = 8.9 Hz, 4H), 7.54 (t, ³*J*_{HH} = 5.6 Hz, 2H), 7.39–7.28 (m, 10H), 7.11 (d, ³*J*_{HH} = 9.0 Hz, 4H), 5.04 (s, 4H), 4.10 (t, ³*J*_{HH} = 5.6 Hz, 4H), 3.42 (q, ³*J*_{HH} = 5.7 Hz, 4H).

¹³C-NMR (101 MHz, (CD₃)₂SO, δ): 160.7, 156.3, 146.2, 137.1, 128.4, 127.8, 127.8, 124.2, 115.0, 66.8, 65.4.

TLC (SiO₂, cyclohexane/EtOAc 1:1, UV): *R*_f = 0.34.

The characterization data are in agreement with the literature.^[319]

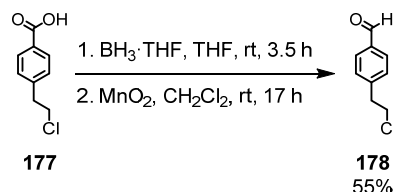
7.5.30 4,4'-Di(γ -aminoethoxy)azobenzene (**176**)Reaction SchemeExperimental Procedure

175 (54.0 mg, 95.0 μmol , 1.0 equiv) was dissolved in HBr (30% in AcOH, 2.00 mL, 10.0 mmol, 106 equiv) and stirred at room temperature for 1 h. The formed red precipitate was filtered off, washed with Et₂O (30 mL), and dried under high vacuum to yield 4,4'-di[γ -aminoethoxy]-azobenzene dihydrobromide (43.0 mg). The red solid was subsequently dissolved in aq. NaOH (1 M, 2 mL) and stirred at room temperature for 1 h. The yellow precipitate was filtered off and washed with H₂O (30 mL) to yield the pure product (23.0 mg, 76.6 μmol , 81%, lit.^[320] 49%) as a yellow solid.

¹H-NMR (400 MHz, (CD₃)₂SO, δ): 7.83 (d, ³ J_{HH} = 8.9 Hz, 4H), 7.11 (d, ³ J_{HH} = 8.9 Hz, 4H), 4.01 (t, ³ J_{HH} = 5.7 Hz, 4H), 2.90 (t, ³ J_{HH} = 5.7 Hz, 4H), 1.56 (s, 4H, NH₂).

¹³C-NMR (101 MHz, (CD₃)₂SO, δ): 161.0, 146.1, 124.1, 115.0, 70.7, 40.9.

The characterization data are in agreement with the literature.^[320]

7.5.31 4-(2-Chloroethyl)benzaldehyde (**178**)Reaction SchemeExperimental Procedure

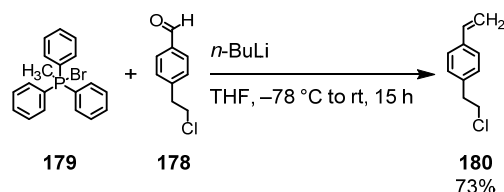
To an oven-dried flask were added 4-(2-chloroethyl)benzoic acid (**177**; 2.00 g, 10.8 mmol, 1.0 equiv) and dry THF (40 mL). The resulting mixture was cooled to 0 °C and $\text{BH}_3 \cdot \text{THF}$ (1 M, 16.0 mL, 16.0 mmol, 1.5 equiv) was added dropwise over 30 min. The suspension was stirred at room temperature for 2 h and aq. H_2SO_4 (1 M, 36 mL) was added. The mixture was stirred at room temperature for 1 h and extracted with EtOAc (2×30 mL). The combined organic layers were washed with brine (40 mL), dried over MgSO_4 , filtered, and the solvent was evaporated under reduced pressure. The residue was dissolved in CH_2Cl_2 (50 mL) and MnO_2 (10.0 g, 100 mmol, 10.6 equiv) was added. The reaction mixture was stirred at room temperature for 17 h. The mixture was filtered through a Celite[®] pad and the filtrate was concentrated under reduced pressure to obtain a yellow liquid, which was purified by column chromatography (SiO_2 , cyclohexane/EtOAc 4:1) to obtain the pure product (998 mg, 5.92 mmol, 55%, lit.^[321] 91%) as a white solid.

GC-MS (EI), m/z (% relative intensity, ion): 168.0 (99.2, $[\text{M}]^+$), 139.0 (29.5, $[\text{M} - \text{CHO}]^+$), 119.8 (100, $[\text{M} - \text{CH}_2\text{Cl}]^+$), 105.1 (21.2, $[\text{M} - \text{EtCl}]^+$).

¹H-NMR (400 MHz, CDCl_3 , δ): 10.00 (s, 1H), 7.87–7.83 (m, 2H), 7.40 (d, $^3J_{\text{HH}} = 8.0$ Hz, 2H), 3.76 (t, $^3J_{\text{HH}} = 7.1$ Hz, 2H), 3.16 (t, $^3J_{\text{HH}} = 7.1$ Hz, 2H).

¹³C-NMR (101 MHz, CDCl_3 , δ): 192.0, 145.3, 135.4, 130.2, 129.7, 44.4, 39.2.

TLC (SiO_2 , cyclohexane/EtOAc 2:1, UV): $R_f = 0.45$.

7.5.32 1-(2-Chloroethyl)-4-vinylbenzene (**180**)Reaction SchemeExperimental Procedure

To an oven-dried flask was added dry THF (40 mL) and cooled to -78 °C. Methyltriphenylphosphonium bromide (**179**; 1.20 g, 3.32 mmol, 1.0 equiv) and *n*-BuLi (1.6 M in hexanes, 2.5 mL, 4.00 mmol, 1.2 equiv) were added and stirred at -78 °C for 30 min. **178** (556 mg, 3.30 mmol, 1.0 equiv) in dry THF (10 mL) was added dropwise over 30 min to the solution. The reaction mixture was warmed to room temperature over 3 h, before it was quenched by the addition of H₂O (50 mL) and diluted with EtOAc (70 mL). The organic layer was separated and the aqueous layer was extracted with EtOAc (2 × 60 mL). The combined organic layers were washed with brine (50 mL), dried over MgSO₄, filtered, and the solvent removed under reduced pressure. The residue was purified by column chromatography (SiO₂, cyclohexane/EtOAc 3:1) to obtain the pure product (400 mg, 2.40 mmol, 73%) as a yellow liquid.

GC-MS (EI), *m/z* (% relative intensity, ion): 166.1 (43.2, [M]⁺), 117.1 (100, [M - CH₂Cl]⁺).

¹H-NMR (400 MHz, CDCl₃, δ): 7.40–7.35 (m, 2H), 7.22–7.17 (m, 2H), 6.71 (dd, ³*J*_{HH} = 17.6 Hz, ³*J*_{HH} = 10.9 Hz, 1H), 5.77–5.70 (m, 1H), 5.26–5.21 (m, 1H), 3.71 (t, ³*J*_{HH} = 7.4 Hz, 2H), 3.06 (t, ³*J*_{HH} = 7.4 Hz, 2H).

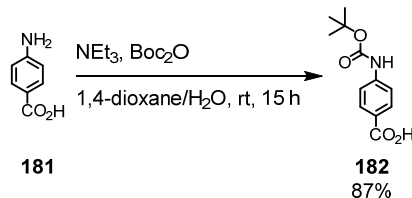
¹³C-NMR (101 MHz, CDCl₃, δ): 137.8, 136.6, 136.4, 129.1, 126.6, 113.8, 45.0, 39.0.

TLC (SiO₂, cyclohexane/EtOAc 2:1, UV): *R*_f = 0.68.

7.6 Syntheses of Linear cNDIs with Different Protecting Groups

7.6.1 4-(*tert*-Butoxycarbonylamino)benzoic acid (**182**)

Reaction Scheme



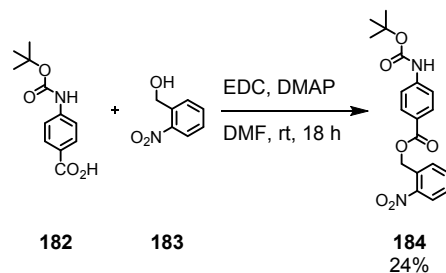
Experimental Procedure

4-Aminobenzoic acid (**181**; 1.37 g, 10.0 mmol, 1.0 equiv) was dissolved in a 26:15 mixture of 1,4-dioxane/H₂O (205 mL) and NEt₃ (2.8 mL, 19.7 mmol, 2.0 equiv) was added, followed by the addition of di-*t*-butyl dicarbonate (4.38 g, 19.7 mmol, 2.0 equiv). The resulting solution was stirred at room temperature for 15 h. The solvents were removed under reduced pressure, the residue was dissolved in aq. HCl (3 M, 100 mL), and the resulting white solid was filtered off to afford the pure product (2.05 g, 8.65 mmol, 87%, lit.^[322] 94%).

¹H-NMR (400 MHz, (CD₃)₂SO, δ): 9.73 (s, 1H, NH), 7.83 (d, ³J_{HH} = 8.8 Hz, 2H), 7.55 (d, ³J_{HH} = 8.8 Hz, 2H), 1.48 (s, 9H).

¹³C-NMR (101 MHz, (CD₃)₂SO, δ): 167.0, 152.5, 143.8, 130.3, 123.9, 117.2, 79.6, 28.0.

The characterization data are in agreement with the literature.^[322]

7.6.2 2-Nitrobenzyl 4-((*tert*-butoxycarbonyl)amino)benzoate (184**)**Reaction SchemeExperimental Procedure

To a solution of **182** (241 mg, 1.01 mmol, 1.0 equiv) in dry DMF (15 mL) were added EDC (200 μ L, 1.12 mmol, 1.1 equiv) and DMAP (29.0 mg, 235 μ mol, 23.2 mol-%). The mixture was stirred at room temperature for 10 min and 2-nitrobenzyl alcohol (**183**; 226 mg, 1.48 mmol, 1.5 equiv) was added. The resulting mixture was stirred at room temperature for 18 h and was diluted with H₂O (50 mL) and CH₂Cl₂ (80 mL). The aqueous layer was extracted with CH₂Cl₂ (2 x 50 mL), the combined organic layers were dried over MgSO₄, and filtered. The solvents were evaporated under reduced pressure and the residue was purified by column chromatography (SiO₂, cyclohexane/EtOAc 3:1) to yield the pure product (91.0 mg, 244 μ mol, 24%) as a yellow solid.

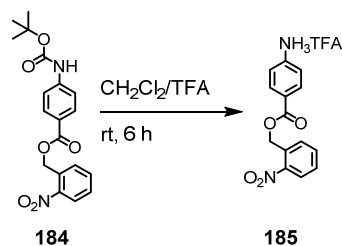
HRMS (ESI): [M + H]⁺ calcd for C₁₉H₂₀N₂O₆: 373.1394; found: 373.1211.

¹H-NMR (400 MHz, (CD₃)₂SO, δ): 9.82 (s, 1H, NH), 8.14 (dd, ³J_{HH} = 8.2 Hz, ⁴J_{HH} = 1.1 Hz, 1H), 7.90 (d, ³J_{HH} = 8.8 Hz, 2H), 7.84–7.75 (m, 2H), 7.69–7.54 (m, 3H), 5.63 (s, 2H), 1.49 (s, 9H).

¹³C-NMR (126 MHz, (CD₃)₂SO, δ): 164.9, 152.5, 147.5, 144.6, 134.2, 131.6, 130.5, 129.4, 129.4, 124.9, 122.2, 117.4, 79.8, 62.8, 28.0.

7.6.3 2-Nitrobenzyl-4-aminobenzoate (185)

Reaction Scheme



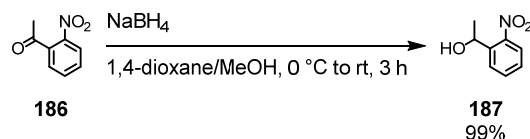
Experimental Procedure

184 (91.0 mg, 244 μmol , 1.0 equiv) was added to a 1:1 mixture of $\text{CH}_2\text{Cl}_2/\text{TFA}$ (8.0 mL) and stirred at room temperature for 6 h. The solvents were removed under reduced pressure to isolate the white product (89.0 mg) as the TFA salt.

GC-MS (EI), m/z (% relative intensity, ion): 272.1 (18.8, $[\text{M}]^+$).

$^1\text{H-NMR}$ (400 MHz, $(\text{CD}_3)_2\text{SO}$, δ): 8.12 (dd, $^3J_{\text{HH}} = 8.2$ Hz, $^4J_{\text{HH}} = 1.3$ Hz, 1H), 7.83–7.72 (m, 2H), 7.71–7.59 (m, 3H), 6.62–6.56 (m, 2H), 5.56 (s, 2H).

$^{13}\text{C-NMR}$ (101 MHz, $(\text{CD}_3)_2\text{SO}$, δ): 165.3, 153.6, 147.5, 134.1, 132.0, 131.3, 129.3, 129.2, 124.8, 115.1, 112.9, 62.1.

7.6.4 1-(2-Nitrophenyl)-ethanol (**187**)Reaction SchemeExperimental Procedure

o-Nitroacetophenone (**186**; 7.31 g, 44.2 mmol, 1.0 equiv) was dissolved in a 6:4 mixture of 1,4-dioxane/MeOH (100 mL) and stirred at 0 °C for 10 min. NaBH₄ (3.51 g, 89.1 mmol, 2.0 equiv) was carefully added to the reaction mixture (highly exothermic). The resulting solution was warmed to room temperature, stirred for 3 h, and quenched by the addition of acetone (50 mL). The solvents were removed under reduced pressure and the residue was dissolved in EtOAc (70 mL). The solution was washed with H₂O (3 × 50 mL), dried over MgSO₄, filtered, and concentrated under reduced pressure to yield the pure product (7.32 g, 43.8 mmol, 99%, lit.^[323] 99%) as a yellow oil.

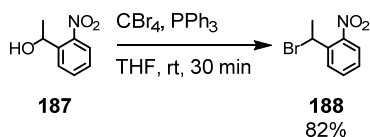
¹H-NMR (400 MHz, (CD₃)₂SO, δ): 7.90–7.78 (m, 2H), 7.72 (td, ³J_{HH} = 7.6 Hz, ⁴J_{HH} = 1.3 Hz, 1H), 7.54–7.44 (m, 1H), 5.50 (d, ³J_{HH} = 4.4 Hz, 1H), 5.12 (qd, ³J_{HH} = 6.4 Hz, ³J_{HH} = 4.3 Hz, 1H), 1.38 (d, ³J_{HH} = 6.4 Hz, 3H).

TLC (SiO₂, cyclohexane/EtOAc 4:1, UV): R_f = 0.13.

The characterization data are in agreement with the literature.^[323]

7.6.5 1-(1-Bromoethyl)-2-nitrobenzene (188)

Reaction Scheme



Experimental Procedure

187 (1.64 g, 9.82 mmol, 1.0 equiv), triphenylphosphine (3.98 g, 15.0 mmol, 1.5 equiv), and CBr₄ (5.04 g, 15.1 mmol, 1.5 equiv) were dissolved in dry THF (10 mL) and the resulting mixture was stirred for 30 min at room temperature. The solution was filtered and concentrated under reduced pressure. The residue was purified by column chromatography (SiO₂, cyclohexane/EtOAc 5:1 to 4:1) to afford the pure product (1.89 g, 8.17 mmol, 82%, lit.^[323] 97%) as a brown oil.

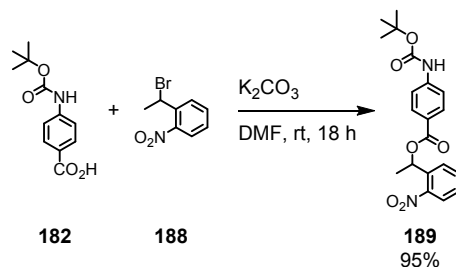
GC-MS (EI), m/z (% relative intensity, ion): 150.1 (100, [M - Br]⁺).

¹H-NMR (400 MHz, CDCl₃, δ): 7.91–7.81 (m, 2H), 7.64 (td, ³ J_{HH} = 7.6, ⁴ J_{HH} = 1.4 Hz, 1H), 7.47–7.40 (m, 1H), 5.81 (q, ³ J_{HH} = 6.9 Hz, 1H), 2.09 (d, ³ J_{HH} = 6.9 Hz, 3H).

¹³C-NMR (101 MHz, CDCl₃, δ): 137.9, 133.5, 130.0, 129.0, 124.5, 41.9, 27.3.

TLC (SiO₂, cyclohexane/EtOAc 4:1, UV): R_f = 0.39.

The characterization data are in agreement with the literature.^[323]

7.6.6 1-(2-Nitrophenyl)ethyl-4-((*tert*-butoxycarbonyl)amino)benzoate (189)Reaction SchemeExperimental Procedure

To an oven-dried two-necked round-bottom flask were added **182** (2.42 g, 10.2 mmol, 1.2 equiv), K_2CO_3 (1.42 g, 10.2 mmol, 1.2 equiv), and dry DMF (80 mL). The mixture was stirred at room temperature for 30 min and **188** (1.96 g, 8.50 mmol, 1.0 equiv) was added. The resulting solution was stirred at room temperature for 17 h and H_2O (40 mL) and EtOAc (50 mL) were added. The organic layer was separated and the aqueous phase was extracted with EtOAc (2×30 mL). The combined organic layers were washed with brine (40 mL), dried over $MgSO_4$, filtered, and the solvent was evaporated under reduced pressure. The residue was purified twice by column chromatography (SiO_2 , cyclohexane/EtOAc 3:1) to yield the pure product (3.11 g, 8.05 mmol, 95%) as a white solid.

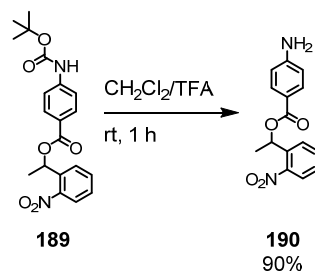
HRMS (ESI): $[M + H]^+$ calcd for $C_{20}H_{22}N_2O_6$: 387.1551; found: 387.1545.

1H -NMR (250 MHz, $CDCl_3$, δ): 8.03–7.92 (m, 3H), 7.71 (dd, $^3J_{HH} = 7.9$ Hz, $^4J_{HH} = 1.5$ Hz, 1H), 7.61 (td, $^3J_{HH} = 7.8$ Hz, $^4J_{HH} = 1.3$ Hz, 1H), 7.50–7.39 (m, 3H), 6.68 (s, 1H, NH), 6.54 (q, $^3J_{HH} = 6.5$ Hz, 1H), 1.77 (d, $^3J_{HH} = 6.5$ Hz, 3H), 1.53 (s, 9H).

1H -NMR (250 MHz, $(CD_3)_2SO$, δ): 9.80 (s, 1H, NH), 7.99 (dd, $^3J_{HH} = 8.1$ Hz, $^4J_{HH} = 1.3$ Hz, 1H), 7.95–7.70 (m, 4H), 7.65–7.50 (m, 3H), 6.30 (q, $^3J_{HH} = 6.5$ Hz, 1H), 1.70 (d, $^3J_{HH} = 6.5$ Hz, 3H), 1.48 (s, 9H).

^{13}C -NMR (101 MHz, $(CD_3)_2SO$, δ): 164.6, 152.4, 147.6, 144.5, 136.8, 134.1, 130.4, 129.1, 127.5, 124.1, 122.3, 117.3, 79.8, 67.7, 28.0, 21.5.

TLC (SiO_2 , cyclohexane/EtOAc 2:1, UV): $R_f = 0.44$.

7.6.7 (2-Nitrophenyl)ethyl-4-aminobenzoate (190)Reaction SchemeExperimental Procedure

189 (3.08 g, 7.98 mmol, 1.0 equiv) was dissolved in a 2:1 mixture of $\text{CH}_2\text{Cl}_2/\text{TFA}$ (30 mL) and stirred at room temperature for 1 h. The solvents were removed under reduced pressure, the residue was dissolved with CH_2Cl_2 (120 mL), and washed with sat. aq. NaHCO_3 (90 mL). The organic layer was separated and the aqueous layer was extracted with CH_2Cl_2 (2 x 30 mL). The combined organic layers were dried over MgSO_4 , filtered, and concentrated under reduced pressure. The pure product (2.06 g, 7.20 mmol, 90%) was isolated as a yellow solid.

GC-MS (EI), m/z (% relative intensity, ion): 286.1 (99.0, $[\text{M}]^+$), 151.1 (6.2, $[\text{M} - \text{C}_7\text{H}_6\text{NO}_2]^+$), 137.0 (88.1, $[\text{M} - \text{C}_8\text{H}_9\text{NO}_2]^+$).

HRMS (ESI): $[\text{M} + \text{H}]^+$ calcd for $\text{C}_{15}\text{H}_{14}\text{N}_2\text{O}_4$: 287.1026; found: 287.1026.

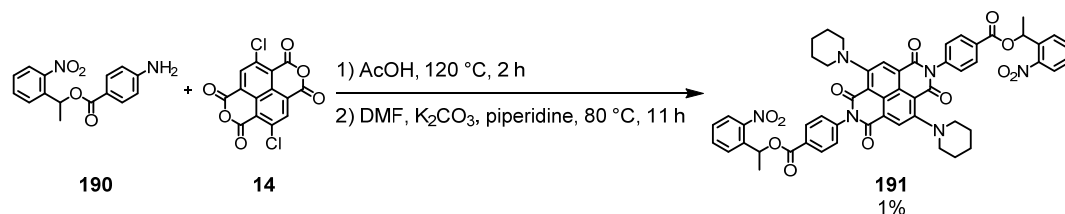
$^1\text{H-NMR}$ (400 MHz, $(\text{CD}_3)_2\text{SO}$, δ): 7.97 (dd, $^3J_{\text{HH}} = 8.2$ Hz, $^4J_{\text{HH}} = 1.3$ Hz, 1H), 7.82–7.73 (m, 2H), 7.70–7.62 (m, 2H), 7.61–7.52 (m, 1H), 6.62–6.52 (m, 2H), 6.24 (q, $^3J_{\text{HH}} = 6.5$ Hz, 1H), 6.03 (s, 2H), 1.67 (d, $^3J_{\text{HH}} = 6.5$ Hz, 3H).

$^{13}\text{C-NMR}$ (101 MHz, $(\text{CD}_3)_2\text{SO}$, δ): 164.9, 153.8, 147.6, 137.3, 134.0, 131.3, 128.9, 127.4, 124.1, 115.1, 112.6, 66.8, 21.6.

TLC (SiO_2 , cyclohexane/EtOAc 2:1, UV): $R_f = 0.22$.

7.6.8 *N,N'*-Di-4'-(1'-(2'-nitrophenyl)ethyl)benzoate-2,6-dipiperidinyl-1,4,5,8-naphthalenetetracarboxylic acid diimide (191)

Reaction Scheme



Experimental Procedure

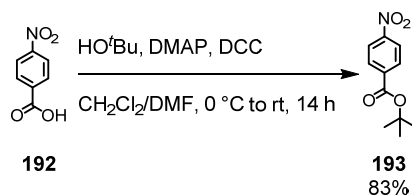
190 (970 mg, 3.39 mmol, 4.0 equiv) and **14** (286 mg, 848 μ mol, 1.0 equiv) were dissolved in AcOH (100 mL) and heated at 120 °C for 2 h. The reaction mixture was cooled to room temperature and the solvent was removed under reduced pressure. The residue was dissolved in CH₂Cl₂ and aq. HCl (1 M, 50 mL) was added. The organic layer was separated and the aqueous phase was extracted with CH₂Cl₂ (2 x 40 mL). The combined organic layers were washed with brine (40 mL), dried over MgSO₄, and filtered. The solvent was evaporated under reduced pressure and the residue was dried under high vacuum. The residue (740 mg), K₂CO₃ (243 mg, 1.74 mmol), dry DMF (15 mL), and piperidine (5.0 mL, 50.1 mmol) were added to a microwave vial. The vial was sealed and heated in the microwave reactor at 80 °C for 11 h. H₂O (80 mL) and CH₂Cl₂ (50 mL) were added and the organic layer was separated. The aqueous layer was extracted with CH₂Cl₂ (2 x 50 mL), the combined organic layers were dried over MgSO₄, and filtered. The solvent was evaporated under reduced pressure and the residue was purified by column chromatography (1st: SiO₂, CH₂Cl₂/EtOAc 20:1 to 15:1 to 10:1; 2nd: SiO₂, CH₂Cl₂/EtOAc 20:1 to 15:1; 3rd: SiO₂, CH₂Cl₂/EtOAc 15:1 to 1:10) to obtain the pure product (11.0 mg, 11.3 μ mol, 1% over two steps) as a blue solid.

HRMS (ESI): [M + H]⁺ calcd for C₅₄H₄₆N₆O₁₂: 971.3246; found: 971.3248.

¹H-NMR (500 MHz, CDCl₃, δ): 8.50 (s, 2H), 8.29–8.24 (m, 4H), 8.01 (dd, ³J_{HH} = 8.2 Hz, ⁴J_{HH} = 1.3 Hz, 2H), 7.75 (dd, ³J_{HH} = 7.9 Hz, ⁴J_{HH} = 1.4 Hz, 2H), 7.65 (td, ³J_{HH} = 7.6 Hz, ⁴J_{HH} = 1.3 Hz, 2H), 7.48–7.44 (m, 2H), 7.43–7.39 (m, 4H), 6.62 (q, ³J_{HH} = 6.5 Hz, 2H), 3.38 (t, ³J_{HH} = 5.3 Hz, 8H), 1.82 (d, ³J_{HH} = 6.5 Hz, 6H), 1.80–1.75 (m, 8H), 1.71–1.67 (m, 4H).

¹³C-NMR (126 MHz, CDCl₃, δ): 164.8, 163.3, 161.8, 152.6, 147.9, 140.6, 138.2, 133.9, 131.0, 130.3, 129.3, 128.6, 127.2, 126.1, 125.9, 125.0, 124.7, 109.3, 69.2, 53.8, 26.4, 24.0, 22.3.

TLC (SiO₂, CH₂Cl₂/EtOAc 10:1, UV): R_f = 0.62.

7.6.9 *tert*-Butyl-4-nitrobenzoate (193)Reaction SchemeExperimental Procedure

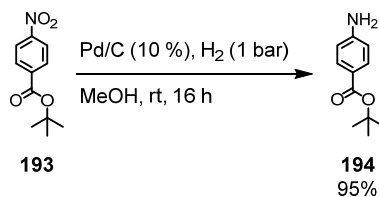
To an oven-dried two-necked round-bottom flask were added 4-nitrobenzoic acid (**192**; 7.69 g, 45.1 mmol, 1.0 equiv), *tert*-butanol (6.50 mL, 67.7 mmol, 1.5 equiv), DMAP (559 mg, 4.53 mmol, 0.1 equiv), and a 10:1 mixture of dry $\text{CH}_2\text{Cl}_2/\text{DMF}$ (220 mL). The solution was cooled to 0 °C and DCC (10.3 g, 49.6 mmol, 1.1 equiv) was added in two portions. The reaction mixture was warmed to room temperature and stirred for 14 h. The formed precipitate was filtered off and washed with CH_2Cl_2 (40 mL). The filtrate was washed with aq. HCl (1 M, 2 \times 50 mL), brine (50 mL), dried over MgSO_4 , and filtered. The solvents were removed under reduced pressure and the resulting oil was purified by column chromatography (SiO_2 , cyclohexane/EtOAc 10:1 to 4:1) to obtain the pure product (8.37 g, 37.5 mmol, 83%, lit.^[324] 72%) as a brown solid.

$^1\text{H-NMR}$ (400 MHz, CDCl_3 , δ): 8.28–8.22 (m, 2H), 8.17–8.12 (m, 2H), 1.62 (s, 9H).

$^{13}\text{C-NMR}$ (101 MHz, CDCl_3 , δ): 163.9, 150.4, 137.6, 130.6, 123.5, 82.7, 28.2.

TLC (SiO_2 , hexane/EtOAc 5:1, UV): $R_f = 0.83$.

The characterization data are in agreement with the literature.^[324]

7.6.10 *tert*-Butyl-4-aminobenzoate (**194**)Reaction SchemeExperimental Procedure

To a two-necked round-bottom flask were added **193** (8.16 g, 36.5 mmol, 1.0 equiv) and MeOH (300 mL). Pd/C (10%, 830 mg, 780 μ mol, 2.13 mol-%) was added and the reaction mixture was purged with H₂, and stirred under H₂ atmosphere (1 bar) at room temperature for 16 h. The mixture was filtered through a Celite[®] pad and the solvent was evaporated under reduced pressure. The residue was purified by column chromatography (SiO₂, cyclohexane/EtOAc 5:1 to 7:2) to yield the pure product (6.78 g, 34.7 mmol, 95%, lit.^[324] quant.) as a white solid.

GC-MS (EI), m/z (% relative intensity, ion): 193.1 (13.4, [M]⁺), 137.1 (100, [M - C₄H₈]⁺), 120.1 (86.8, [M - C₄H₉O]⁺).

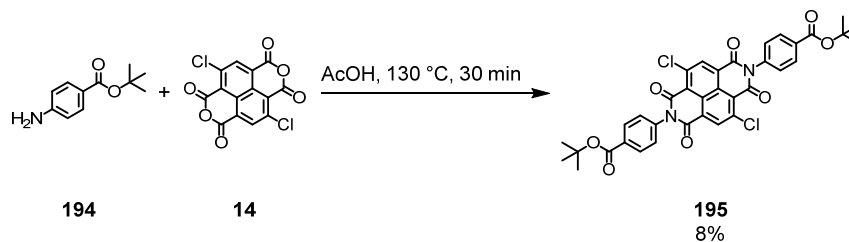
¹H-NMR (400 MHz, (CD₃)₂SO, δ): 7.60–7.55 (m, 2H), 6.57–6.51 (m, 2H), 5.85 (s, 2H, NH₂), 1.49 (s, 9H).

¹³C-NMR (101 MHz, (CD₃)₂SO, δ): 165.3, 153.0, 130.9, 117.6, 112.5, 78.8, 28.0.

TLC (SiO₂, cyclohexane/EtOAc 5:1, UV): R_f = 0.01.

TLC (SiO₂, cyclohexane/EtOAc 2 :1, UV): R_f = 0.36.

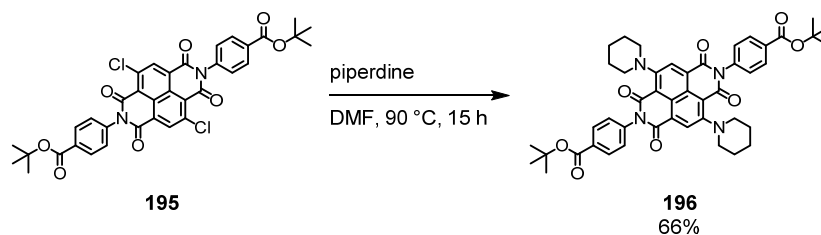
The characterization data are in agreement with the literature.^[324]

7.6.11 *N,N'*-Di-(4'-*tert*-butylbenzoate)-2,6-dichloro-1,4,5,8-naphthalenetetracarboxylic acid diimide (195)Reaction SchemeExperimental Procedure

To a flask were added **194** (254 mg, 1.31 mmol, 4.4 equiv) and AcOH (40 mL). The solution was heated at 130 °C and **14** (103 mg, 306 μ mol, 1.0 equiv) was added. The resulting mixture was stirred for 30 min at 130 °C. After cooling to room temperature, the solvent was removed under reduced pressure and the residue was purified by column chromatography (SiO₂, cyclohexane/EtOAc 2:1) to afford the pure product (17.0 mg, 24.7 μ mol, 8%) as a red solid.

MS (MALDI-TOF), m/z : 686.8 ([M]⁻).

TLC (SiO₂, cyclohexane/EtOAc 2:1, UV): R_f = 0.36.

7.6.12 *N,N'*-Di-(4'-*tert*-butylbenzoate)-2,6-dipiperidinyl-1,4,5,8-naphthalenetetracarboxylic acid diimide (196)Reaction SchemeExperimental Procedure

To an oven-dried two-necked round-bottom flask were added **195** (17.0 mg, 24.7 μmol , 1.0 equiv), piperidine (1.20 mL, 12.0 mmol, 487 equiv), and dry DMF (40 mL). The reaction mixture was stirred at 90 °C for 15 h. After cooling to room temperature, the mixture was poured into aq. HCl (1 M, 100 mL) and diluted with CH_2Cl_2 (80 mL). The aqueous layer was separated and the organic layer was washed with H_2O (3×40 mL). The organic layer was dried over MgSO_4 , filtered, and the solvent was removed under reduced pressure. The crude product was purified by column chromatography (SiO_2 , cyclohexane/EtOAc 2:1) to obtain the pure product (12.8 mg, 16.3 μmol , 66%) as a blue solid.

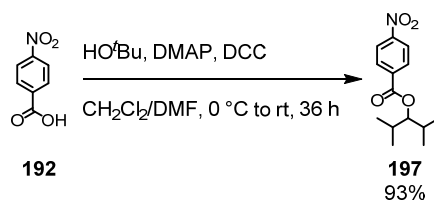
HRMS (ESI): $[\text{M} + \text{H}]^+$ calcd for $\text{C}_{46}\text{H}_{48}\text{N}_4\text{O}_8$: 785.3545; found: 785.3547.

MS (MALDI-TOF), m/z : 785.2 ($[\text{M}]^-$).

$^1\text{H-NMR}$ (500 MHz, CDCl_3 , δ): 8.50 (s, 2H), 8.21–8.16 (m, 4H), 7.38–7.34 (m, 4H), 3.41–3.34 (m, 8H), 1.80–1.74 (m, 8H), 1.71–1.66 (m, 4H), 1.63 (s, 18H).

$^{13}\text{C-NMR}$ (126 MHz, CDCl_3 , δ): 165.2, 163.3, 161.8, 152.6, 139.8, 132.4, 130.7, 128.9, 126.1, 125.9, 125.0, 109.4, 81.5, 53.8, 28.4, 26.4, 24.0.

TLC (SiO_2 , cyclohexane/EtOAc 2:1, UV): $R_f = 0.44$.

7.6.13 2,4-Dimethylpentan-3-yl-4-nitrobenzoate (197)Reaction SchemeExperimental Procedure

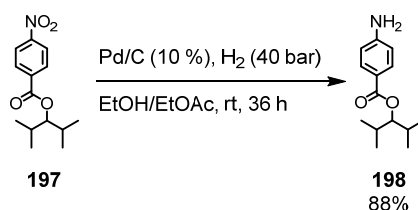
To an oven-dried two-necked round-bottom flask were added **192** (3.42 g, 20.1 mmol, 1.0 equiv), 2,4-dimethyl-3-pentanol (2.60 mL, 32.0 mmol, 1.5 equiv), DMAP (253 mg, 2.05 mmol, 0.1 equiv), and a 20:3 mixture of dry CH₂Cl₂/DMF (115 mL). The resulting solution was cooled to 0 °C and DCC (4.60 g, 22.1 mmol, 1.1 equiv) was added in one portion. The reaction mixture was warmed to room temperature and stirred for 36 h. The precipitate was filtered off and washed with CH₂Cl₂ (50 mL). The filtrate was washed with aq. HCl (1 M, 100 mL), brine (50 mL), dried over MgSO₄, filtered, and the solvent was evaporated under reduced pressure. The resulting oil was purified by column chromatography (SiO₂, cyclohexane/EtOAc 1:5) to yield the pure product (4.98 g, 18.8 mmol, 93%) as a colorless solid.

GC-MS (EI), *m/z* (% relative intensity, ion): 222.0 (14.6, [M - C₃H₇]⁺), 150.0 (100, [M - C₇H₁₅O]⁺).

¹H-NMR (400 MHz, CDCl₃, δ): 8.32–8.28 (m, 2H), 8.25–8.19 (m, 2H), 4.88 (t, ³J_{HH} = 6.1 Hz, 1H), 2.06 (hept, ³J_{HH} = 6.7 Hz, 2H), 0.95 (d, ³J_{HH} = 5.8 Hz, 12H).

¹³C-NMR (101 MHz, CDCl₃, δ): 164.8, 150.6, 136.2, 130.8, 123.7, 84.9, 29.7, 19.7, 17.5.

TLC (SiO₂, cyclohexane/EtOAc 5:1, UV): R_f = 0.60.

7.6.14 2,4-Dimethylpentan-3-yl-4-aminobenzoate (198)Reaction SchemeExperimental Procedure

To a reaction vial were added **197** (4.73 g, 17.8 mmol), Pd/C (10%, 305 mg, 1.61 mol-%) dissolved, and a 5:8 mixture of EtOH/EtOAc (13 mL). The vial was placed in an autoclave and the reaction was performed under H₂ atmosphere (40 bar) at room temperature over 36 h. The suspension was filtrated through a Celite[®] pad and washed with EtOAc (90 mL) and CH₂Cl₂ (80 mL). The solvents were evaporated under reduced pressure and the residue was purified by column chromatography (SiO₂, cyclohexane/EtOAc 1:2 to 1:1) to yield the pure product (3.73 g, 15.9 mmol, 88%) as a bright orange solid.

GC-MS (EI), *m/z* (% relative intensity, ion): 235.1 (56.6, [M]⁺), 136.8 (97.2, [M - C₇H₁₅]⁺), 120.7 (99.8, [M - C₇H₁₅O]⁺).

HRMS (ESI): [M + H]⁺ calcd for C₁₄H₂₁NO₂: 236.1645; found: 236.1643.

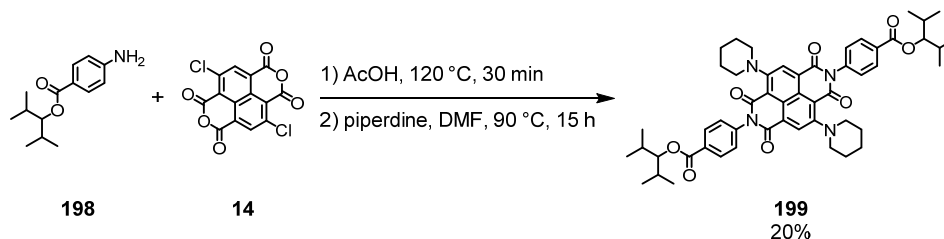
¹H-NMR (400 MHz, (CD₃)₂SO, δ): 7.71–7.60 (m, 2H), 6.63–6.52 (m, 2H), 5.93 (s, 2H, NH₂), 4.63 (t, ³J_{HH} = 6.1 Hz, 1H), 2.00–1.87 (m, 2H), 0.85 (dd, ³J_{HH} = 6.7 Hz, ⁴J_{HH} = 2.3 Hz, 9H).

¹³C-NMR (101 MHz, (CD₃)₂SO, δ): 165.9, 153.4, 131.0, 116.1, 112.7, 80.9, 19.5, 17.2.

TLC (SiO₂, cyclohexane/EtOAc 3:1, UV and ninhydrin): R_f = 0.18.

7.6.15 *N,N'*-Di-4'-(2',4'-dimethylpentan-3'-yl)benzoate-2,6-dipiperidinyl-1,4,5,8-naphthalenetetracarboxylic acid diimide (**199**)

Reaction Scheme



Experimental Procedure

198 (284 mg, 1.21 mmol, 4.0 equiv) and **14** (103 mg, 306 μmol , 1.0 equiv) were dissolved in AcOH (60 mL) and heated at 120 °C for 30 min. After cooling to room temperature, the solvent was removed under reduced pressure and the residue was dried under high vacuum. The residue (232 mg), piperidine (5.0 mL, 50.1 mmol), and dry DMF (10 mL) were added to a microwave vial. The vial was sealed and heated at 90 °C for 15 h. The solvent was evaporated under reduced pressure before the residue was dissolved in CH_2Cl_2 (100 mL) and aq. HCl (1 M, 40 mL). The organic layer was separated and the aqueous phase was extracted with CH_2Cl_2 (2 \times 50 mL). The combined organic layers were dried over MgSO_4 , filtered, and concentrated under reduced pressure. The residue was repeatedly purified by column chromatography (SiO_2 , cyclohexane/EtOAc 2:1) to isolate the pure product (54.0 mg, 62.1 μmol , 20% over two steps) as a blue solid.

HRMS (ESI): $[\text{M} + \text{H}]^+$ calcd for $\text{C}_{52}\text{H}_{60}\text{N}_4\text{O}_8$: 869.4484; found: 869.4489.

MS (MALDI-TOF), m/z : 868.4 ($[\text{M}]^-$).

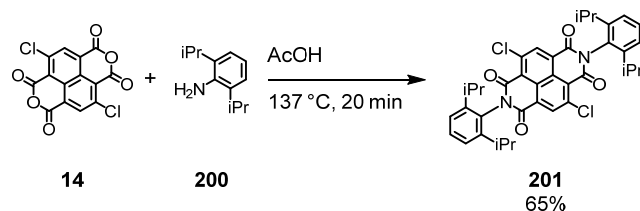
$^1\text{H-NMR}$ (400 MHz, CDCl_3 , δ): 8.50 (s, 2H), 8.28–8.24 (m, 4H), 7.42–7.37 (m, 4H), 4.89 (t, $^3J_{\text{HH}} = 6.1$ Hz, 2H), 3.39 (t, $^3J_{\text{HH}} = 5.1$ Hz, 8H), 1.83–1.60 (m, 16H), 0.99–0.96 (m, 24H).

TLC (SiO_2 , cyclohexane/EtOAc 2:1, UV): $R_f = 0.48$.

7.7 Miscellaneous Target Structures

7.7.1 *N,N'*-Di-(2',6'-diisopropylphenyl)-2,6-dichloronaphthalene-1,4,5,8-tetracarboxylic acid diimide (**201**)

Reaction Scheme



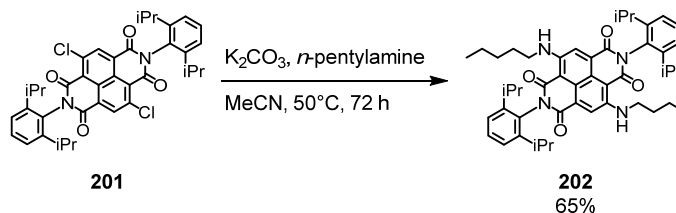
Experimental Procedure

To an oven-dried two-necked round-bottom flask were added **14** (873 mg, 2.59 mmol, 1.0 equiv) and AcOH (50 mL). The solution was stirred at 137 °C and 2,6-diisopropylaniline (**200**; 3.7 mL, 17.7 mmol, 6.8 equiv) was added in one portion. The resulting mixture was stirred at 137 °C for 20 min. After cooling to room temperature, the solvent was removed under reduced pressure and the residue was poured into MeOH (40 mL). The precipitated solid was filtered off, dried, and recrystallized from AcOH to obtain the pure product (1.10 g, 1.68 mmol, 65%, lit.^[325] 44%) as a pink solid.

¹H-NMR (400 MHz, CDCl₃, δ): 8.91 (s, 2H), 7.52 (t, ³J_{HH} = 7.8 Hz, 2H), 7.36 (d, ³J_{HH} = 7.8 Hz, 4H), 2.65 (hept, ³J_{HH} = 6.8 Hz, 4H), 1.17 (d, ³J_{HH} = 6.8 Hz, 24H).

¹³C-NMR (101 MHz, CDCl₃, δ): 161.2, 160.7, 145.5, 141.0, 136.6, 130.3, 129.8, 128.2, 126.4, 124.5, 122.9, 29.6, 24.1.

The characterization data are in agreement with the literature.^[325]

7.7.2 *N,N'*-Di-(2',6'-dipylphenyl)-2,6-di-*n*-pentylaminonaphthalene-1,4,5,8-tetracarboxylic acid diimide (202)Reaction SchemeExperimental Procedure

To an oven-dried two-necked round-bottom flask were added **201** (100 mg, 153 μmol , 1.0 equiv), K_2CO_3 (254 mg, 1.84 mmol, 12.0 equiv), and MeCN (10 mL). The solution was heated at 50 $^\circ\text{C}$ and *n*-pentylamine (213 μL , 1.84 mmol, 12.0 equiv) was added in one portion. The resulting mixture was stirred at 50 $^\circ\text{C}$ for 72 h before the solvent was removed under reduced pressure, and the residue was twice purified by column chromatography (SiO_2 , CH_2Cl_2) to yield the pure product (80.1 mg, 106 μmol , 69%) as a blue solid.

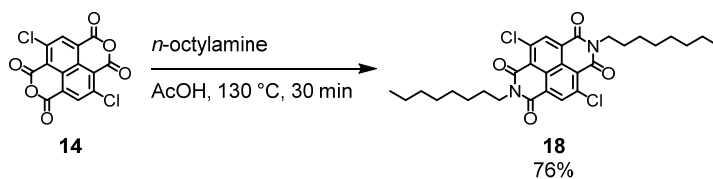
$^1\text{H-NMR}$ (400 MHz, CDCl_3 , δ): 9.38 (t, $^3J_{\text{HH}} = 5.1$ Hz, 2H), 8.30 (s, 2H), 7.53 (t, $^3J_{\text{HH}} = 7.8$ Hz, 2H), 7.38 (d, $^3J_{\text{HH}} = 7.7$ Hz, 4H), 3.53 (q, $^3J_{\text{HH}} = 7.0$ Hz, 4H), 2.74 (hept, $^3J_{\text{HH}} = 6.6$ Hz, 4H), 1.77 (p, $^3J_{\text{HH}} = 7.0$ Hz, 4H), 1.46–1.35 (m, 8H), 1.22–1.16 (m, 24H), 0.91 (t, $^3J_{\text{HH}} = 7.1$ Hz, 6H).

$^{13}\text{C-NMR}$ (101 MHz, CDCl_3 , δ): 166.6, 163.2, 149.8, 145.7, 130.9, 129.8, 126.4, 124.2, 122.2, 119.3, 101.9, 43.4, 29.3, 29.3, 29.0, 24.1, 24.0, 22.5, 14.1.

TLC (SiO_2 , CH_2Cl_2): $R_f = 0.69$.

7.7.3 *N,N'*-Di-*n*-octyl-2,6-dichloro-1,4,5,8-naphthalenetetracarboxylic acid diimide (18)

Reaction Scheme



Experimental Procedure

To an oven-dried flask were added **14** (1.01 g, 2.98 mmol, 1.0 equiv), 1-aminooctane (**17**; 2.5 mL, 15.1 mmol, 5.1 equiv), and AcOH (30 mL). The solution was stirred at 130 °C for 30 min and cooled to room temperature. The solvent was removed under reduced pressure and the residue was poured into MeOH (20 mL). The precipitate was dried over MgSO₄, filtered, and recrystallized from AcOH to afford the pure product (1.27 g, 2.27 mmol, 76%, lit.^[55] 70%) as a yellow solid.

MS (MALDI-TOF), m/z : 558.5 ($[M]^-$).

¹H-NMR (400 MHz, CDCl₃, δ): 8.78 (s, 2H), 4.52–4.00 (m, 4H), 1.76–1.70 (m, 4H), 1.45–1.27 (m, 20H), 0.89–0.86 (m, 6H).

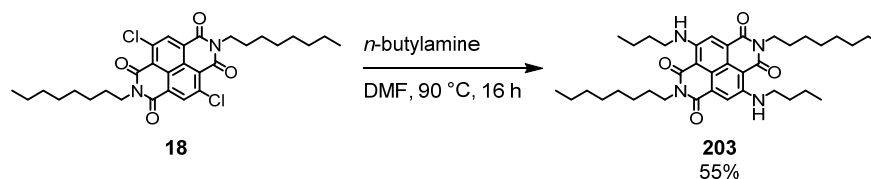
¹³C-NMR (101 MHz, CDCl₃, δ): 161.0, 160.7, 140.2, 136.1, 126.1, 122.5, 41.6, 31.9, 29.4, 29.3, 28.1, 27.2, 22.8, 14.2.

TLC (SiO₂, CH₂Cl₂): R_f = 0.44.

The characterization data are in agreement with the literature.^[55]

7.7.4 *N,N'*-Di-*n*-octyl-2,6-di-*n*-butylamino-1,4,5,8-naphthalenetetracarboxylic acid diimide (**203**)

Reaction Scheme



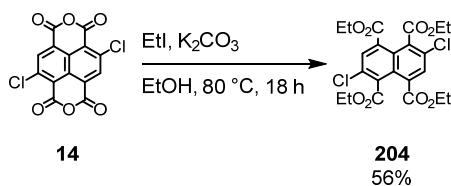
Experimental Procedure

To an oven-dried flask were added **18** (335 mg, 599 μ mol, 1.0 equiv), butan-1-amine (1.50 mL, 15.2 mmol, 25.3 equiv), and dry DMF (25 mL). The resulting mixture was stirred at 90 °C for 16 h. After evaporation of the solvent under reduced pressure, the residue was purified by column chromatography (SiO_2 , CH_2Cl_2) to yield the pure product (210 mg, 332 μ mol, 55%) as a blue solid.

MS (MALDI-TOF), m/z : 632.6 ($[\text{M}]^-$).

$^1\text{H-NMR}$ (400 MHz, CDCl_3 , δ): 9.23 (s, 2H, NH), 8.08–7.83 (m, 2H), 4.21–4.01 (m, 4H), 3.51–3.37 (m, 4H), 1.79 (p, $^3J_{\text{HH}} = 7.4$ Hz, 4H), 1.74–1.63 (m, 4H), 1.55 (h, $^3J_{\text{HH}} = 7.5$ Hz, 4H), 1.45–1.23 (m, 20H), 1.03 (t, $^3J_{\text{HH}} = 7.3$ Hz, 6H), 0.94–0.83 (m, 6H).

$^{13}\text{C-NMR}$ (101 MHz, CDCl_3 , δ): 166.1, 162.9, 149.0, 125.5, 120.9, 118.1, 43.0, 40.6, 32.0, 31.6, 29.5, 29.4, 28.2, 27.4, 22.8, 20.5, 14.3, 14.0.

7.7.5 2,6-Dichloro-1,4,5,8-naphthalenetetracarboxylic acid tetraethyl ester (204)Reaction SchemeExperimental Procedure

14 (1.01 g, 2.99 mmol, 1.0 equiv), iodoethane (9.00 mL, 110 mmol, 36.9 equiv), K_2CO_3 (2.50 g, 17.9 mmol, 6.0 equiv), and EtOH (9.0 mL) were added to a round-bottom flask and the reaction mixture was stirred at 80 °C for 18 h. The solvents were evaporated under reduced pressure and the residue was dissolved in CH_2Cl_2 (70 mL) and H_2O (50 mL). The organic layer was separated and the aqueous layer was extracted with CH_2Cl_2 (3×30 mL). The combined organic layers were dried over Na_2SO_4 , filtered, and the solvent was removed under reduced pressure. The residue was purified by column chromatography (SiO_2 , EtOAc/hexane 1:6 to 1:4) to obtain the pure product (817 mg, 1.68 mmol, 56%) as a white solid.

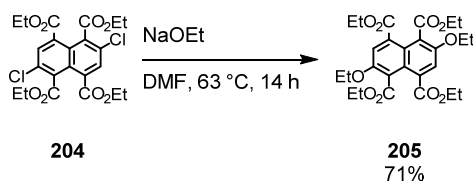
MS (MALDI-TOF), m/z : 484.1 ($[M]^-$).

1H -NMR (400 MHz, $CDCl_3$, δ): 7.94 (s, 2H), 4.42–4.36 (m, 8H), 1.42 (t, $^3J_{HH} = 7.2$ Hz, 12H).

^{13}C -NMR (101 MHz, $CDCl_3$, δ): 166.6, 165.7, 133.2, 132.5, 132.0, 132.0, 128.2, 62.5, 62.4, 14.2, 14.0.

TLC (SiO_2 , EtOAc/hexane 1:6): $R_f = 0.63$.

7.7.6 2,6-Diethoxy-1,4,5,8-naphthalenetetracarboxylic acid tetraethyl ester (205)

Reaction SchemeExperimental Procedure

204 (2.44 g, 34.1 mmol, 14.9 equiv) and sodium ethoxide (1.11 g, 2.29 mmol, 1.0 equiv) were dissolved in dry DMF (20 mL) and the resulting mixture was stirred at 63 °C for 14 h. The solvent was removed under reduced pressure and the residue was dissolved in H₂O (30 mL), CH₂Cl₂ (100 mL), and brine (30 mL). The organic layer was separated and the aqueous phase was extracted with CH₂Cl₂ (5 × 40 mL). The combined organic layers were washed with brine (50 mL), dried over Na₂SO₄, filtered, and the solvent was removed under reduced pressure. The residue was purified by column chromatography (SiO₂, EtOAc/hexane 1:3 to 1:2 to 1:1) to afford the pure product (824 mg, 1.63 mmol, 71%) as a yellow solid.

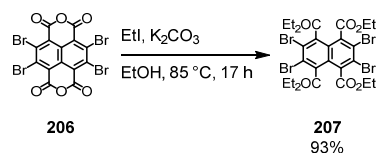
MS (MALDI-TOF), m/z : 504.2 ([M]⁻).

¹H-NMR (500 MHz, CDCl₃, δ): 7.65 (s, 2H), 4.38–4.33 (m, 8H), 4.26–4.17 (m, 4H), 1.43 (t, ³J_{HH} = 7.0 Hz, 6H), 1.38 (t, ³J_{HH} = 7.1 Hz, 12H).

¹³C-NMR (126 MHz, CDCl₃, δ): 167.9, 166.9, 153.4, 133.2, 125.1, 120.5, 119.5, 66.2, 61.9, 61.4, 15.1, 14.3, 14.2.

TLC (SiO₂, cyclohexane/EtOAc 1:1, UV): R_f = 0.42.

The characterization data are in agreement with the literature.^[326]

7.7.7 2,3,6,7-Tetrabromo-1,4,5,8-naphthalenetetracarboxylic acid tetraethyl ester (207)Reaction SchemeExperimental Procedure

2,3,6,7-Tetrabromo-1,4,5,8-naphthalenetetracarboxylic acid dianhydride (**206**; 858 mg, 1.47 mmol, 1.0 equiv), iodoethane (8.50 mL, 106 mmol, 72.3 equiv), and K₂CO₃ (1.66 g, 12.0 mmol, 8.2 equiv) were dissolved in EtOH (8.5 mL). The reaction mixture was heated at 85 °C for 17 h. The solvent was removed under reduced pressure and the residue was dissolved in H₂O (50 mL) and CH₂Cl₂ (100 mL). The aqueous layer was separated and the organic layer was dried over Na₂SO₄, filtered, and concentrated under reduced pressure. The crude product was purified by column chromatography (SiO₂, CH₂Cl₂) to yield the pure product (1.00 g, 1.37 mmol, 93%) as a yellow solid.

MS (MALDI-TOF), *m/z*: 731.9 ([M]⁻).

¹H-NMR (400 MHz, CDCl₃, δ): 4.38 (q, ³*J*_{HH} = 7.2 Hz, 8H), 1.39 (t, ³*J*_{HH} = 7.2 Hz, 12H).

¹³C-NMR (101 MHz, CDCl₃, δ): 165.8, 135.2, 125.8, 125.1, 63.3, 13.7.

7.8 Solid State Structures

7.8.1 Structure Determination by X-ray Diffraction Analysis

The structure determination by X-ray diffraction analyses were performed in close collaboration with Dr. Markus Neuburger at the University of Basel. The molecular structures or ORTEP plots were created with the programs Diamond^[327] and Mercury.^[328]

Crystal data for **37**: formula $C_{54}H_{54}N_2O_4S_2$, $M = 859.17$, $F(000) = 912$, orange plate, size $0.020 \cdot 0.070 \cdot 0.220 \text{ mm}^3$, monoclinic, space group $P 2_1/n$, $Z = 2$, $a = 17.9255(11) \text{ \AA}$, $b = 6.1027(4) \text{ \AA}$, $c = 21.6330(13) \text{ \AA}$, $\alpha = 90^\circ$, $\beta = 106.335(4)^\circ$, $\gamma = 90^\circ$, $V = 2271.0(2) \text{ \AA}^3$, $D_{\text{calc.}} = 1.256 \text{ Mg} \cdot \text{m}^{-3}$. The crystal was measured on a Bruker Kappa Apex2^[329] diffractometer at 123 K using graphite-monochromated Cu K_α -radiation with $\lambda = 1.54178 \text{ \AA}$, $\Theta_{\text{max}} = 67.042^\circ$. Minimal/maximal transmission 0.90/0.97, $\mu = 1.444 \text{ mm}^{-1}$. The Apex2 suite has been used for data collection and integration. From a total of 15467 reflections, 3999 were independent (merging $r = 0.041$). From these, 2923 were considered as observed ($I > 2.0\sigma(I)$) and were used to refine 280 parameters. The structure was solved by Other methods using the program^[330] Superflip. Least-squares refinement against F was carried out on all non-hydrogen atoms using the program^[331] CRYSTALS. $R = 0.0398$ (observed data), $wR = 0.0634$ (all data), $GOF = 1.0424$. Minimal/maximal residual electron density = $-0.25/0.29 \text{ e} \text{ \AA}^{-3}$. Chebychev polynomial weights^[332] were used to complete the refinement. Plots were produced using CAMERON.

Crystal data for **84**: formula $C_{54}H_{50}N_2O_4S_2$, $M = 855.13$, $F(000) = 452$, yellow needle, size $0.020 \cdot 0.090 \cdot 0.220 \text{ mm}^3$, triclinic, space group $P -1$, $Z = 1$, $a = 7.3687(5) \text{ \AA}$, $b = 11.1564(8) \text{ \AA}$, $c = 13.3648(9) \text{ \AA}$, $\alpha = 79.770(4)^\circ$, $\beta = 89.723(5)^\circ$, $\gamma = 75.936(5)^\circ$, $V = 1047.97(13) \text{ \AA}^3$, $D_{\text{calc.}} = 1.355 \text{ Mg} \cdot \text{m}^{-3}$. The crystal was measured on a Bruker Kappa Apex2 diffractometer at 123 K using graphite-monochromated Cu K_α -radiation with $\lambda = 1.54178 \text{ \AA}$, $\Theta_{\text{max}} = 67.823^\circ$. Minimal/maximal transmission 0.87/0.97, $\mu = 1.564 \text{ mm}^{-1}$. The Apex2 suite has been used for data collection and integration. From a total of 13673 reflections, 3669 were independent (merging $r = 0.032$). From these, 3077 were considered as observed ($I > 2.0\sigma(I)$) and were used to refine 280 parameters. The structure was solved by Other methods using the program Superflip. Least-squares refinement against F was carried out on all non-hydrogen atoms using the program CRYSTALS. $R = 0.0510$ (observed data), $wR = 0.0852$ (all data), $GOF = 1.0583$. Minimal/maximal residual electron density = $-0.17/0.45 \text{ e} \text{ \AA}^{-3}$. Chebychev polynomial weights were used to complete the refinement. Plots were produced using CAMERON.

8 Appendix

8.1 Contributions

All molecules in this doctoral thesis except of 2,3,6,7-tetrabromo-1,4,5,8-naphthalenetetracarboxylic acid dianhydride (**206**) and 2,6-dichloronaphthalene-1,4,5,8-tetracarboxylic acid dianhydride (**14**), which were synthesized by Mathias Fischer at Karlsruhe Institute of Technology, were synthesized and characterized by Pascal Hess.

All transient-absorption spectra were recorded by Dr. Igor Pugliesi in the group of Prof. Dr. Eberhard Riedle at the Ludwig Maximilian University of Munich.

The described STM image was taken and analyzed by Katharina Scheil in the group of Prof. Dr. Richard Berndt at the Christian-Albrechts-Universität zu Kiel.

The conductance measurements in the squeezable break junction were performed and analyzed by Michal Vadai in the group of Dr. Yoram Selzer at the Tel Aviv University.

All NOESY experiments were recorded and subsequently analyzed by Kaspar Zimmermann in the group of PD. Dr. Daniel Häussinger at the University of Basel.

All 2D-NMR spectra were recorded by Heiko Gsellinger, Kaspar Zimmermann, or Pascal Hess and the signal assignment was conducted by Pascal Hess or Kaspar Zimmermann.

The ^1H -NMR studies of isomerization of **123** and **137** were performed with the help of PD Dr. Daniel Häussinger at the University of Basel.

X-ray diffraction analyses were performed by Dr. Markus Neuburger at the University of Basel.

All HR-ESI/MALDI-FTICR mass spectra were recorded by the mass spectrometry service at the ETH Zürich.

All HR-ESI-TOF mass spectra were recorded by Dr. Heinz Nadig at the University of Basel.

Elemental analyses were either measured by Werner Kirsch or by Sylvie Mittelheisser at the University of Basel.

All fluorescence quantum yields were determined by Dr. Jonas Schönle in the group of Prof. Dr. Edwin Constable at the University of Basel.

9 Literature

- [1] Vögtle, F. *Cyclophan-Chemie*; Teubner Studienbücher Chemie; Vieweg+Teubner Verlag: Wiesbaden, 1990.
- [2] Pellegrin, M. *Recl. Trav. Chim. Pays-Bas Belg.* **1899**, *18*, 457.
- [3] Brown, C. J.; Farthing, A. C. *Nature* **164**, 915.
- [4] Cram, D. J.; Steinberg, H. *J. Am. Chem. Soc.* **1951**, *73*, 5691.
- [5] Cram, D. J.; Cram, J. M. *Acc. Chem. Res.* **1971**, *4*, 204.
- [6] Burley, S. K.; Petsko, G. A. *Science* **1985**, *229*, 23.
- [7] Hunter, C. A.; Sanders, J. K. M. *J. Am. Chem. Soc.* **1990**, *112*, 5525.
- [8] Cozzi, F.; Cinquini, M.; Annuziata, R.; Siegel, J. S. *J. Am. Chem. Soc.* **1993**, *115*, 5330.
- [9] Cockroft, S. L.; Hunter, C. A.; Lawson, K. R.; Perkins, J.; Urch, C. J. *J. Am. Chem. Soc.* **2005**, *127*, 8594.
- [10] Sinnokrot, M. O.; Sherrill, C. D. *J. Phys. Chem. A* **2006**, *110*, 10656.
- [11] Tsuzuki, S.; Uchamaru, T.; Mikami, M. *J. Phys. Chem. A* **2006**, *110*, 2027.
- [12] Martinez, C. R.; Iverson, B. L. *Chem. Sci.* **2012**, *3*, 2191.
- [13] Garau, C.; Frontera, A.; Quiñonero, D.; Ballester, P.; Costa, A.; Deyà, P. M. *ChemPhysChem* **2003**, *4*, 1344.
- [14] Mareda, J.; Matile, S. *Chem. – Eur. J.* **2009**, *15*, 28.
- [15] Schottel, B. L.; Chifotides, H. T.; Dunbar, K. R. *Chem. Soc. Rev.* **2007**, *37*, 68.
- [16] Mascal, M.; Armstrong, A.; Bartberger, M. D. *J. Am. Chem. Soc.* **2002**, *124*, 6274.
- [17] Quiñonero, D.; Garau, C.; Rotger, C.; Frontera, A.; Ballester, P.; Costa, A.; Deyà, P. M. *Angew. Chem. Int. Ed.* **2002**, *41*, 3389.
- [18] McCurdy, A.; Jimenez, L.; Stauffer, D. A.; Dougherty, D. A. *J. Am. Chem. Soc.* **1992**, *114*, 10314.
- [19] Schirch, P. F. T.; Boekelheide, V. *J. Am. Chem. Soc.* **1979**, *101*, 3125.
- [20] Kawai, H.; Suzuki, T.; Ohkita, M.; Tsuji, T. *Chem. – Eur. J.* **2000**, *6*, 4177.
- [21] Haenel, M.; Staab, H. A. *Chem. Ber.* **1973**, *106*, 2203.
- [22] Sauer, M.; Staab, H. A. *Liebigs Ann. Chem.* **1984**, *1984*, 615.
- [23] Umemoto, T.; Satani, S.; Sakata, Y.; Misumi, S. *Tetrahedron Lett.* **1975**, *16*, 3159.
- [24] Mitchell, R. H.; Carruthers, R. J.; Zwinkels, J. C. M. *Tetrahedron Lett.* **1976**, *17*, 2585.
- [25] Irngartinger, H.; Kirrstetter, R. G. H.; Krieger, C.; Rodewald, H.; Staab, H. A. *Tetrahedron Lett.* **1977**, *18*, 1425.
- [26] Ziegler, K.; Eberle, H.; Ohlinger, H. *Justus Liebigs Ann. Chem.* **1933**, *504*, 94.
- [27] O’Sullivan, M. C.; Sprafke, J. K.; Kondratuk, D. V.; Rinfray, C.; Claridge, T. D. W.; Saywell, A.; Blunt, M. O.; O’Shea, J. N.; Beton, P. H.; Malfois, M.; Anderson, H. L. *Nature* **2011**, *469*, 72.

- [28] Sprafke, J. K.; Kondratuk, D. V.; Wykes, M.; Thompson, A. L.; Hoffmann, M.; Drevinskas, R.; Chen, W.-H.; Yong, C. K.; Kärnbratt, J.; Bullock, J. E.; Malfois, M.; Wasielewski, M. R.; Albinsson, B.; Herz, L. M.; Zigmantas, D.; Beljonne, D.; Anderson, H. L. *J. Am. Chem. Soc.* **2011**, *133*, 17262.
- [29] Liu, P.; Neuhaus, P.; Kondratuk, D. V.; Balaban, T. S.; Anderson, H. L. *Angew. Chem. Int. Ed.* **2014**, n/a.
- [30] Sprafke, J. K.; Odell, B.; Claridge, T. D. W.; Anderson, H. L. *Angew. Chem. Int. Ed.* **2011**, *50*, 5572.
- [31] Beves, J. E.; Campbell, C. J.; Leigh, D. A.; Pritchard, R. G. *Angew. Chem. Int. Ed.* **2013**, *52*, 6464.
- [32] Ayme, J.-F.; Beves, J. E.; Leigh, D. A.; McBurney, R. T.; Rissanen, K.; Schultz, D. *Nat. Chem.* **2012**, *4*, 15.
- [33] Ayme, J.-F.; Beves, J. E.; Leigh, D. A.; McBurney, R. T.; Rissanen, K.; Schultz, D. *J. Am. Chem. Soc.* **2012**, *134*, 9488.
- [34] Barran, P. E.; Cole, H. L.; Goldup, S. M.; Leigh, D. A.; McGonigal, P. R.; Symes, M. D.; Wu, J.; Zengerle, M. *Angew. Chem. Int. Ed.* **2011**, *50*, 12280.
- [35] Bravo, J. A.; Raymo, F. M.; Stoddart, J. F.; White, A. J. P.; Williams, D. J. *Eur. J. Org. Chem.* **1998**, *1998*, 2565.
- [36] Chichak, K. S.; Cantrill, S. J.; Pease, A. R.; Chiu, S.-H.; Cave, G. W. V.; Atwood, J. L.; Stoddart, J. F. *Science* **2004**, *304*, 1308.
- [37] Williams, A. R.; Northrop, B. H.; Chang, T.; Stoddart, J. F.; White, A. J. P.; Williams, D. *J. Angew. Chem. Int. Ed.* **2006**, *45*, 6665.
- [38] Dichtel, W. R.; Miljanić, O. Š.; Spruell, J. M.; Heath, J. R.; Stoddart, J. F. *J. Am. Chem. Soc.* **2006**, *128*, 10388.
- [39] Lozac'h, N.; Goodson, A. L.; Powell, W. H. *Angew. Chem. Int. Ed. Engl.* **1979**, *18*, 887.
- [40] Lozac'h, N.; Goodson, A. L. *Angew. Chem. Int. Ed. Engl.* **1984**, *23*, 33.
- [41] IUPAC Gold Book - energy transfer in photochemistry
<http://goldbook.iupac.org/E02116.html> (accessed Aug 5, 2014).
- [42] IUPAC Gold Book - charge-transfer (CT) transition <http://goldbook.iupac.org/C01008.html>
(accessed Aug 5, 2014).
- [43] Jaboski, A. *Nature* **1933**, *131*, 839.
- [44] Valeur, B.; Berberan-Santos, M. N. *Molecular Fluorescence: Principles and Applications*; John Wiley & Sons, 2013.
- [45] Basics about how LEDs work, how manufacturers characterize them, and how they are driven. | Components content from Electronic Design

- <http://electronicdesign.com/components/understanding-led-application-theory-and-practice> (accessed Jul 14, 2014).
- [46] Fukumura, H.; Irie, M.; Iwasawa, Y.; Masuhara, H.; Uosaki, K. *Molecular Nano Dynamics*; John Wiley & Sons, 2009.
- [47] Masuhara, H.; Kawata, S. *Nanophotonics: Integrating Photochemistry, Optics and Nano/Bio Materials Studies: Proceedings of the International Nanophotonics Symposium Handai, July 24-26th 2003, Suita Campus of Osaka University, Osaka, Japan*; Elsevier, 2004.
- [48] Megerle, U.; Pugliesi, I.; Schrieber, C.; Sailer, C. F.; Riedle, E. *Appl. Phys. B* **2009**, *96*, 215.
- [49] The Nobel Prize in Chemistry 1999
http://www.nobelprize.org/nobel_prizes/chemistry/laureates/1999/ (accessed Jul 30, 2014).
- [50] Corkum, P. B.; Krausz, F. *Nat. Phys.* **2007**, *3*, 381.
- [51] Förster, T. *Ann. Phys.* **1948**, *437*, 55.
- [52] Valeur, B. In *Molecular Fluorescence*; Wiley-VCH Verlag GmbH, 2001; pp. i – xiv.
- [53] Dexter, D. L. *J. Chem. Phys.* **1953**, *21*, 836.
- [54] Vollmann, H.; Becker, H.; Corell, M.; Streeck, H. *Justus Liebigs Ann. Chem.* **1937**, *531*, 1.
- [55] Thalacker, C.; Röger, C.; Würthner, F. *J. Org. Chem.* **2006**, *71*, 8098.
- [56] Würthner, F.; Ahmed, S.; Thalacker, C.; Debaerdemaeker, T. *Chem. – Eur. J.* **2002**, *8*, 4742.
- [57] Kishore, R. S. K.; Kel, O.; Banerji, N.; Emery, D.; Bollot, G.; Mareda, J.; Gomez-Casado, A.; Jonkheijm, P.; Huskens, J.; Maroni, P.; Borkovec, M.; Vauthey, E.; Sakai, N.; Matile, S. *J. Am. Chem. Soc.* **2009**, *131*, 11106.
- [58] Banerji, N.; Fürstenberg, A.; Bhosale, S.; Sisson, A. L.; Sakai, N.; Matile, S.; Vauthey, E. *J. Phys. Chem. B* **2008**, *112*, 8912.
- [59] Doria, F.; di Antonio, M.; Benotti, M.; Verga, D.; Freccero, M. *J. Org. Chem.* **2009**, *74*, 8616.
- [60] Thalacker, C.; Miura, A.; Feyter, S. D.; Schryver, F. C. D.; Würthner, F. *Org. Biomol. Chem.* **2005**, *3*, 414.
- [61] Cat, I. D.; Röger, C.; Lee, C. C.; Hoeben, F. J. M.; Pouderoijen, M. J.; Schenning, A. P. H. J.; Würthner, F.; Feyter, S. D. *Chem. Commun.* **2008**, 5496.
- [62] Jazwinski, J.; Blacker, A. J.; Lehn, J.-M.; Cesario, M.; Guilhem, J.; Pascard, C. *Tetrahedron Lett.* **1987**, *28*, 6060.
- [63] Dawson, R. E.; Hennig, A.; Weimann, D. P.; Emery, D.; Ravikumar, V.; Montenegro, J.; Takeuchi, T.; Gabutti, S.; Mayor, M.; Mareda, J.; Schalley, C. A.; Matile, S. *Nat. Chem.* **2010**, *2*, 533.
- [64] Miller, L. L.; Mann, K. R. *Acc. Chem. Res.* **1996**, *29*, 417.

- [65] Katz, H. E.; Lovinger, A. J.; Johnson, J.; Kloc, C.; Siegrist, T.; Li, W.; Lin, Y.-Y.; Dodabalapur, A. *Nature* **2000**, *404*, 478.
- [66] Röger, C.; Müller, M. G.; Lysetska, M.; Miloslavina, Y.; Holzwarth, A. R.; Würthner, F. *J. Am. Chem. Soc.* **2006**, *128*, 6542.
- [67] Röger, C.; Miloslavina, Y.; Brunner, D.; Holzwarth, A. R.; Würthner, F. *J. Am. Chem. Soc.* **2008**, *130*, 5929.
- [68] Bhosale, S. *Science* **2006**, *313*, 84.
- [69] Buncel, E.; Mailloux, N. L.; Brown, R. S.; Kazmaier, P. M.; Dust, J. *Tetrahedron Lett.* **2001**, *42*, 3559.
- [70] Hamilton, D. G.; Feeder, N.; Teat, S. J.; Sanders, J. K. M. *New J. Chem.* **1998**, *22*, 1019.
- [71] Hansen, J. G.; Feeder, N.; Hamilton, D. G.; Gunter, M. J.; Becher, J.; Sanders, J. K. M. *Org. Lett.* **2000**, *2*, 449.
- [72] Fallon, G. D.; Lee, M. A.-P.; Langford, S. J.; Nichols, P. J. *Org. Lett.* **2004**, *6*, 655.
- [73] Bruns, C. J.; Li, J.; Frascioni, M.; Schneebeli, S. T.; Iehl, J.; Jacquot de Rouville, H.-P.; Stupp, S. I.; Voth, G. A.; Stoddart, J. F. *Angew. Chem. Int. Ed.* **2014**, *53*, 1953.
- [74] Avestro, A.-J.; Gardner, D. M.; Vermeulen, N. A.; Wilson, E. A.; Schneebeli, S. T.; Whalley, A. C.; Belowich, M. E.; Carmieli, R.; Wasielewski, M. R.; Stoddart, J. F. *Angew. Chem. Int. Ed.* **2014**, *53*, 4442.
- [75] Gabutti, S.; Schaffner, S.; Neuburger, M.; Fischer, M.; Schäfer, G.; Mayor, M. *Org. Biomol. Chem.* **2009**, *7*, 3222.
- [76] Gabutti, S. An investigation of naphthalenediimides as central building blocks in model compounds for scanning tunneling microscope induced light emission experiments and förster resonance energy transfer studies, Basel: Basel, 2010.
- [77] Pugliesi, I.; Krok, P.; Lochbrunner, S.; Błaszczuk, A.; von Hänisch, C.; Mayor, M.; Riedle, E. *J. Phys. Chem. A* **2010**, *114*, 12555.
- [78] Pugliesi, I.; Megerle, U.; Suraru, S.-L.; Würthner, F.; Riedle, E.; Lochbrunner, S. *Chem. Phys. Lett.* **2011**, *504*, 24.
- [79] Shiratori, H.; Ohno, T.; Nozaki, K.; Yamazaki, I.; Nishimura, Y.; Osuka, A. *J. Org. Chem.* **2000**, *65*, 8747.
- [80] Debreczeny, M. P.; Svec, W. A.; Wasielewski, M. R. *Science* **1996**, *274*, 584.
- [81] Ganesan, P.; Baggerman, J.; Zhang, H.; Sudhölter, E. J. R.; Zuilhof, H. *J. Phys. Chem. A* **2007**, *111*, 6151.
- [82] Chaignon, F.; Buchet, F.; Blart, E.; Falkenström, M.; Hammarström, L.; Odobel, F. *New J. Chem.* **2009**, *33*, 408.
- [83] Morton, J. J. L.; McCamey, D. R.; Eriksson, M. A.; Lyon, S. A. *Nature* **2011**, *479*, 345.
- [84] Moore, G. E. *IEEE Solid-State Circuits Soc. Newsl.* **2006**, *11*, 33.

- [85] 26, S. A. on J.; Am, 2013 at 9:54. 7nm, 5nm, 3nm: The new materials and transistors that will take us to the limits of Moore's law <http://www.extremetech.com/computing/162376-7nm-5nm-3nm-the-new-materials-and-transistors-that-will-take-us-to-the-limits-of-moores-law> (accessed Jul 15, 2014).
- [86] Binnig, G.; Rohrer, H. *IBM J Res Dev* **1986**, *30*, 355.
- [87] Press Release: The 1986 Nobel Prize in Physics http://www.nobelprize.org/nobel_prizes/physics/laureates/1986/press.html (accessed Jul 15, 2014).
- [88] Bowker, M.; Davies, P. R. *Scanning Tunneling Microscopy in Surface Science*; 1 edition.; Wiley-VCH: Weinheim, 2010.
- [89] Wolf, E. L. *Principles of Electron Tunneling Spectroscopy: Second Edition*; Oxford University Press, 2012.
- [90] Binnig, G. K. Atomic force microscope and method for imaging surfaces with atomic resolution. US4724318 A, February 9, 1988.
- [91] Haugstad, G. *Atomic Force Microscopy: Understanding Basic Modes and Advanced Applications*; John Wiley & Sons, 2012.
- [92] Petty, M. C. *Molecular Electronics: From Principles to Practice*; John Wiley & Sons, 2007.
- [93] ...: Universidad De Colima ... Laboratorio de Microscopía <http://fejer.ucol.mx/meb/galeria.php> (accessed Jul 17, 2014).
- [94] Moreland, J.; Ekin, J. W. *J. Appl. Phys.* **1985**, *58*, 3888.
- [95] Muller, C. J.; van Ruitenbeek, J. M.; de Jongh, L. J. *Phys. Rev. Lett.* **1992**, *69*, 140.
- [96] Brunner, J. G. Gaining microscopic insight into molecular junctions by transport experiments, Basel: Basel, 2013.
- [97] Turanský, R.; Konôpka, M.; Doltsinis, N. L.; Štich, I.; Marx, D. *Phys. Chem. Chem. Phys.* **2010**, *12*, 13922.
- [98] Van Wees, B. J.; van Houten, H.; Beenakker, C. W. J.; Williamson, J. G.; Kouwenhoven, L. P.; van der Marel, D.; Foxon, C. T. *Phys. Rev. Lett.* **1988**, *60*, 848.
- [99] Wharam, D. A.; Thornton, T. J.; Newbury, R.; Pepper, M.; Ahmed, H.; Frost, J. E. F.; Hasko, D. G.; Peacock, D. C.; Ritchie, D. A.; Jones, G. a. C. *J. Phys. C Solid State Phys.* **1988**, *21*, L209.
- [100] Wu, S. Electrical conductance of single conjugated oligomers, Basel: Basel, 2010.
- [101] Moreland, J.; Alexander, S.; Cox, M.; Sonnenfeld, R.; Hansma, P. K. *Appl. Phys. Lett.* **1983**, *43*, 387.
- [102] Vadai, M.; Nachman, N.; Ben-Zion, M.; Bürkle, M.; Pauly, F.; Cuevas, J. C.; Selzer, Y. *J. Phys. Chem. Lett.* **2013**, *4*, 2811.
- [103] Tang, Y.; Zeng, X.; Liang, J. *J. Chem. Educ.* **2010**, *87*, 742.

- [104] Raether, H. *Surface Plasmons on Smooth and Rough Surfaces and on Gratings*; Springer Berlin Heidelberg, 2013.
- [105] Sarid, D.; Challener, W. *Modern Introduction to Surface Plasmons: Theory, Mathematical Modeling, and Applications*; Cambridge University Press, 2010.
- [106] Nitzan, A.; Ratner, M. A. *Science* **2003**, *300*, 1384.
- [107] Yokota, K.; Taniguchi, M.; Kawai, T. *J. Am. Chem. Soc.* **2007**, *129*, 5818.
- [108] Jia, C.; Guo, X. *Chem. Soc. Rev.* **2013**, *42*, 5642.
- [109] Nielsen, M. B. *Organic Synthesis and Molecular Engineering*; John Wiley & Sons, 2013.
- [110] Bain, C. D.; Whitesides, G. M. *Angew. Chem. Int. Ed. Engl.* **1989**, *28*, 506.
- [111] Chen, F.; Li, X.; Hihath, J.; Huang, Z.; Tao, N. *J. Am. Chem. Soc.* **2006**, *128*, 15874.
- [112] Frei, M.; Aradhya, S. V.; Hybertsen, M. S.; Venkataraman, L. *J. Am. Chem. Soc.* **2012**, *134*, 4003.
- [113] McCreery, R. L.; Bergren, A. J. *Adv. Mater.* **2009**, *21*, 4303.
- [114] Hong, W.; Manrique, D. Z.; Moreno-García, P.; Gulcur, M.; Mishchenko, A.; Lambert, C. J.; Bryce, M. R.; Wandlowski, T. *J. Am. Chem. Soc.* **2012**, *134*, 2292.
- [115] Bagrets, A.; Arnold, A.; Evers, F. *J. Am. Chem. Soc.* **2008**, *130*, 9013.
- [116] Mishchenko, A.; Zotti, L. A.; Vonlanthen, D.; Bürkle, M.; Pauly, F.; Cuevas, J. C.; Mayor, M.; Wandlowski, T. *J. Am. Chem. Soc.* **2011**, *133*, 184.
- [117] Jones, D. R.; Troisi, A. *J. Phys. Chem. C* **2007**, *111*, 14567.
- [118] Pauly, F.; Viljas, J. K.; Cuevas, J. C.; Schön, G. *Phys. Rev. B* **2008**, *77*, 155312.
- [119] Dell'Angela, M.; Kladnik, G.; Cossaro, A.; Verdini, A.; Kamenetska, M.; Tamblyn, I.; Quek, S. Y.; Neaton, J. B.; Cvetko, D.; Morgante, A.; Venkataraman, L. *Nano Lett.* **2010**, *10*, 2470.
- [120] Chen, F.; Tao, N. J. *Acc. Chem. Res.* **2009**, *42*, 429.
- [121] Salomon, A.; Cahen, D.; Lindsay, S.; Tomfohr, J.; Engelkes, V. b.; Frisbie, C. d. *Adv. Mater.* **2003**, *15*, 1881.
- [122] Kaliginedi, V.; Moreno-García, P.; Valkenier, H.; Hong, W.; García-Suárez, V. M.; Buitter, P.; Otten, J. L. H.; Hummelen, J. C.; Lambert, C. J.; Wandlowski, T. *J. Am. Chem. Soc.* **2012**, *134*, 5262.
- [123] Mayor, M.; Weber, H. B.; Reichert, J.; Elbing, M.; von Hänisch, C.; Beckmann, D.; Fischer, M. *Angew. Chem. Int. Ed.* **2003**, *42*, 5834.
- [124] Venkataraman, L.; Klare, J. E.; Nuckolls, C.; Hybertsen, M. S.; Steigerwald, M. L. *Nature* **2006**, *442*, 904.
- [125] Vonlanthen, D.; Mishchenko, A.; Elbing, M.; Neuburger, M.; Wandlowski, T.; Mayor, M. *Angew. Chem. Int. Ed.* **2009**, *48*, 8886.
- [126] Desvergne, J.-P.; Bouas-Laurent, H. *J. Chem. Soc. Chem. Commun.* **1978**, 403.

- [127] Bouas-Laurent, H.; Castellan, A.; Desvergne, J.-P. *Pure Appl. Chem.* **1980**, *52*.
- [128] Yamashita, I.; Fujii, M.; Kaneda, T.; Misumi, S.; Otsubo, T. *Tetrahedron Lett.* **1980**, *21*, 541.
- [129] Shinkai, S.; Nakaji, T.; Nishida, Y.; Ogawa, T.; Manabe, O. *J. Am. Chem. Soc.* **1980**, *102*, 5860.
- [130] Shinkai, S.; Nakaji, T.; Ogawa, T.; Shigematsu, K.; Manabe, O. *J. Am. Chem. Soc.* **1981**, *103*, 111.
- [131] Green, J. E.; Wook Choi, J.; Boukai, A.; Bunimovich, Y.; Johnston-Halperin, E.; DeIonno, E.; Luo, Y.; Sheriff, B. A.; Xu, K.; Shik Shin, Y.; Tseng, H.-R.; Stoddart, J. F.; Heath, J. R. *Nature* **2007**, *445*, 414.
- [132] Vögtle, F.; Müller, W. M.; Müller, U.; Bauer, M.; Rissanen, K. *Angew. Chem. Int. Ed. Engl.* **1993**, *32*, 1295.
- [133] Bissell, R. A.; Córdova, E.; Kaifer, A. E.; Stoddart, J. F. *Nature* **1994**, *369*, 133.
- [134] Soares, B. F.; MacDonald, K. F.; Fedotov, V. A.; Zheludev, N. I. *Nano Lett.* **2005**, *5*, 2104.
- [135] Auwärter, W.; Seufert, K.; Bischoff, F.; Ecija, D.; Vijayaraghavan, S.; Joshi, S.; Klappenberger, F.; Samudrala, N.; Barth, J. V. *Nat. Nanotechnol.* **2011**, *7*, 41.
- [136] Worm, A. T.; Brewster, J. H. *J. Org. Chem.* **1970**, *35*, 1715.
- [137] trans-Stilbene 96% | Sigma-Aldrich
<http://www.sigmaaldrich.com/catalog/product/aldrich/139939?lang=de®ion=CH> (accessed Jul 16 2014).
- [138] Likhtenshtein, G. I. *Stilbenes: Applications in Chemistry, Life Sciences and Materials Science*; Wiley, 2010.
- [139] Märcker. *Justus Liebigs Ann. Chem.* **1865**, *136*, 88.
- [140] Straus. *Justus Liebigs Ann. Chem.* **1905**, *342*, 257.
- [141] Strömer. *Chem. Ber.* **1909**, *42*, 4866.
- [142] trans-Stilbene UV-Vis <http://omlc.org/spectra/PhotochemCAD/html/110.html> (accessed Jul 16, 2014).
- [143] cis-Stilbene UV-Vis <http://omlc.org/spectra/PhotochemCAD/html/163.html> (accessed Jul 16, 2014).
- [144] Repinec, S. T.; Sension, R. J.; Szarka, A. Z.; Hochstrasser, R. M. *J. Phys. Chem.* **1991**, *95*, 10380.
- [145] Bansal. *Organic Reaction Mechanisms*; Tata McGraw-Hill Education, 1998.
- [146] Saltiel, J.; Klima, R. F. *Photochem. Photobiol.* **2006**, *82*, 38.
- [147] Maeda, H.; Nishimura, K.; Mizuno, K.; Yamaji, M.; Oshima, J.; Tobita, S. *J. Org. Chem.* **2005**, *70*, 9693.
- [148] Imai, M.; Arai, T. *Tetrahedron Lett.* **2002**, *43*, 5265.

- [149] Waldeck, D. H. *Chem. Rev.* **1991**, *91*, 415.
- [150] Liu, R. S. H.; Hammond, G. S. *Proc. Natl. Acad. Sci.* **2000**, *97*, 11153.
- [151] Imamoto, Y.; Kuroda, T.; Kataoka, M.; Shevyakov, S.; Krishnamoorthy, G.; Liu, R. S. H. *Angew. Chem. Int. Ed.* **2003**, *42*, 3630.
- [152] Jung, Y. O.; Lee, J. H.; Kim, J.; Schmidt, M.; Moffat, K.; Šrajer, V.; Ihse, H. *Nat. Chem.* **2013**, *5*, 212.
- [153] Tamai, N.; Miyasaka, H. *Chem. Rev.* **2000**, *100*, 1875.
- [154] Fuß, W.; Kosmidis, C.; Schmid, W. E.; Trushin, S. A. *Angew. Chem. Int. Ed.* **2004**, *43*, 4178.
- [155] IUPAC Gold Book - one-bond-flip <http://goldbook.iupac.org/OT07432.html> (accessed Jul 17, 2014).
- [156] Mulliken, R. S.; Roothaan, C. C. J. *Chem. Rev.* **1947**, *41*, 219.
- [157] Liu, R. S.; Asato, A. E. *Proc. Natl. Acad. Sci.* **1985**, *82*, 259.
- [158] IUPAC Gold Book - hula-twist (HT) mechanism <http://goldbook.iupac.org/HT07393.html> (accessed Jul 17, 2014).
- [159] IUPAC Gold Book - bicycle-pedal (BP) mechanism <http://goldbook.iupac.org/BT07330.html> (accessed Jul 17, 2014).
- [160] Seltzer, S. *J. Am. Chem. Soc.* **1987**, *109*, 1627.
- [161] Warshel, A. *Nature* **1976**, *260*, 679.
- [162] Tapavicza, E.; Meyer, A. M.; Furche, F. *Phys. Chem. Chem. Phys.* **2011**, *13*, 20986.
- [163] Wang, Z.; Yin, G.; Qin, J.; Gao, M.; Cao, L.; Wu, A. *Synthesis* **2008**, *2008*, 3675.
- [164] Barton, D. H. R.; Willis, B. J. *J. Chem. Soc. Chem. Commun.* **1970**, 1225.
- [165] Kellogg, R. M.; Wassenaar, S. *Tetrahedron Lett.* **1970**, *11*, 1987.
- [166] Wiel, M. K. J. ter; Vicario, J.; Davey, S. G.; Meetsma, A.; Feringa, B. L. *Org. Biomol. Chem.* **2005**, *3*, 28.
- [167] Fu, G. C.; Nguyen, S. T.; Grubbs, R. H. *J. Am. Chem. Soc.* **1993**, *115*, 9856.
- [168] Heck, R. F.; Nolley, J. P. *J. Org. Chem.* **1972**, *37*, 2320.
- [169] Mizoroki, T.; Mori, K.; Ozaki, A. *Bull. Chem. Soc. Jpn.* **1971**, *44*, 581.
- [170] Kantam, M. L.; Srinivas, P.; Yadav, J.; Likhar, P. R.; Bhargava, S. *J. Org. Chem.* **2009**, *74*, 4882.
- [171] Stille, J. K. *Angew. Chem. Int. Ed. Engl.* **1986**, *25*, 508.
- [172] Gallagher, W. P.; Maleczka, R. E. *J. Org. Chem.* **2005**, *70*, 841.
- [173] McMurry, J. E.; Fleming, M. P. *J. Am. Chem. Soc.* **1974**, *96*, 4708.
- [174] Perkin, W. H. *J. Chem. Soc.* **1868**, *21*, 181.
- [175] Sinha, A. K.; Kumar, V.; Sharma, A.; Sharma, A.; Kumar, R. *Tetrahedron* **2007**, *63*, 11070.
- [176] Lindlar, H. *Helv. Chim. Acta* **1952**, *35*, 446.

- [177] Wittig, G.; Schöllkopf, U. *Chem. Ber.* **1954**, *87*, 1318.
- [178] Tanner, D.; Wennerström, O. *Tetrahedron Lett.* **1981**, *22*, 2313.
- [179] Horner, L.; Hoffmann, H.; Wippel, H. G. *Chem. Ber.* **1958**, *91*, 61.
- [180] Wadsworth, W. S.; Emmons, W. D. *J. Am. Chem. Soc.* **1961**, *83*, 1733.
- [181] Ianni, A.; Waldvogel, S. *Synthesis* **2006**, *2006*, 2103.
- [182] Anger, I.; Sandros, K.; Sundahl, M.; Wennerstroem, O. *J. Phys. Chem.* **1993**, *97*, 1920.
- [183] Sundahl, M.; Wennerström, O.; Raston, I.; Norinder, U.; Wittman, G.; Gera, L.; Bartók, M.; Pelczer, I.; Dombi, G. *Acta Chem. Scand.* **1988**, *42b*, 367.
- [184] Raston, I.; Wennerström, O.; Strömberg, S.; Norin, T.; Hjeds, H. *Acta Chem. Scand.* **1982**, *36b*, 655.
- [185] Norinder, U.; Tanner, D.; Wennerström, O. *Tetrahedron Lett.* **1983**, *24*, 5411.
- [186] Thulin, B.; Wennerström, O.; Somfai, I.; Sandström, J.; Enzell, C. R.; Berg, J.-E.; Pilotti, A.-M. *Acta Chem. Scand.* **1978**, *32b*, 109.
- [187] Tanner, D.; Wennerström, O.; Chattopadhyaya, J.; Carlberg, G. E.; Sterner, O.; Wickberg, B. *Acta Chem. Scand.* **1983**, *37b*, 693.
- [188] Tanner, D.; Thulin, B.; Wennerström, O.; Enzell, C. R.; Åkeson, Å.; Lundquist, G. *Acta Chem. Scand.* **1979**, *33b*, 443.
- [189] Thulin, B.; Wennerström, O.; Jie-Cheng, X.; Björkroth, U.; Yi-An, L.; Yin-Zeng, L. *Acta Chem. Scand.* **1983**, *37b*, 297.
- [190] Mateo, C.; Pérez-Melero, C.; Peláez, R.; Medarde, M. *J. Org. Chem.* **2005**, *70*, 6544.
- [191] Darabi, H. R.; Darestani Farahani, A.; Hashemi Karouei, M.; Aghapoor, K.; Firouzi, R.; Herges, R.; Mohebbi, A. R.; Näther, C. *Supramol. Chem.* **2012**, *24*, 653.
- [192] Rojanathanes, R.; Tuntulani, T.; Bhanthumnavin, W.; Sukwattanasinitt, M. *Org. Lett.* **2005**, *7*, 3401.
- [193] Reuter, R.; Wegner, H. A. *Chem. Commun.* **2011**, *47*, 12267.
- [194] IUPAC Gold Book - azo compounds <http://goldbook.iupac.org/A00560.html> (accessed Jul 17, 2014).
- [195] Zollinger, H. *Color Chemistry: Syntheses, Properties, and Applications of Organic Dyes and Pigments*; Wiley, 2003.
- [196] Hunger, K. *Industrial Dyes: Chemistry, Properties, Applications*; John Wiley & Sons, 2007.
- [197] Mitscherlich, E. *Ann. Pharm.* **1834**, *12*, 311.
- [198] Hartley, G. S. *Nature* **1937**, *140*, 281.
- [199] Robertson, J. M. *J. Chem. Soc. Resumed* **1939**, 232.
- [200] De Maria, P.; Fontana, A.; Gasbarri, C.; Siani, G.; Zanirato, P. *Arkiv* **2009**, *8*, 16.
- [201] Brown, E. V.; Granneman, G. R. *J. Am. Chem. Soc.* **1975**, *97*, 621.
- [202] Kumar, G. S.; Neckers, D. C. *Chem. Rev.* **1989**, *89*, 1915.

- [203] Rabek, J. F.; Scott, G. W. *Photochemistry and Photophysics*; CRC Press, 1989.
- [204] Sekkat, Z.; Knoll, W. *Photoreactive Organic Thin Films*; Academic Press, 2002.
- [205] Rau, H. *Angew. Chem. Int. Ed. Engl.* **1973**, *12*, 224.
- [206] Bandara, H. M. D.; Burdette, S. C. *Chem. Soc. Rev.* **2012**, *41*, 1809.
- [207] Chang, C.-W.; Lu, Y.-C.; Wang, T.-T.; Diao, E. W.-G. *J. Am. Chem. Soc.* **2004**, *126*, 10109.
- [208] Shin, D. M.; Whitten, D. G. *J. Am. Chem. Soc.* **1988**, *110*, 5206.
- [209] Marcandalli, B.; Liddo, L. P.-D.; Fede, C. D.; Bellobono, I. R. *J. Chem. Soc. Perkin Trans. 2* **1984**, 589.
- [210] Nishimura, N.; Tanaka, T.; Asano, M.; Sueishi, Y. *J. Chem. Soc. Perkin Trans. 2* **1986**, 1839.
- [211] Rau, H.; Lueddecke, E. *J. Am. Chem. Soc.* **1982**, *104*, 1616.
- [212] Crecca, C. R.; Roitberg, A. E. *J. Phys. Chem. A* **2006**, *110*, 8188.
- [213] Kessler, H.; Leibfritz, D. *Tetrahedron Lett.* **1970**, *11*, 1423.
- [214] Tamaoki, N.; Ogata, K.; Koseki, K.; Yamaoka, T. *Tetrahedron* **1990**, *46*, 5931.
- [215] Wei-Guang Diao, E. *J. Phys. Chem. A* **2004**, *108*, 950.
- [216] Merino, E. *Chem. Soc. Rev.* **2011**, *40*, 3835.
- [217] Angeli; Valori. *Atti Accad Lincei* **1913**, *22*, 132.
- [218] Haselbach, E. *Helv. Chim. Acta* **1970**, *53*, 1526.
- [219] Velema, W. A.; van der Toorn, M.; Szymanski, W.; Feringa, B. L. *J. Med. Chem.* **2013**, *56*, 4456.
- [220] Norikane, Y.; Tamaoki, N. *Org. Lett.* **2004**, *6*, 2595.
- [221] Reuter, R.; Wegner, H. A. *Chem. – Eur. J.* **2011**, *17*, 2987.
- [222] Gattermann, L.; Rüdtt, H. *Berichte Dtsch. Chem. Ges.* **1894**, *27*, 2293.
- [223] Müri, M.; Schuermann, K. C.; De Cola, L.; Mayor, M. *Eur. J. Org. Chem.* **2009**, *2009*, 2562.
- [224] Bigelow, H. E.; Robinson, D. B. *Org Synth* **1942**, *22*, 28.
- [225] Opolonick, N. *Ind. Eng. Chem.* **1935**, *27*, 1045.
- [226] Lim, Y.-K.; Lee, K.-S.; Cho, C.-G. *Org. Lett.* **2003**, *5*, 979.
- [227] Kang, H.-M.; Jung, J.-W.; Cho, C.-G. *J. Org. Chem.* **2007**, *72*, 679.
- [228] Wang, Z.; Skerlj, R. T.; Bridger, G. J. *Tetrahedron Lett.* **1999**, *40*, 3543.
- [229] Tanaka, K.; Fukuoka, S.; Miyanishi, H.; Takahashi, H. *Tetrahedron Lett.* **2010**, *51*, 2693.
- [230] Becker, K.; Lagoudakis, P. G.; Gaefke, G.; Höger, S.; Lupton, J. M. *Angew. Chem.* **2007**, *119*, 3520.
- [231] Becker, K.; Lagoudakis, P. G.; Gaefke, G.; Höger, S.; Lupton, J. M. *Angew. Chem. Int. Ed.* **2007**, *46*, 3450.

- [232] Gleiter, R.; Hopf, H. *Modern Cyclophane Chemistry*; John Wiley & Sons, 2006.
- [233] Ramaiah, D.; Neelakandan, P. P.; Nair, A. K.; Avirah, R. R. *Chem. Soc. Rev.* **2010**, *39*, 4158.
- [234] Griffiths, J. *Chem. Soc. Rev.* **1972**, *1*, 481.
- [235] Funke, U.; Grützmacher, H.-F. *Tetrahedron* **1987**, *43*, 3787.
- [236] Gräf, D.; Nitsch, H.; Ufermann, D.; Sawitzki, G.; Patzelt, H.; Rau, H. *Angew. Chem. Int. Ed. Engl.* **1982**, *21*, 373.
- [237] Röttger, D.; Rau, H. *J. Photochem. Photobiol. Chem.* **1996**, *101*, 205.
- [238] Tamaoki, N.; Koseki, K.; Yamaoka, T. *Angew. Chem. Int. Ed. Engl.* **1990**, *29*, 105.
- [239] Tamaoki, N.; Koseki, K.; Yamaoka, T. *Angew. Chem.* **1990**, *102*, 66.
- [240] Norikane, Y.; Kitamoto, K.; Tamaoki, N. *Org. Lett.* **2002**, *4*, 3907.
- [241] Norikane, Y.; Kitamoto, K.; Tamaoki, N. *J. Org. Chem.* **2003**, *68*, 8291.
- [242] Norikane, Y.; Tamaoki, N. *Eur. J. Org. Chem.* **2006**, *2006*, 1296.
- [243] Norikane, Y.; Katoh, R.; Tamaoki, N. *Chem. Commun.* **2008**, 1898.
- [244] Nagamani, S. A.; Norikane, Y.; Tamaoki, N. *J. Org. Chem.* **2005**, *70*, 9304.
- [245] Shinkai, S.; Minami, T.; Kusano, Y.; Manabe, O. *J. Am. Chem. Soc.* **1983**, *105*, 1851.
- [246] Ferri, V.; Elbing, M.; Pace, G.; Dickey, M. D.; Zharnikov, M.; Samorì, P.; Mayor, M.; Rampi, M. A. *Angew. Chem. Int. Ed.* **2008**, *47*, 3407.
- [247] Muraoka, T.; Kinbara, K.; Wakamiya, A.; Yamaguchi, S.; Aida, T. *Chem. – Eur. J.* **2007**, *13*, 1724.
- [248] Muraoka, T.; Kinbara, K.; Aida, T. *Nature* **2006**, *440*, 512.
- [249] Sasaki, T.; Tour, J. M. *Org. Lett.* **2008**, *10*, 897.
- [250] Vives, G.; Tour, J. M. *Acc. Chem. Res.* **2009**, *42*, 473.
- [251] Irie, M. *Chem. Rev.* **2000**, *100*, 1685.
- [252] Tsujioka, T.; Irie, M. *J. Photochem. Photobiol. C Photochem. Rev.* **2010**, *11*, 1.
- [253] Katsonis, N.; Kudernac, T.; Walko, M.; van der Molen, S. J.; van Wees, B. J.; Feringa, B. L. *Adv. Mater.* **2006**, *18*, 1397.
- [254] Dulić, D.; van der Molen, S. J.; Kudernac, T.; Jonkman, H. T.; de Jong, J. J. D.; Bowden, T. N.; van Esch, J.; Feringa, B. L.; van Wees, B. J. *Phys. Rev. Lett.* **2003**, *91*, 207402.
- [255] Feringa, B. L.; Browne, W. R. *Molecular Switches*; John Wiley & Sons, 2011.
- [256] Katsonis, N.; Lubomska, M.; Pollard, M. M.; Feringa, B. L.; Rudolf, P. *Prog. Surf. Sci.* **2007**, *82*, 407.
- [257] Tian, H.; Yang, S. *Chem. Soc. Rev.* **2004**, *33*, 85.
- [258] Grunder, S.; Huber, R.; Horhoiu, V.; González, M. T.; Schönenberger, C.; Calame, M.; Mayor, M. *J. Org. Chem.* **2007**, *72*, 8337.
- [259] Fernández-Rodríguez, M. A.; Hartwig, J. F. *J. Org. Chem.* **2009**, *74*, 1663.

- [260] Eibl, H.; Hottkowitz, T. Novel Phospholipids with Unsaturated Alkyl and Acyl Chains. EP1102775 (A1) Abstract of corresponding document: DE19835611 (A1), May 30, 2001.
- [261] Stuhr-Hansen, N. *Synth. Commun.* **2003**, *33*, 641.
- [262] Vonlanthen, D.; Rotzler, J.; Neuburger, M.; Mayor, M. *Eur. J. Org. Chem.* **2010**, *2010*, 120.
- [263] Farrera-Sinfreu, J.; Royo, M.; Albericio, F. *Tetrahedron Lett.* **2002**, *43*, 7813.
- [264] Chelucci, G.; Falorni, M.; Giacomelli, G. *Synthesis* **1990**, *1990*, 1121.
- [265] Bergmann, M.; Zervas, L. *Berichte Dtsch. Chem. Ges. B Ser.* **1932**, *65*, 1192.
- [266] Li, Y.; Manickam, G.; Ghoshal, A.; Subramaniam, P. *Synth. Commun.* **2006**, *36*, 925.
- [267] Bonnet, É.; Gangneux, P.; Marcéchal, E. *Bull. Soc. Chim. Fr.* **1974**, 504.
- [268] Liao, S.; Alfaro-Lopez, J.; Shenderovich, M. D.; Hosohata, K.; Lin, J.; Li, X.; Stropova, D.; Davis, P.; Jernigan, K. A.; Porreca, F.; Yamamura, H. I.; Hruby, V. J. *J. Med. Chem.* **1998**, *41*, 4767.
- [269] Sabitha, G.; Babu, R. S.; Rajkumar, M.; Srividya, R.; Yadav, J. S. *Org. Lett.* **2001**, *3*, 1149.
- [270] Ahmad, S.; Phillips, R. S.; Stammer, C. H. *J. Med. Chem.* **1992**, *35*, 1410.
- [271] Bruckner, R. *Advanced Organic Chemistry: Reaction Mechanisms*; 1 edition.; Academic Press: San Diego, 2001.
- [272] Clayden, J. *Organic Chemistry*; 2 edition.; Oxford University Press: Oxford ; New York, 2012.
- [273] Alder, R. W.; Bowman, P. S.; Steele, W. R. S.; Winterman, D. R. *Chem. Commun. Lond.* **1968**, 723.
- [274] Staab, H. A.; Saupe, T. *Angew. Chem. Int. Ed. Engl.* **1988**, *27*, 865.
- [275] Raab, V.; Kipke, J.; Gschwind, R. M.; Sundermeyer, J. *Chem. – Eur. J.* **2002**, *8*, 1682.
- [276] Brzeziński, B.; Schroeder, G.; Grzegorz Schroeder, E. G.; Malarski, Z.; Rospenk, M.; Sobczyk, L. *J. Chem. Res. Synop.* **1997**, 151.
- [277] Pedersen, C. J. *J. Am. Chem. Soc.* **1967**, *89*, 7017.
- [278] Pedersen, C. J. *J. Am. Chem. Soc.* **1967**, *89*, 2495.
- [279] Błaszczuk, A.; Fischer, M.; von Hänisch, C.; Mayor, M. *Helv. Chim. Acta* **2006**, *89*, 1986.
- [280] Pugliesi, I.; Megerle, U.; Suraru, S.-L.; Würthner, F.; Riedle, E.; Lochbrunner, S. *Chem. Phys. Lett.* **2011**, *504*, 24.
- [281] Suzuki, H. *Electronic absorption spectra and geometry of organic molecules: An application of molecular orbital theory*; Elsevier, 2012.
- [282] Guilbault, G. G. *Pure Appl. Chem.* **2009**, *57*, 495.
- [283] Valkenier, H.; Huisman, E. H.; van Hal, P. A.; de Leeuw, D. M.; Chiechi, R. C.; Hummelen, J. C. *J. Am. Chem. Soc.* **2011**, *133*, 4930.
- [284] Yu, C. J.; Chong, Y.; Kayyem, J. F.; Gozin, M. *J. Org. Chem.* **1999**, *64*, 2070.

- [285] Reinders, F. Azobenzenes and dithiocarbamates in molecular film devices, Basel: Basel, 2012.
- [286] Flatt, A. K.; Dirk, S. M.; Henderson, J. C.; Shen, D. E.; Su, J.; Reed, M. A.; Tour, J. M. *Tetrahedron* **2003**, *59*, 8555.
- [287] Grunder, S.; Huber, R.; Wu, S.; Schönenberger, C.; Calame, M.; Mayor, M. *Eur. J. Org. Chem.* **2010**, *2010*, 833.
- [288] Shirai, Y.; Cheng, L.; Chen, B.; Tour, J. M. *J. Am. Chem. Soc.* **2006**, *128*, 13479.
- [289] Grundberg, H.; Andergran, M.; Nilsson, U. J. *Tetrahedron Lett.* **1999**, *40*, 1811.
- [290] Tewari, N.; Nizar, H.; Mane, A.; George, V.; Prasad, M. *Synth. Commun.* **2006**, *36*, 1911.
- [291] Housecroft, C.; Sharpe, A. G. *Inorganic Chemistry*, 4 edition.; Prentice Hall: Harlow, England ; New York, 2012.
- [292] Wierschke, S. G.; Chandrasekhar, J.; Jorgensen, W. L. *J. Am. Chem. Soc.* **1985**, *107*, 1496.
- [293] Gabutti, S.; Knutzen, M.; Neuburger, M.; Schull, G.; Berndt, R.; Mayor, M. *Chem. Commun.* **2008**, 2370.
- [294] Konishi, Y. Lithographic Printing Plate. JP2007232836 (A), September 13, 2007.
- [295] Poeylout-Palena, A. A.; Testero, S. A.; Mata, E. G. *J. Org. Chem.* **2008**, *73*, 2024.
- [296] Xu, Y.; Smith, M. D.; Krause, J. A.; Shimizu, L. S. *J. Org. Chem.* **2009**, *74*, 4874.
- [297] Younes, S.; Tchani, G.; Baziard-Mouysset, G.; Stigliani, J.; Payard, M.; Bonnafous, R.; Tisne-Versailles, J. *Eur. J. Med. Chem.* **1994**, *29*, 87.
- [298] Toyoshima, S.; Sato, R.; Ito, K.; Shinohara, T.; Yamamoto, Y. Anti-tumor agent comprising an organosilicon compound. EP0046242 (A1), February 24, 1982.
- [299] Ghosh, S.; Tochtrop, G. P. *Tetrahedron Lett.* **2009**, *50*, 1723.
- [300] Rajagopalan, R. Nitrogen-sulfur ligands as opiate receptor drug mimics. US5330737 (A), July 19, 1994.
- [301] Anderson, M. B.; Ranasinghe, M. G.; Palmer, J. T.; Fuchs, P. L. *J. Org. Chem.* **1988**, *53*, 3125.
- [302] Chambert, S.; Désiré, J.; Décout, J.-L. *Synthesis* **2002**, 2319.
- [303] Scarpetti, D.; Fuchs, P. L. *J. Am. Chem. Soc.* **1990**, *112*, 8084.
- [304] Li, W.; Fishkin, N.; Zhao, R.; Miller, M.; Chari, R. Novel Benzodiazepine Derivatives. WO2010091150 (A1), August 12, 2010.
- [305] Brückner, R. *Reaktionsmechanismen: Organische Reaktionen, Stereochemie, Moderne Synthesemethoden*; Auflage: 3., Aufl. 2004. 3., korr. Nachdruck 2009.; Spektrum Akademischer Verlag: München; Heidelberg, 2009.
- [306] IUPAC Gold Book - isobestic point <http://goldbook.iupac.org/I03310.html> (accessed Aug 22, 2014).

- [307] Armarego, W. L. F.; Chai, C. *Purification of Laboratory Chemicals*; Butterworth-Heinemann, 2012.
- [308] Calcagno, P.; Kariuki, B. M.; Kitchin, S. J.; Robinson, J. M. A.; Philp, D.; Harris, K. D. M. *Chem. – Eur. J.* **2000**, *6*, 2338.
- [309] Harzmann, G. D.; Neuburger, M.; Mayor, M. *Eur. J. Inorg. Chem.* **2013**, *2013*, 3334.
- [310] Grunder, S.; Huber, R.; Wu, S.; Schönenberger, C.; Calame, M.; Mayor, M. *Chim. Int. J. Chem.* **2010**, *64*, 140.
- [311] Sek, S.; Breczko, J.; Plonska-Brzezinska, M. E.; Wilczewska, A. Z.; Echegoyen, L. *ChemPhysChem* **2013**, *14*, 96.
- [312] Olsen, M. T.; Gray, D. L.; Rauchfuss, T. B.; Gioia, L. D.; Zampella, G. *Chem. Commun.* **2011**, *47*, 6554.
- [313] Guo, W.; Li, J. J.; Wang, Y. A.; Peng, X. *J. Am. Chem. Soc.* **2003**, *125*, 3901.
- [314] Wang, F.; Good, J. A. D.; Rath, O.; Kaan, H. Y. K.; Sutcliffe, O. B.; Mackay, S. P.; Kozielski, F. *J. Med. Chem.* **2012**, *55*, 1511.
- [315] Refat, M. S.; Grabchev, I.; Chovelon, J.-M.; Ivanova, G. *Spectrochim. Acta. A. Mol. Biomol. Spectrosc.* **2006**, *64*, 435.
- [316] Vanoppen, P.; Grim, P. C. M.; Rücker, M.; De Feyter, S.; Moessner, G.; Valiyaveetil, S.; Müllen, K.; De Schryver, F. C. *J. Phys. Chem.* **1996**, *100*, 19636.
- [317] Aissaoui, H.; Binkert, C.; Clozel, M.; Mathys, B.; Mueller, C.; Nayler, O.; Scherz, M.; Velker, J.; Weller, T. 4-(piperidyl- and Pyrrolidyl-Alkyl-Ureido) -Quinolines as Urotensin II Receptor Antagonists. WO03048154 (A1), June 12, 2003.
- [318] Cahiez, G.; Gager, O.; Moyeux, A.; Delacroix, T. *Adv. Synth. Catal.* **2012**, *354*, 1519.
- [319] Wei, W.; Tomohiro, T.; Kodaka, M.; Okuno, H. *J. Org. Chem.* **2000**, *65*, 8979.
- [320] Shimogaki, T.; Oshita, S.; Matsumoto, A. *Macromol. Chem. Phys.* **2011**, *212*, 1767.
- [321] Yamamoto, T.; Chiba, A.; Fujita, K.; Kataba, Y.; Ohsumi, K.; Asari, S.; Fukuchi, N.; Noguchi, M.; Tanabe, I.; Ijichi, C.; Oohmuta, N.; Iida, Y.; Iwayama, S.; Fujita, K.; Oomuta, N. Novel azole compound. US2006194850 (A1), August 31, 2006.
- [322] Jones, M. W.; Mantovani, G.; Blindauer, C. A.; Ryan, S. M.; Wang, X.; Brayden, D. J.; Haddleton, D. M. *J. Am. Chem. Soc.* **2012**, *134*, 7406.
- [323] Su, M.; Wang, J.; Tang, X. *Chem. – Eur. J.* **2012**, *18*, 9628.
- [324] Moses, J. E.; Neidle, S.; Moorhouse, A. D.; Moore, M. Ureylene Derivatives. WO2008122667 (A2), October 16, 2008.
- [325] Würthner, F.; Ahmed, S.; Thalacker, C.; Debaerdemaeker, T. *Chem. – Eur. J.* **2002**, *8*, 4742.
- [326] Kishore, R. S. K.; Ravikumar, V.; Bernardinelli, G.; Sakai, N.; Matile, S. *J. Org. Chem.* **2008**, *73*, 738.

- [327] Pennington, W. T. *J. Appl. Crystallogr.* **1999**, *32*, 1028.
- [328] Macrae, C. F.; Bruno, I. J.; Chisholm, J. A.; Edgington, P. R.; McCabe, P.; Pidcock, E.; Rodriguez-Monge, L.; Taylor, R.; van de Streek, J.; Wood, P. A. *J. Appl. Crystallogr.* **2008**, *41*, 466.
- [329] Bruker. *APEX2*; Madison, 2006.
- [330] Palatinus, L.; Chapuis, G. *J. Appl. Crystallogr.* **2007**, *40*, 786.
- [331] Betteridge, P. W.; Carruthers, J. R.; Cooper, R. I.; Prout, K.; Watkin, D. J. *J. Appl. Crystallogr.* **2003**, *36*, 1487.
- [332] Carruthers, J. R.; Watkin, D. J. *Acta Crystallogr. Sect. A* **1979**, *35*, 698.